Coordination Chemistry and Recognition of Some Metal Ions Using *N*- or *N*,*O*-Donor Ligands

A Dissertation Submitted to the
Indian Institute of Technology Guwahati as
Partial Fulfillment for the Degree of Doctor of Philosophy
in Chemistry

by

Nibedita Behera
Roll No. 126122034

Department of Chemistry
Indian Institute of Technology Guwahati
Guwahati – 781 039

January 2018

Dedicated to My Parents, Brother and Sister

DEPARTMENT OF CHEMISTRY
INDIAN INSTITUTE OF TECHNOLOGY GUWAHATI
GUWAHATI–781039

DECLARATION

I hereby declare that this thesis entitled "**Coordination Chemistry and Recognition of Some Metal Ions Using *N*- or *N,O*-Donor Ligands**" is the outcome of research work carried out by me under the supervision of Dr. V. Manivannan, at the Department of Chemistry, Indian Institute of Technology Guwahati, Assam, India.

In keeping with the general practice of reporting scientific observations, due acknowledgement has been made whenever work described here has been based on the findings of other investigators.

January 2018
IIT Guwahati

Nibedita Behera
(Roll. No. 126122034)

DEPARTMENT OF CHEMISTRY
INDIAN INSTITUTE OF TECHNOLOGY GUWAHATI
GUWAHATI–781039

Certificate

This is to certify that Miss Nibedita Behera has been working under my supervision since July, 2012 as a regular registered Ph. D. student. I am forwarding his thesis entitled "**Coordination Chemistry and Recognition of Some Metal Ions Using *N*- or *N,O*-Donor Ligands**" being submitted for the Ph. D. Degree (Chemistry) of this Institute.

I certify that he has fulfilled all the requirements according to the rules of this institute regarding the investigations embodied in his thesis and this work has not been submitted elsewhere for a degree.

January 2018
IIT Guwahati

Dr. V. Manivannan
(Thesis Supervisor)

Acknowledgements

The journey of my PhD started with encouragement, optimistic thinking, emotional and moral support from people of my acquaintance. At the verge of completing my thesis work I offer my sincerest gratitude to every supportive individual who helped me with their kind advises and indigenous ideas.

A special thanks to my supervisor Dr V. Manivannan for all his kind support and encouragement he has given me over the last four years. I will always be grateful for his patience to make me learn minor things while writing the Thesis and manuscripts.

I would like to express my profound respect to my parents and regard sister and brother for their moral and emotional support for defying the odds. Your unconditional love and faith on me brought this journey to a fruitful end.

I always feel lucky that I have friends like Rajendra Maity, Prajna Sucharita Das and Bibhudatta Mishra. They are my inspiration and encouragement of my life. I also feel proud that I have friends like Mitali Sahu, Pratika Basumatary, Rakhee Das, Abhradip Pal, V. V. Kulkarni, Ardhendu S. Choudhary, Bebina Chakma, Neha Arora, Ruchira Bajpai, Ananya Berman, R. Unnava, Bedika Phukan whose honest criticism helped me to improve. Together we spent quality times amidst fun, which helped me to carry forward my work smoothly. I also take this opportunity to convey my deepest regard to my dear friend Late Richa Rakshit, without whom I could not even think about overcoming the obstacles, from the beginning of my journey in doctoral studies.

Specially, I am delighted to have lab mates Jugal Bori, Araghni Bhattacharya and Satyajit Mahata who are very cooperative and helpful.

Besides, I am thankful to my seniors Kameli di, Suchandra di, Samir Da, Sujit Da, Kanhu Da, and juniors Dillip, Niranjan, Avisek, Manoranjan, Subas, Archana for their helps and suggestions in these five years while doing experiments and instrumental analysis.

Along with, I wish to thank Dr. Bigan Jali and Dr. Babulal das for helping me in crystal analysis and Dr. Santosh K. Behera for his guidance in DFT calculations. I am thankful to CIF operators, HRMS operators and staff members of Dept. of Chemistry for their kind help in operating the instruments and sample analysis.

Preface

This Thesis contains five chapters. Chapter 1 is the introduction, which describes self-assembly of the coordination complexes by supramolecular interactions based on selected recent literature reports. Some highlights on fluorescence sensors containing different fluorophore moieties for the detection of various metal ions have been described. Chapter 2 describes molecular structures of nine metal complexes synthesized using a monodentate *N*-substituted imidazole ligand, 1-(4-acetylphenyl)imidazole (**L**) and coligands. Weak interactions present in three pairs of isomorphous and isostructural mononuclear complexes, a mononuclear complex, a 1D coordination polymer and a 2D-coordination polymer have been described. In Chapter 3, a trisubstituted imidazole, 2,4-bis(2-pyridyl)-5-(4-pyridyl)imidazole (**L1H**) has been employed which acts as a fluorophore and selectively detect Zn^{2+} ion by a characteristic fluorescence response. The Zn^{2+} ion can be detected within a calculated limit of 6.5×10^{-7} M. A complex of composition $[Zn_2(\mathbf{L1})Cl_3(H_2O)]$ was isolated as a crystalline solid by reacting **L1H** with $ZnCl_2$ which was structurally characterized. In this complex, **L1H** got deprotonated and bound to Zn^{2+} ion in pentadentate fashion as $\mathbf{L1}^-$ ion, by using all the five donor atoms. In Chapter 4, two new hydrazones *viz.*, 2-(2-(2,3-dihydroxy)benzylidenehydrazinyl)benzothiazole (**L2H**) and 2-((2-(2-hydroxy)(4-*N*,*N*-diethylamino))benzylidenehydrazinyl)benzothiazole (**L3H**), were synthesized which are weakly emissive in nature due to PET process and gave "*turn-on*" responses with $AlCl_3$. The detection limits of **L2H** and **L3H** for Al^{3+} ion were calculated to be 3.6×10^{-9} M and 2.4×10^{-9} M respectively. The DFT/TDDFT calculations performed on **L2H**, **L3H** and their Al(III) complexes revealed that HOMO-LUMO energy gap got reduced upon complexation. In Chapter 5, a hydrazide 6-(hydroxymethyl)-*N*'-((2-hydroxy-1-naphthyl)methylene)picolinohydrazide (**L4H**) was synthesized by condensation of 2-hydroxy-1-napthaldehyde and 6-(hydroxymethyl)picoloinohydrazide. This probe act as "*turn on*" fluorescent sensor for multi detection of Al^{3+}, Zn^{2+} and Cd^{2+} ions at distinct emission maxima. The resultant Al(III) complex gave "*turn–off"* response towards F^- ion. Similar quenching responses were also exhibited in case of Zn^{2+} and Cd^{2+} complexes upon addition of $H_2PO_4^-$ ion. The DFT/TDDFT calculations performed on **L4H**, $[Al(\mathbf{L4})_2]^+$, $[Zn(\mathbf{L4})Cl(H_2O)_2]$ and $[Cd(\mathbf{L4})Cl(H_2O)_2]$ are support the experimentally observed results. This hydrazide probe **L4H** can also be utilized in real water samples.

Abbreviations

a	Unit cell dimension a
b	Unit cell dimension b
c	Unit cell dimension c
D	Density of the crystal
α	Interfacial angle α in a unit cell
β	Interfacial angle β in a unit cell
γ	Interfacial angle γ in a unit cell
Z	Unit cell formula units
λ	Wave length
ν	Wave number
μ	Absorption coefficient
ε	Molar extinction coefficient
μ_{eff}	Effective magnetic moment
θ	Temperature

Contents

Chapter 1

Introduction, Materials and Methods

Abstract:

In this Chapter, an attempt has been made to give concise view of self-assembly of the coordination complexes by supramolecular interactions based on selected recent literature reports. Along with this, some highlights on fluorescence sensors containing different fluorophore moieties for the detection of various metal ions have been discussed. The materials used in this study, their commercial sources, methods of spectral analysis, specifications of the instruments used for the characterization of the compounds, procedures of crystallographic data collection and refinement *etc*., are also briefed at the end.

1. Introduction:

1.1. Coordination chemistry:

Coordination compounds are the assembly comprising a central metal atom/ion to which is attached a surrounding array of other groups of atoms from the ligand molecules. Metal ions play vital role in all living systems.[1] In biological systems, metal ions are essential for transport and storage of oxygen, electron transfer processes, enzymatic regulation of several biological processes *etc*.[2] In addition coordination complexes are also used as medicines and employed in diagnostic procedures.[3] Coordination chemistry of many transition metal ions has also considerable importance due to their intriguing structures[4] and extensive applications. Various applications of coordination compounds are catalysis,[5] molecular magnetism,[6] luminescence,[7] gas storage and separation[8] *etc*. Choice of the metal ion and design of appropriate ligand framework play the principal role in the construction of coordination architectures with fascinating structures and functions.

Ligands having nitrogen donor centers are one of the most important aspects of coordination complexes. Among them, multi-dentate ligands having nitrogen heterocyclic groups such as imidazole, pyridine, pyrrole, pyrazole, pyrazine and triazole have been useful linkers for the construction of coordination networks.[9] Importantly, the imidazole motifs have been widely utilized as excellent candidates for synthesis of complexes. Imidazole ring containing ligands are also used for anion and cation sensing,[10-11] molecular recognition[12] and in supramolecular chemistry.[13] The imidazole moiety has two N-atoms, one of them can be used as donor for metal atom or can be protonated in acidic medium. Because of delocalization of six electrons on five atoms it is more basic than pyridine and has higher electron density and stronger coordination ability. In addition, it is capable of acting as a bidentate bridging ligand as imidazolate anion formed through deprotonation. Along with, imidazole moiety is found in many biologically relevant molecules such as histidyl residue in proteins and have an important role in biological systems and their derivatives have many pharmacological activities such as antibacterial, antifungal,[14] as well as antitumoral effects.[15]

1.2. Supramolecular chemistry:

The concept of "supramolecular chemistry" was introduced by Jean-Marie Lehn who was awarded noble prize for his work in this area in 1978. The term "supramolecular chemistry" is alternatively expressed as "chemistry beyond the molecule" or "non-molecular chemistry" or "the chemistry of non-covalent bond". According to J. -M. Lehn, "the supramolecular chemistry is the chemistry of the intermolecular bond, covering the structures and functions of the entities formed by the association of two or more chemical species".[16] This interdisciplinary field of science has great impact in chemical, physical and biological domains.[13,17-20] Studies on crystals with applications in solid-state chemistry, crystal engineering, catalysis and material science, organic, inorganic, bio-organic and bioinorganic chemistries, chemistry at interfaces, transport phenomena, polymer sciences, molecular sensors, molecular switches *etc.*, utilize the concept of supramolecular chemistry.[13] Traditional chemistry focus on the formation of covalent and coordinate bonds whereas, non-covalent intermolecular forces play crucial role to assemble large molecular structure in supramolecular chemistry.[21] Intermolecular forces are weak in comparison with covalent and coordinate bonds, so that supramolecular species are thermodynamically less stable, kinetically labile and more flexible in nature. Supramolecular species incorporate many interactions such as, electrostatic force, hydrogen bonding, π···π stacking, ion-ion, ion-dipole and dipole-dipole, cation···π and van der Waals forces.[22] Accumulation of these interactions gives rise to a stable supramolecular arrangements by their components with the resultant architecture/superstructure being determined by the nature of intermolecular forces holding them together.[16] Many interactions with varying degrees of strength and directionality constitute the supramolecular assemblies which also depend on bond distances and angles.[16]

Hydrogen bonding interactions are one kind of dipole-dipole interaction which is directional, electrostatic in nature and having certain geometry. Typically this can be represented as D–H···A, (where D = electronegative atoms such as C, O, N, F and S; A = partially negative atom having at least on one lone-pair of electrons or polarisable π electrons) in which hydrogen atom carries a partially positive charge due to large

difference of electronegativity between hydrogen and atoms to which it is attached *via* covalent bond. Hydrogen bonding is a dominant interaction in supramolecular chemistry, helps in close packing arrangements with particular geometry and also minimizes energy of the system. In biology, DNA and RNA form the double helical structure by the help of hydrogen bonding of base pairs (Scheme 1).[23] Besides the role of H-bonding in various chemical and biological processes,[24] it has also pivotal role in water networks[25] and peptide interactions.[26] In addition, H-bonding interactions are often subcategorised into three types such as weak, moderate and strong. Other common weak interactions are π-interactions of the type D–H···π, π···π, cation···π, anion···π, *etc*.

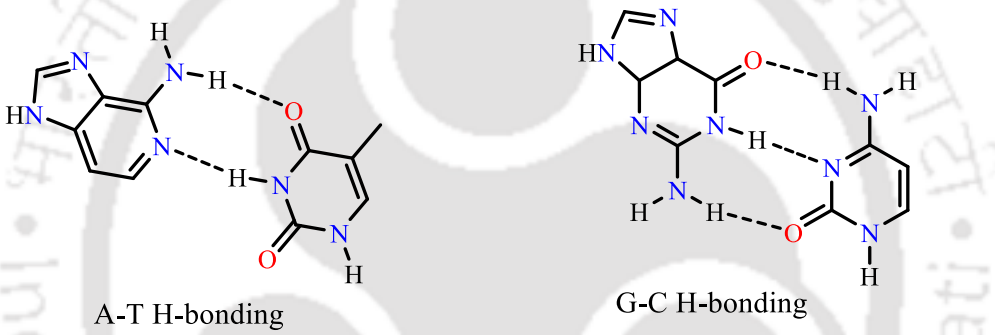

Scheme 1. Base pairing by H-bonding.

1.2.1. Supramolecular interaction in coordination complex:

Because of tremendous impact of supramolecular chemistry, many studies were focused on different weak and non-covalent interactions. Although, non-covalent interactions are relatively weak in comparison with covalent bond, their simultaneous interactions influence structural topologies which lead to several physical and chemical characteristic of the molecules or coordination complexes. Specifically, tuning of the hydrogen-bond formation sites, various application such as supramolecular electronics,[27] host guest chemistry,[28] self-assembly of molecular capsules,[29] nanotubes,[30] and so forth have been achieved. Etter and co-workers analyzed variety of hydrogen-bonding patterns by applying graph set theory.[31] Weak interactions led to supramolecular networks by forming simple patterns such as chains, rings, inter-molecular hydrogen-bonded patterns, and other finite patterns. Few selected reports containing some or more of these

interactions, effect of hydrogen bonding on magnetic properties and existence of salt-bridge···π interaction has been listed below, for representative purpose.

Sadhukhan *et al.*[32] synthesised and determined molecular structures of Ni(II) complexes using three ligands **1**, **1a-b**, which show 1D, 2D and 3D H-bonded network structures. A moderate antiferromagnetic interaction has been found to operate between phenoxo bridged Ni(II) dimers isolated using **1** (Figure 1a) and **1a** (Figure 1b). Interestingly, the O–H···O bridged dimeric complex containing **1b** has been reported to exhibit very weak antiferromagnetic exchange through hydrogen bonding and π···π stacking interactions (Figure 2).

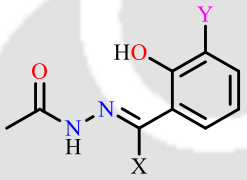

1: X = H, Y = H
1a: X = CH_3, Y = H
1b: X = H, Y = OH

Scheme 2. Schematic diagram of ligand **1**, **1a-b**.

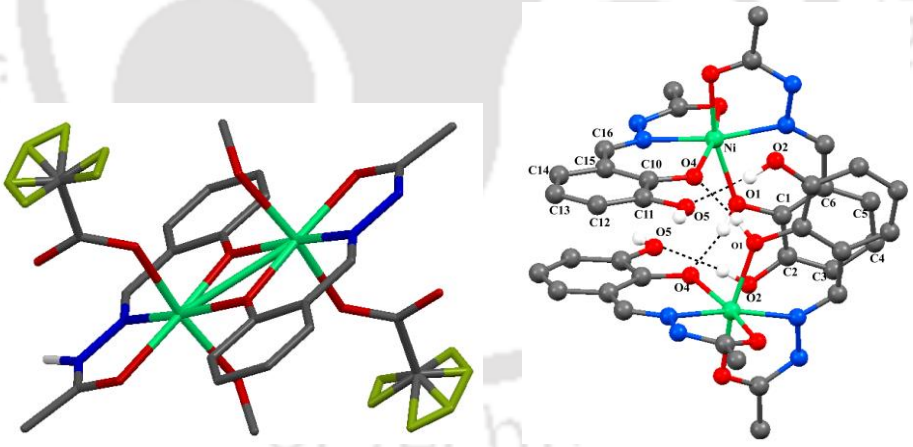

(**a**) (**b**)

Figure 1. (a) Molecular structure of **1**. (b) Dimeric unit formed by intermolecular H-bonding interaction in **1b** (Hydrogen atoms not involved in hydrogen bonding are omitted) along with π···π interactions.

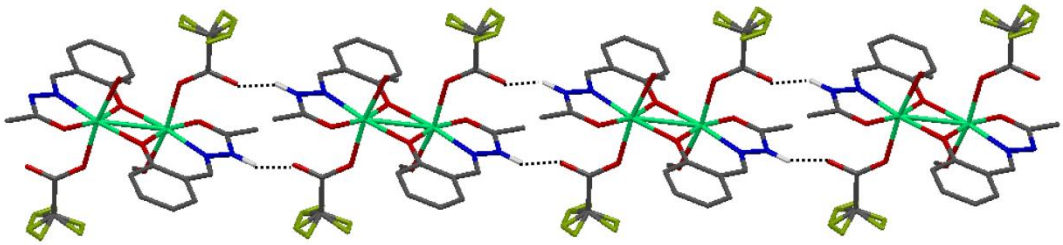

Figure 2. Packing diagram of **1** depicting the 1D H-bonded network (hydrogen atoms, not involved in H-bonding, are omitted for clarity).

Sadhukhan *et al.*[33] also reported mononuclear and dinuclear Mn(II) complexes of **1** and **1b**, and in all of these compounds, hydrogen-bonded self assemblies of different dimensionalities and architectures were observed. Along with this, C–H···π and π···π interactions also contribute in forming supramolecular assemblies.

Mitra *et al.*[34a] synthesized and determined the molecular structure of a Cu(II) malonate complex (**2**) using protonated 2-aminopyridine as the auxiliary ligand, which is acting as the counter cation. In self assembly of this Cu(II) complex, salt-bridge···π interaction has been found to exist apart from the presence of O–H···O, π···π stacking and anion···π interactions (Figure 3).

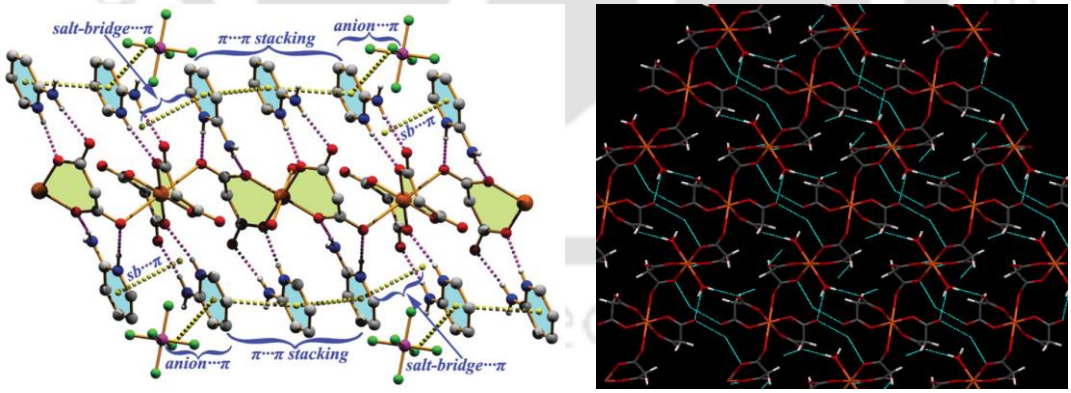

Figure 3. Salt-bridge···π interaction (left, which has been adopted without permission) and O–H···O interactions (right) in **2**.

The proton conduction properties of a 2D, flexible MOF and a 1D coordination polymer having the molecular formulae $\{[Zn(C_{10}H_2O_8)_{0.5}(C_{10}S_2N_2H_8)]\cdot 5H_2O]\}_n$ (**3a**) and $\{[Zn\text{-}(C_{10}H_2O_8)_{0.5}(C_{10}S_2N_2H_8)]\cdot 2H_2O]\}_n$ (**3b**), {$C_{10}H_2O_8$ = 1,2,4,5-benzenetetracarboxylate ion; $C_{10}S_2N_2H_8$ = 4,4'-dipyridyldisulfide} respectively have

been reported.[34b] Both these compounds have been reported to show high conductivity due to their dimensionalities and the internal hydrogen bonding connectivities (Figure 4).

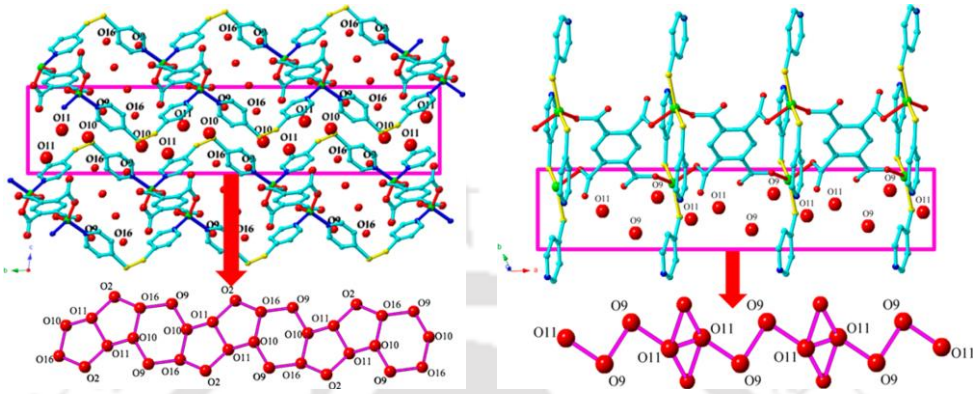

(**a**) (**b**)

Figure 4. (a) 2D structure and H-bonding network present in lattice water of **3a**. (b) 1D structure and H-bonding network present in lattice water of **3b**. (Colour code: C, cyan; N, blue; O, red; S, yellow; Zn, green) (These two figures have been adopted without permission).

Five Hg(II) complexes synthesized using *N*-(2-quinolinyl)pyrazine-2-carboxamide (**3c**) and *N*-(3-quinolinyl)pyrazine-2-carboxamide (**3d**) have been structurally characterized.[34c] Molecular structures of these compounds have been reported to contain 1D and 2D polymeric structures linked through supramolecular interactions in three of them and 3D coordination polymers in two compounds. These C–H···π, π···π and C–H···O interactions affect the coordination geometry and structural assembly and also help in stabilization of some of the crystal structures reported here (Figure 5).

Four Zn(II) complexes of 6-chloro-4-phenyl-2-(2-pyridyl)quinazoline ligand (**3e**) were synthesized using different salts of zinc.[34d] Varying the anions in zinc salts yields different conformations of the ligand due to twisting of the pyridyl ring with respect to the quinazoline ring. As a result complexes with different nuclearities as well as different coordination geometries were observed. The packing diagrams of these complexes contain intermolecular interactions such as C–H···π, π···π, C–H···O, C–H···N and C–H···Cl interactions (Figure 6).

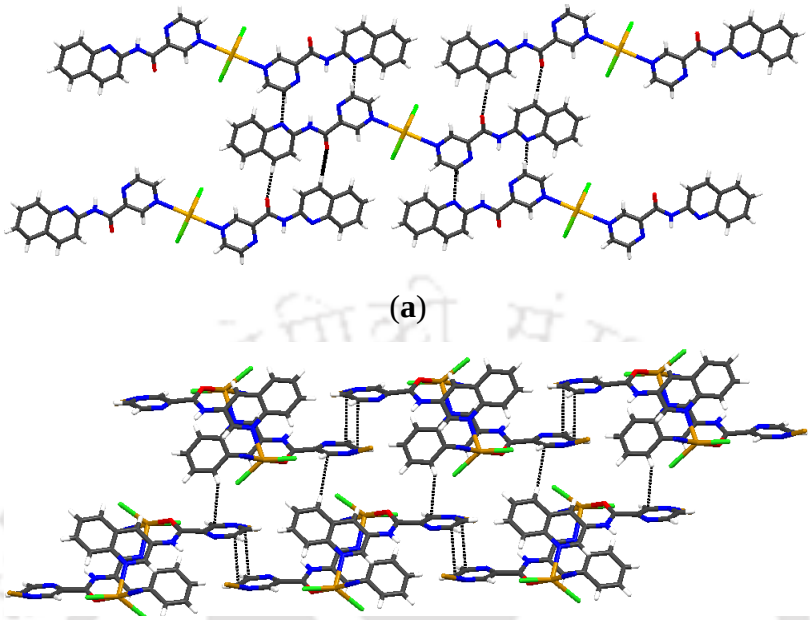

(**a**)

(**b**)

Figure 5. Representation of Hg(II) complex of (a) **3c** and (b) **3d** showing C–H···π, π···π and C–H···O interactions.

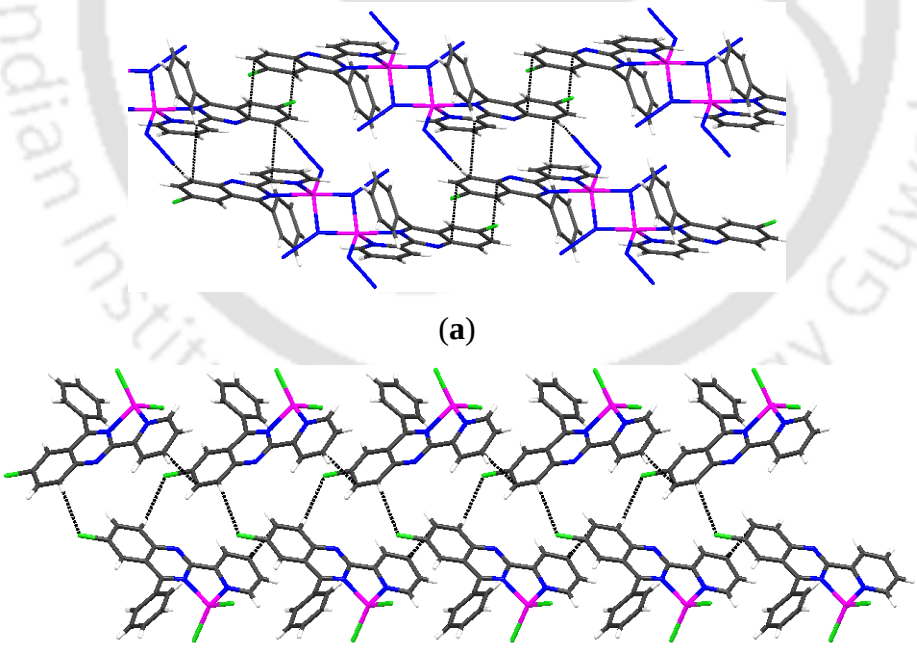

(**a**)

(**b**)

Figure 6. Representation of some of Zn(II) complexes of **3e** and showing C–H···Cl, π···π and C–H···N interactions.

1.3. Fluorescence Sensor:

This sensing technique has had a great impact recently in analyte detection. In this technique, object is the one which has to be detected and is known as the analyte. Analytes can be a small molecules or ions or large molecules or living cells. Another one is the probe or sensor. A sensor unit provides binding site and an informative signal about the object, upon binding. Many physical principles are applied in sensors for generating a specific signal upon interaction between probe and analyte. These physical principles may be optical (light absorption, reflection, fluorescence), electrochemical and heat. Mechanisms responsible for generating signal may be electronic, conformational, change in medium or by chemical or electrochemical reactions. Many optical bioassays and chemical sensing probes use fluorescence technique highly because of the easy operational process, simple set up, high sensitivity and selectivity. In this technique, sensors interact with analyte and give rise to a change which is correlated with the quantity of analyte. Typically, fluorescent sensors for metal ions have two essential features: a metal chelating or binding moiety and at least one fluorophore capable of absorbing and emitting light. Metal ions upon binding with probe change either the electronic structure or the molecular structure of the sensor. Consequently, change in the electronic structure can lead to a change in the intensity or wavelength of light absorption or emission, while changes in the molecular structure can also alter the distance or orientation of fluorophore. Generally, probe-analyte interaction can modulate:

a) the UV-visible absorption properties of the probe in terms of bathochromic or hypsochromic shifts in the absorption bands
b) change in fluorescence intensity by "*turn on*" or "*turn off*" process or generating new emission band(s)
c) bathochromic shift in emission spectra.

Such measurable and quantifiable changes lead to information about binding constants, formation and stoichiometry of receptor-analyte species, limits of detection, sensitivity, as well as selectivity of the sensing process. As probes exhibit colour and emission changes in the presence of a guest species have emerged as ideal candidates for use in optical fibre devices. Besides experimental analysis, theoretical calculations have

also been used and gained significance as because of its support to the proposed binding hypothesis. By using DFT/TDDFT calculation, molecular structure and geometry of probe and probe-metal ion species are optimised for evaluation of the energies of the participating frontier molecular orbitals (FMOs), highest occupied and lowest unoccupied molecular orbitals (HOMO and LUMO, respectively) of the probe as well as probe-metal ion species and correlation of the molecular electronic transitions, energy, atomic charges *etc*. Thus, it helps to understand the sensing mechanism and design more efficient sensors. Usually, detection of analytes by probes occurs by three different approaches[35] such as binding site-signalling, displacement and chemodosimeter approach. In the "binding site-signalling subunit" approach, both host and guest interacts by forming covalent bond.[36] The displacement approach is due to the formation of molecular assemblies of binding site-signalling subunit, which upon coordination of anion to the binding site results in the release of the signalling subunit into the solution. Thus change in their optical properties has been revealed.[37] In the chemodosimeter approach, chemical reaction occurs in presence of a specific anion which results in an optical signal. Numerous reports are available based on ICT (Internal Charge Transfer), CHEF (Chelation Enhanced Fluorescence), EET (electronic Energy Transfer), PET (Photoinduced Electron Transfer), FRET (Förster Resonance Energy Transfer), MEF (Monomer-Excimer formation) mechanisms which alter the fluorescence signals in metal ion detection.[38-46] Among all approaches, probes are designed and synthesised based on binding site-signalling and displacement approaches as well as emphasising on PET and deprotonation processes. In this thesis, properties of these probes towards metal ions recognition have been investigated in detail. Some of the recently reported literatures on metal ions detection have been highlighted below and relevant literature reports related to the Chapters of the thesis has been referred appropriately in the Chapters.

1.3.1. Recent developments in fluorogenic metal ion sensing:

Tian *et al.*[47] used the molecule **4** that acts as a selective and sensitive fluorescent sensor for Zn^{2+} ion. This "8-oxalamidoquinoline" based sensor upon binding Zn^{2+} ion, gives rise to "*turn on*" emission enhancement with emission maximum at 490 nm in buffered aqueous solution at pH = 7.2. Complexation of **4** with Zn^{2+} ion is accompanied

by deprotonation of 8-amide group and results in increasing the electron-donating ability of this amide nitrogen atom to the quinoline ring. The fluorescent signals of **4** were utilized to construct an INHIBIT logic gate at the molecular level and **4** was used for fluorescence imaging in living yeast cells.

Wang *et al.*[48] reported a cell permeable, ESIPT based fluorescence sensor **5** which gives highly selective "*turn on*" response towards zinc ion at 545 nm and also NIR emission at 720 nm. In this zinc ion recognition process, complex formation between **5** and Zn^{2+} ion occur through imine-N, pyridine-N and phenolic-O atom that lie ortho to imine bond. One of the advantages of **5** is that due to the strict binding requirement associated with the chelate rings **5** is silent to Cd^{2+}, which often interferes with Zn^{2+} detection.

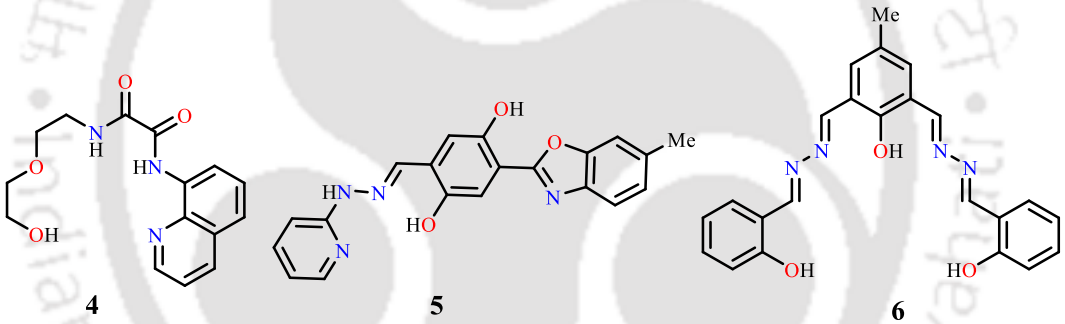

Scheme 3. Schematic diagram of probes **4**-**6**.

Compound **6** having two azine groups has been developed by Nandi *et al.*[49] for the naked eye and fluorescence recognition of I^- ion. The probe has been reported to show intense red color in the presence of I^- in THF and solvent dependent multiple signaling, *viz.*, green emission with Al^{3+} in aqueous methanol and ratiometric yellow emission with Zn^{2+} in DMSO. Routine Al^{3+} and Zn^{2+} imaging in human breast cancer cell, MCF7, under fluorescence microscope has also been performed. The developed method is used for analysis of real samples.

Sinha *et al.*[50] reported the usefulness of probe **7** having a imidazole ring fused to 9,10-phenanthrene, for selective recognition of Al^{3+} ion. Selectivity and recognition properties of **7** towards Al^{3+} ion were examined using UV-Visible, steady-state and time-resolved fluorescence spectroscopic studies. The fluorescence emission of free **7** in

acetonitrile at 445 nm blue shifted to 412 nm with ~2.3-fold enhancement in emission intensity upon addition of Al^{3+} ion. Density functional theoretical (DFT) calculations were carried out on the proposed aluminium complex $[Al_2(\mathbf{7})_2(\mu\text{-}OH)_2]^{2+}$ to support the experimental results.

A rhodamine–isatin hybrid probe **8**[51] has been synthesised and reported to selectively detect Al^{3+} ion in aqueous solution at physiological pH. The fluorescence "*off-on*" response has been due to opening of spirolactum ring upon complexation with Al^{3+} ion. The resultant **8**–Al^{3+} complex was utilized as a secondary fluorescence chemosensor for PPi ($P_2O_7^{4-}$). These changes in fluorescence signals of the **8** towards Al^{3+} and PPi ions have been reported to mimic the INHIBIT logic gate operation.

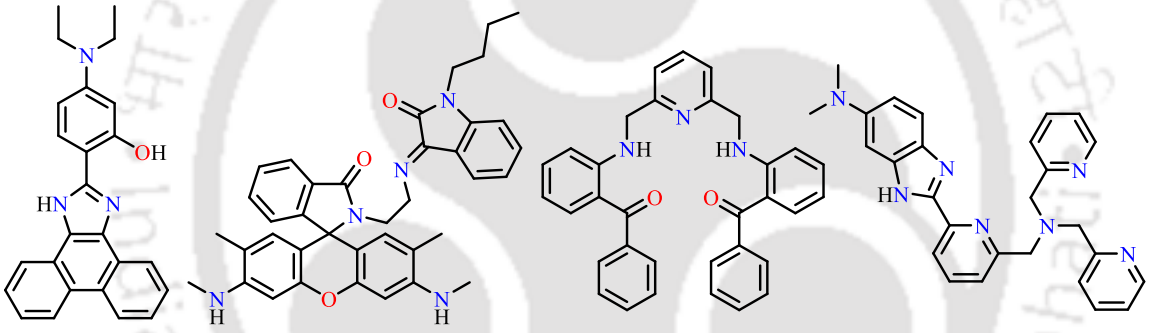

7 **8** **9** **10**

Scheme 4. Schematic diagram of probes **7**-**10**.

A fluorescence sensor **9** was developed by Chithiraikumar *et al.*[52] which selectively detects Cd^{2+} ion in presence of various other metal ions. Enhancement of fluorescence intensity of **9** by Cd^{2+} ion has been reported to occur because of blocking of photoinduced electron transfer (PET) process by the complexation of Cd^{2+} ion through oxygen and nitrogen atoms of the ligand. The ^1H NMR titrations and ESI-mass studies revealed binding ratio of **9** to Cd^{2+} ion to be 1:1.

Liu *et al.*[53] has reported the use of **10** as a ratiometric Cd^{2+} ion sensor in aqueous media. Mechanism of ratiometric sensing is due to metal ion chelation induced co-planation of 2,2′-azo-1,1′-biaryl fluorophore in **10** and hence internal charge transfer ICT effect has become prominent in **10** that provides red emission shift (53 nm) in presence of Cd^{2+} ion. A benzothiazole-functionalized fluorescein derivative (**11**) reported by Gao

et al.,[54] exhibits highly selective and sensitive "*turn-on*" fluorescence and naked-eye color change to Fe^{3+}. The probe **11** has been reported to exhibit low cytotoxicity and cell-membrane permeability, thus making it capable of Fe^{3+} bioimaging in living Hep G2 cells.

A fluorescence probe **12**, containing pyrene moiety and its di-sulfide linked dimer have been reported as trivalent (Fe^{3+}, Cr^{3+} and Al^{3+}) metal ion sensor through fluorescence ''*off–on*'' response.[55] Selectivity towards trivalent metal ions in presence of other metal ions is due to inhibition of PET process along with excimer formation by pyrene ring. The 2:1 stoichiometry of **12**-M^{3+} (M = Fe/Cr/Al) sensor complexes were obtained from Job's plot calculations. In addition, the binding ratio was supported by ^1H NMR titrations, ESI(+) mass and FTIR analysis.

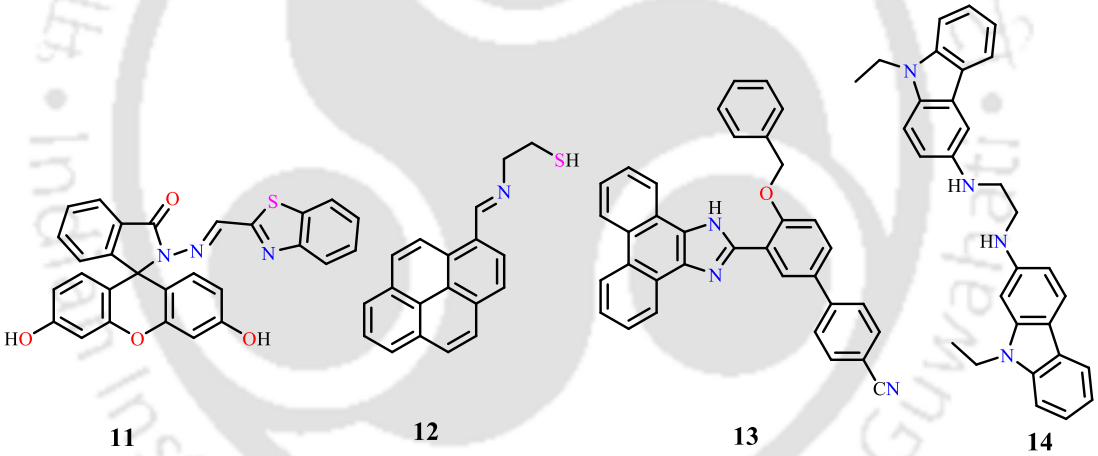

11 **12** **13** **14**

Scheme 5. Schematic diagram of probes **11**-**14**.

A fluorescent sensor **13** containing phenanthro[9,10-d]oxazole moiety was synthesized by Fan *et al.*[56] It acts as a fast-response, highly selective and sensitive chemosensor towards Cr^{3+} ion by giving "*turn-on*" fluorescence response at the physiological pH. The phenanthro[9,10-d]oxazole moiety in **13**, acts both as the electron donor and a potential binding site, while the electron deficient nitrile group acts as electron acceptor. Addition of Cr^{3+} to solution of **13** gave rise to red shifted emission from 393 to 412 nm. The quantum yield increased from 0.127 for the free probe to 0.917

upon Cr^{3+} ion binding. The reason behind the "*turn on*" selectivity mechanism of **13** for Cr^{3+} ion was based on combined interference of inhibition of ICT and CHEF process.

Zhang *et.al.*[57] synthesized the carbazole **14**, by reacting 3-amino-9-ethylcarbazole with glyoxal and then reducing the diimine with $NaBH_4$. Upon excitation at 370 nm, **14** exhibited strong fluorescence emission at 438 nm. Addition of Cr^{3+} to an ethanol–H_2O solution of **14** has been reported to result in quenching of fluorescence with the **14**:Cr^{3+} (1:1) ratio.

Zhao *et al.*[58] synthesised two isomeric fluorescence probes (**15** and **16**) having phenanthro[9,10-d]imidazolecoumarin moiety. Both were found to give selective "*turn-off*" fluorescence responses towards Fe^{3+} ion caused by paramagnetic quenching effect in a 1:1 sensor-Fe^{3+} ratio. The fluorescence detection mechanism had been supported by Job's plot, ^1H NMR and ESI-MS analysis.

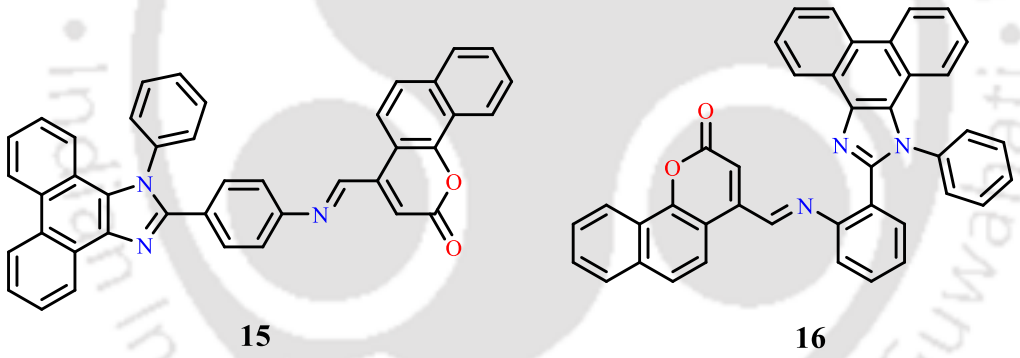

15 **16**

Scheme 6. Schematic diagram of probes **15** and **16**.

A 1,8-diaminonaphthalene based fluorescent probe **17**[59] has been employed to detect Cu^{2+} ion in a ratiometric and selective colorimetric "*off-on*" type of responses. Interaction of Cu^{2+} ion with **17** resulted in a red shift in both UV-Vis and emission spectra, due to ICT process. Such red shift has been reported to be specific to Cu^{2+} ion, effected by coordination through the N-atom of pyrimidine core *via* deprotonation.

A benzothiazole[60] ring bearing chemosensor **18** has been used as a molecular fluorescent sensor for Hg^{2+}, based on metal induced inhibition of the ESIPT mechanism. Free probe **18** has been reported to be weakly emissive having low intensity at 377 nm upon excitation at 340 nm, due to ESIPT being operational. With increase in Hg^{2+} ion

concentration, **18** gave a strong emission band centered at 530 nm. Engagement of phenolate-O in coordination to Hg^{2+} ion, has been the cause of preventing ESIPT.

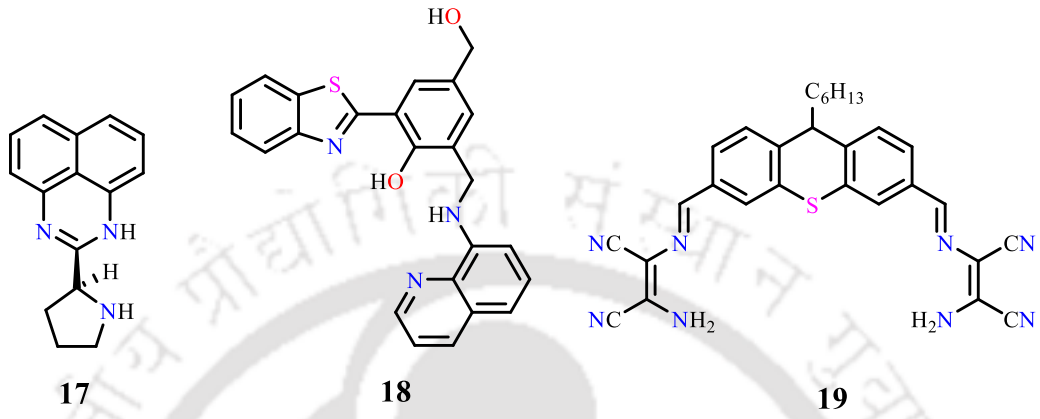

17 **18** **19**

Scheme 7. Schematic diagram of probes **17-19**.

A phenothiazine[61] having diamino-malenonitrile linkage as in **19**, was reported as chromogenic and fluorogenic sensor for specific detection of Hg^{2+} and S^{2-} ions. Upon excitation at 450 nm **19** gave emission maximum at 575 nm, which got quenched with increase in Hg^{2+} ion concentration. This quenching effect is because of inhibition of ICT process from the phenothiazine group to the diaminomalenonitrile moiety. DFT calculations on **19** and its Hg^{2+} complex also supported the disturbance of ICT upon coordination with Hg^{2+} ion. Addition of S^{2-} ion to resultant solution of **19**-Hg^{2+} complex species has been reported to reverse the quenching by releasing fluorescent **19** into the solution. The **19** also has the advantage of low cell toxicity and can be used for selective imaging of Hg^{2+} in living cells.

Spirobenzopyran derivative[62] **20** was designed, synthesized and its binding behaviour towards metal ions were studied by UV-Vis and fluorescence titration experiments and was supported by DFT calculations. The free probe has absorption maximum at 373 nm. Incremental addition of Cr^{3+} and Cu^{2+} ions to the solution of **20** gave raise to new absorption peaks at 477 and 550 nm, exhibiting yellow and pink colours, respectively. Difference in colour arose due to difference in ICT caused by Cr^{3+} and Cu^{2+} ions, because of their different oxidation states. Free probe **20** gave weak emission and addition of Cr^{3+} ion showed 27-fold increase in fluorescence at 675 nm. "*Turn On*"

response was observed due to internal charge transfer (ICT) as well as chelation-enhanced fluorescence (CHEF) processes.[63]

Alam *et al.* reported a 1:1 condensation product of diformyl-*p*-cresol with 8-aminoquinoline[64] **21** which is a useful chromogenic and fluorogenic dual sensor for Mg^{2+} and Zn^{2+} ions. Upon addition of both ions to free probe **21**, original absorption peaks at 369 and 500 nm decreased in intensity and a new peak grew at 456 nm along with isosbestic points. Whereas in fluorescence titration experiments, addition of Zn^{2+} and Mg^{2+} ions, blue shifted the 562 nm peak of **21** to 539 and 526 nm respectively. Metal ion competition studies revealed that detection of Mg^{2+} and Zn^{2+} ions were not affected by biologically abundant Na^{+}, K^{+}, Ca^{2+} ions *etc*., as well as several transition and heavy metal ions. Fluorescence "*off-on*" responses due to both Zn^{2+} and Mg^{2+} ions arose as a consequence of increase in rigidity and on set of CHEF[65] effect upon coordination of metal ions to **21**. The probe **21** could also be used for *in vitro*/*in vivo* cell imaging of Zn^{2+} and Mg^{2+} ions with negligible cytotoxicity. The DFT/TDDFT calculations were carried out on **21** and its Mg^{2+} and Zn^{2+} ions complexes where in calculated absorption spectra matched well with the experimental one.

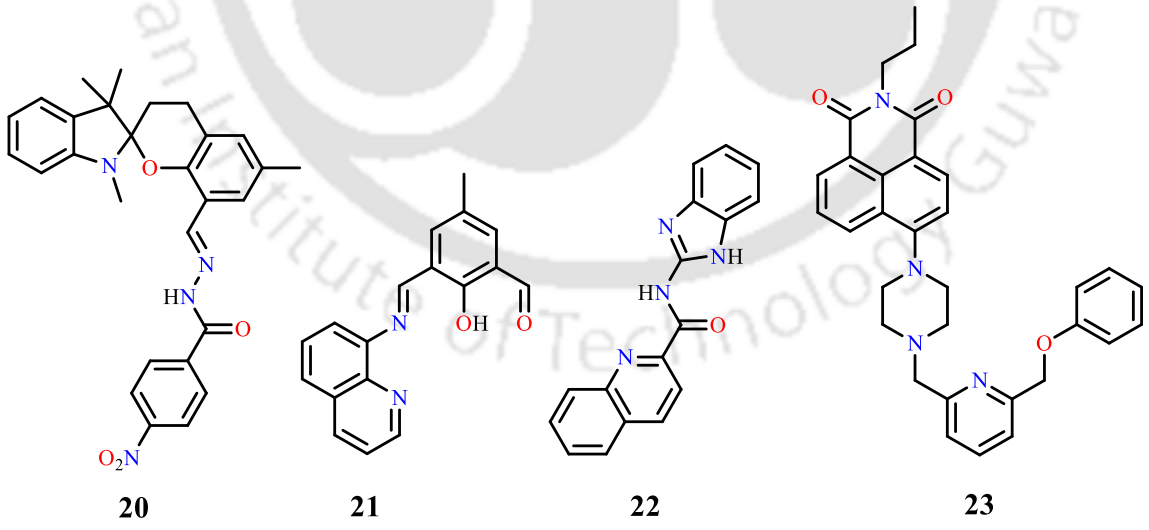

Scheme 8. Schematic diagram of probes **20**-**23**.

A fluorescence probe **22** containing quinoline and benzimidazole rings[66] was developed to simultaneously recognise Cu^{2+} and Fe^{3+} ions. Free probe gave strong

emission at 508 nm upon excitation at 370 nm. Titration of Cu^{2+} and Fe^{3+} ions with **22** quenched the emission hence green fluorescence became colourless under UV light. The quenching in emission has been reported to occur because of chelation-enhanced fluorescence quenching (CHEQ) effect of paramagnetic Cu^{2+} and Fe^{3+} ions.[67] Ascorbic acid has been reported to distinguish between Cu^{2+} and Fe^{3+} ion by further reduction of **22**-Fe^{3+} to fluorescent **22** and Fe^{2+} while **22**-Cu^{2+} remaining intact. Moreover, the sensor has been used in fluorescence imaging of HeLa cells due to low cytotoxicity of **22**.

Synthesis and metal ion recognition properties of a naphthalimide based fluorescent probe **23** was reported.[68] The probe **23** is weakly fluorescent due to the photoinduced electron transfer from piperazine-N to naphthalimide and became highly fluorescent only in presence of Fe^{3+} ions. Theoretical calculations on **23** and its Fe^{3+} complex supported the Fe^{3+} induced reduction in the PET in probe **23**. Probe **23** has been used for the imaging of intracellular Fe^{3+} ions with its "*turn-on*" fluorescence response.

1.4. Objective of thesis:

Taking inspiration from the literature, an attempt has been made in Chapter 2 of this Thesis to evaluate the "Supramolecular Interactions" in a set of coordination complexes formed by a mono-dentate *N*-substituted imidazole ligand along with co-ligands. Some fluorophores containing quinoline, benzimidazole, napthalimide, benzothiazole, benzoxazole, rhodamine, spirobenzopyran, napthyl moieties were reported in the literature to be useful for the detection of metal ions. They function either as "*turn on*" or "*turn off*" or "ratiometric" sensors towards metal ions. Having used a imidazole moiety, then continued with the use of a 2,4,5-trisubstituted imidazole and some new ligands containing benzothiazole and napthyl moieties were scrutinized as fluorogenic metal ion sensors subsequently, in Chapters 3, 4 and 5.

1.5. Materials and Methods:

1.5.1. Materials:

$CoCl_2 \cdot 6H_2O$, $Co(NO_3)_2 \cdot 6H_2O$, $Co(OAc)_2 \cdot 4H_2O$, $ZnCl_2$, $Mn(OAc)_2 \cdot 4H_2O$, $Zn(NO_3)_2 \cdot 6H_2O$, fumaric acid, anahydrous Na_2SO_4, K_2CO_3, KSCN, $NH_2NH_2 \cdot H_2O$ and $NaBH_4$ were purchased from Merck India. 1-(4-acetylphenyl)imidazole, 2-hydrazinylbenzothiazole, 2,3-dihydroxybenzaldehyde, 4-(diethylamino)-2-hydroxybenzaldehyde, 2–hydroxy–1–naphthaldehyde, 2,6-pyridinedicarboxylic acid, HEPES, $CDCl_3$, DMSO–d_6 and KBr were from M/S Aldrich, USA. All the chemicals and solvents were of reagent grade and were used as received without further purifications.

1.5.2. Instrumentation and Methods:

A Perkin–Elmer Series II CHNS/O Analyzer 2400, and a Lakshore VSM Setup were used for performing relevant measurements. The absorption spectra were recorded with Perkin-Elmer Lambda-750 UV-visible spectrometer using 10 mm path length quartz cuvettes with the wavelength in the range of 250-800 nm. Fluorescence measurements were made on Horiba Fluoromax-4 spectrofluorometer using 10 mm path length quartz cuvettes with a slit width of 5 nm at 298 k with a xenon lamp as excitation source. NMR spectra were recorded using a Varian FT-400 MHz instrument. A FT-IR spectrum was taken using Perkin–Elmer Spectrum One spectrometer.

1.5.3. X-ray Crystallography:

Diffraction data were collected at 292 K with MoKα radiation (λ = 0.71073 Å) using a Bruker Nonius SMART APEX CCD diffractometer equipped with graphite monochromator and Apex CD camera. The SMART software was used for data collection and for indexing the reflections and determining the unit cell parameters. Data reduction and cell refinement were performed using SAINT[69,70] software and the space groups of these crystals were determined from systematic absences by XPREP and further justified by the refinement results. The structures were solved by direct methods and refined by full-matrix least-squares calculations using SHELXTL-97[71] software. All

the non-H atoms were refined in the anisotropic approximation against F^2 of all reflections.

1.5.4. Thermal Measurements:

Thermogravimetry were studied by a computer controlled METTLER TOLEDO STARe system of module TGA/SDTA851e under static nitrogen atmosphere using platinum pan at a heating rate of 10ºC/min in the temperature range 20–800ºC. The instrument was calibrated using RTypSDTA sensor. Onset temperature obtained from DTG curve is used to evaluate the onset decomposition temperature of the samples.

1.5.5. UV-Vis and fluorescence spectral studies:

Stock solutions of metal chlorides (1×10^{-3} mol L^{-1}) were prepared in DMSO and in deionised water. Stock solutions of probes (1×10^{-3} mol L^{-1}) were also prepared in DMSO. The solution of probes was then diluted to 1×10^{-5} mol L^{-1} in DMSO or DMSO/HEPES or MeOH/HEPES solutions. In each titration experiment, 2.50 mL solution of probe (1×10^{-5} mol L^{-1}) were placed in a quartz optical cell with 1 cm optical path length, and then metal chloride stock solutions were gradually added into the optical cell using a micropipette. Spectra were recorded for each addition after waiting for 1 min. In selectivity experiments, the test samples were prepared by adding appropriate volume of stock solution of the cations into solutions probes (2.0 mL of 2×10^{-5} mol L^{-1}). Stock solutions (1×10^{-1} mol L^{-1}) of sodium salts of citrate, lactate and carbonate ions in H_2O:DMSO (*v*/*v*, 2:9) and tetra-butyl ammonium or sodium salts of F^-, Br^-, Cl^-, I^-, SO_4^{2-}, S^{2-}, SCN^-, OH^-, PF_6^-, NO_3^-, HSO_4^-, $H_2PO_4^-$, PO_4^{3-}, $P_2O_7^{4-}$, OAc^-, $S_2O_3^{2-}$, CO_3^{2-}, $C_2O_4^{2-}$, HCO_3^- and ClO_4^- in DMSO or MeOH/HEPES were prepared and used. In the titration experiment, a quartz cell of 1.0 cm path length was filled with a 2.0 mL solution of probes (1×10^{-5} mol L^{-1}) to which 3 equivalents of various anions (0.1 mM) prepared by diluting the stock solutions in DMSO or MeOH/HEPES were added and then titrated with up to 2 equivalents of $ZnCl_2$ using a micropipette.

1.5.6. Calculation of detection limit:

The detection limits were calculated on the basis of fluorescence titrations. The fluorescence emission spectra of probes were repeated for 15/20 times, and the standard deviation of blank measurement was obtained. In order to obtain the slope, the

fluorescence emission was plotted as a concentration of M^{n+}. The detection limits were calculated using the following equation:

$$\text{Detection limit} = 3\sigma/k$$

Where σ is the standard deviation of the blank measurement, and k is the slope between the fluorescence emission intensity *versus* [M^{n+}] (M = metal ions).

1.5.7. Time–resolved fluorescence spectroscopy:

The fluorescence transients were measured by a time correlated single photon counting set up from Horiba. The laser diode 375 or LED 405 was used as a source with excitation wavelength of 375 or 405 nm. The fluorescence decays were fitted using DAS6 software.

1.5.8. Fluorescence Quantum Yield in Solution:

Fluorescence quantum yield was determined in CH_3OH/aqueous HEPES buffer (5 mM, pH = 7.3, 7:3, *v*/*v*) using optically matching solutions of Fluorescein (Φ_r = 0.79 in 0.1M NaOH) as standard at an excitation wavelength of 425 nm. The quantum yield is calculated using the following equation

$$\Phi_s = \Phi_r (A_r F_s / A_s F_r)(\eta_s / \eta)^2$$

Here, A_s and A_r are absorbance value of sample and reference solutions, respectively, at the same excitation wavelength, F_s and F_r are the corresponding relative integrated fluorescence intensities, and η is the refractive index of the solvents.

1.5.9. Computational Methods:

The geometry optimisation were carried out using the density functional theory (DFT/TDDFT) method at the B3LYP level for ligands and its complexes of Al^{3+}, Zn^{2+}, Cd^{2+} ions. The lanl2dz basis set was assigned for all the elements. All calculations were performed with Gaussian09 program[72] with the aid of Gauss View visualization program.

1.5.10. Appendices:

The Chapter appendix has been included at the end of reference section of each Chapter.

References:

1. (a) A. I. Bush, W. H. Pettingell, G. Multhaup, M. D. Paradis, J. P. Vonsattel, J. F. Gusella, K. Beyreuther, C. L. Masters and R. E. Tanzi, *Science*, 1994, **265**, 1464-1467; (b) L. A. Finney and T. V. O'Halloran, *Science*, 2003, **300**, 931-936; (c) J. F. B. Mercer, J. Livingston, B. Hall, J. A. Paynter, C. Begy, S. Chandrasekharappa, P. Lockhart, A. Grimes, M. Bhave, D. Siemieniak and T. W. Glover, *Nature Genetics*, 1993, **3**, 20–25; (d) V. M. Ingram, *Nature*, 1957, **180**, 326–328; (e) F. D. Dunn and K. Dittmer, *Science*, 1950, **111**, 173-175.
2. S. J. Lippard and J. M. Berg, *Principles of Bioinorganic Chemistry*, University Science Books, Mill Valley, CA, 1st ed., 1994.
3. I. Bertini, H. B. Gray, S. J. Lippard and J. S. Valentine, *Bioinorganic Chemistry*, University Science Books, Mill Valley, California, 1st ed., 1994.
4. (a) S. R. Batten and R. Robson, *Angew. Chem., Int. Ed.*, 1998, **37**, 1460-1494; (b) L. Carlucci, G. Ciani and D. M. Proserpio, *Coord. Chem. Rev.*, 2003, **246**, 247-289; (c) A. Harada, A. Hashidzume, H. Yamaguchi and Y. Takashima, *Chem. Rev.*, 2009, **109**, 5974-6023.
5. (a) J. W. Liu, L. F. Chen, H. Cui, J. Y. Zhang, L. Zhang and C. Y. Su, *Chem. Soc. Rev.*, 2014, **43**, 6011-6061; (b) A. Dhakshinamoorthy, A. M. Asiri and H. Garcia, *Chem. Soc. Rev.*, 2015, **44**, 1922-1947.
6. (a) G. Rogez, N. Viart and M. Drillon, *Angew. Chem., Int. Ed.*, 2010, **49**, 1921-1923; (b) M. Clemente-Leon, E. Coronado, C. Marti-Gastaldo and F. M. Romero, *Chem. Soc. Rev.*, 2011, **40**, 473-497.
7. (a) L. E. Kreno, K. Leong, O. K. Farha, M. Allendorf, R. P. V. Duyne and J. T. Hupp, *Chem. Rev.*, 2012, **112**, 1105-1125; (b) X. Sun, Y. Wang and Y. Lei, *Chem. Soc. Rev.*, 2015, **44**, 8019-8061.
8. (a) A. Phan, C. J. Doonan, F. J. Uribe-Romo, C. B. Knobler, M. O'Keeffe and O. M. Yaghi, *Acc. Chem. Res.*, 2010, **43**, 58-67; (b) G. Ferey, C. Serre, T. Devic, G. Maurin, H. Jobic, P. L. Llewellyn, G. De Weireld, A. Vimont, M. Daturi and J. S.

Chang, *Chem. Soc. Rev.*, 2011, **40**, 550-562; (c) Q. Wang, J. Bai, Z. Lu, Y. Pan and X. You, *Chem. Commun.*, 2016, **52**, 443-452.

9. (a) Y. He, B. Li, M. O'Keeffe and B. Chen, *Chem. Soc. Rev.*, 2014, **43**, 5618-5656; (b) M. Eddaoudi, D. F. Sava, J. F. Eubank, K. Adil and V. Guillerm, *Chem. Soc. Rev.*, 2015, **44**, 228-249; (c) Q. Chen, Z. Chang, W. C. Song, H. Song, H. B. Song, T. L. Hu and X. H. Bu, *Angew. Chem., Int. Ed.*, 2013, **52**, 11550-11553.
10. P. Rothemund and A. R. Mennotti, *J. Am. Chem. Soc*., 1941, **63**, 267-270.
11. S.-P. Wu, R.-Y. Huang and K.-J. Du, *Dalton Trans.*, 2009, 4735-4740.
12. (a) O. R. Evans and W. Lin, *Acc. Chem. Res*., 2002, **35**, 511-522; (b) S. Kitagawa, R. Kitaura and S. Noro, *Angew. Chem., Int. Ed*., 2004, **43**, 2334-2375; (c) D. Bradshaw, J. B. Claridge, E. J. Cussen, T. J. Prior and M. Rosseinsky, *J. Acc. Chem. Res*., 2005, **38**, 273-282; (d) C. D. Wu, A. Hu, L. Zhang and W. Lin, *J. Am. Chem. Soc*., 2005, **127**, 8940-8941; (e) J. L. C. Rowsell and O. M. Yaghi, *Angew. Chem., Int. Ed*., 2005, **44**, 4670-4679.
13. J.-M. Lehn, *Angew. Chem., Int. Ed.*, 1988, **27**, 89-112.
14. H. Sigel, A. Saha, N. Saha, P. Carloni, L.E. Kapinos and R. Griesser, *J. Inorg. Biochem.*, 2000, **78**, 129-137.
15. (a) S. S. Block, *Disinfection sterilization and preservation*, 4th ed., Lea & Febiger, Philadelphia, USA, 1991, pp 40; (b) A. D. Russell, W. B. Hugo and G. A. J. Ayliffe, *Principles and practice of disinfection, preservation and sterilization*, 2nd ed., Blackwell Scientific Publications, Oxford, 1992, pp 64.
16. J. M. Lehn, '*Supramolecular Chemistry: Concepts and Perspectives*', ed. VCH, 1995.
17. M. Albrecht, *Chem. Soc. Rev.*, 1998, **27**, 281-287.
18. G. R. Desiraju (1996). Editor. *The Crystal as a Supramolecular Entity in Perspectives in Supramolecular Chemistry*, Vol. 2. New York: John Wiley and Sons.

19. H. J. Schneider and H. Dürr, (1991). Editors. *Frontiers in Supramolecular Organic Chemistry and Photochemistry*. New York: VCH.
20. J. L. Atwood and J. W. Steed, (2004). Editors. *Encyclopedia of Supramolecular Chemistry*. Dekker.
21. J. W. Steed and J. L. Atwood, *Supramolecular Chemistry*, 2nd ed. New York: John Wiley and Sons, 2009.
22. M. J. Hannon and L. J. Childs, *Supramolecular Chemistry*, 2004, **16**, 7-22.
23. (a) G. R. Desiraju, *Chem. Commun.*, 1997, 1475-1482; (b) G. R. Desiraju, *J. Chem. Sci.*, 2010, **122**, 667-675.
24. (a) W. C. Hamilton and J. A. Ibers, *Hydrogen Bonding in Solids: Methods of Molecular Structure Determination*, W. A. Benjamin, 1968; (b) G. A. Jeffrey and W. Saenger, *Hydrogen Bonding in Biological Structures*, Springer-Verlag, 1991; (c) T. S. Moore and T. F. Winmill, *J. Chem. Soc., Trans.*, 1912, **101**, 1635–1676; (d) W. M. Latimer and W. H. Rodebush, *J. Am. Chem. Soc.*, 1920, **42**, 1419–1433; (e) L. Pauling, *The Nature of the Chemical Bond and the Structure of Molecules and Crystals: An Introduction to Modern Structural Chemistry*, Cornell University Press, 1939; (f) E. Arunan, G. R. Desiraju, R. A. Klein, J. Sadlej, S. Scheiner, I. Alkorta, D. C. Clary, R. H. Crabtree, J. J. Dannenberg, P. Hobza, H. G. Kjaergaard, A. C. Legon, B. Mennucci and D. J. Nesbitt, *Pure Appl. Chem.*, 2011, **83**, 1619–1636.
25. M. C. R. Symons, *Nature*, 1972, **239**, 257–259.
26. (a) L. Pauling and R. B. Corey, *J. Am. Chem. Soc.*, 1950, **72**, 5349; (b) G. R. Desiraju, *Acc. Chem. Res.*, 1996, **29**, 441–449.
27. A. El-ghayoury, E. Peeters, A. P. H. J. Schenning and E. W. Meijer, *Chem. Commun.*, 2000, 1969–1970.
28. (a) T. W. Bell and Z. Hou, *Angew. Chem., Int. Ed.*, 1997, **36**, 1536–1538; (b) S. K. Chang, D. Van Engen, E. Fan and A. D. Hamilton, *J. Am. Chem. Soc.*, 1991, **113**, 7640–7645.
29. (a) J. Rebek, Jr., *Chem. Soc. Rev.*, 1996, **25**, 255–264; (b) M. M. Conn and J. Rebek, Jr., *Chem. Rev.*, 1997, **97**, 1647–1668; (c) F. Hof, S. L. Craig, C. Nuckolls and J. Rebek, Jr., *Angew. Chem., Int. Ed.*, 2002, **41**, 1488–1508.

30. D. T. Bong, T. D. Clark, J. R.Granja and M. R. Ghadiri, *Angew. Chem., Int. Ed.*, 2001, **40**, 988–1011.
31. (a) M. C. Etter, *Acc. Chem. Res.*, 1990, **23**, 120–126; (b) M. C. Etter, J. M. MacDonald and J. Bernstein, *Acta Crystallogr., Sect. B*, 1990, **46**, 256–262. (c) J. Bernstein, L. Shimoni, R. E. Davis and N.-L.Chang, *Angew. Chem., Int. Ed. Engl.*, 1995, **34**, 1555–1573.
32. D. Sadhukhan, A. Ray, G. Pilet, C. Rizzoli, G. M. Rosair, C. J. Gómez-García, S. Signorella, S. Bellú, and S. Mitra, *Inorg. Chem.*, 2011, **50**, 8326–8339.
33. D. Sadhukhan, M. Maiti, G. Pilet, A. Bauzá, A. Frontera and S. Mitra, *Eur. J. Inorg. Chem.*, 2015, 1958–1972.
34. (a) M. Mitra, P. Manna, S. K. Seth, A. Das, J. Meredith, M. Helliwell, A. Bauzá, S. Ray Choudhury, A. Frontera and S. Mukhopadhyay, *CrystEngComm.*, 2013, **15**, 686–696; (b) S. Sanda, S. Biswas and S. Konar, *Inorg. Chem.*, 2015, **54**, 1218−1222; (c) H. R. Khavasi and B. M. M. Sadegh, *Dalton Trans.*, 2015, **44**, 5488–5502; (d) N. Dwivedi, S. K. Panja, Monika, S. Saha and S. S. Sunkari, *Dalton Trans.*, 2016, **45**, 12053–12068.
35. R. Martínez-Máñez and F. Sancenón, *Chem. Rev*., 2003, **103**, 4419.
36. R. Bissell, A. P. de Silva, P. H. Q. N. Gunaratne, P. L. M. Lynch, G. E. M. Maguire and K. R. A. S. Sandanayake, *Chem. Soc. Rev*., 1992, 187-195.
37. S. L. Wiskur, H. Aït-Haddou, J. J. Lavigne and E. V. Anslyn, *Acc. Chem. Res.*, 2001, **34**, 963-972.
38. J. F. callan, A. P. De Silva and D. C. Magri, *Tetrahedron*, 2005, **61**, 8551-8588.
39. H. N. Kim, M. H. Lee, H. J. Kim, J. S. Kim and J. Yoon, *Chem. Soc. Rev.*, 2008, **37**, 1465-1472.
40. C. Lodeiro and F. Pina, *Coord. Chem. Rev.*, 2009, **253**, 1353-1383.
41. G. Accorsi, A. Listorti, K. Yoosaf, and N. Armaroli, *Chem. Soc. Rev.*, 2009, **38**, 1690-1700.
42. R. Martínez-Máñez and F. Sancenón, *Chem. Rev.*, 2003, **103**, 4419-4476.
43. T. Gunnlaugsson, H. D. Paduka, M. Glynn, P. E. kruger, G. M. hussey, F. M. Pfeffer, C. M. Dos Santos and J. Tierney, *J. Fluoresc*., 2005, **15**, 287-299.

44. E. J. O'Neil and B. D. Smith, *Coord. Chem. Rev.*, 2006, **250**, 3068-3080.
45. V. Amendola and L. Fabbrizzi, *Chem. Commun.*, 2009, 513-531.
46. L. Prodi, *New J. Chem.*, 2005, **29**, 20-31.
47. X. Tian, X. Guo, F. Yu and L. Jia, *Sens. .Actuators, B*, 2016, **232**, 181–187.
48. J. Wang, Y. Li, E. Duah, S. Paruchuri, D. Zhou and Y. Pang, *J. Mater. Chem. B*, 2014, **2**, 2008-2012.
49. S. Nandi and D. Das, *ACS Sens.*, 2016, **1**, 81−87.
50. S. Sinha, B. Chowdhury and P. Ghosh, *Inorg. Chem.*, 2016, **55**, 9212−9220.
51. S. Paul, A. Manna and S. Goswami, *RSC Adv.*, 2013, **3**, 10639–10643.
52. S. Chithiraikumar, C. Balakrishnan and M. A. Neelakantan, *Sens. Actuators, B*, 2017, **249**, 235–245.
53. Z. Liu, C. Zhang, W. He, Z. Yang, X. Gao and Z. Guo, *Chem. Commun.*, 2010, **46**, 6138–6140.
54. Y. Gao, H. Liu, Q. Liu and W. Wang, *Tetrahedron Lett.*, 2016, **57**, 1852–1855.
55. M. Shellaiah, T. Simon, V. Srinivasadesikan, C. M. Lin, K. W. Sun, F. H. Ko, M. C. Lin and H. C. Lin, *J. Mater. Chem. C*, 2016, **4**, 2056-2071.
56. C. Fan, X. Huang, C. A. Black, X. Shen, J. Qi, Y. Yi, Z. Lu, Y. Ni and G. Sun, *RSC Adv.*, 2015, **5**, 70302-70308.
57. J. Zhang, L. Zhang, Y. Wei, J. Chao, S. Wang, S. Shuang, Z. Cai and C. Dong, *Anal. Methods*, 2013, **5**, 5549–5554.
58. B. Zhao, T. Liu, Y. Fang, L. Wang, B. Song and Q. Deng, *Tetrahedron Lett.*, 2016, **57**, 4417–4423.
59. S. Goswami, D. Sen and N. K. Das, *Org. Lett.*, 2010, **12**, 856-859.
60. S. Sahana, G. Mishra, S. Sivakumar and P. K. Bharadwaj, *Dalton Trans.*, 2015, **44**, 20139–20146.
61. K. M. Vengaian, C. D. Britto, K. Sekar, G. Sivaraman and S. Singaravadivel, *RSC Adv.*, 2016, **6**, 7668–7673.
62. S. Goswami, A. K. Das, A. K. Maity, A. Manna, K. Aich, S. Maity, P. Saha and T. K. Mandal, *Dalton Trans.*, 2014, **43**, 231–239.

63. (a) S. Aoki, D. Kagata, M. Shiro, K. Takeda and E. Kimura, *J. Am. Chem. Soc.*, 2004, **126**, 13377-13390; (b) R. Badugu, J. R. Lakowicz and C. D. Geddess, *J. Am. Chem. Soc.*, 2005, **127**, 3635-3641.
64. R. Alam, T. Mistri, A. Katarkar, K. Chaudhuri, S. K. Mandal, A. R. K. Bukhsh, K. K. Das and M. Ali, *Analyst*, 2014, **139**, 4022–4030.
65. (a) P. Ashokkumar, V. T. Ramakrishnan and P. Ramamurthy, *J. Phys. Chem. A*, 2011, **115**, 14292–14299; (b) T. Mistri, M. Dolai, D. Chakraborty, A. R. Khuda-Bukhsh, K. K. Das and M. Ali, *Org. Biomol. Chem.*, 2012, **10**, 2380–2384; (c) T. Mistri, R. Alam, M. Dolai, S. K. Mandal, A. R. K. Bukhsh and M. Ali, *Org. Biomol. Chem.*, 2013, **11**, 1563–1569.
66. B. Zhang, H. Liu, F. Wu, G. Hao, Y. Chen, C. Tan, Y. Tan, and Y. Jiang, *Sens. Actuators, B*, 2017, **243**, 765–774.
67. J. P. Holland, P. J. Barnard, S. R. Bayly, H. M. Betts, G. C. Churchill and J. R. Dilworth, *Eur. J. Inorg. Chem.*, 2008, **12,** 1985–1993.
68. N. R. Chereddy, M. V. N. Raju, P. Nagaraju, V. R. Krishnaswamy, P. S.Korrapati, P. R. Bangal and V. J. Rao, *Analyst*, 2014, **139**, 6352-6356.
69. G. M. Sheldrick, SADABS, 1996, based on the method described in: R. H. Blessing, *Acta Crystallogr.* 1995, **A51**, 33–38.
70. SMART and SAINT, Siemens Analytical X-ray Instruments Inc., Madison, WI, 1996.
71. G. M. Sheldrick, *Acta Crystallogr.*, 2008, **A64**, 112–122.
72. M. J. Frisch, , G. W. Trucks, H. B. Schlegel, G. E. Scuseria, M. A. Robb, J. R. Cheeseman, G. Scalmani, V. Barone, B. Mennucci, G. A. Petersson, H. Nakatsuji, M. Caricato, X. Li, H. P. Hratchian, A. F. Izmaylov, J. Bloino, G. Zheng, J. L. Sonnenberg, M. Hada, M. Ehara, K. Toyota, R. Fukuda, J. Hasegawa, M. Ishida, T. Nakajima, Y. Honda, O. Kitao, H. Nakai, T. Vreven, J. A. Montgomery, Jr., J. E. Peralta, F. Ogliaro, M. Bearpark, J. J. Heyd, E. Brothers, K. N. Kudin, V. N. Staroverov, R. Kobayashi, J. Normand, K. Raghavachari, A. Rendell, J. C. Burant, S. S. Iyengar, J. Tomasi, M. Cossi, N. Rega, J. M. Millam, M. Klene, J. E. Knox, J. B. Cross, V. Bakken, C. Adamo, J. Jaramillo, R. Gomperts, R. E. Stratmann, O.

Yazyev, A. J. Austin, R. Cammi, C. Pomelli, J. W. Ochterski, R. L. Martin, K. Morokuma, V. G. Zakrzewski, G. A. Voth, P. Salvador, J. J. Dannenberg, S. Dapprich, A. D. Daniels, Ö. Farkas, J. B. Foresman, J. V. Ortiz, J. Cioslowski, and D. J. Fox, Gaussian 09, Revision D.01, Gaussian, Inc., Wallingford CT, 2009.

Chapter 2

Molecular Structures of Some Bivalent Metal Complexes of 1-(4-Acetylphenyl)imidazole and Co-Ligands

Abstract:

In this Chapter, a series of bivalent metal complexes having compositions $[Co(\mathbf{L})_2Cl_2]$(**1**), $[Zn(\mathbf{L})_2Cl_2]$(**2**), $[Co(\mathbf{L})_2(H_2O)_4](NO_3)_2{\cdot}2H_2O$(**3**), $[Zn(\mathbf{L})_2(H_2O)_4](NO_3)_2{\cdot}2H_2O$(**4**), $[Co(\mathbf{L})_2(OAc)_2(H_2O)]{\cdot}3H_2O$ (**5**), $[Mn(\mathbf{L})_2(OAc)_2(H_2O)]{\cdot}3H_2O$ (**6**) $[Co(\mathbf{L})_4(NCS)_2]$(**7**), $\{[Co(\mathbf{L})_2(\mathbf{Fum})(H_2O)_2]{\cdot}2H_2O\}_n$ (**8**) and $\{[Mn(\mathbf{L})_2(\mathbf{Fum})]\}_n$ (**9**) were synthesized using **L** {**L** = 1-(4-acetylphenyl)imidazole} and respective co-ligands. The mononuclear sets **1**–**2**, **3**–**4** and **5**–**6** are isomorphous and isostructural in nature. Complex **7** is a mononuclear complex, **8** is a 1D coordination polymer and **9** is a 2D-coordination polymer. All the compounds were structurally characterized using IR spectroscopy, thermogravimetric analyses, powder X-ray and single crystal X-ray diffraction studies. In general, coordinated / lattice water molecules are found to be involved in O–H···O hydrogen bonding and counter ions, in other weak interactions like C–H···S, C–H···Cl and C–H···O. The aromatic ring of **L** also is involved in C–H···π and π···π stacking interactions. In **3** and **4**, hydrogen bonding interactions between coordinated water molecules, lattice water and nitrate ion contain cyclic hydrogen-bonded architectures. In **5** and **6,** acetyl group present in **L** act as hydrogen bond acceptor through O···H–O interaction. In **8** and **9 Fum** coordinate to metal center in μ-η^1:η^1 bidentate and μ_4-η^1:η^1:η^1:η^1 tetradentate fashions resulting in formation of 1D and 2D coordination polymers, respectively.

2.1. Introduction:

Design and synthesis of transition metal complexes with structural features have attracted much attention due to not only to their intriguing architectures and topologies but also to their potential applications as important functional materials in the fields of magnetism,[1] sensors,[2] adsorption,[3] catalysis,[4] and ion-exchange.[2d, 5] The assemblies of metal complexes are not only governed by strong and highly directional coordination bonds but also directed by various weak non-covalent forces such as hydrogen bonding, π···π, C-H···π *etc*.[6] From last decade, imidazole based metal complexes have attracted much attention because of their versatile coordination binding modes of the both N-atoms in imidazole ring. Both N atoms play an important role in hydrogen bond donor and acceptor properties as well as in making complexes with various dimensionalities.[7] Among substituted imidazole ligands, 1-imidazolyl or 4-imidazolyl moieties have been intensively utilized.[8] However, design and synthesis of imidazole based ligands are still a challenging field. It is well known that the imidazole moiety plays an important role in biological systems. Imidazole based metal complexes pose diverse range of pharmacological activity such as antibacterial, antifungal, as well as antitumor effects.[9a] Recently, Song *et al*.[9b] reported a series of transition metal complexes of 4-imidazolecarboxylate ligand and their structural diversities, luminescence, and gas adsorption properties. In this study, six new mononuclear isomorphs and isostructural complexes, a mononuclear complex and two coordination polymers of bivalent metal ions were successfully synthesized using the *N*-substituted imidazole, 1-(4-acetylphenyl)imidazole and other coligands.

2.2. Experimental Section:

2.2.1. Synthesis of 1-9:

2.2.1.1. $[Co(L)_2Cl_2]$ (1):

To a methanolic (25 mL) solution of **L** (186 mg, 1 mmol), solid $CoCl_2·6H_2O$ (120 mg, 0.5 mmol) was added and stirred overnight. The reaction mixture was filtered and filtrate was kept for crystallization. Block shaped blue colored crystals, suitable for SXRD, were obtained after 10 days. Crystals were collected and washed with ice-cold

methanol. Yield 200 mg, (80%). Anal. calcd. for $C_{22}H_{20}Cl_2N_4O_2Co$: C, 52.61; H, 4.01; N, 11.15% Found: C, 52.41; H, 3.95; N, 11.04%. IR (KBr, cm^{-1}): 3168(w), 3124(m), 2913(w), 1674(vs), 1606(s), 1520(s), 1499(m), 1422(m), 1376(s), 1331(m), 1305(m), 1273(m), 1262(w), 1242(m), 1187(w), 1125(m), 1109(m), 1081(w), 1064(s), 1018(w), 963(m), 840(s), 746(s), 654(m), 618(m), 597(m). UV-Vis [λ_{max}, nm (ε, $M^{-1}cm^{-1}$) DMSO solution]: 670(114); 284(27910). μ_{eff}, 4.01 B.M.

2.2.1.2. [Zn(L)$_2$Cl$_2$](2):

Complex **2** was prepared as described for complex **1** by using $ZnCl_2$ (70 mg, 0.5 mmol) instead of $CoCl_2 \cdot 6H_2O$. The block shaped crystals were obtained after two weeks. Yield 190 mg (75%). Anal. calcd. for $C_{22}H_{20}Cl_2N_4O_2Zn$: C, 51.94; H, 3.96; N, 11.01% Found: C, 51.80; H, 3.88; N, 10.92%. IR (KBr, cm^{-1}): 3429(br), 3168(w), 3124(w), 1674(vs), 1606(s), 1521(s), 1499(w), 1425(w), 1358(m), 1331(w), 1305(m), 1273(m), 1244(m), 1187(w), 1127(m), 1109(w), 963(m), 946(w), 841(m), 747(m), 655(m), 619(w). UV-Vis [λ_{max}, nm (ε, $M^{-1}cm^{-1}$) DMSO solution]: 279(28725).

2.2.1.3. [Co(L)$_2$(H$_2$O)$_4$](NO$_3$)$_2$·2H$_2$O (3):

Cobalt nitrate hexahydrate (310 mg, 1.07 mmol) and **L** (400 mg, 2.15 mmol) were dissolved in methanol (50 mL) and stirred overnight. Then the pink colored solution was filtered and kept for crystallization. The block shaped crystals were obtained after two weeks. Yield 540 mg (78%). Anal. calcd. for $C_{22}H_{32}N_6O_{14}Co$: C, 39.83; H, 4.86; N, 12.67% Found: C, 39.75; H, 4.81; N, 12.59%. IR (KBr, cm^{-1}): 3430 (b), 3123(w), 2923(w), 1674(s), 1606(m), 1520(m), 1499(w), 1384(vs), 1330(w), 1305(w), 1272(w), 1242(w), 1187(w), 1125(w), 1063(m), 963(w), 839(m), 743(m), 654(m). UV-Vis [λ_{max}, nm (ε, $M^{-1}cm^{-1}$) DMSO solution]: 535(14); 280(39765). μ_{eff}, 4.50 B.M.

2.2.1.4. [Zn(L)$_2$(H$_2$O)$_4$](NO$_3$)$_2$·2H$_2$O (4):

Complex **4** was obtained by the same procedure as described as in complex **3**, except that $Zn(NO_3)_2 \cdot 6H_2O$ (320 mg, 1.07 mmol) was added to the methanolic solution. Yield 575 mg, (80%). Anal. calcd. for $C_{22}H_{32}N_6O_{14}Zn$: C, 39.44; H, 4.81; N, 12.55% Found: C 39.30; H 4.78; N 12.44%. IR (KBr, cm^{-1}): 3460(br), 3167(w), 3123(w), 2923(w), 1674(vs), 1606(m), 1521(m), 1499(w), 1477(w), 1384(vs), 1358(w), 1305(m),

1272(m), 1244(m), 1187(w), 1127(m), 1109(w), 1064(m), 1081(m), 839(m), 745(m), 654(m). UV-Vis [λ_{max}, nm (ε, $M^{-1}cm^{-1}$) DMSO solution]: 281(55700).

2.2.1.5. [Co(L)$_2$(OAc)$_2$(H$_2$O)]·3H$_2$O (5) and [Mn(L)$_2$(OAc)$_2$(H$_2$O)]·3H$_2$O (6):

Complexes **5** and **6** were also obtained by the same procedure as described as in complex **3**, except that $Co(OAc)_2·4H_2O$ (270 mg, 1.07 mmol) and $Mn(OAc)_2·4H_2O$ (260 mg, 1.07 mmol) and using **L** (400 mg, 2.15 mmol). (Yield = 465 mg, 70% for **5** and 300 mg, 45% for **6**). For complex **5**: Anal. calcd. for $C_{26}H_{34}N_4O_{10}Co$: C, 50.25; H, 5.51; N, 9.01% Found: C, 50.17; H, 5.46; N, 8.95%. IR (KBr, cm^{-1}): 3400(br), 3142(w), 3129(w), 2923(w), 1682(vs), 1608(s), 1579(w), 1525(m), 1425(m), 1367(w), 1334(w), 1309(w), 1265(m), 1248(m), 1193(w), 1119(m), 1068(m), 1022(w), 965(m), 939(w), 844(m), 800(w), 748(m), 658(m), 617(w), 596(m). UV-Vis [λ_{max}, nm (ε, $M^{-1}cm^{-1}$) DMSO solution]: 549(102); 281(15940). μ_{eff}, 5.19 B.M. For complex **6**: Anal. calcd. for $C_{26}H_{34}N_4O_{10}Mn$: C, 50.57; H, 5.55; N, 9.07% Found: C, 50.52; H, 5.46; N, 9.01%. IR (KBr, cm^{-1}): 3412(br), 3140(w), 2923(w), 1682(vs), 1608(s), 1573(m), 1525(m), 1448(w), 1423(m), 1384(w), 1367(w), 1333(w), 1307(w), 1266(w), 1248(m), 1119(m), 1067(m), 965(m), 933(w), 842(m), 748(m), 656(m), 616(w), 596(m). UV-Vis [λ_{max}, nm (ε, $M^{-1}cm^{-1}$) DMSO solution]: 284(29785). μ_{eff}, 6.18 B.M.

2.2.1.6. [Co(L)$_4$(NCS)$_2$] (7):

Ligand **L** (250 mg, 1.344 mmol) and $CoCl_2·6H_2O$ (80 mg, 0.34 mmol) were dissolved in methanol (20 mL) and stirred for 5h. Then KSCN (130 mg, 0.67 mmol) was added and stirred for another 3h. The solution was concentrated and the precipitate was dissolved in minimum amount of hot DMF and left undisturbed. Brown colour crystals suitable for SXRD were obtained after 10 days (Yield = 200 mg, 64%). Anal. calcd. for $C_{46}H_{40}CoN_{10}O_4S_2$: C, 60.06; H, 4.38; N, 15.23% Found: C, 60.01; H, 4.33; N, 15.16%. IR (KBr, cm^{-1}): 3129(m), 2923(m), 2854(w), 2075(vs), 1690(vs), 1604(s), 1516(s), 1492(m), 1420(w), 1372(w), 1356(w), 1304(m), 1273(w), 1259(w), 1249(w), 1114(w), 1056(m), 956(m), 931(w), 847(w), 657(m), 596(w). UV-Vis [λ_{max}, nm (ε, $M^{-1}cm^{-1}$) DMSO solution]: 660(101); 284(33370). μ_{eff}, 4.80 B.M.

2.2.1.7. {[Co(L)$_2$(Fum)(H$_2$O)$_2$]·2H$_2$O}$_n$ (8):

Ligand **L** (200 mg, 1.07 mmol) was dissolved in methanol and $CoCl_2 \cdot 6H_2O$ (130 mg, 0.55 mmol) was added then stirred for 5 h. Fumaric acid (125 mg, 1.07 mmol) was added to the reaction mixture and stirred for additional 3 h. The solution was concentrated and the precipitate was dissolved in minimum amount of hot DMF left undisturbed for crystallization. The crystals obtained after 10 days were collected and used for further studies. (Yield = 260 mg, 77%). Anal. calcd. for $C_{26}H_{28}N_4O_{10}Co$: C, 50.54; H, 4.59; N, 9.10% Found: C, 50.48; H, 4.54; N, 9.02%. IR (KBr, cm^{-1}): 3424(br), 3129(w), 3112(w), 1677(vs), 1652(w), 1605(s), 1522(m), 1492(m), 1420(w), 1365(w), 1333(w), 1315(w), 1255(m), 1192(w), 1063(m), 994(m), 961(m), 845(w),832(m), 770(m), 786(w), 657(w), 590(w). UV-Vis [λ_{max}, nm (ε, $M^{-1}cm^{-1}$) DMSO solution]: 284(36370).

2.2.1.8. {[Mn(L)$_2$(Fum)]}$_n$ (9):

Complex **9** was obtained by the same procedure as described as in complex **8**, by using $Mn(OAc)_2 \cdot 4H_2O$ (130 mg, 0.55 mmol). (Yield = 180 mg, 60%). Anal. calcd. for $C_{26}H_{22}N_4O_6Mn$: C, 57.68; H, 4.10; N, 10.35% Found: C, 57.49; H, 4.02; N, 10.28%. IR (KBr, cm^{-1}): 3429(br), 3127(w), 3106(w), 1678(vs), 1634(w), 1665(s),1522(w), 1492(w),1420(w), 1365(w), 1332(w), 1314(w), 1281(w), 1259(m), 1191(m), 1110(w), 1062(m), 983(w), 960(w), 832(w), 770(w), 589(w). UV-Vis [λ_{max}, nm (ε, $M^{-1}cm^{-1}$) DMSO solution]: 284(32760).

2.3. Results and discussions:

2.3.1. Synthesis and spectra:

Imidazole moiety is known to coordinate through nitrogen and allowing NH arm to involve in supramolecular interactions as a hydrogen bond donor. Here we have utilised the ligand **L** in which proton of NH has been substituted with a 4-acetylphenyl group and synthesised its coordination complexes along with some co-ligands. As 4-acetylphenyl substitution has blocked the hydrogen bond donor ability, thus has allowed evaluating the supramolecular interaction arising from the co-ligands as well as from the acetyl group. In the context, mononuclear isomorphs and isostructural complexes (**1-6**),

mononuclear complexes (**7**) and coordination polymer (**8-9**) were synthesised (Scheme 1) by controlling the ratio of **L** ligand as well as the selection of reaction conditions such as reaction temperature, solvent systems, counter ions and co-ligand such as aliphatic dicarboxylic acid (Fumaric acid). These complexes **1**–**9** crystallised readily as single crystals, thus allowing the determination of their structures.

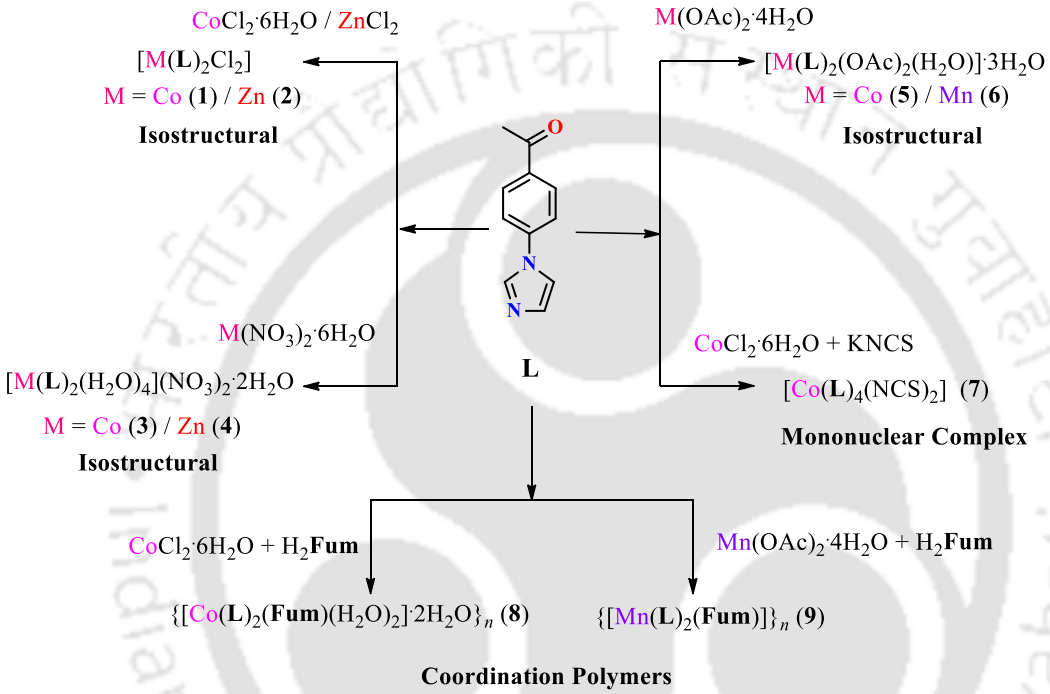

Scheme 1. Synthesis of **1**–**9**.

The electronic spectra of the complexes **1**–**9** have been recorded in DMSO (Figure A1). Higher energy band around 280-285 nm has been observed in all the nine complexes which corresponds to the allowed π→π* intra-ligand transition. Lower energy band observed in the visible region around 670, 535, 550 and 660 nm, respectively for complexes **1**, **3**, **5** and **7** are of *d-d* transition in origin. The quantitative spectrum of **8** in the visible region could not be recorded due to its poor solubility in DMSO and other common solvents. Both **6** and **9**, having high-spin manganese(II) center, did not exhibit appreciable absorption in the visible region as there are no spin allowed *d-d* transitions in them. The IR spectra of the complexes show strong peaks around 1680 cm^{-1} and 1605 cm^{-1} which respectively correspond to ν_{CO} and aromatic ν_{CN} stretching vibrations. In addition, other characteristic peaks found are: ~1384 cm^{-1} (for ν_{NO} of NO_3^-) in **3**–**4**,

1572-1579 cm^{-1} (for ν_{CO} of OAc^-) in **5**–**6**, ~2075 cm^{-1} (for ν_{NC} of NCS^-) in **7**, 1651 cm^{-1} (for ν_{CO} of **Fum**) in **8**, 1633 cm^{-1} (for ν_{CO} of **Fum**) in **9**. The 28 cm^{-1} difference in ν_{CO} of **Fum** is in agreement with μ-η^1:η^1 and μ_4-η^1:η^1:η^1:η^1 modes of binding in **8** and **9**, respectively.

2.3.2. Molecular Structures:

2.3.2.1. $[Co(L)_2Cl_2]$ (1) and $[Zn(L)_2Cl_2]$ (2):

Both **1** and **2** crystallized in the space group *Pnma* (Table 1) and the asymmetric unit contains half molecule of the coordination complex. Ligand **L** expectedly behaves as monodentate ligand by coordinating through nitrogen atom of imidazole moiety to the central metal ion along with two chloride ions. As a result, the bivalent metal ion has distorted tetrahedral coordination geometry having N_2Cl_2 environments with a plane of symmetry passing through MCl_2 unit. A schematic view of **1** is shown in Figure 1 as a representative and **2** in Figure A2.

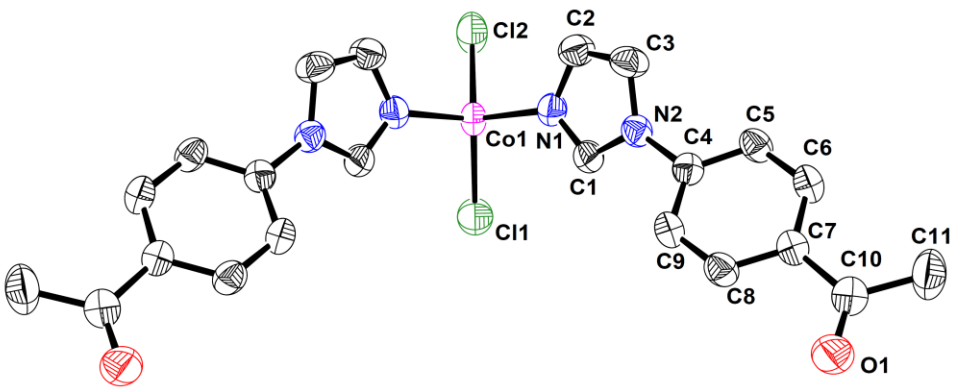

Figure 1. ORTEP diagram (50% probability) of **1** (all hydrogen atoms are omitted for clarity). Selected bond lengths (Å) and angles (º): Co1–N1, 2.015(2); Co1–Cl1, 2.237(1); Co1–Cl2, 2.251(1); N1–Co1–N1′, 104.36(12); N1–Co1–Cl1, 107.97(6); N1–Co1–Cl2, 106.48(6); Cl1–Co1–Cl2, 122.23(5).

The Co–N_I and Zn–N_I bond lengths {imidazole-N = N_I; thiocyanate-N = N_T; water-O = O_W; acetate-O = O_A; fumarate-O = O_F} do not show much deviation. Among the two Co–Cl and Zn–Cl bond distances in each molecule, one of it is nearly same in both, while second is longer in **1**, by 0.0510(11) Å. The angles at the metal center are close to

tetrahedral values with small deviations. The bond parameters found in **2** are comparable to those in other Zn(II) imidazole complexes.[10]

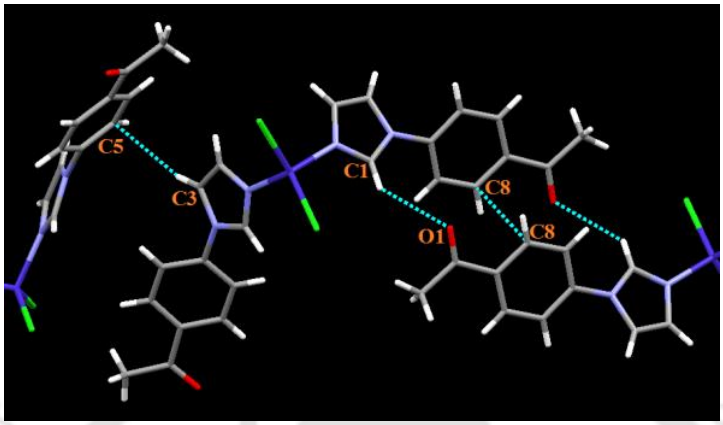

Figure 2. C–H···O, C–H···π and π···π interactions in **1**.

The pattern and types of inter-molecular interactions present in **1** and **2** are identical as well as the non-bonded distances being nearly same, hence such interactions observed in **1** are elaborated here. The O-atom of carbonyl group form hydrogen bond of the type O···H–C (O1···C1, 3.433(3) Å; O1···C3, 3.324(3) Å) of imidazole moiety and the phenyl ring (O1···C5, 3.268(3) Å). Apart from this, hydrogen atom (C3–H3) of imidazole ring interacts with benzene ring of **L** to form inter-molecular C–H···π (C3···C5, ~3.58 Å) interaction (Figure 2).

Thus the mononuclear units of **1** are linked together by this set of charge-assisted hydrogen bonds to *zig-zag* structures. The benzene rings of **L** are further connected by π···π interactions between C8···C8 with distance 3.393(3) Å (3.397(5) Å in **2**), thus constructing a 3D supramolecular architecture as shown in Figure 3. In addition, centro-symmetric C–H···Cl interaction between an H-atom of phenyl ring and the coordinated chlorine is present having the non-bonded C9···Cl2 distance of ~3.78 Å (Figure 4).

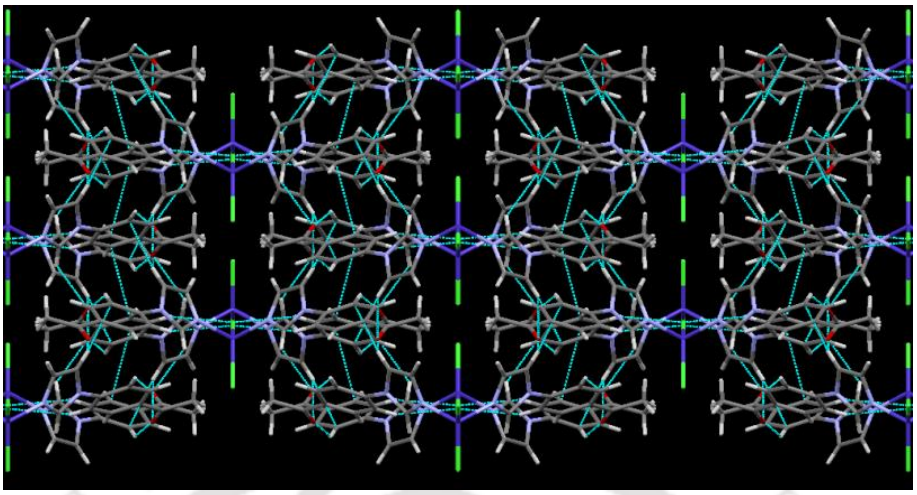

Figure 3. Packing diagram upon viewing down *a*-axis of **1**.

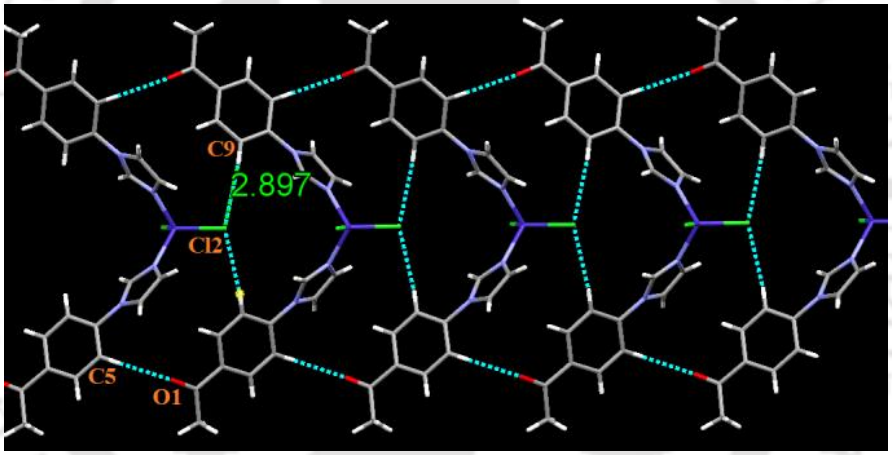

Figure 4. C–H···O, C–H···Cl interaction in **1**.

2.3.2.2. $[Co(L)_2(H_2O)_4](NO_3)_2{\cdot}2H_2O$ (3) and $[Zn(L)_2(H_2O)_4](NO_3)_2{\cdot}2H_2O$ (4):

Complexes **3** and **4** crystallized in $P2_1/c$ space group with similar cell parameters (Table 1 and 2), and the results of X-ray crystallographic analysis indicate that they are isomorphous and isostructural. The reaction of two equivalents of **L** with $M(NO_3)_2{\cdot}6H_2O$ {M = Co, Zn}, resulted in the formation of complex of composition $[M(\mathbf{L})_2(H_2O)_4](NO_3)_2{\cdot}2H_2O$. The asymmetric unit has half of complex ion with M(II) ion sitting at the center of symmetry, one each of nitrate ion and water molecule. The bivalent metal ion is bound by two **L** ligands and four water molecules, having *trans*-$(N_I)_2(O_W)_4$ coordination environment. The bond distances at the cobalt lie in the range 2.094(5)–2.155(5) Å consistent with the high-spin nature of the bivalent cobalt.[11] The

bond length orders Co–O2 < Co–N1 < Co–O3 and Zn–N1 < Zn–O2 < Zn–O3 were observable and the difference within M(II)–O_W distances may be due to Jahn Teller distortions.[12] A schematic view of **3** is shown in Figure 5 as a representative and **4** in

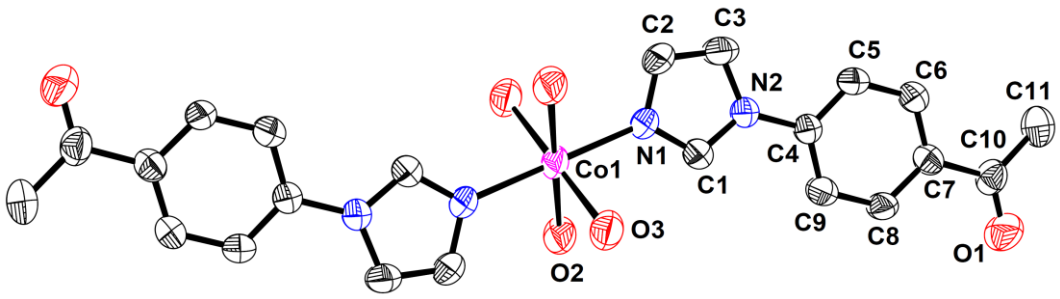

Figure 5. ORTEP diagram (50% probability) of **3** (all hydrogen atoms are omitted for clarity). Selected bond lengths (Å) and angles (º): Co1–O2, 2.094(5); Co1–O3, 2.155(5); Co1–N1, 2.104(6); O2–Co1–O3, 87.5(2); O2–Co1–O3, 92.5(2); O2–Co1–N1, 91.7(2); O2–Co1–N1, 88.3(2); O2–Co1–O2, 180.00(1);O3–Co1–O3, 180.00(1); N1–Co1–N1, 180.00(1); N1–Co1–O3, 89.9(2); N1–Co1–O3, 90.1(2).

Figure A3. The pattern and types of inter-molecular interactions present in **3** and **4** are identical as well as the non-bonded distances being nearly same, hence such interactions observed in **4** are elaborated here. From the crystal structure, it is observed that hydrogen bonding interaction is dominant of all the inter-molecular interactions. The carbonyl oxygen of the acetyl group is inter-molecularly hydrogen bonded to the coordinated water molecule having the non-bonded contact O1···O2, 2.816(9) Å (Figure 6 and 7). This makes two aromatic rings slipped away but closer together to have π-stacking interactions within the calculated distance of ~3.56 Å between the two planes formed by ring containing C4,C5,C6,C7,C8,C9 atoms. The O2 of coordinated water molecule is hydrogen bonded to nitrate oxygen with non-bonded distances O2···O4, 2.93(1) and O2···O5, 2.901(9) Å which has a cyclic $R^2_1(4)$ architecture and lead to a chain-like structure. Same architecture is also present as the lattice water interacts with the nitrate oxygen through interactions O7···O6, 2.968(9) and O7···O5, 3.03(1) Å, but this is a cross-linked two chain-like structures. Other two hydrogen bond present involving lattice water and coordinated water are O7···O6, 2.93(1) and O7···O3, 2.780(8) Å. Overall, hydrogen bonding interactions involving coordinated water molecules, lattice water and

nitrate ion contain cyclic hydrogen-bonded architectures $R^2_2(5)$ and $R^2_3(6)$ as shown in Figure 8. The π-stacking and hydrogen-bonded interactions are inter-twined infinitely along the *c*-axis that cross at the metal center, thus form a doubled stranded chains as shown in Figure 6.

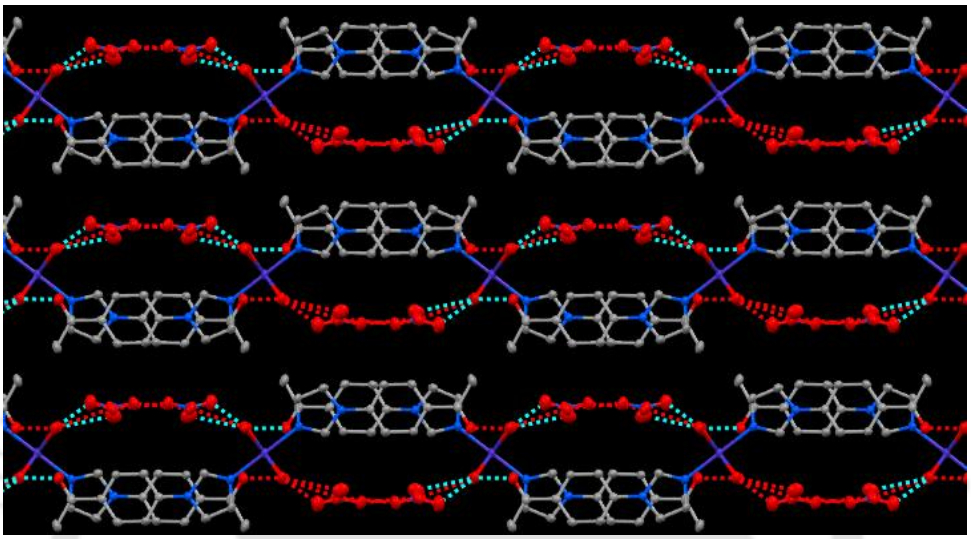

Figure 6. Doubled stranded chains in **3**.

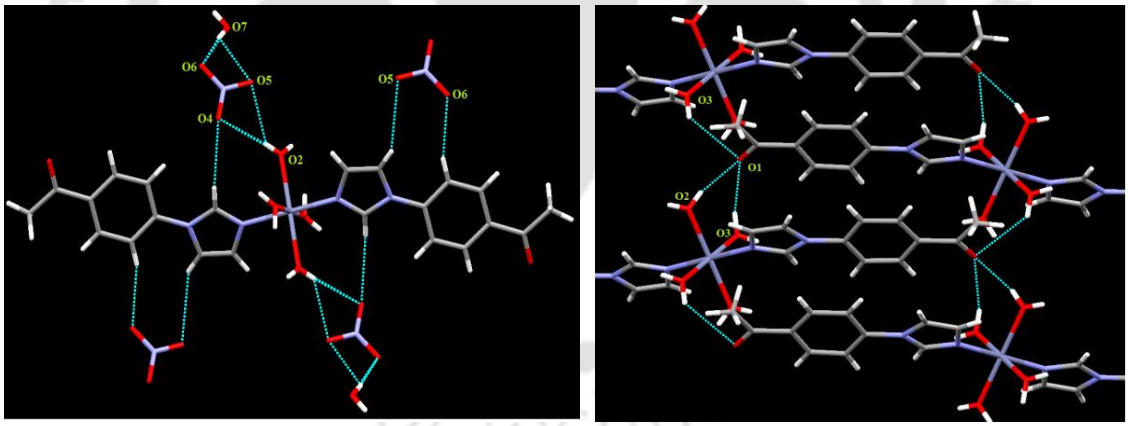

Figure 7. Bifurcated H-bond (left) and trifurcated H-bond (right) present in **3**.

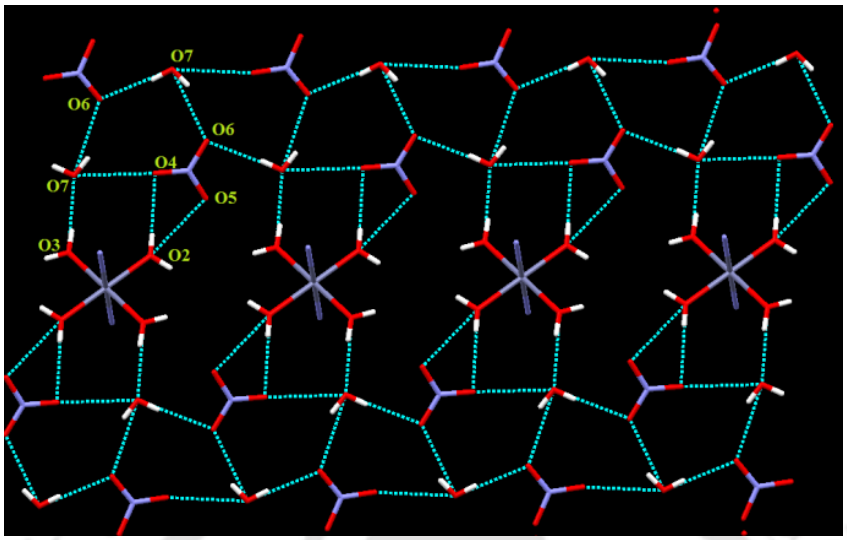

Figure 8. Cyclic hydrogen-bonded architectures in **3**.

2.3.2.3. [Co(L)$_2$(OAc)$_2$(H$_2$O)]·3H$_2$O (5) and [Mn(L)$_2$(OAc)$_2$(H$_2$O)]·3H$_2$O (6):

Complexes **5** and **6** are isomorphous and isostructural in nature having the general formula [M(**L**)$_2$(OAc)$_2$(H$_2$O)]·2H$_2$O and crystallized in *P*bcn space group with similar cell parameters (Table 2 and 3). The asymmetric unit has a half molecule of complex unit, namely; a M(II) atom and coordinated water molecules each with half occupancy, one each of **L** ligand and coordinated acetate ion. In both complexes, the coordination geometry around M(II) ion can be described as pentagonal bipyramidal. The equatorial positions are occupied by five oxygen atoms from two η^2-acetate ions and one water molecule. Two axial sites are coordinated by N_I atoms of **L**. Out of the two distances between metal to acetate oxygen atoms, one is shorter than the other suggesting that the η^2-acetate binding is asymmetric. The metal to ligand distances in cobalt complex is shorter than in manganese, consistent with the relative size of these two ions. The difference in M–N_I, M–O_W and M–O_A, respectively are 0.114(2), 0.075(3) and 0.121(2) Å. The trend Mn–O_W < Mn–N_I < Mn–O_A was observable in **5** but in **6**, it is Co–N_I ≈ Co–O_W < Co–O_A. The difference between two Mn–O_A distance is 0.098(2) Å and the same in Co–O_A is 0.265(2) Å. The pentagonal plane formed by the O_A and O_W atoms is planar as the sum of the angles is 360.07(7)°. The *axial* N_I–Mn–N_I angle deviates from linearity by ~6.5°. A representative schematic diagram of complex **6** is shown in Figure 9 and **5** in Figure A4.

In **5** and **6**, pattern and types of inter-molecular interactions present are identical and non-bonded distances are nearly same. Packing diagram of **6** indicate the presence of H-bonded architectures involving the oxygen atoms of lattice water, coordinated water and acetate ion. It is notable that three lattice water molecules form a V-shaped trimer in which the O6 atom sit on a 2-fold rotational axis, and the unique non-bonded O5···O6 distance is 2.779(3) Å. This O6 is a double hydrogen bond acceptor from O5 and double hydrogen bond donor to O3 of acetate group. However, O5 in addition act as a single hydrogen bond acceptor from coordinated water molecule and single hydrogen bond donor to O4 of acetate group. This H-bonded architecture contains cyclic fused five- and six-membered $R^2_2(5)$ and $R^2_3(6)$ patterns (Figure 10) having the non-bonded contacts O2···O5, 2.757(3); O3···O6, 2.723(3) and O4···O5, 2.796(3) Å. These hydrogen bonding interactions lead a 2D network of hydrophilic layer which separates the hydrophobic aromatic ring of the ligand (Figure 11). It is also notable that the carbonyl oxygen does not participate in hydrogen bonding.

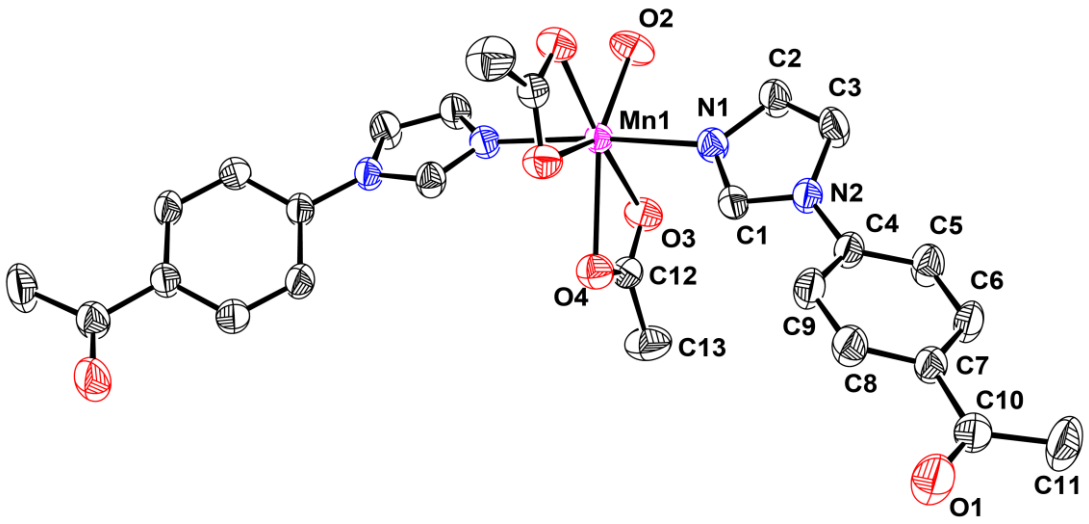

Figure 9. ORTEP diagram (50% probability) of **6** (all hydrogen atoms are omitted for clarity). Selected bond lengths (Å) and angles (º): Mn1–N1, 2.243(2); Mn1–O2, 2.207(3); Mn1–O3, 2.295(2); Mn1–O4, 2.393(2); O2–Mn1–N1, 93.23(5); N1–Mn1–N1, 173.54(10); O2–Mn1–O3, 86.15(5); N1–Mn1–O3, 93.02(7); N1–Mn1–O3, 87.41(7); O3–Mn1–O3, 172.31(9); O2–Mn1–O4, 141.38(4); N1–Mn1–O4, 87.72(7); N1–Mn1–O4, 87.24(7); O3–Mn1–O4, 55.27(6); O3–Mn1–O4, 132.42(6); O4–Mn1–O4, 77.23(9).

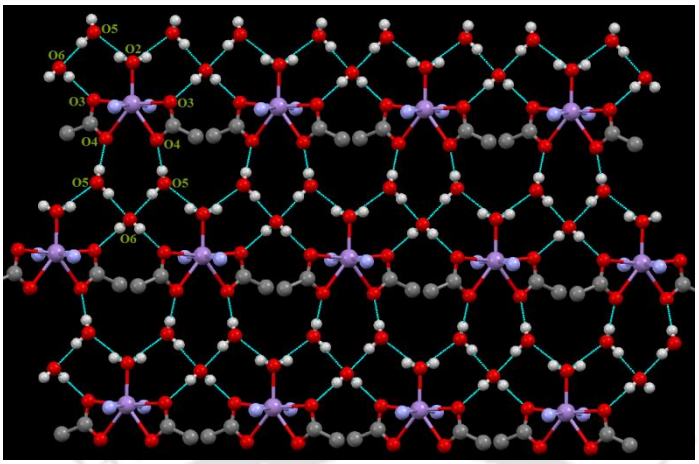

Figure 10. H-bonded architecture between the water molecules and acetate ion containing cyclic fused five- and six-membered in **6**.

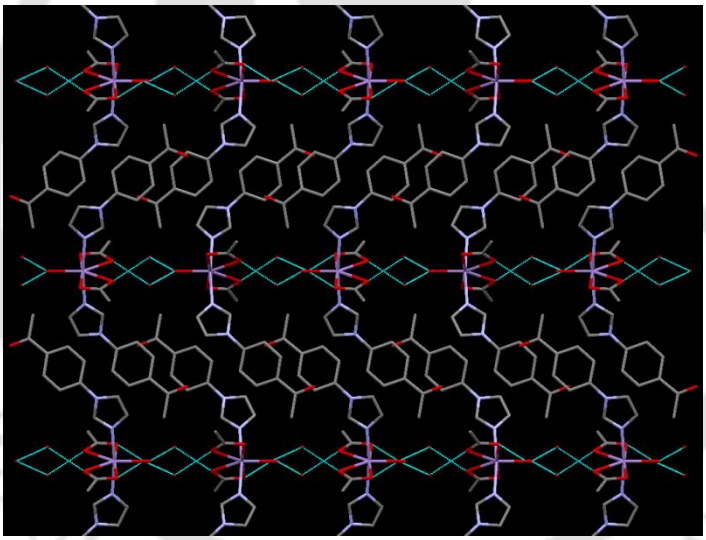

Figure 11. 2D network of hydrophilic layer and hydrophobic layer along *a*-axis of **5**.

2.3.2.4. [Co(L)$_4$(NCS)$_2$] (7):

X-ray crystallographic analysis revealed that complex **7** crystallized in space group *P*-1. The bivalent cobalt is surrounded by four nitrogen atoms of **L** and two nitrogen atoms from thiocyanate ion. The Co^{2+} ion is hexa-coordinated having the coordination environment *trans*-$(N_I)_4(N_T)_2$. A representative view is shown in Figure 12. The high-spin Co(II) has a $t_2^5e^2$ electronic configuration and hence is expected to show a week distortion. The observed Co–N bond lengths are consistent with this and the three unique bond distances are Co1–N1, 2.144(1); Co1–N3, 2.174(1) and Co1–N5, 2.133(1) Å, the

shortest being Co–N_T. Since the central cobalt sits at the crystallographic center of symmetry, three *trans* angles are exactly linear. All the ligands are mono-dentate in nature and do not impose angular strain, hence the *cis* angles lies in the range 86.30(7) – 93.70(7)°, closer towards 90°.

Significant among the short contacts is the intermolecular C–H···O interactions between the O-atoms of two acetyl groups of two units of complex and H-atoms of phenyl (C17···O1, 3.487(3) Å) and CH_3 groups (C11···O2, 3.666(4) Å) of **L** which form a $R_2^2(9)$ type of cyclic hydrogen bond motif (Figure 13). Imidazole moieties (carbon atom C2) interact with benzene ring (carbon atom C16) of **L** forming π···π (C2···C16, 3.313(3) Å) interaction and C–S bond of thiocyanate interacting with aromatic ring (C23···C9, 3.662(4); S1···C9, 3.790(3) and S1···C20, 3.818(3) Å) (Figure 14).

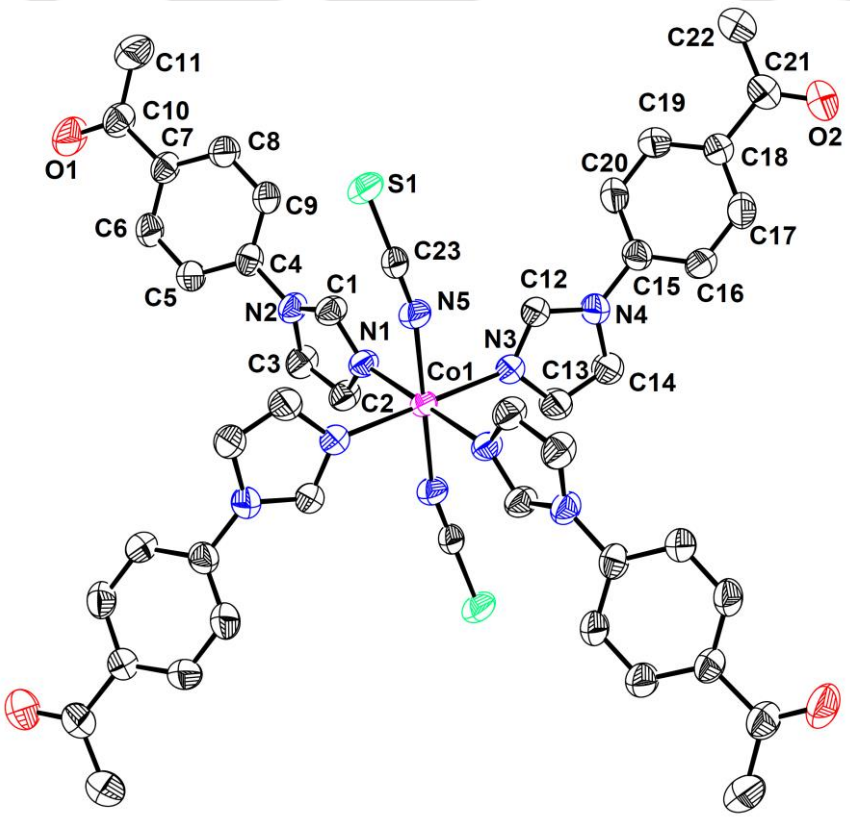

Figure 12. ORTEP diagram (50% probability) of **7** (all hydrogen atoms are omitted for clarity). Selected bond angles (°): N5–Co1–N1, 91.29(7); N5–Co1–N1, 88.71(7); N5–Co1–N3, 89.21(7); N5–Co1–N3, 90.79(7); N1–Co1–N3, 93.70(7); N1–Co1–N3, 86.30(7); N1–Co1–N3, 93.70(7).

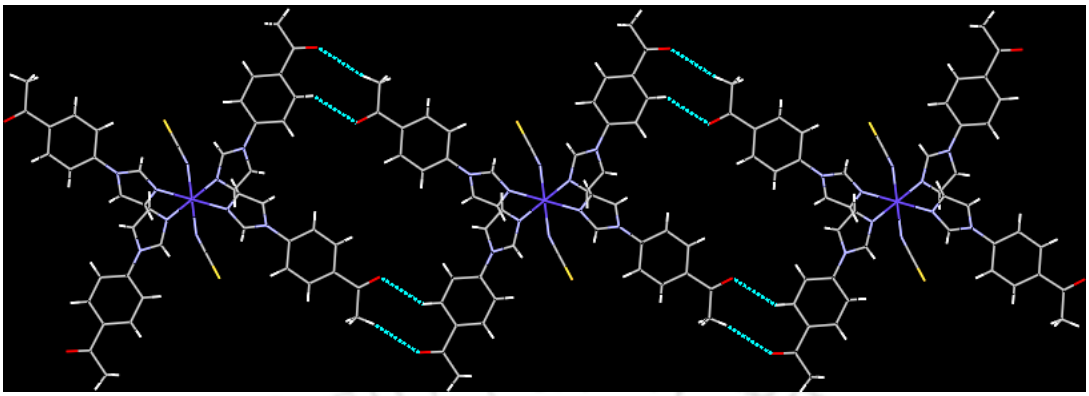

Figure 13. C–H···O interactions present in **7**.

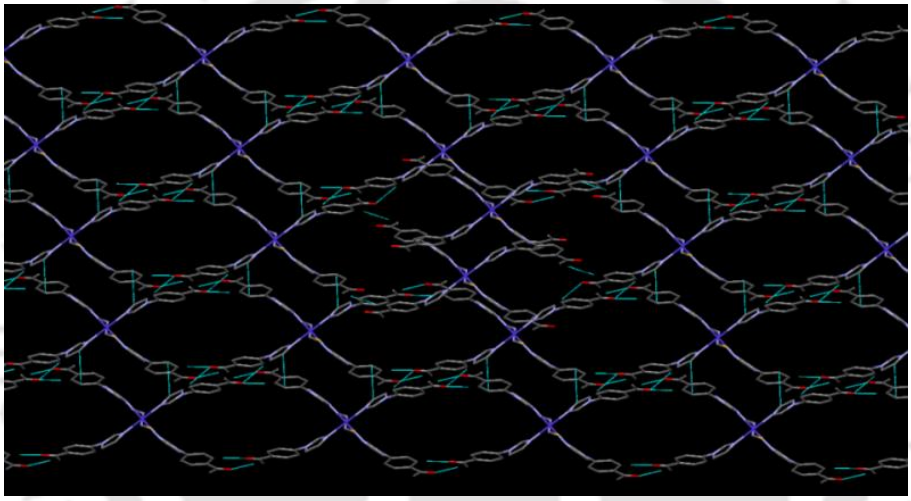

Figure 14. Packing diagram depicting C···S and π···π interaction in **7**.

2.3.2.5. {[Co(L)$_2$(Fum)(H$_2$O)$_2$]·2H$_2$O}$_n$ (8) and {[Mn(L)$_2$(Fum)]}$_n$ (9):

Further, an attempt has been made to prepare isomorphous and isostructural complexes by using Co(II) and Mn(II) chlorides with **L** and a planar aliphatic dicarboxylic acid (H$_2$**Fum**) as coligand but could not succeed in isolating isomorphous and isostructural complexes from them. On the other hand, coordination polymers of composition {[Co(**L**)$_2$(**Fum**)(H$_2$O)$_2$]·2H$_2$O}$_n$ and {[Mn(**L**)$_2$(**Fum**)]}$_n$ {**Fum** = fumarate dianion} could be isolated as shown in Scheme 1, from the said reactants.

The X-ray diffraction analysis revealed that complex **8** crystallized in *P*-1 space group. The asymmetric unit has one **Fum** linked in μ-η^1:η^1 fashion to two cobalt centers both of which are sitting at a center of symmetry (Figure 15).

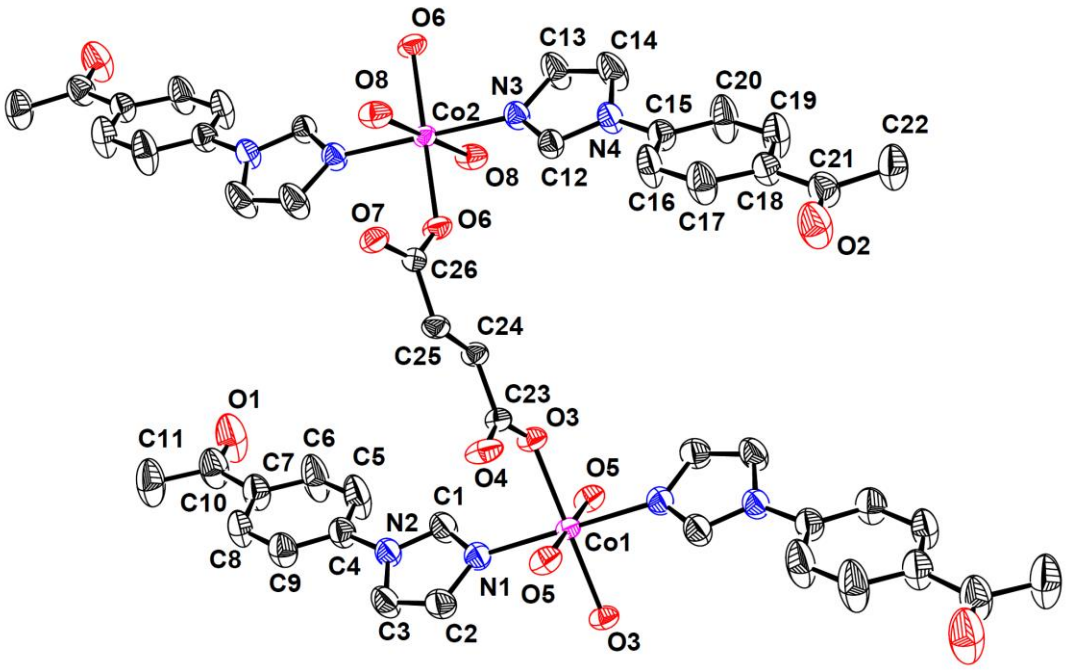

Figure 15. ORTEP diagram (50% probability) of **8** (all hydrogen atoms are omitted for clarity). Selected bond angles (°) in **8**: O6–Co2–N3, 91.74(8); O6–Co2–N3, 88.26(8); O6–Co2–N3, 88.26(8); O6–Co2–N3, 91.74(8); O6–Co2–O8, 89.38(7); O6–Co2–O8, 90.62(7); N3–Co2–O8, 94.45(9); N3–Co2–O8, 85.55(9); O6–Co2–O8, 90.62(7); O6–Co2–O8, 89.38(7); N3–Co2–O8, 85.55(9); N3–Co2–O8, 94.45(9); O3–Co1–O5, 94.19(7); O3–Co1–O5, 85.81(8); O3–Co1–O5, 85.81(7); O3–Co1–O5, 94.19(7); O3–Co1–N1, 87.37(8); O3–Co1–N1, 92.63(8); O5–Co1–N1, 87.13(10); O5–Co1–N1, 92.87(10); O3–Co1–N1, 92.63(8); O3–Co1–N1 87.37(8); O5–Co1–N1, 92.87(10); O5–Co1–N1, 87.13(10); O8–Co2–O8, 180.000(1); O3–Co1–O3, 180.000(1); O6–Co2–O6, 180.000(1); N3–Co2–N3, 180.000(1); O5–Co1–O5, 180.000(1); N1–Co1–N1 180.00(5).

The bond distances at the metal center Co1–O3, 2.093(2); Co2–O8, 2.065(2); Co1–N1, 2.131(2); Co2–N3, 2.156(2); Co1–O5, 2.122(2) and Co2–O8, 2.158(2) Å are consistent with the high-spin nature of the cobalt(II) center.[11] Since the bridging arm of the fumarate ion is longer with a non-bonded distances O3···O6, 4.999(3) Å; O4···O7, 4.986(3) Å; two cobalt centers are separated by a distance of 9.01(1) Å, in the 1D polymer (Figure 16). Generally, aliphatic dicarboxylic acids such as adipic acid or fumaric acid forms wide varieties of Co(II) complexes either as monomer,[13a] or as

coordination polymer.[13b-c] On the other hand, double bond geometry of maleate based cobalt(II) complex can be isomerised to a fumarate complex in presence of ligands such as pyridine or bipyridine.[13d]

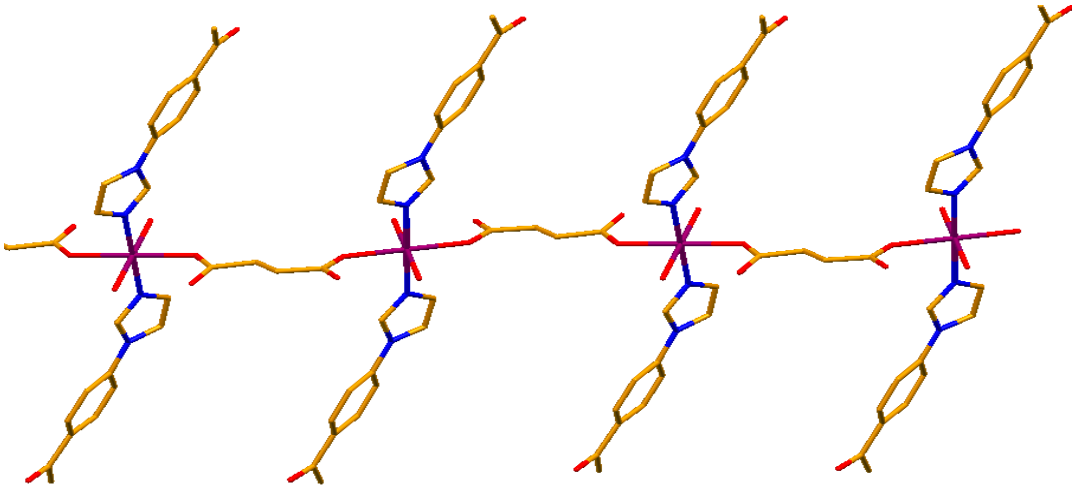

Figure 16. 1D co-ordination polymer of **8**.

Uncoordinated carbonyl oxygen atom of **Fum** takes part in intermolecular hydrogen bonding interactions. Both O4 and O7 atoms of the carboxylate group is involved as H-bond acceptor with the coordinated water molecule O8 having the non-bonded distances of O4···O8, 2.855(3) Å; O7···O8, 2.666(3) Å. Further, O4 is also hydrogen bonded with another coordinated water molecule O5 having a O5···O4 contact of 2.640(4) Å. It is also relevant to note that O7···O8 and O4···O6 interactions occur within the coordination sphere. Two lattice water molecules exists as a dimer O9···O10, 2.784(4) Å and one of them is H-bonded to the coordinated water molecule O10···O5, 2.844(4) Å. The O4···O8 H-bonding interaction interlinks the coordination polymer chains with the inter-strand Co1···Co1/Co2···Co2 distance of 8.10(1) Å. The shortest Co1···Co2 distance is 7.65(1) Å and the longest one is 15.32 Å. In addition the aromatic rings of **L** zip two adjacent polymeric chains through π-stacking interactions (Figure 17). Apart from these, carbon atom (C24) of double bond interact with methyl group of **L** forming C–H···π (dc_3···π, 3.81 Å) interaction.

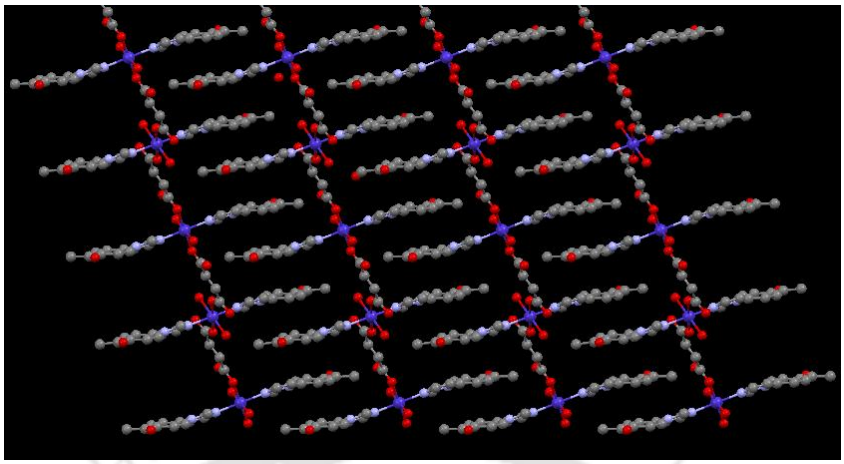

Figure 17. π-stacking diagram of **8**.

The molecular structure of complex **9** has also been determined using X-ray diffraction method, which crystallized in *P*-1 space group. The asymmetric unit has half-molecule of **Fum**, one **L** and a Mn(II) atom sitting on a special position. The **Fum** is bound in μ_4-η^1:η^1:η^1:η^1 fashion to four manganese centers and each manganese centers is further bound by two **L** ligands, thus leading to the 2D-coordination polymer entity {[Mn(**L**)$_2$(μ_4-**Fum**)]}. The bivalent manganese ion has a distorted octahedral coordination geometry having an *trans*-$(N_I)_2(O_F)_4$ environment as shown in Figure 18. The Mn–N_I distance of 2.279(1) Å and Mn–O_F distances of 2.214(1) and 2.177(1) Å are comparable with those of reported bivalent manganese complexes.[14] The μ_4-mode of binding by **Fum** brings about a diamond shaped Mn_4 unit having the non-bonded Mn···Mn edges of 5.054(1), 7.398(1) Å with angles at corners being 85.1(1)° and 94.9(1)°. Within this coordination polymer, there are eight and fourteen membered cyclic ring structure involving the manganese atoms and that of **Fum** ion (Figure 19). Among the weak inter-molecular interactions, notable is that the acetyl group of **L** is involved in C–H···O type interaction. The oxygen atom (O1) has a non-bonded contact of 3.338(4) Å with C3 of imidazole ring and of 3.520(4) Å with C11 of methyl group.

The experimentally observed powder X-ray diffraction patterns of **1**–**9**, are consistent with that of calculated from the single crystal X-ray diffraction data (Figure A5).

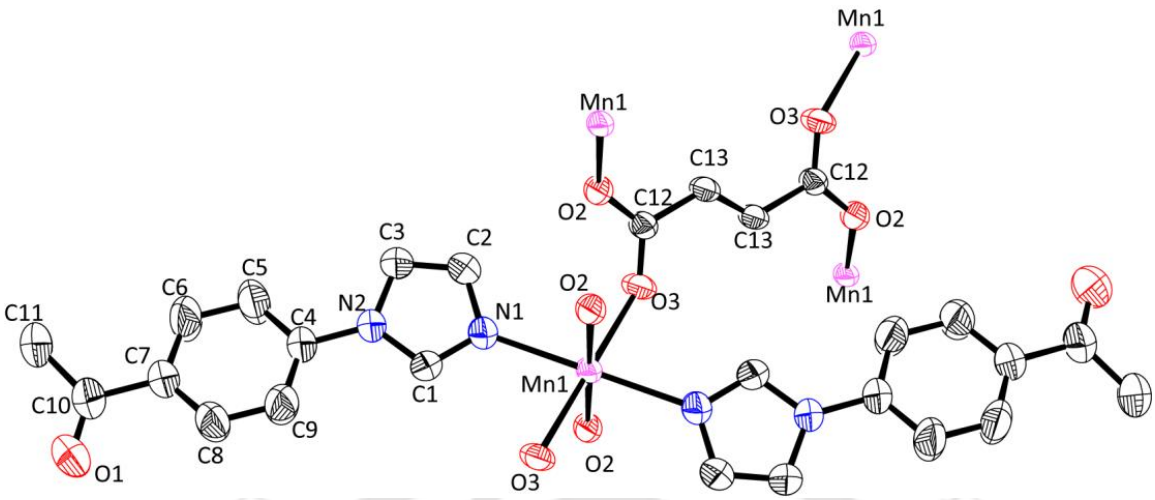

Figure 18. ORTEP diagram (50% probability) of **9** (all hydrogen atoms are omitted for clarity). Selected bond angles (°) in **9**: O3–Mn1–O3, 180.0; O3–Mn1–O2, 88.25(6); O3–Mn1–O2, 91.75(6); O2–Mn1–O2, 180.00(9); O3–Mn1–N1, 90.47(7); O3–Mn1–N1, 89.53(7); O2–Mn1–N1, 85.12(7); O2–Mn1–N1, 94.88(7); O3–Mn1–N1, 90.47(7); N1–Mn1–N1, 180.00(2).

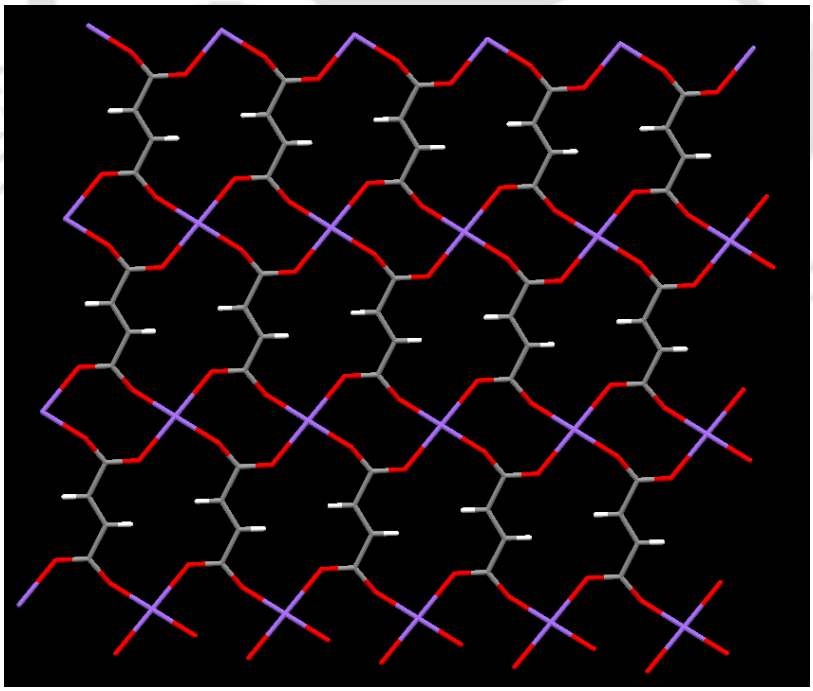

Figure 19. Metallocycles formed in **9**.

2.3.3. Thermogravimetry:

The thermal decomposition of **3**–**6** and **8** were studied using TGA in the temperature range 20-800ºC in N_2 atmosphere (Figure 20 and 21). Complex **3** shows a continuous weight loss of 16.3% in the temperature range 50-150ºC corresponding to loss of two lattice and four co-ordinated water molecules (calc. 16.3%). The iso-structural complex **4**, show gradual weight loss of 16.1% (calc. 16.1% for 6 water molecules) in the range 48-210ºC, accompanied by loss of other volatiles beyond this temperature. In complexes **5** weight loss of 11.8% (calcd. 11.6%) was observed in the temperature range of ca. 20-180ºC corresponding to liberation of three lattice and one coordinated water molecule. The complex **6**, shows a two-step weight loss. The first occurs in the range 39-94°C (2.8%, calcd. 2.8%) corresponding to the loss of one water molecule and second in the range 94-133°C (8.8%, calcd. 8.8%) for the loss of rest of three water molecules. Complex **8** shows a weight loss of 11.6% from 50-116ºC corresponding to the loss of two lattice and two co-ordinated molecules (calc. 11.7%).

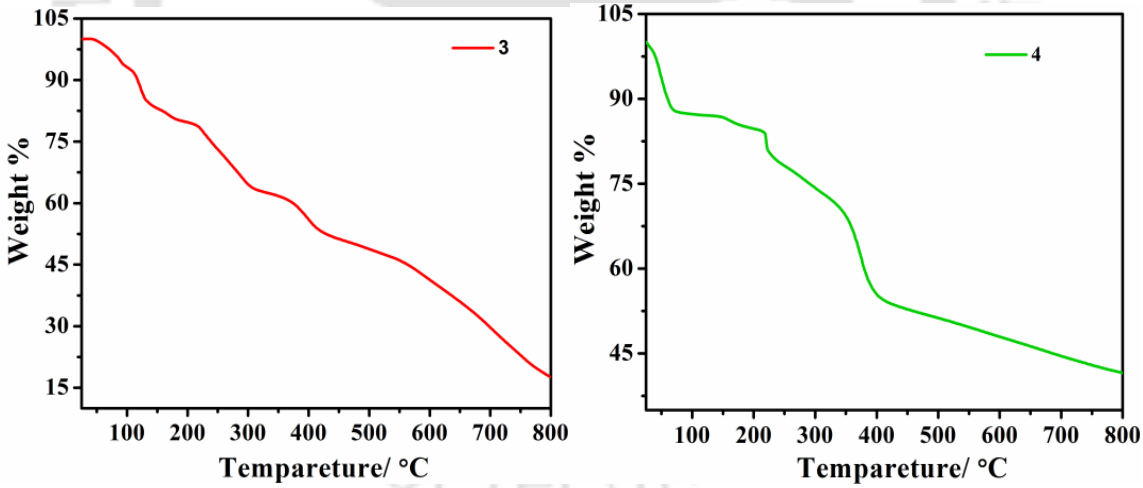

Figure 20. Thermogravimetric profiles of **3** and **4**.

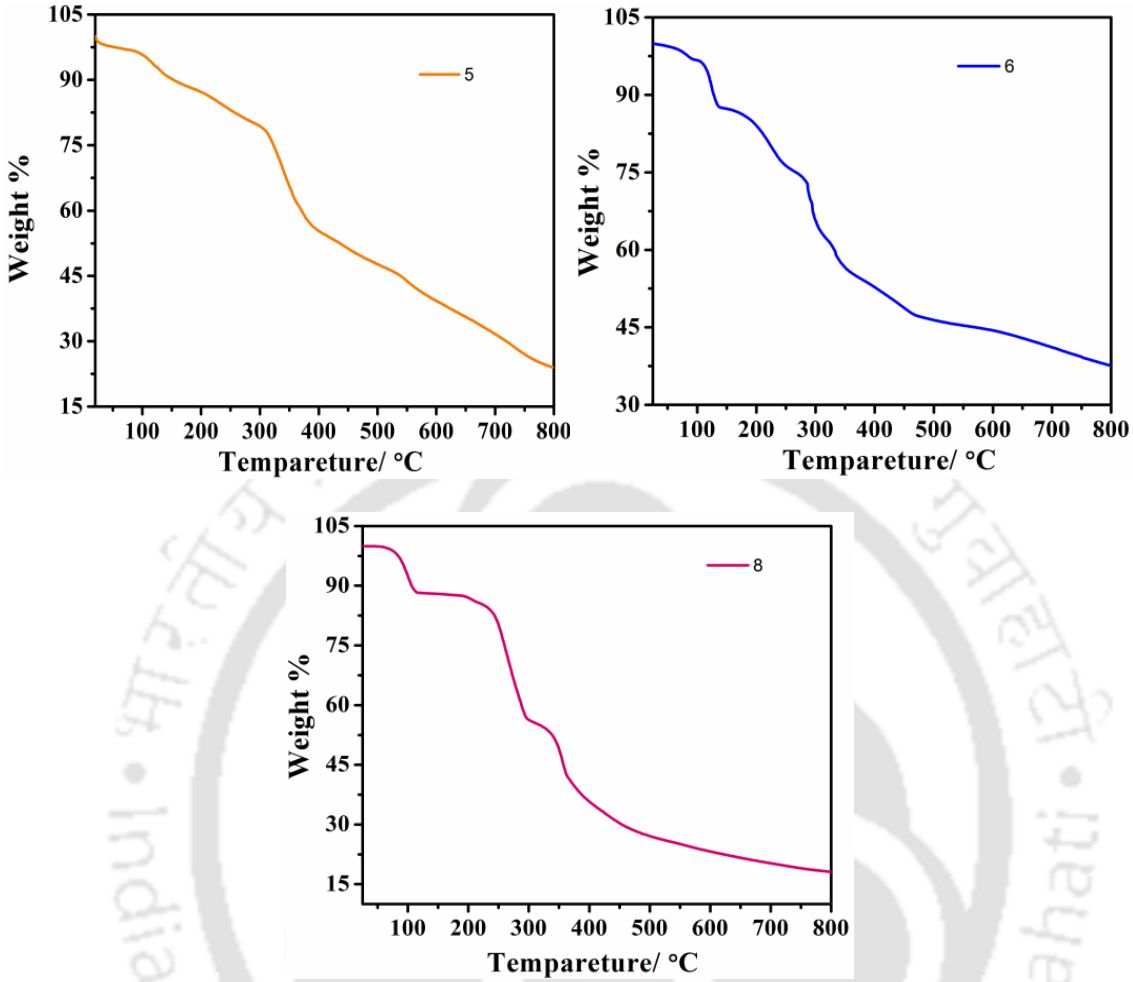

Figure 21. Thermogravimetric profiles of **5**, **6** and **8**.

2.4. Conclusion:

In summary, nine bivalent metal complexes of 1-(4-acetylphenyl)imidazole were synthesized along with coligands including Cl^-, NO_3^-, OAc^-, NCS^- and fumarate ion. Determination of their molecular structures revealed that there are three pairs of iso-structural complexes, one mononuclear complex and two coordination polymers. In these complexes counter ions, co-ordinated and/or lattice water molecules are involved in O–H···O hydrogen bonding and other weak interactions like C–H···π, C–H···S, C–H···Cl and C–H···O, while in some cases the aromatic ring of **L** is found to involve in π···π stacking interactions. The acetyl group of **L** plays an important role as hydrogen bond acceptor through O···H–O_W in **3**–**4** and O···H–C interactions in **1**, **2**, **5**–**9**. In complex **1**–**2**, inter-molecular interactions present are of C–H···O, C–H···π and C–H···Cl type. In **3**–**4**, O–

H···O type hydrogen-bonded cross-linked doubled stranded chain structures have been observed along with π-stacking interactions. In **3**-**4** and **5**-**6**, the counter ion nitrate / acetate along with the coordinated and lattice aqua molecule form fused cyclic H-bonding network. The H-bonding are of $R^2_1(4)$, $R^2_2(5)$, $R^2_3(6)$ type in **3**-**4** and of $R^2_2(5)$, $R^2_3(6)$ type in **5**-**6**. The H-bonding network in **5**-**6** is a 2D hydrophilic layer which separate hydrophobic layer formed by aromatic ring of **L**. While changing the counter ion from Cl^- to NCS^-, a conversion from tetrahedral (**1**) to octahedral (**7**) geometry around the Co^{2+} ion has occurred. In **8**-**9**, co-ligand **Fum** coordinate to metal center in μ-η^1:η^1 bidentate and μ_4-η^1:η^1:η^1:η^1 tetradentate fashions. As a result, 1D and 2D coordination polymer was found in case of cobalt and manganese ions, each having a distorted octahedral coordination geometry with *trans*-*trans*-*trans*-$(N_I)_2(O_F)_2(O_W)_2$ and *trans*-$(N_I)_2(O_F)_4$ environments respectively. In **8**, two cobalt centers are separated by a distance of 9.01(1) Å within the chain and H-bonding interactions interlink the chain with inter-chain Co1···Co1 distance of 8.10(1) Å. In the 2D coordination polymer **9**, eight and fourteen membered cyclic ring like structures is present having Mn···Mn distances of 5.054(1) and 7.398(1) Å and supported by the C–H···O interaction.

Table 1. Crystallographic data of **1**–**3**.

	1	**2**	**3**
Formula	$C_{22}H_{20}Cl_2N_4O_2Co$	$C_{22}H_{20}Cl_2N_4O_2Zn$	$C_{22}H_{32}N_6O_{14}Co$
CCDC number	1553365	1553366	1553368
Formula weight	502.25	508.71	663.45
T (K)	296(2)	296(2)	296(2)
Crystal system	Orthorhombic	Orthorhombic	Monoclinic
Space group	*Pnma*	*Pnma*	$P2_1/c$
a (Å)	14.9055(5)	14.866(3)	9.0120(12)
b (Å)	20.1666(7)	20.083(4)	22.157(3)
c (Å)	7.5540(3)	7.5340(15)	7.4899(9)
α (°)	90.00	90.00	90.00
β (°)	90.00	90.00	105.262(8)
γ (°)	90.00	90.00	90.00
V (Å^3)	2270.68(14)	2249.3(8)	1442.8(3)
Z	4	4	2
D_{calcd} (g m^{-3})	1.469	1.502	1.499
μ (mm^{-1})	1.017	1.356	0.672
F(000)	1030.9	1040.0	750.0
Reflections collected	6373	12806	12701
Unique reflections	2052	2011	2515
Goodness-of-fit (GOF)[a]	1.005	1.032	1.016
R_1[b], wR_2[c] ($I \geq 2\sigma(I)$)	0.0354, 0.0896	0.0475, 0.0691	0.0959, 0.2413
R_1[b], wR_2[c] (all data)	0.0437, 0.0978	0.1006, 0.0815	0.1258, 0.2557

[a]GOF = $[\Sigma[w(F_0^2-F_c^2)^2]/M–N]^{1/2}$ (M = number of reflections, N = number of parameters refined). [b]$R_1 = \Sigma||F_0|-|F_c||\Sigma|F_0|$. [c]$wR_2 = [\Sigma\,[w(F_0^2-F_c^2)^2]/\Sigma\,[w(F_0^2)^2]]^{1/2}$.

Table 2. Crystallographic data of **4**–**6**.

	4	**5**	**6**
Formula	$C_{22}H_{32}N_6O_{14}Zn$	$C_{26}H_{33}N_4O_{10}Co$	$C_{26}H_{33}N_4O_{10}Mn$
CCDC number	1553367	1553369	1553370
Formula weight	669.93	616.50	616.50
T (K)	296(2)	296(2)	296(2)
Crystal system	Monoclinic	Orthorhombic	Orthorhombic
Space group	$P2_1/c$	Pbcn	Pbcn
a (Å)	8.9229(6)	7.7185(9)	7.7802(5)
b (Å)	22.1775(14)	16.0246(18)	15.9278(10)
c (Å)	7.5240(5)	23.433(3)	23.6276(18)
α (°)	90.00	90.00	90.00
β (°)	104.987(3)	90.00	90.00
γ (°)	90.00	90.00	90.00
V (Å^3)	1438.26(16)	2898.3(6)	2928.0(3)
Z	2	4	4
D_{calcd} (g m^{-3})	1.538	1.424	1.399
μ (mm^{-1})	0.932	0.653	0.511
F(000)	688.0	1296.0	1288.0
Reflections collected	15469	23943	7271
Unique reflections	2438	2554	2573
Goodness-of-fit (GOF)[a]	1.007	1.044	1.070
R_1[b], wR_2[c] ($I \geq 2\sigma(I)$)	0.0426, 0.1137	0.0311, 0.0578	0.0414, 0.1106
R_1[b], wR_2[c] (all data)	0.0623, 0.1260	0.0381, 0.0605	0.0493, 0.1174

[a]GOF = $[\Sigma[w(F_0^2-F_c^2)^2]/M–N]^{1/2}$ (M = number of reflections, N = number of parameters refined). [b]$R_1 = \Sigma||F_0|-|F_c||\Sigma|F_0|$. [c]$wR_2 = [\Sigma\,[w(F_0^2-F_c^2)^2]/\Sigma\,[w(F_0^2)^2]]^{1/2}$.

Table 3. Crystallographic data of **7**–**9**.

	7	**8**	**9**
Formula	$C_{46}H_{40}CoN_{10}O_4S_2$	$C_{26}H_{26}N_4O_{10}Co$	$C_{26}H_{22}MnN_4O_6$
CCDC number	1553371	1553372	1553374
Formula weight	919.93	613.44	541.42
T (K)	296(2)	296(2)	296(2)
Crystal system	Triclinic	Triclinic	Triclinic
Space group	*P*-1	*P*-1	*P*-1
a (Å)	8.5365(4)	8.0965(5)	5.0538(2)
b (Å)	8.9375(4)	12.7701(8)	7.3979(3)
c (Å)	15.0402(6)	14.6217(9)	15.6641(7)
α (°)	85.864(2)	70.777(6)	100.722(2)
β (°)	87.947(3)	79.035(5)	91.926(2)
γ (°)	73.745(2)	81.004(5)	94.929(2)
V (Å^3)	1098.61(8)	1394.25(15)	572.55(4)
Z	1	2	1
D_{calcd} (g m^{-3})	1.390	1.461	1.570
μ (mm^{-1})	0.542	0.678	0.630
F(000)	477.0	634.0	279.0
Reflections collected	12304	10211	6503
Unique reflections	3820	4910	1757
Goodness-of-fit (GOF)[a]	1.001	1.038	1.032
R_1[b], wR_2[c] ($I \geq 2\sigma(I)$)	0.0344, 0.1137	0.0428, 0.1264	0.0307, 0.0748
R_1[b], wR_2[c] (all data)	0.0436, 0.1350	0.0566, 0.1412	0.0327, 0.0757

[a]GOF = $[\Sigma[w(F_0^2-F_c^2)^2]/M–N]^{1/2}$ (M = number of reflections, N = number of parameters refined). [b]$R_1 = \Sigma||F_0|-|F_c||\Sigma|F_0|$. [c]$wR_2 = [\Sigma\,[w(F_0^2-F_c^2)^2]/\Sigma\,[w(F_0^2)^2]]^{1/2}$.

References:

1. (a) M. Sakamoto, K. Manseki and H. Õkawa, *Coord. Chem. Rev*., 2001, **219-221**, 379-414; (b) A. Mishra, W. Wernsdorfer, K. A. Abboud and G. Christou, *J. Am. Chem. Soc*., 2004, **126**, 15648-15649; (c) C. Aronica, G. Pilet, G. Chastanet, W. Wernsdorfer, J. F. Jacquot and D. Luneau, *Angew. Chem., Int. Ed*., 2006, **45**, 4659-4662; (d) T. K. Prasad, M. V Rajasekharan and J. P. Costes, *Angew. Chem., Int. Ed.*, 2007, **46**, 2851-2854; (e) F. Pointillart, K. Bernot, R. Sessoli and D. Gatteschi, *Chem-Eur. J*., 2007, **13**, 1602-1609; (f) V. Chandrasekhar, B. M. Pandian, R. Boomishankar, A. Steiner, J. J. Viftal, A. Houri and R. Clerac, *Inorg. Chem*., 2008, **47**, 4918-4929; (g) A. M. Ako, V. Mereacre, R. Clerac, I. J. Hewitt, Y. H. Lan, G. Buth, C. E. Anson and A. K. Powell, *Inorg. Chem*., 2009, **48**, 6713-6722; (h) M. N. Akhtar, Y. Z. Zheng, Y. H. Lan, V. Mereacre, C. E. Anson and A. K. Powell, *Inorg. Chem*., 2009, **48**, 3502-3504; (i) M. Nippe, J. F Wang, E. Bill, H. Hope, N. S. Dalal and J. F. Berry, *J. Am. Chem. Soc*., 2010, **132**, 14261-14272; (j) Y. Z. Zheng, M. Evangelisti and R. E. P. Winpenny, *Chem. Sci*., 2011, **2**, 99-102.

2. (a) S. J. A. Pope, B. J. Coe, S. Faulkner, E. V. Bichenkova, X. Yu and K. Douglas, *J. Am. Chem. Soc*., 2004, **126**, 9490-9491; (b) B. Zhao, X. Y. Chen, P. Cheng, D. Z. Liao, S. P. Yan and Z. H. Jiang, *J. Am. Chem. Soc*., 2004, **126**, 15394-15395; (c) B. Zhao, H. L. Gao, X. Y. Chen, P. Cheng, W. Shi, D. Z. Liao, S. P. Yan and Z. H. Jiang, *Chem. Eur. J*., 2006, **12**, 149-158; (d) P. Wang, J. P. Ma, Y. B. Dong and R. Q. Huang, *J. Am. Chem. Soc*., 2007, **129**, 10620-10621; (e) B. Zhao, X. Y. Chen, Z. Chen, W. Shi, P. Cheng, S. P. Yan and D. Z. Liao, *Chem. Commun*., 2009, 3113-3115; (f) Y. J. Cui, Y. F. Yue, G. D. Qian and B. L. Chen, *Chem. Rev*., 2012, **112**, 1126-1162.

3. (a) B. Zhao, P. Cheng, X. Y. Chen, C. Cheng, W. Shi, D.Z. Liao, S. P. Yan and Z. H. Jiang, *J. Am. Chem. Soc*., 2004, **126**, 3012-3013; (b) O. Guillou, C. Daiguebonne, M. Camara and N. Kerbellec, *Inorg.Chem*., 2006, **45**, 8468-8470; (c) Y. Wang, P. Cheng, J. Chen, D. Z. Liao and S. P. Yan, *Inorg. Chem*., 2007, **46**, 4530-4534; (d) C. J. Li, Z. J. Lin, M. X. Peng, J. D. Leng, M. M. Yang and M. L. Tong, *Chem.*

Commun., 2008, 6348-6350; (e) P. Mahata, K. V. Ramya and S. Natarajan, *Inorg. Chem*., 2009, **48**, 4942-4951.

4. (a) M. Shibasaki and N. Yoshikawa, *Chem. Rev*., 2002, **102**, 2187-2210; (b) S. Handa, V. Gnanadesikan, S. Matsunaga and M. Shibasaki, *J. Am. Chem. Soc*., 2007, **129**, 4900-4901; (c) S. Handa, V. Gnanadesikan, S. Matsunaga and M. Shibasaki, *J. Am. Chem. Soc*., 2010, **132**, 4925-4934.

5. (a) Z. Y. Li, J. W. Dai, S. T. Yue and Y. L. Liu, *CrystEngComm*, 2010, **12**, 2014-2017.

6. (a) M. T. Allen, A. D. Burrows and M. F. Mahon, *J. Chem. Soc., Dalton Trans*., 1999, 215-221; (b) C. B. Aakeröy, J. Desper and N. Schultheiss, *Inorg. Chem*., 2005, **44**, 4983-4991; (c) C. J. Janiak, *J*. Chem. Soc., *Dalton Trans*., 2000, 3896; (d) H. W. Roesky and M. Andruh, *Coord. Chem. Rev*., 2003, **236**, 91-119; (e) M. B. Zaman, K. A. Udachin and J. A. Ripmeester, *Cryst. Growth Des*., 2004, **4**, 585-589; (f) B. L. Schottel, H. T. Chifotides, M. Shatruk, A. Chouai, L. M. Pérez, J. Bacsa and K. R. Dunbar, *J. Am. Chem. Soc*., 2006, **128**, 5895-5912; (g) S. Noro, R. Kitaura, M. Kondo, S. Kitagawa, T. Ishii, H. Matsuzaka and M. Yamashita, *J. Am. Chem. Soc*., 2002, **124**, 2568-2583.

7. (a) T. Panda, T. Kundu and R. Banerjee, *Chem. Commun*., 2012, **48**, 5464; (b) S. S. Iremonger, R. Vaidhyanathan, R. K. Mah and G. K. H. Shimizu, *Inorg. Chem*., 2013, **52**, 4124-4126; (c) H. Wu, J. Yang, Y. Y. Liu and J. F. Ma, *Cryst. Growth Des*., 2012, **12**, 2272-2276; (d) K. Liu, W. Shi and P. Cheng, *Dalton Trans*., 2011, **40**, 8475-8490; (e) S. Q. Zhang, F. L. Jiang, M. Y. Wu, J. Ma, Y. Bu and M. C. Hong, *Cryst. Growth Des*., 2012, **12**, 1452-1463; (f) S. Q. Su, W. Chen, C. Qin, S. Y. Song, Z. Y. Guo, G. H. Li, X. Z. Song, M. Zhu, S. Wang, Z. M. Hao and H. J. Zhang, *Cryst. Growth Des*., 2012, **12**, 1808-1815; (g) N. Behera and V. Manivannan, *ChemistrySelect*, 2016, **1**, 4016-4023.

8. (a) J. Fan, W. Y. Sun, T. Okamura, W. X. Tang and N. Ueyama, *Inorg. Chem*., 2003, **42**, 3168-3175; (b) J. Fan, L. Gan, H. Kawaguchi, W. Y. Sun, K. B. Yu and W. X. Tang, *Chem. Eur. J*., 2003, **9**, 3965-3973; (c) W. Zhao, J. Fan, Y. Song, H.

Kawaguchi, T. Okamura, W. Y. Sun and N. Ueyama, *Dalton Trans*., 2005, 1509-1517; (d) J. Fan, M. H. Shu, T. Okamura, Y. Z. Li, W. Y. Sun, W. X. Tang and N. Ueyama, *New J. Chem*., 2003, **27**, 1307-1309; (e) X. F. Wang, Y. Lv, T. Okamura, H. Kawaguchi, G. Wu, W. Y. Sun and N. Ueyama, *Cryst. Growth Des*., 2007, **7**, 1125-1133; (f) S. S. Chen, M. Chen, S. Takamizawa, M. S. Chen, Z. Su and W. Y. Sun, *Chem. Commun*., 2011, **47**, 752-754; (g) S. S. Chen, M. Chen, S. Takamizawa, P. Wang, G. C. Lv and W. Y. Sun, *Chem. Commun*., 2011, **47**, 4902-4904; (h) S. S. Chen, G. C. Lv, J. Fan, T. Okamura, M. Chen and W. Y. Sun, *Cryst. Growth Des*., 2011, **11**, 1082-1090; (i) S. S. Chen, Y. Zhao, J. Fan, T. Okamura, Z. S. Bai, Z. H. Chen and W. Y. Sun, *CrystEngComm.*, 2012, **14**, 3564-3576.

9. (a) H. Sigel, A. Saha, N. Saha, P. Carloni, L.E. Kapinos and R. Griesser, *J. Inorg. Biochem*., 2000, **78**, 129-137; (b) S.-S. Chen, Q. Liu, Y. Zhao, R. Qiao, L.-Q. Sheng, Z.-D. Liu, S. Yang and C.-F. Song, *Cryst. Growth Des*., 2014, **14**, 3727-3741.

10. (a) W. L. Steffen and G. J. Palenik, *Inorg. Chem*., 1978, **17**, 1338-1340; (b) C. I. H. Ashby, C. P. Cheng, E. N. Duesler and T. L. Brown, *J. Am. Chem. Soc.*, 1978, **30**, 6057-6063; (c) E. Kimura, Y. Kurogi, M. Shionoya and M. Shiro, *Inorg. Chem*., 1991, **30**, 4524-4530; (d) X. -M. Chen, B. -H. Ye, Z. -T. Xu and X. -C. Huang, *J. Chem. Soc., Dalton Trans*., 1996, 3465-3468.

11. (a) J. Tong, S. Demeshko, M. John, S. Dechert and F. Meyer, *Inorg. Chem.*, 2016, **55**, 4362-4372; (b) J. Vallejo, I. Castro, L. Cañadillas-Delgado, C. Ruiz-Pérez, J. Ferrando-Soria, R. Ruiz-García, J. Cano, F. Lloret and M. Julve., *Dalton Trans.*, 2010, **39**, 2350-2358; (c) S. Pandey, P. P. Das, A. K. Singh and R. Mukherjee, *Dalton Trans.*, 2011, **40**, 10758-10768; (d) Y. Mulyana, K. G. Alley, K. M. Davies, B. F. Abrahams, B. Moubaraki, K. S. Murray and C. Boskovic, *Dalton Trans.*, 2014, **43**, 2499-2511.

12. (a) H. A. Jahn and E. Teller, *Proc. R. Soc. London A*, 1937, **161**, 220-235; (b) C. Housecroft and A. G. Sharpe, *Inorganic Chemistry*, Prentice Hall, 3rd Ed., 2008, p. 644. ISBN: 978-0-13-175553-6.

13. (a) Z. Setifi, F. Setifi, G. Smith, M. El-Ghozzi, D.-A. Rouag, D. Avignant and H. Merazig, *ActaCrystallogr*., 2013, **69E**, m334-m336; (b) S. L. Beko, J. W. Batts and

M. U. Schmidt, *ActaCrystallogr*., 2009, **65C**, m347-m351; (c) J.-F. Ma, J. Yang and J.-F. Liu, *ActaCrystallogr*., 2003, **C59**, m304-m306; (d) M. Padmanabhan, J. C. Joseph, A. Thirumurugan and C. N. R. Rao, *Dalton Trans*., 2008, 2809-2811.

14. (a) S. Brooker and V. McKee, *J. Chem.* Soc., *Dalton Trans.*, 1990, 2397-2401; (b) P. Singh, D. P. Singh, K. Tiwari, M. Mishra, A. K. Singh and V. P. Singh, *RSC Adv.*, 2015, **5**, 45217-45230; (c) S. Biswas, S. Naiya, C. J. Gómez-García and A. Ghosh, *Dalton Trans.*, 2012, **41**, 462-473.

Appendix:

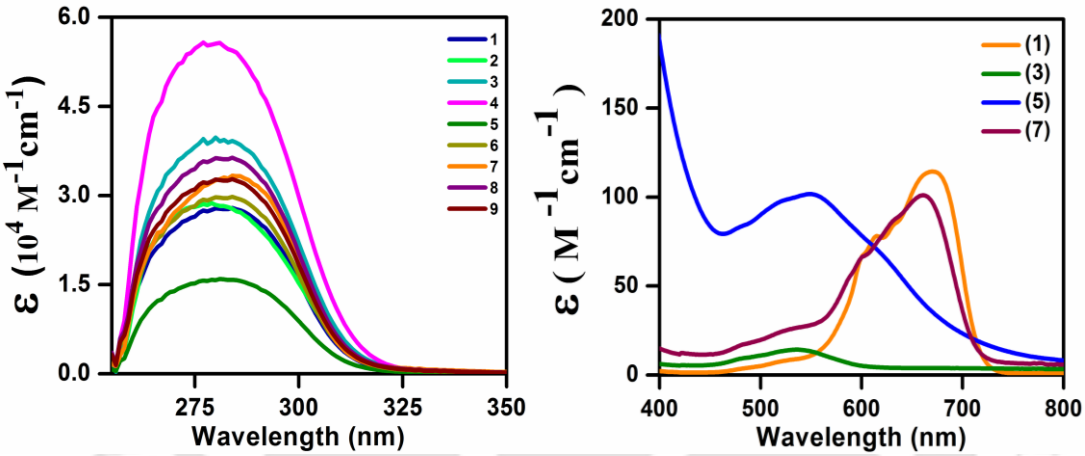

Figure A1. UV-Vis spectra of **1**–**9**.

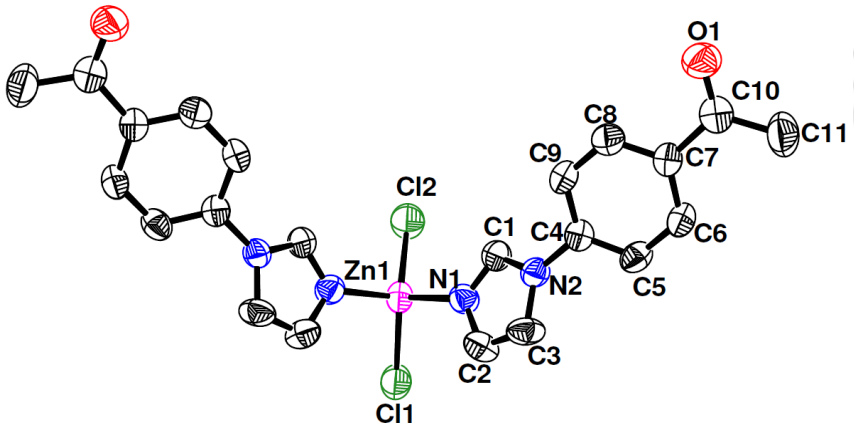

Figure A2. ORTEP diagram (50% probability) of **2** (all hydrogen atoms are omitted for clarity). Selected bond lengths (Å) and angles (º): Zn1–Cl1, 2.2298(16), Zn1–Cl2, 2.2094(18); Zn1–N1, 2.011(3); N1–Zn1–N1′, 102.92(18); N1–Zn1–Cl1, 106.49(10); N1–Zn1–Cl2, 108.31(11); Cl1–Zn1–Cl2, 122.62(7).

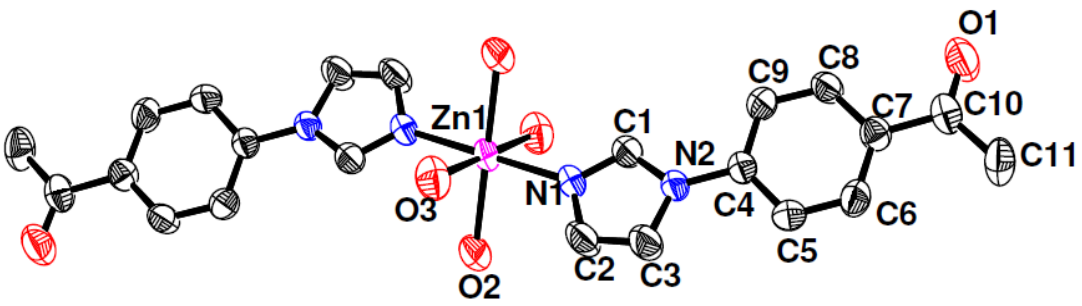

Figure A3. ORTEP diagram (50% probability) of **4** (all hydrogen atoms are omitted for clarity). Selected bond lengths (Å) and angles (º): Zn1–N1, 2.074(2); Zn1–N1, 2.074(2); Zn1–O2, 2.106(2); Zn1–O2, 2.106(2); Zn1–O3, 2.189(2); Zn1–O3, 2.189(2); N1–Zn1–N1, 180.0 (1); N1–Zn1–O2, 91.90(9); N1–Zn1–O2, 88.10(9); N1–Zn1–O2, 88.10(9); N1–Zn1–O2, 91.90(9); N1–Zn1–O3, 90.70(9); N1–Zn1–O3, 90.70(9); N1–Zn1–O3, 89.30(9); N1–Zn1–O3, 89.30(9); O2–Zn1–O2, 180.00(12); O2–Zn1–O3, 87.31(9); O2–Zn1–O3, 92.69(9); O2–Zn1–O3, 87.31(9); O2–Zn1–O3, 92.69(9); O3–Zn1–O3, 180.00(11).

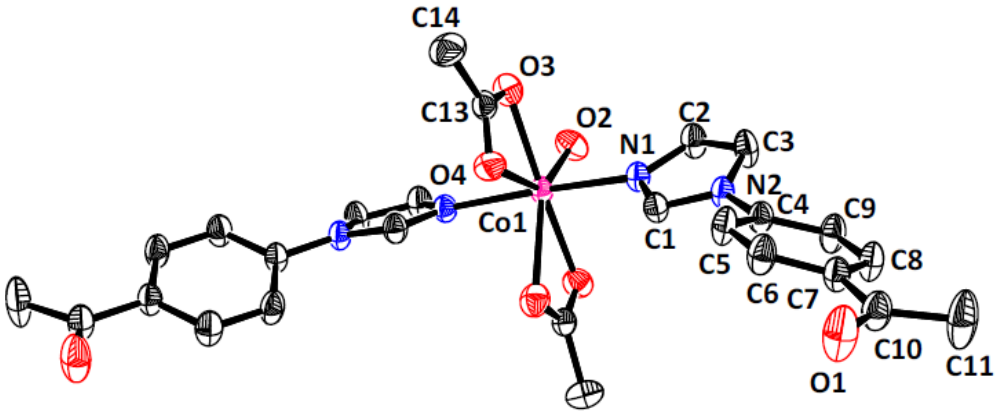

Figure A4. ORTEP diagram (40% probability) of **5** (all hydrogen atoms are omitted for clarity). Selected bond lengths (Å) and angles (º): Co1–O3, 2.1744(16); Co1–O3, 2.1744(16); Co1–O2, 2.132(2); Co1–N1, 2.1286(16); Co1–N1, 2.1286(16); O3–Co1–O3, 174.53(8); O2–Co1–O3, 87.26(4); O2–Co1–O3, 87.26(4); N1–Co1–O3; 88.19(6); N1–Co1–O3, 92.15(6); N1–Co1–O3, 88.18(6); N1–Co1–O3, 92.15; N1–Co1–O2, 93.51(4); N1–Co1–O2, 93.51(4); N1–Co1–N1, 172.98(9).

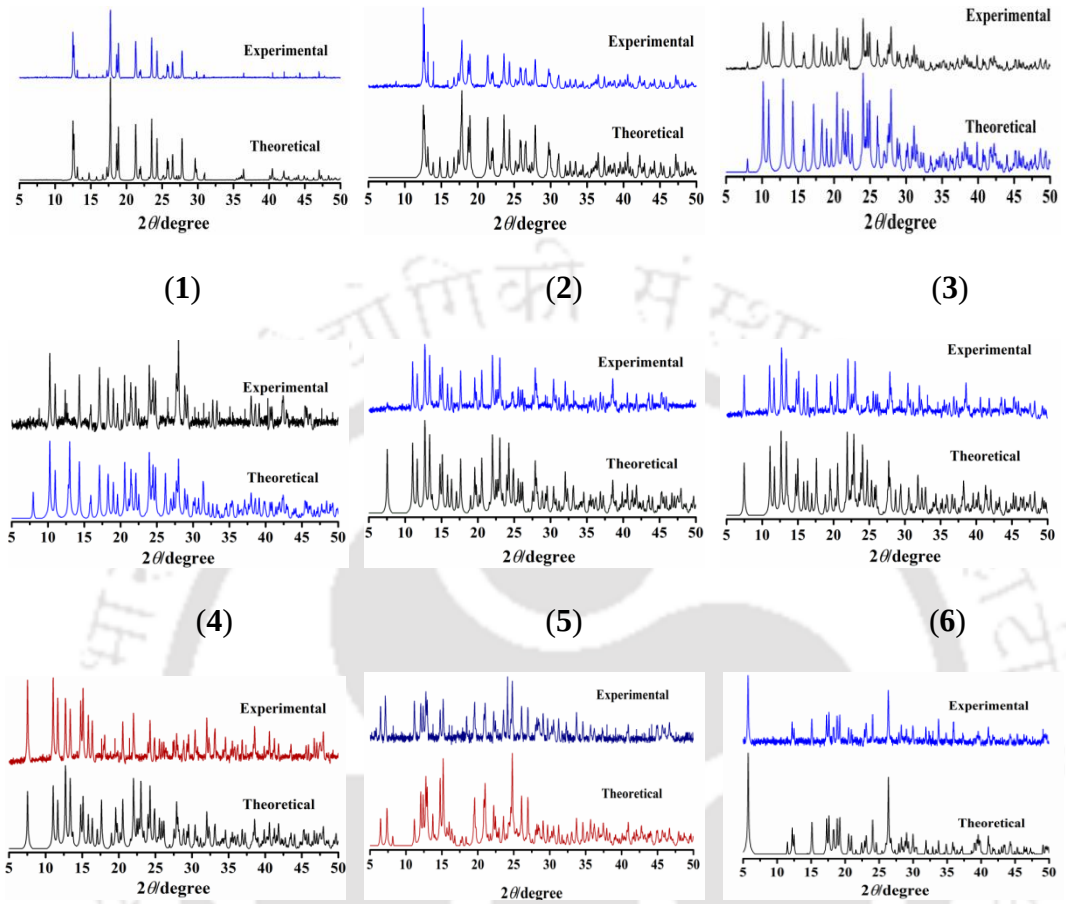

Figure A5. Powder X-ray diffraction patterns of **1**–**9**.

Chapter 3

Selective Recognition of Zn^{2+} Ion Using 2,4-Bis(2-pyridyl)-5-(4-pyridyl)imidazole: Spectra and Molecular Structure*

Abstract:

In this Chapter, a trisubstituted imidazole, 2,4-bis(2-pyridyl)-5-(4-pyridyl)imidazole (**L1H**) in presence of other cations, selectively binds Zn^{2+} ion by exhibiting characteristic absorption and fluorescence spectral behaviors. Upon gradual addition of $ZnCl_2$ to DMSO solution of **L1H**, intensity of peak at 318 nm decreased. A new peak appeared at 364 nm along with an isosbestic point at 337 nm. The DMSO solution of **L1H** upon irradiation with λ = 320 nm exhibited an emission peak at 391 nm, which decreased gradually with increase in Zn^{2+} ion concentrations. A new emission peak also appeared at 445 nm along with a quasi isoemissive point at 413 nm. The HEPES buffered aqueous DMSO solution (pH = 7.4, 2:8, *v*/*v*) of free **L1H**, upon excitation with 320 nm radiation gave emission at 396 nm which shifted to 445 nm during incremental additions of Zn^{2+} ion. The red shift is due to the binding of Zn^{2+} ion to **L1H**. The binding is accompanied by deprotonation of acidic hydrogen from imidazole ring and orientation of two 2-pyridyl rings in near-planarity with the imidazolate ring. The Zn^{2+} ion can be detected with a calculated limit of 6.5×10^{-7} M. The Job's plot revealed that ligand binds to Zn^{2+} ion in 1:2 ratio and it was further confirmed by single crystal X-ray diffraction method.

* This work has been published in:

N. Behera and V. Manivannan, *ChemistrySelect*, 2016, **1**, 4016–4023.

3.1. Introduction:

The design and synthesis of novel fluorescent probes for metal ion detection continues to be an active research field in biology and environmental chemistry. Among the first row transition metal ions, zinc is one of the essential elements in biological systems. Also this is the second most abundant transition metal ion in human body. Due to its electronic and structural preferences, Zn^{2+} ion plays a central role in regulating cellular metabolism.[1,2] High concentrations of zinc(II) ion is present in Central Nervous System (CNS), that is required for signal transmissions. In various biological processes, it plays a diverse role including regulation of enzyme functions,[3-7] DNA binding, as structural cofactors, neural signal transmission, associated diseases, catalytic center and others.[8-11] However, it is recognized that alteration of zinc homeostasis can lead to disorders in metabolism as well as its excessive accumulation in brain cells. The Zn^{2+} ion may also be crucial in various neurodegenerative disorders, such as Alzheimer's disease, Amyotrophic lateral sclerosis (ALS), Parkinson's disease, ischemia, and epilepsy.[12-14] In its free hydrated form, zinc(II) ions are also involved in regulation of apoptosis.[15-17]

Among the several methods available for determination of Zn^{2+} ion, fluorescence has become more useful and popular method in environmental chemistry, medicine and biology. The most common fluorescent probes for detection of Zn^{2+} ion are coumarin,[18,19] Schiff bases,[20-22] calixarene,[23] hydroxyflavone,[24] 8-hydroxyquinoline,[25,26] and imidazoline.[27] Prime reason for lesser development of zinc(II) ion specific sensors is the poor coordination of ligands towards bivalent zinc, in comparison with other common transition metal ions. However, design and synthesis of Zn^{2+} ion specific fluorescent probes have received intense attention. Thus, a sensitive and non-invasive technique to trace and visualize free zinc(II) ions would be of high demand. Zinc(II) ion itself is spectroscopically silent due to its $3d^{10}$ $4s^{0}$ electronic configuration. In addition, it is still a challenge to develop fluorescent sensor which can discriminate Zn^{2+} ion from Cd^{2+} ion, as both belong to same group of the periodic table having similar properties, thus rendering similar changes after interacting with fluorescent sensors.[28-35] Among imidazoles, compounds containing benzimidazole ring,[36,37] 2-(imidazol-2-yl)phenol,[38] imidazoles substituted with 1-10-phenanthroline[39] or pyridine[40] were widely used as

cation and anion sensors. In spite of these few reports, sensing of Zn^{2+} ion using imidazole ring bearing pyridyl groups is lacking. In this sense, development of highly sensitive and selective fluorescent sensors for zinc(II) ion is of critical importance.[41-47] In this report, we describe selective recognition of zinc(II) ion using a tris-pyridyl substituted imidazole *viz*., 2,4-bis(2-pyridyl)-5-(4-pyridyl)imidazole (**L1H**, Scheme 1) by fluorescence titration technique, supported by single crystal X-ray diffraction analysis.

3.2. Experimental section:

*3.2.1. Synthesis of [Zn_2(**L1**)Cl_3(H_2O)] (**1**)*

A methanol solution of $ZnCl_2$ (816 mg, 6 mmol) was added slowly to a magnetically stirred methanol solution (20 mL) of **L1H** (897 mg, 3 mmol). Stirring was continued for about 6 h, the yellow precipitate deposited was filtered, washed with cold methanol several times and kept in air till it is dry. Yield 1.25 g (75%). A part of the precipitate was dissolved in DMF, left undisturbed at ambient temperature and block shaped single crystals suitable for X-ray crystallography were collected after 15 days. FT-IR (KBr, cm^{-1}): 3436(br), 1621(w), 1607(vs), 1570(w) 1516(w), 1497(m), 1463(s), 1427(w), 1289(w), 1258(w), 1221(w), 1190(w), 1160(w), 1105(w), 1065(w), 1028(m), 995(m), 848(m), 793(m), 753(m), 713(m), 706(m), 6434(m), 551(w), 504(w), 478(w), 414(w). ESI-MS(+): *m/z* calcd. for $C_{18}H_{12}Cl_2N_5Zn_2$ 497.902 found 497.890 (Figure A1). Anal. calcd. for $C_{18}H_{14}Cl_3N_5OZn_2$ C 39.06; H 2.55; N 12.65 found C 38.90; H 2.48; N 12.51.

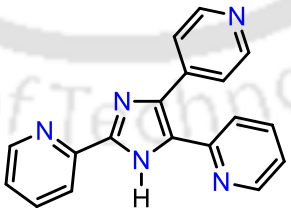

L1H

Scheme 1. Ligand used in this Chapter.

3.3. Result and discussion:

The selectivity of **L1H** towards cations in DMSO and HEPES buffered aqueous DMSO solution (pH = 7.4, 2:8, *v*/*v*) was examined using UV-visible and fluorescence

spectroscopy. Absorption and fluorescence emission spectra were recorded for the titrations of **L1H** with chloride salts of group I (Li^+, Na^+ and K^+), group II (Mg^{2+} and Ba^{2+}), and transition metal ions (Mn^{2+},Cr^{3+}, Fe^{3+}, Co^{2+}, Ni^{2+}, Cu^{2+}, Zn^{2+}, Cd^{2+}, Hg^{2+} and Ag^+) as well as Al^{3+} and Pb^{2+}.

3.3.1. UV-Vis spectroscopic studies of L1H in presence of metal ions:

UV-Vis spectrum of **L1H** in DMSO (1.0×10^{-5} mol L^{-1}) exhibited an absorption maximum at 318 nm, which possibly be attributed to $\pi \rightarrow \pi^*$ transition (*vide infra*). The absorption maximum of **L1H** remains unchanged upon addition up to five equivalents of univalent alkali metal and alkaline earth metal chlorides. Upon addition of Al^{3+}, Cr^{3+}, Fe^{3+}, Mn^{2+}, Cd^{2+}, Hg^{2+}, Pb^{2+} and Ag^+ spectrum remained unaltered (Figure 1). Interestingly, it was observed that in cases of Co^{2+}, Ni^{2+}, Cu^{2+} and Zn^{2+} chlorides, the absorption of **L1H** at 318 nm gradually decreased with increase in metal ion concentration.

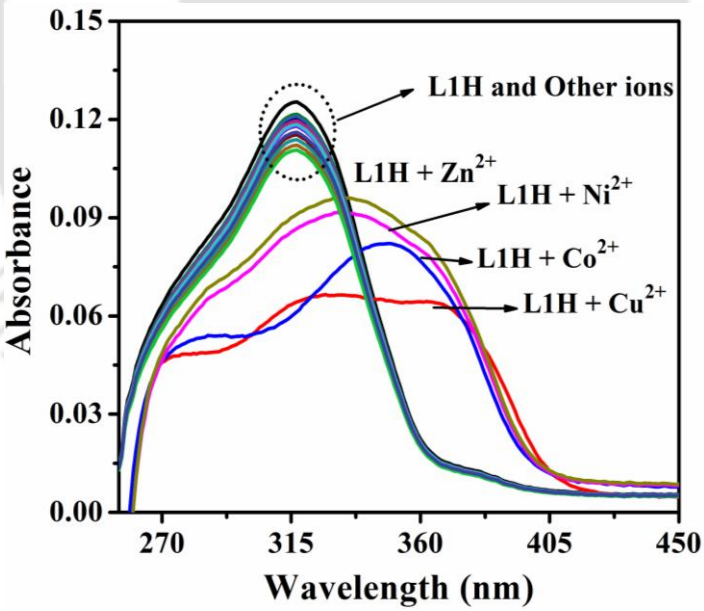

Figure 1. Changes in UV-Vis spectra of receptor **L1H** (10 μM) upon incremental addition of other metal ions Li^+, Na^+, K^+, Mg^{2+}, Ba^{2+}, Al^{3+}, Cr^{3+}, Fe^{3+}, Mn^{2+}, Cd^{2+}, Hg^{2+}, Pb^{2+}, Ag^+, Co^{2+}, Ni^{2+}, Cu^{2+} and Zn^{2+} in DMSO.

A new band (red shift) appeared at 352-366 nm and grew in intensity along with formation of isosbestic point at ~337 nm. Presence of an isosbestic point is a clear

indication of existence of only two chemical species at equilibrium in solution (Figure 2–4).

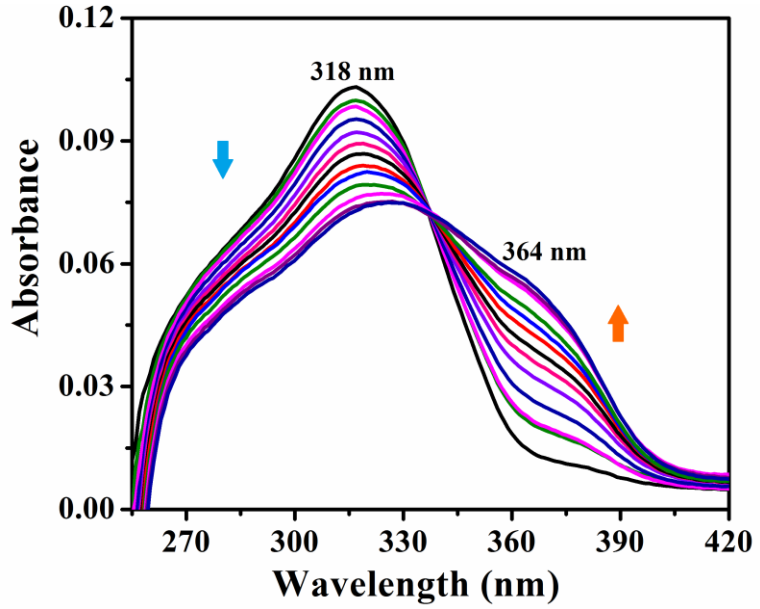

Figure 2. Changes in UV-Vis spectra of receptor **L1H** (10 μM) upon incremental addition of $ZnCl_2$ in DMSO.

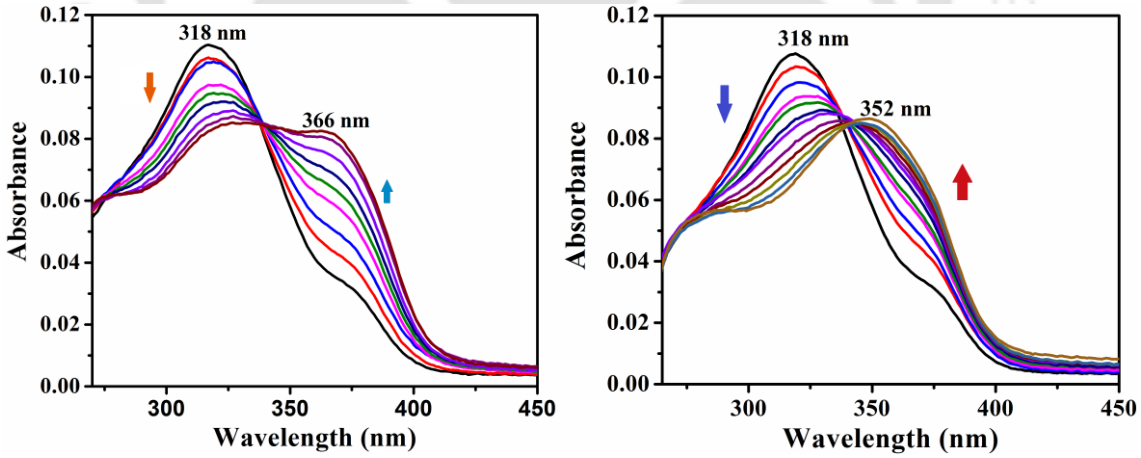

(**a**) (**b**)

Figure 3. Changes in UV-Vis spectra of receptor **L1H** (10 μM) upon incremental addition of (a) $CuCl_2$ (b) $CoCl_2$ in DMSO.

To check the sensitivity of Zn^{2+} ion in aqueous media, UV-Vis spectrum of **L1H** in HEPES buffered aqueous DMSO solution (5 mM, pH = 7.4, 2:8, *v*/*v*) had also been carried out and exhibited same pattern as observed in pure DMSO medium (Figure 5).

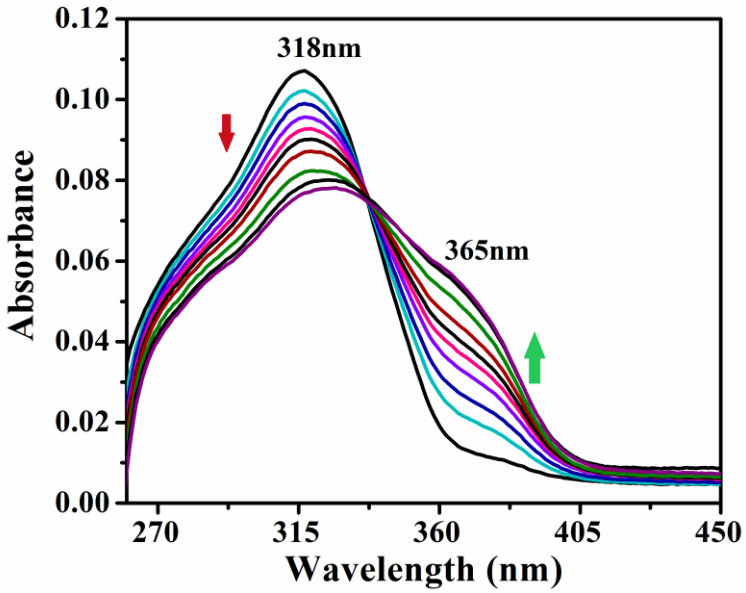

Figure 4. Changes in UV-Vis spectra of receptor **L1H** (10 μM) upon incremental addition of $NiCl_2$ (0-3 equivalents) in DMSO.

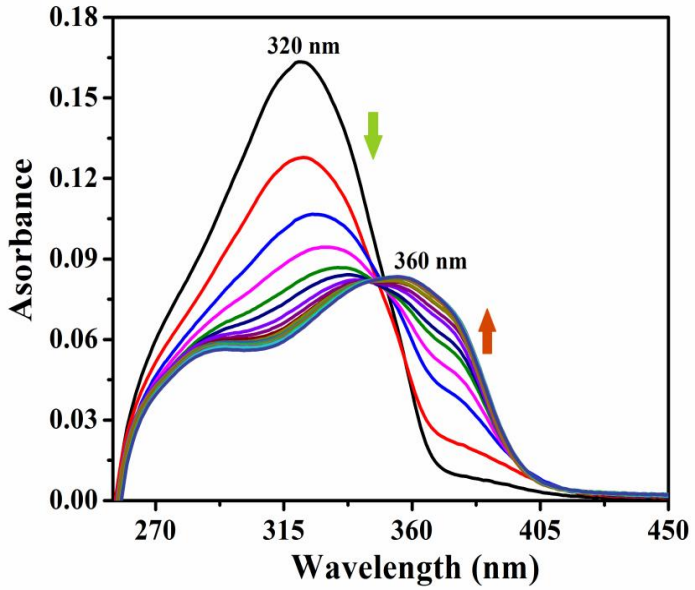

Figure 5. Changes in UV-Vis spectra of receptor **L1H** (10 μM) upon incremental addition of $ZnCl_2$ (0-3 equivalents) in HEPES buffered aqueous DMSO solution (5 mM, pH = 7.4, 2:8, *v*/*v*). Same for Co^{2+}, Cu^{2+}, and Ni^{2+} ions have been displayed in Figure A2.

3.3.2. Fluorescence spectroscopic studies of L1H in presence of metal ions:

The DMSO solution of **L1H** upon irradiation with λ = 320 nm shows an emission at λ_{em} = 391 nm. In order to find out the possible selective behaviour of **L1H** towards metal

chlorides noted in the UV-Vis spectroscopic studies, a series of fluorometric titrations of **L1H** by adding different metal salts were examined. On titration of **L1H** with metal chlorides of Na^{+}, Li^{+}, K^{+}, Ca^{2+}, Mg^{2+}, Ba^{2+}, Hg^{2+}, Pb^{2+}, Al^{3+} and Cr^{3+} no change in the emission of λ_{em} = 391 nm was observed. However, addition of Mn^{2+}, Cd^{2+} and Fe^{3+} ions resulted in a partial (~40%) quenching of fluorescence emission (Figure A3). In case of Cu^{2+}, Ni^{2+} and Co^{2+} ions a near complete quenching of the fluorescence emission at λ_{em} = 391 nm was observed understandably, due to the paramagnetic nature of these metal salts (Figure A3).

Importantly, it was observed in case of $ZnCl_2$ that addition of Zn^{2+} ion to **L1H** solution lead to gradual decrease in emission band intensity at 391 nm along with appearance of a new emissive band (red shift) at 445 nm, which grew in intensity with increasing Zn^{2+} ion concentration. This was accompanied by a quasi isoemissive point at 413 nm as shown in Figure 6.

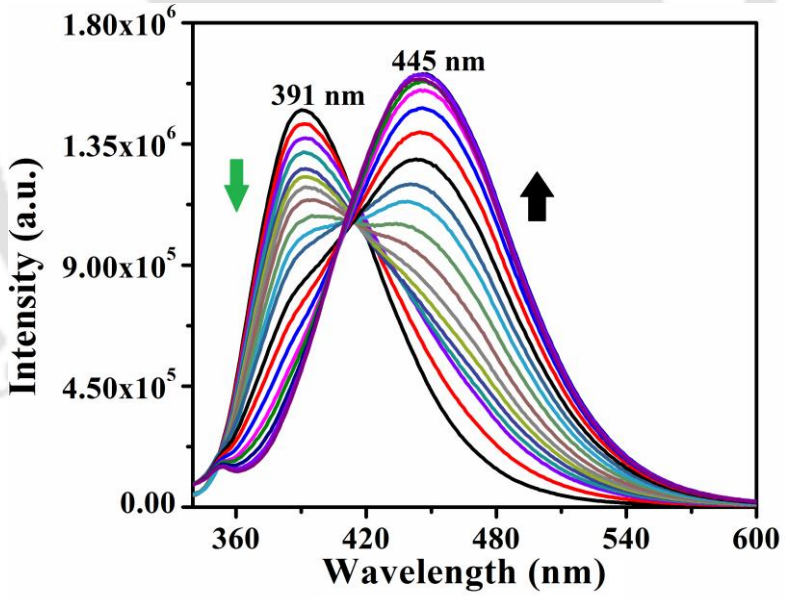

Figure 6. Fluorescence titration spectra of **L1H** (10 μM) upon incremental additions of $ZnCl_2$ (0-3 equivalents) in DMSO (λ_{ex} = 320 nm).

Binding of Zn^{2+} to **L1H** led to red shift due to the capture of Zn^{2+} ion by the receptor **L1H** whereas other metal ions did not display any spectral shift in fluorescence emission and this indicated a difference in binding of zinc with **L1H** with respective to other metal ions (Figure 7).

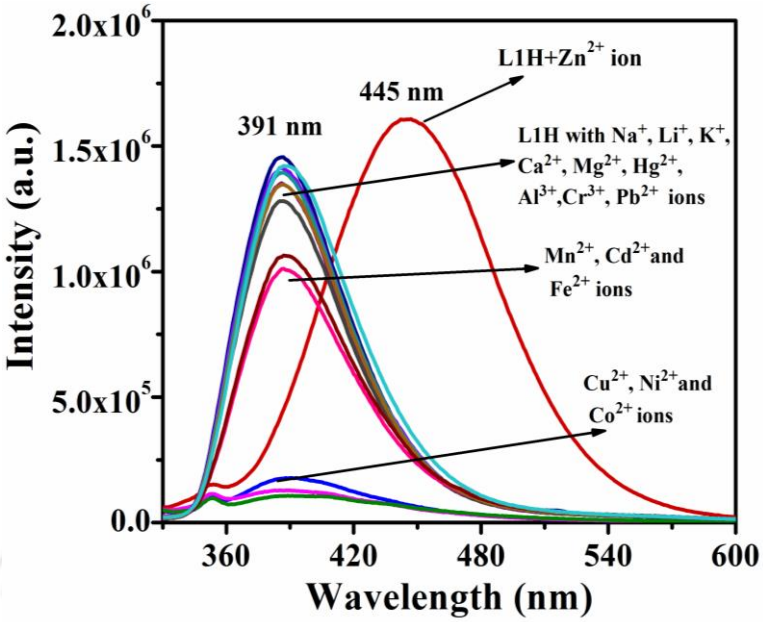

Figure 7. Changes in fluorescence emission of receptor **L1H** (10 μM) observed upon addition of chloride salts (50 μM) of metal ions in DMSO.

Titration experiment to understand the sensing ability of **L1H** towards Zn^{2+} ion was also carried out in buffered aqueous DMSO solution (pH = 7.4, 2:8, *v*/*v*). In this solution **L1H** showed the emission maximum at 396 nm upon excitation with 320 nm and with the increase in Zn^{2+} ion concentrations emission at 445 nm was observed (Figure 8). Upon increasing ratio of water beyond 20%, the quasi isoemissive point starts disappearing due to the broadening of emission band (Figure 9). This broadening is probably due to insolubility of complex molecule in water resulting in its crystallization from the medium.

The large red shift observed for **L1H** upon addition of Zn^{2+} ion originates from deprotonation of acidic hydrogen from imidazole ring. This is necessary for retaining aromaticity of the ring as well as to coordinate in *bis*-bidentate fashion. Two 2-pyridyl rings in the uncoordinated **L1H** are twisted, which as a consequence of deprotonation and *bis*-bidentate coordination upon complexation with zinc ion, attain a near-planar orientation with imidazolate ring. This results in efficient π-electron delocalization and a distinct red shift in emission spectrum which correspond to the high selectivity of bivalent zinc by **L1H**.

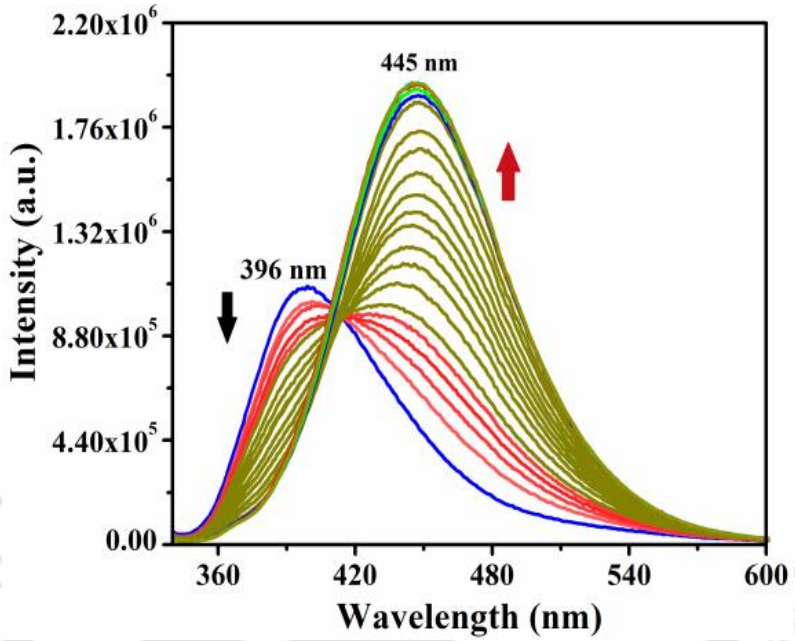

Figure 8. Fluorescence responses of **L1H** (λ_{ex} = 320 nm) with Zn^{2+} ion in HEPES buffer-DMSO (pH = 7.4, 2:8, *v*/*v*).

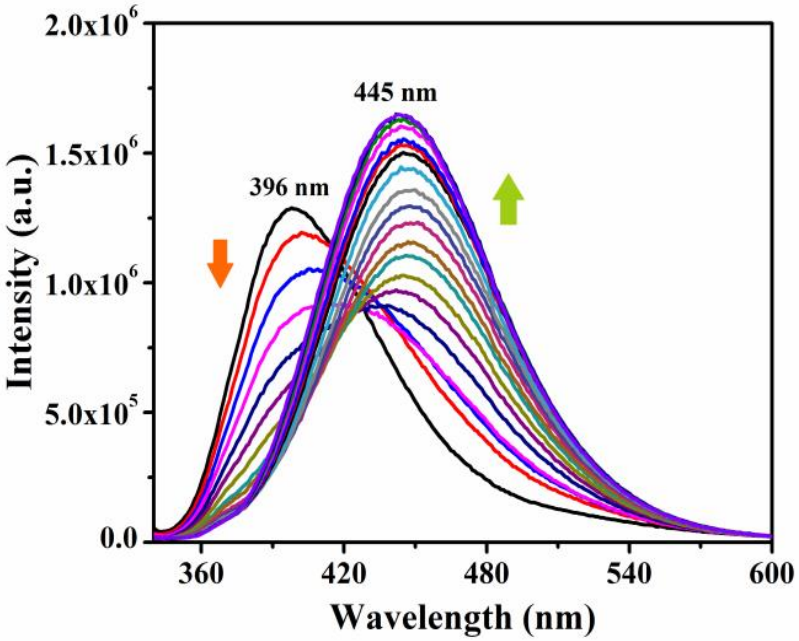

Figure 9. Fluorescence responses of **L1H** with Zn^{2+} ion in HEPES buffer-DMSO (pH = 7.4, 7:3, *v*/*v*).

Job's plot analysis (Figure 10) reveals the maximum emission at 2:1 ratio (Zn^{2+}:**L1H**), which is also in good agreement with X-ray crystal structure of zinc

complex. The binding constant of **L1H** with Zn^{2+} has been determined using the Benesi–Hildebrand equation $1/\Delta I = 1/\Delta I_{max} + (1/K[C]^n) \times (1/\Delta I_{max})$ by the fluorescence method.[48] Here $\Delta I = (I_x - I_0)$ and $\Delta I_{max} = I_\infty - I_0$, where I_0, I_x, and I_∞ are the emission intensities of **L1H** in the absence of Zn^{2+} ion, at an intermediate Zn^{2+} ion concentration, and at a concentration of the complete interaction, respectively. K is the binding constant, C is the concentration of Zn^{2+} ion and *n* is the number of Zn^{2+} ion bound to each **L1H** (here $n = 2$). The value of K was found to be 3.5×10^8 M^{-2} in DMSO and 6.67×10^7 M^{-2} (Figure 11) in buffer-DMSO solution. According to the IUPAC convention using equation mentioned above, the detection limit was calculated to be 6.5×10^{-7} M, which is below the US EPA permissible levels for Zn^{2+} ion in drinking water (Figure 12).

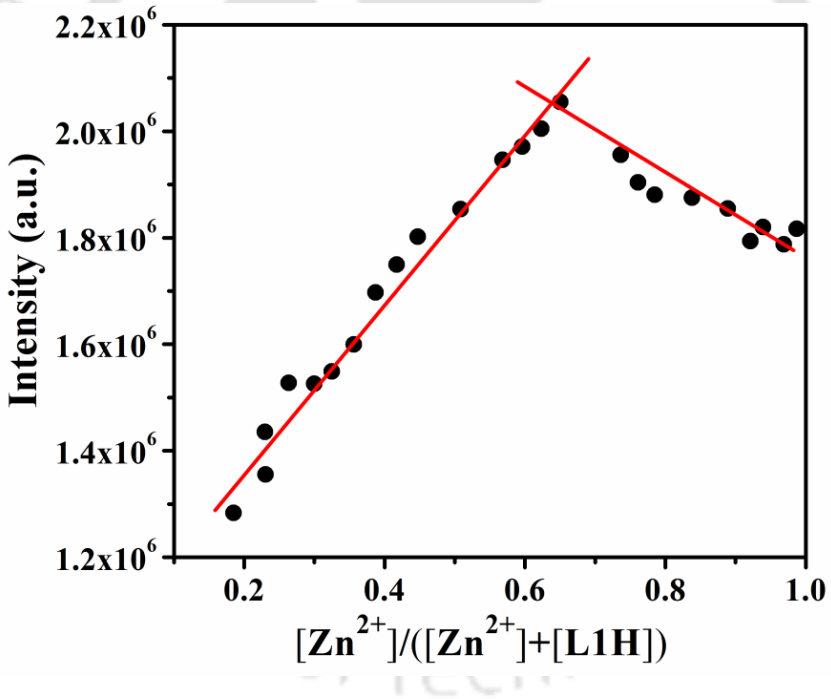

Figure 10. Job's plot shows the 1:2 binding of **L1H** to Zn^{2+} ion.

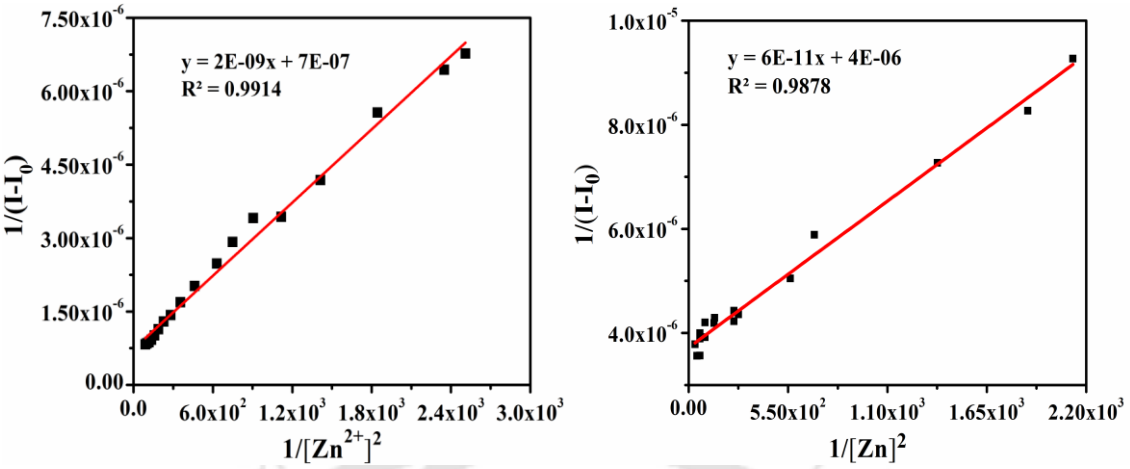

(**a**) (**b**)

Figure 11. Benesi-Hildebrand plot for determination of binding constant of **L1H** (10 μM) with Zn^{2+} ion in (a) DMSO and (b) HEPES buffer-DMSO (pH = 7.4, 2:8, *v*/*v*).

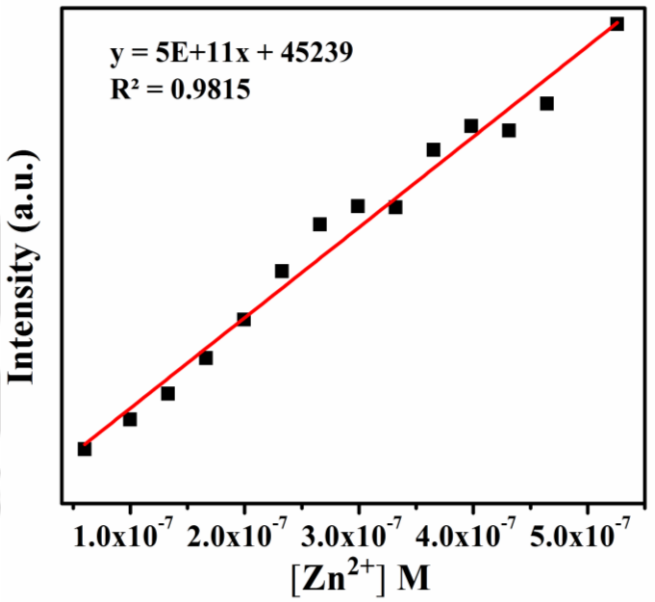

Figure 12. Fluorescence intensity *vs.* concentration of Zn^{2+} ion plot for determination of detection limit ([**L1H**] = 10 μM).

3.3.3. ^{1}H-NMR titration:

The ^{1}H-NMR titration experiment was carried out (Figure 13) for receptor **L1H** with the $ZnCl_2$. Interestingly, the broad peak at 11.049 ppm (for -NH proton) gradually decreased in intensity along with slight shift towards down field. In addition other signals shifted slightly and showed signs of small peak broadening. The acidic proton

completely disappeared due to the binding of Zn^{2+} ion. Whereas, other proton signals shifted in certain degrees, the peak shapes broadened and some new signals appeared and this revealed the co-ordination of **L1H** with Zn^{2+} metal ion.

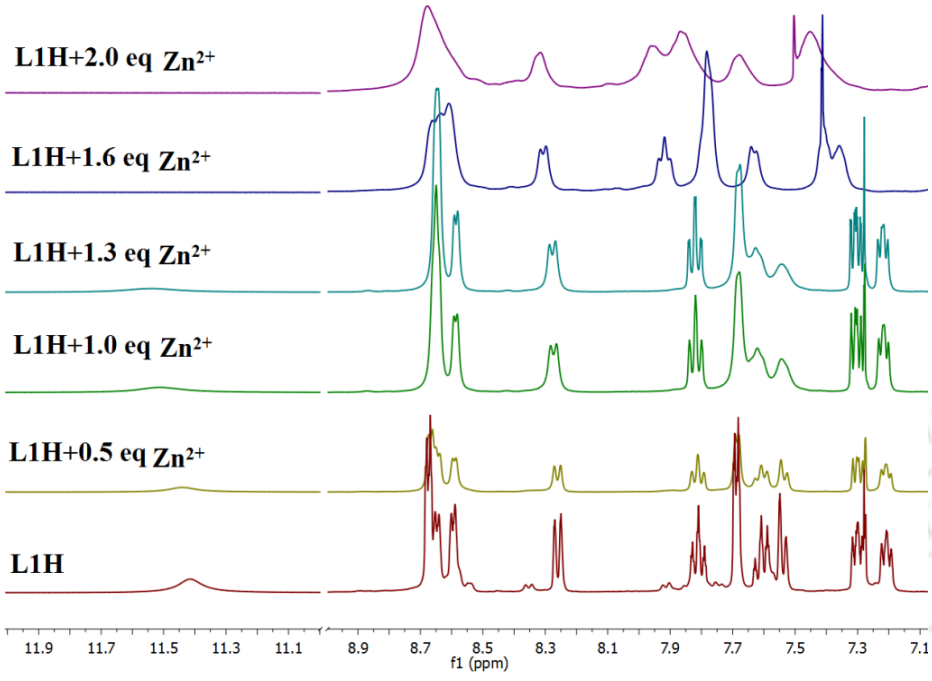

Figure 13. ^{1}H NMR (400 MHz) spectral changes of **L1H** in $CDCl_3$ upon addition of $ZnCl_2$ in 1:4 mixture of CD_3OD and $CDCl_3$.

3.3.4. Effect of pH:

The fluorescence intensities of free **L1H** and in presence of Zn^{2+} ion at various pH values were also measured. The fluorescence intensity of **L1H** decreased slightly at acidic pH and reached the maximum intensity in the pH range 6-10. At higher pH 11-14, emission at 396 nm was very weak (Figure 14). There is no appreciable sensing of Zn^{2+} ion at acidic pH due to the competition of H^{+} ion at pH below 6. However, Zn^{2+} ion induced a red shift in emission of **L1H** occurring in the pH range 6-9. The emission intensity at 445 nm, induced by Zn^{2+} ion, was quenched at higher pH (Figure 14). The quenching effect at alkaline solutions could be due to the formation of $Zn(OH)^{-}$ or $Zn(OH)_2$ that hindered formation of the complex.[49]

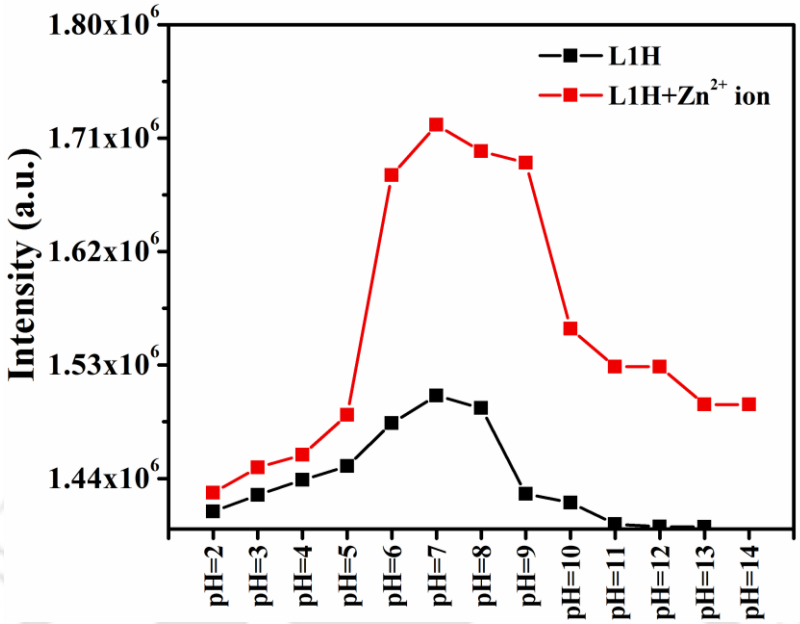

Figure 14. Fluorescence intensities of **L1H** (λ_{em} = 396 nm) and **L1**–Zn^{2+} (λ_{em} = 445nm) at various pH values in HEPES buffer-DMSO solution (5 mM, 2:8, *v*/*v*, λ_{ex} = 320 nm). ([**L1H**] = 0.10 μM).

3.3.5. Metal ion competition studies:

The individual emission response of **L1H** against different transition metal ions revealed a remarkable selectivity of Zn^{2+} ion binding. However, the most important criterion for selective cation probe is the ability to detect the specific cation in the vicinity of other competitive ions. To further explore the selectivity of **L1H** for Zn^{2+} ion, we measured the fluorescence intensity of **L1H** in presence of Zn^{2+}, mixed with various metal ions in DMSO. The emission intensity of Zn^{2+} bound **L1H** is unperturbed in presence of 5 equivalents of metal ions such as Na^{+}, K^{+}, Li^{+}, Ca^{2+}, Mg^{2+}, Mn^{2+}, Hg^{2+}, Pb^{2+}, Cd^{2+}, Ag^{+}, Al^{3+} and Cr^{3+} indicating the high selectivity for Zn^{2+} ion over these biologically competing cations (Figure 15). Addition of metal ions up to 8 equivalents doesn't lower the selectivity but beyond this about 10-15% decrease in intensity was observable. While metal ions Cu^{2+}, Co^{2+} and Ni^{2+} quenched the fluorescence intensity obtained by the Zn^{2+} ion bound **L1H** (Figure A4). The quenching of emission may be originated from the spin-orbit quenching mechanism associated with the heavy metals or displacement of Zn^{2+} by Cu^{2+}, Co^{2+} and Ni^{2+} from **L1**-Zn^{2+} complex.[49-52]

Additionally, we investigated the absorption titration of Cu^{2+}, Co^{2+} and Ni^{2+} and these were similar to that of **L1**-Zn^{2+} (Figure 3, 4). The stability constant of Cu^{2+}, Co^{2+} and Ni^{2+} were 3.85×10^8 M^{-1}, 3.63×10^8 M^{-1} and 3.59×10^8 M^{-1} respectively (Figure 16, 17), which are greater than that of **L1**-Zn^{2+}. This result concluded that Cu^{2+}, Co^{2+} and Ni^{2+} ions could form the complex with **L1H** and quench the fluorescence. There are many fluorescence sensors which have exhibited similar depressed responses due to the competition from these ions (Cu^{2+}, Co^{2+} and Ni^{2+}).[53-57] However these free cations would have little influence *in vivo* because they exist in very low concentration.[22, 58-60] Thus **L1H** has high binding affinity and low detection limit which can be used to detect Zn^{2+} ion in chemical, environmental, and biological systems. Also Zn^{2+} ion can be selectively detected by **L1H** without any interference from same group ions Cd^{2+} and Hg^{2+} at physiological pH.

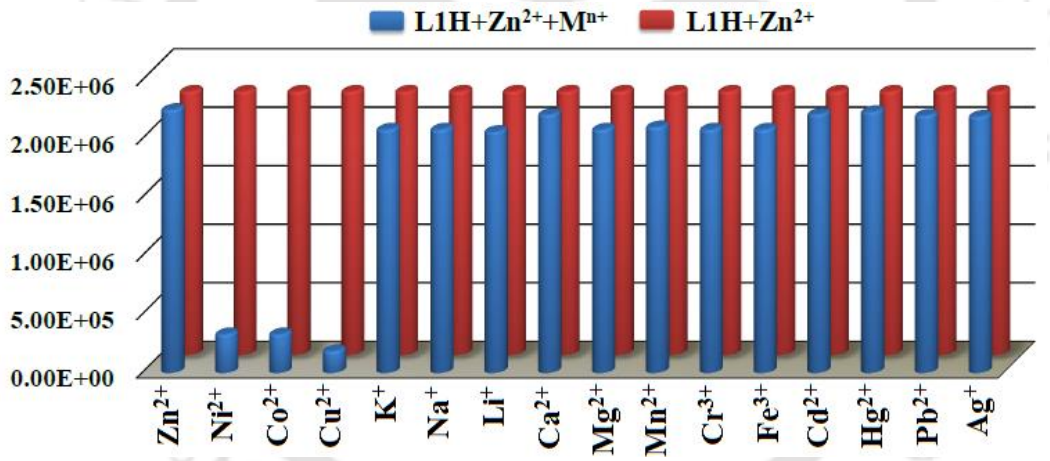

Figure 15. Fluorescence response of **L1H** (10 µM) in presence of Zn^{2+} ion with addition of various metal ions in DMSO (λ_{em} = 445 nm). The blue bars represent the Fluorescence emission of solution containing **L1H** (10 µM) and 2.5 equivalents of Zn^{2+} ion. The red bars show the fluorescence change that occurs upon addition of 5 equivalents of corresponding cations to the above solution.

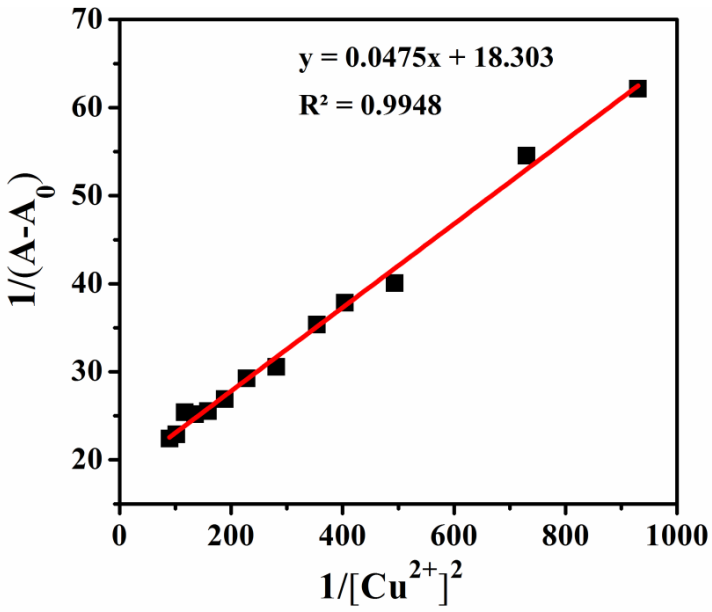

Figure 16. Benesi-Hildebrand plot for **L1H**-Cu^{2+} ion complex obtained from the UV-Vis studies in DMSO.

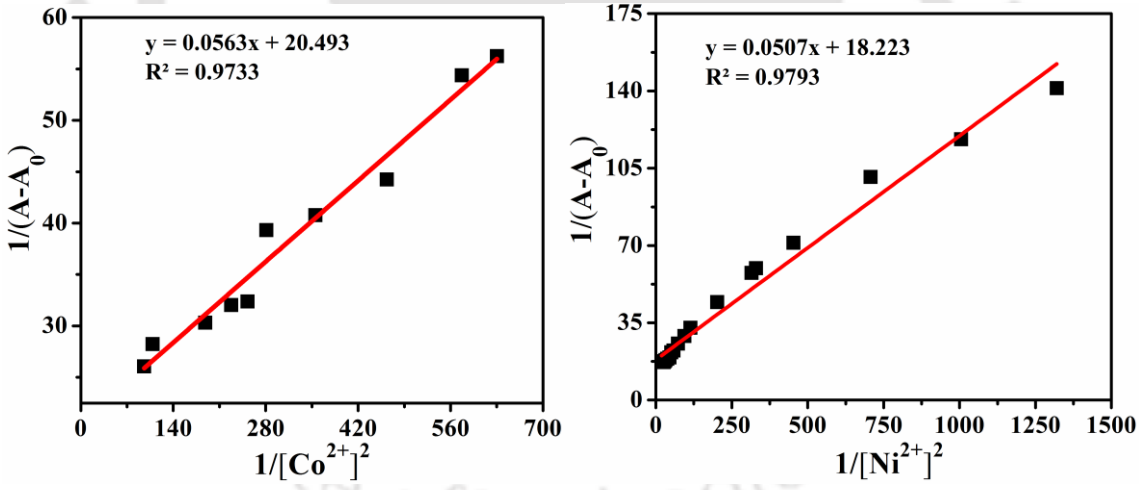

Figure 17. Benesi-Hildebrand plot for (a) **L1H**-Co^{2+} (b) **L1H**-Ni^{2+} ion complex obtained from the UV-Vis studies in DMSO.

3.3.6. Selectivity of L1H toward Zn^{2+} ion in presence of various anions:

The selectivity of **L1H** toward Zn^{2+} ion in presence of various anions such as citrate, lactate, carbonate, F^-, Br^-, Cl^-, I^-, HCO_3^-, SO_4^{2-}, PF_6^-, NO_3^-, HPO_4^{2-}, $H_2PO_4^-$, OAc^- and ClO_4^- were checked. In presence of all other anions except $H_2PO_4^-$, emission

intensity at 445 nm increased with concomitant decrease in intensity of 391 nm, while increasing concentrations of Zn^{2+} ion. Only in presence of $H_2PO_4^-$, red shifted band at 445 nm was not observed (Figure 18 and 19).

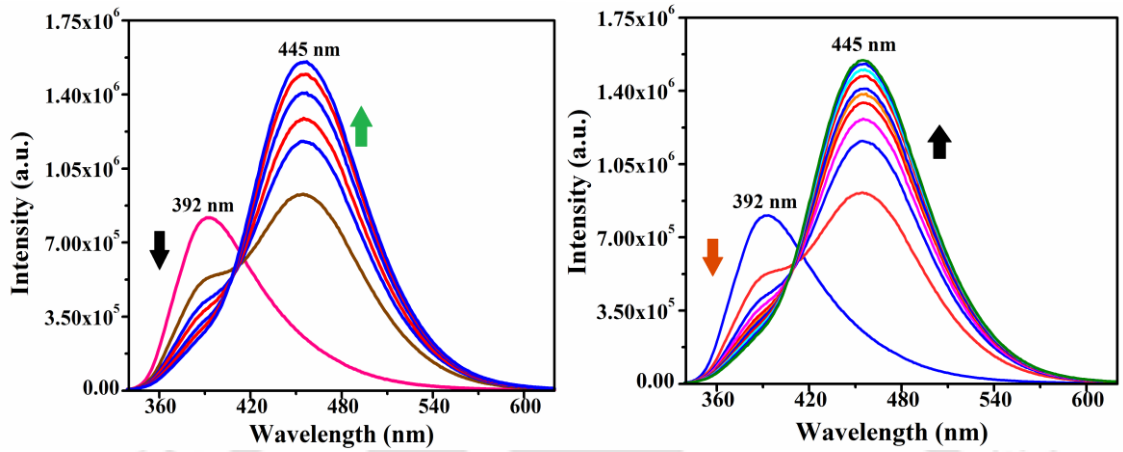

Figure 18. Fluorescence response of **L1H** (10 µM) toward Zn^{2+} ion in presence of (a) Citrate and (b) Lactate ions.

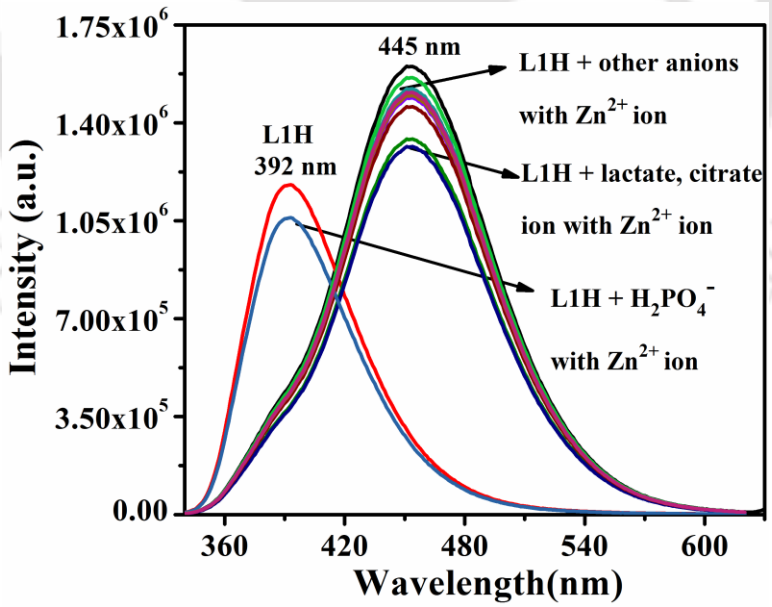

Figure 19. Fluorescence response of **L1H** (10 µM) toward Zn^{2+} ion in presence of various anions such as citrate, lactate, carbonate, F^-, Br^-, Cl^-, I^-, HCO_3^-, SO_4^{2-}, PF_6^-, NO_3^-, HPO_4^{2-}, $H_2PO_4^-$, OAc^- and ClO_4^- in DMSO.

3.3.7. X-ray diffraction studies:

*3.3.7.1. Crystal structure of **1**:*

In order to ascertain the nature of binding of **L1H**[61] to zinc and to analyze orientation of pyridyl rings relative to the imidazole ring, molecular structures of **1** and **L1H** were determined using single crystal X-ray diffraction analysis. The crystallographic refinement parameters are listed in Table 1. Compound **1** crystallized in *R*-3*c* space group and the asymmetric unit contains (i) one ligand in its conjugate base (**L1**$^{-}$) form; (ii) three coordinated chloride ions; (iii) a full occupancy zinc (Zn3); (iv) two half-occupancy zinc centers (Zn1 and Zn2) lying on a two-fold axis and (v) a coordinated water molecule bound with Zn1. A schematic diagram is shown in Figure 20 and selected bond distances and angles are appended.

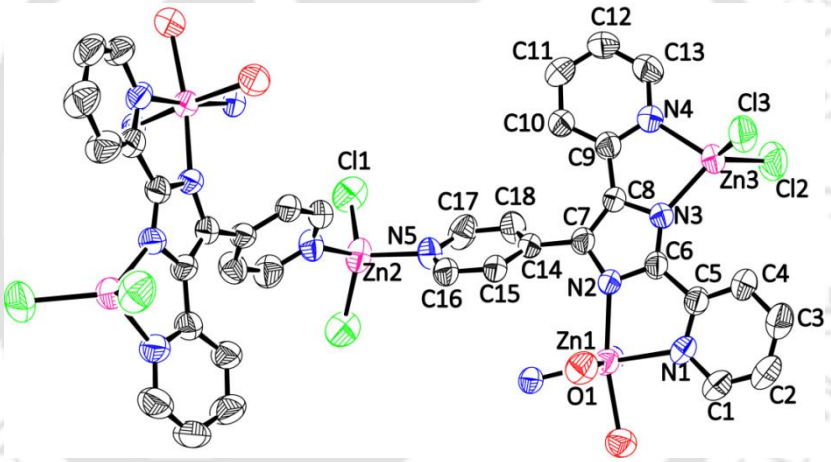

Figure 20. ORTEP (40% probability level) diagram of **1** (all hydrogen atoms are omitted for clarity). Selected bond lengths (Å) and angles (°): Zn1-N2, 2.121(5); Zn1-N2, 2.121(5); Zn1-O1, 2.172(6); Zn1-O1, 2.172(6); Zn1-N1, 2.172(6); Zn2-N5, 2.017(6); Zn2-Cl1, 2.224(3); Zn2-Cl1, 2.224(3); Zn3-N3, 2.020(5); Zn3-N4, 2.069(6); Zn3-Cl3, 2.225(3); Zn3-Cl2, 2.226(3). N2-Zn1-N2, 92.4(3); N2-Zn1-O1, 167.1(2); N2-Zn1-O1, 90.5(2); N2-Zn1-O1, 90.5(2); N2-Zn1-O1, 167.1(2); O1-Zn1-O1, 89.4(3); N2-Zn1-N1, 106.6(2); N2-Zn1-N1, 77.8(2); O1-Zn1-N1, 86.3(2); O1-Zn1-N1, 89.3(2); N2-Zn1-N1, 77.8(2); N2-Zn1-N1, 106.6(2); O1-Zn1-N1, 89.3(2); O1-Zn1-N1, 86.3(2); N1-Zn1-N1, 173.8(3); N5-Zn2-N5, 111.8(4); N5-Zn2-Cl1, 105.6(2); N5-Zn2-Cl1, 108.6(2); N5-Zn2-Cl1, 108.6(2); N5-Zn2-Cl1, 105.6(2); Cl1-Zn2-Cl1, 116.77(14); N3-Zn3-N4, 81.6(2); N3-Zn3-Cl3, 119.12(19); N4-Zn3-Cl3, 113.0(2); N3-Zn3-Cl2, 113.81(18); N4-Zn3-Cl2, 112.2(2); Cl3-Zn3-Cl2, 113.25(11).

In **1**, **L1**$^{-}$ ion acts as a penta-dentate ligand and is bound to all the three types of zinc(II) ions thus bridging them. Specifically, it is bound in *bis*-bidentate fashion coordinating through two pairs of 2-pyridyl and imidazolate nitrogen atoms (N_{2P} and N_I) as well as in the mono-dentate fashion coordinating through 4-pyridyl nitrogen (N_{4P}). Three Zn^{2+} ions differ in their coordination environments with (i) Zn1 having a distorted octahedral *trans-cis-cis*-$(N_{2P})_2(N_I)_2(O_W)_2$; (ii) Zn2 and Zn3 respectively having a distorted tetrahedral $(N_{4P})_2Cl_2$ and $N_{2P}N_ICl_2$ centers {N_{2P} = 2-pyridyl-N; N_{4P} = 4-pyridyl-N; N_I = imidazolate-N; O_W = water-O}. Additionally, the two zinc ions Zn1 and Zn3 bridged by the planar arm of imidazolate ring further clamped by node at Zn2 through the 4-pyridyl rings of two different ligand units generate a bowl shaped unit. These two types of metal to ligand connections *viz.*, (a) Zn1 and Zn3 centers bridged by imidazolate ring; (b) Zn2 center linked by 4-pyridyl rings make a one dimensional coordination polymer along *c*-axis as shown in Figure 21. Probably this fashion of binding is unique for bivalent zinc as its chloride salt with **L1H** over the rest of the metal ions discussed in this work.

In Zn1, both five membered chelate rings are *cis* to each other, and bond distances at metal center follow the trend $Zn–N_I < Zn–N_{2P} \cong Zn–O_W$, with $Zn–N_I$ being shorter by ~0.051(6) Å. Whereas in Zn2, the central metal is tetra-coordinated having a distorted tetrahedral geometry, and the $Zn–N_{4P}$ distance being expectedly shorter than Zn–Cl distance by 0.207(6) Å. In Zn3, the bivalent zinc also adopts a distorted tetrahedral geometry, $Zn–N_I$ being shorter than $Zn–N_{2P}$ by ~0.049(6) Å and two Zn–N distances are shorter than Zn–Cl distances which lie in the range 0.157(6)–0.206(6) Å. Overall, on comparing all the metal to ligand bond distance, the trend $Zn–N_I < Zn–N_{2P} \cong Zn–N_{4P} \cong Zn–O_W < Zn–Cl$ is observable. The hydrogen bonding interaction O1···Cl1 (3.117(7) Å) and the supramolecular interactions C10–H10···Cl2 (C10···Cl2, 3.58(1) Å) and C16–H16···Cl2 (C16···Cl2, 3.69(1) Å) generate a honey-comb like structure with large voids (Figure 22) having volume of ~9143 Å^3 having a 3-fold rotational axis its center.

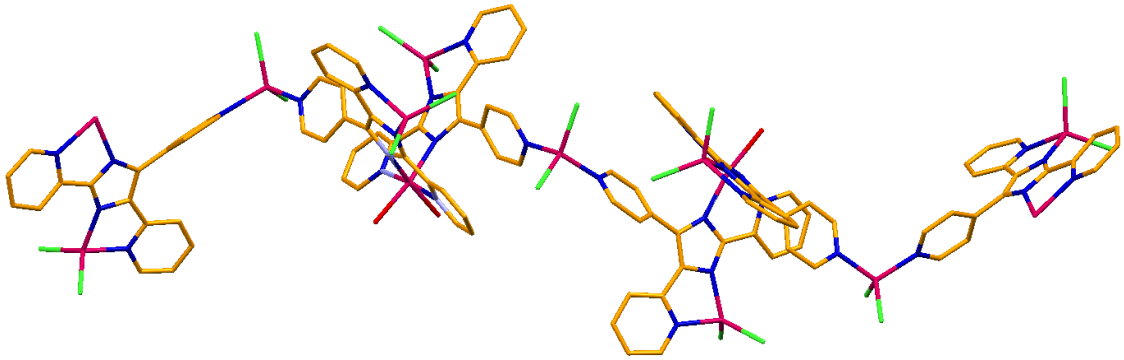

Figure 21. 1D-coordination polymer of **1** (all hydrogen atoms are omitted for clarity).

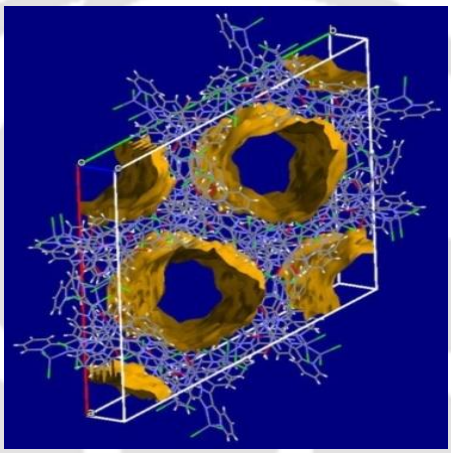

Figure 22. Large voids in complex **1**.

*3.3.7.2. Crystal structure of **L1H**:*

The single crystal of ligand **L1H·6H$_2$O** was obtained by slow evaporation of methanol solution, which crystallized in $P2_1/n$ space group and a schematic diagram is shown in Figure 23. Important difference between **L1H** and **1** lie in dihedral angles between imidazole ring and three pendent pyridyl rings. The major difference in torsional angle is observed along one of the 2-pyridyl rings. In **L1H**, the dihedral angle at C7C8C9N4 is 61(1)° which is about 56(1)° higher than that is observed in **1** (175.5(9)°). While a comparable angle for N1C5C6N2, 7(1)° (in **L1H**) and 9(1)° (in **1**) observed may be due to interaction of lone-pair of electron present in N2 with N1–H of the imidazole ring in **L1H**, but this N1–H has been replaced with N1–Zn1 coordinate bond in **1**. The dihedral angle C8C7C14C15, 27(1)° (in **L1H**) and 127.2(9)° (in **1**) of the 4-pyridyl ring also differ by ~26(1)°.

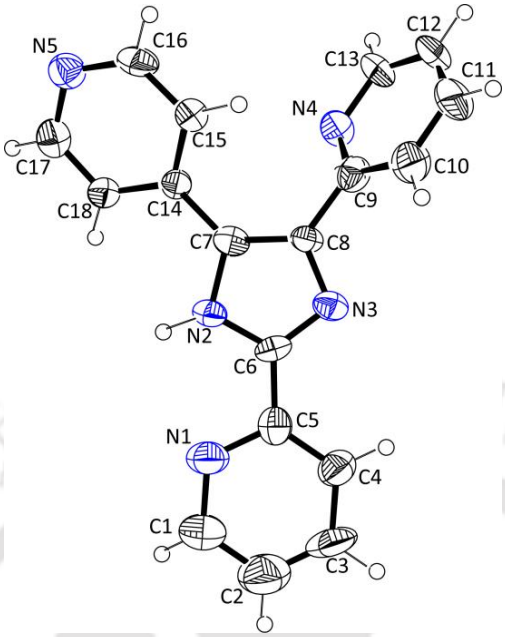

Figure 23. ORTEP (40% probability level) diagram of **L1H**.

The ligand **L1H** form the 1D chain like structure linked by N–H···N (N2···N4, 2.90(1) Å) interaction that occur between the imidazole N–H and nitrogen 2-pyridyl ring of another unit of ligand. In addition, π···π interactions (Figure 24) between adjacent rings are present with non-bonded distances of C5·· C16 3.30(1); C6·· C15 3.34(1); C6·· C18 3.36(1) Å. These 1D chain like structure are arranged to a 2D channels through hydrophobic interactions (Figure 25). These are further separated by hydrophilic channels formed by H-bonded lattice water molecules interlinked by tetrameric, pentameric and hexameric cyclic H-bonds (Figure 24).

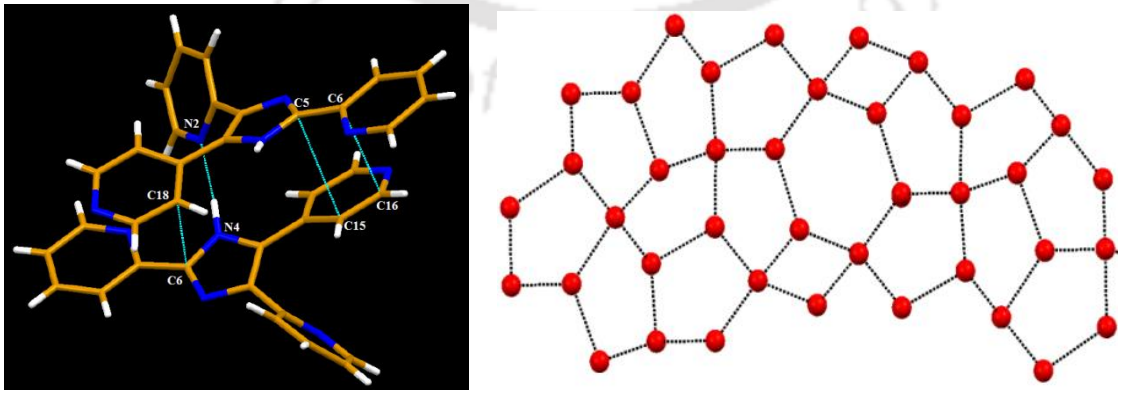

Figure 24. π···π and N–H···N interactions (left) and hydrogen-bonding interactions between the aqua molecules (right, broken lines represent hydrogen bonds) in **L1H**.

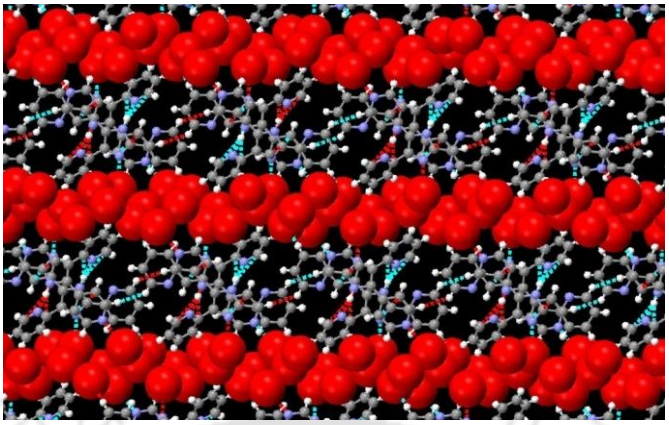

Figure 25. Water channel present along *b* axis in packing diagram of **L1H**.

3.3.8. Computational studies:

Electronic structure calculations employing density functional theory (DFT/TDDFT) have been carried out on the fixed crystal geometry of **L1H** with the B3LYP/6-31G(d,p) basis set using the Gaussian 09 program.[62] Major observation is that HOMO-LUMO energy gap in **L1H** is calculated to be 4.1097 eV (Figure 26). The HOMO electron density is distributed on a π orbital of **L1H**, while the LUMO is of π* type. From TDDFT calculation, results revealed that the major band in the UV region is at 326 nm due to the transitions from HOMO to LUMO which is closer to the experimental UV-Vis absorption maxima at 318 nm (Figure 27). Even though we could not successfully complete the calculation on complex 1, but it is likely that binding of the Zn^{2+} ions stabilize LUMO to a greater extent than HOMO and effectively lowering the HOMO-LUMO energy gap, thus a red shift in fluorescence emission was observed. It is also relevant to note that in a recent report,[63] calculations on structurally related molecule, 2,4,5-tris(2-pyridyl)imidazole predicted that UV-Vis spectrum observed at a maximum of 334 nm arose due to HOMO-LUMO transition and the value of HOMO-LUMO energy gap was found to be 4.385 eV.

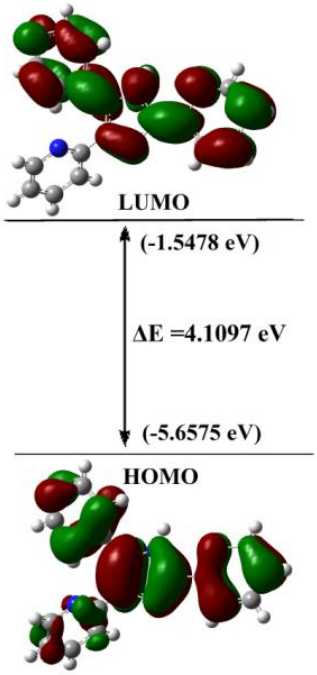

Figure 26. Energy level diagram depicting HOMO and LUMO of **L1H**.

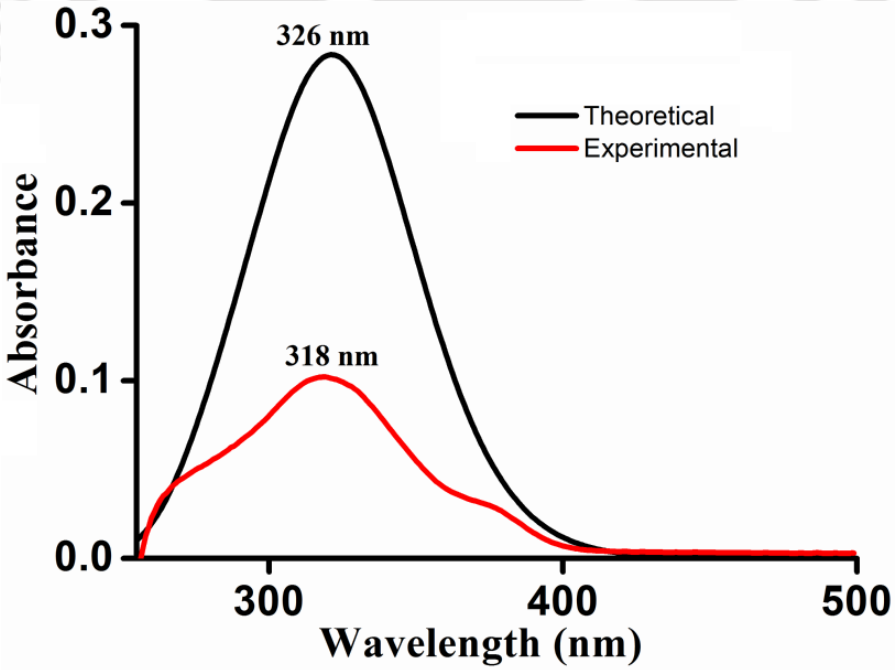

Figure 27. Experimental and simulated UV-Vis absorption spectra of **L1H**.

3.4. Conclusion:

Using 2,4-bis(2-pyridyl)-5-(4-pyridyl)imidazole as a chromophore, selective recognition of Zn^{2+} ions in presence of other cations was achieved in DMSO. The ligand **L1H** exhibits a characteristic electronic and fluorescence spectral behaviours with $ZnCl_2$. Emission maximum at 391 nm of **L1H** decreased with increase in Zn^{2+} ion concentration and new emission band appeared at 445 nm along with a quasi isoemissive point at 413 nm. Binding constant K was found to be 3.5×10^8 M^{-2}. In HEPES buffer-DMSO solution (5 mM, 2:8, *v*/*v*, pH = 7.4), upon excitation at 320 nm, **L1H** exhibited maximum emission at 396 nm and with increase in concentration of Zn^{2+} ion the emission band red shifted to 445 nm. The binding constant found to be 6.67×10^7 M^{-2} with limit of detection being 6.5×10^{-7} M. A complex of composition $[Zn_2(\mathbf{L1})Cl_3(H_2O)]$ was isolated as crystalline solid by reacting **L1H** with $ZnCl_2$ which was structurally characterized. In this complex $\mathbf{L1}^-$ is bound to three Zn^{2+} ions by using all the five donor atoms thus acting as pentadentate ligand. Upon on comparing the ligand moiety in **1** and **L1H**, co-planarity of the 2-pyridyl ring with the imidazolate ring is increased and this may reduce the loss of energy *via* non-radative transition resulting red shift in the emission spectra. From the DFT studied it is observed that the HOMO-LUMO band gap of **L1H** is 4.10979 eV and it is likely that Zn^{2+} ions stabilize the LUMO to a greater extent than it does to the HOMO.

Table 1. Crystallographic data of **L1H** and **1**.

	L1H	**1**
Empirical formula	$C_{18}H_{13}N_5O_6$	$C_{18}H_{14}Cl_3N_5OZn_2$
CCDC number	1449730	1449731
Formula weight	395.33	553.47
T (K)	296(2)	296(2)
Crystal system	Monoclinic	Hexagonal
Space group	$P2_1/n$	R-3c
a (Å)	15.750(10)	28.136(2)
b (Å)	6.826(3)	28.136(2)
c (Å)	20.198(11)	38.869(4)
α (°)	90.00	90.00
β (°)	95.15(3)	90.00
γ (°)	90.00	120.00
V (Å^3)	2163(2)	26648(4)
Z	4	36
D_{calcd} (g m^{-3})	1.214	1.242
μ (mm^{-1})	0.094	1.905
F(000)	816.0	9936.0
Reflections collected	4441	38208
Unique reflections	3901	5180
Goodness-of-fit (GOF)[a]	1.188	1.004
R_1[b], wR_2[c] ($I \geq 2\sigma(I)$)	R_1 = 0.0849, wR_2 = 0.2095	R_1 = 0.0616, wR_2 = 0.1726
R_1[b], wR_2[c] (all data)	R_1 = 0.1599, wR_2 = 0.2487	R_1 = 0.1206, wR_2 = 0.2198

[a]GOF = $[\Sigma[w(F_0^2-F_c^2)^2]/M–N]^{1/2}$ (M = number of reflections, N = number of parameters refined). [b]$R_1 = \Sigma||F_0|-|F_c||\Sigma|F_0|$. [c]$wR_2 = [\Sigma [w(F_0^2-F_c^2)^2]/\Sigma [w(F_0^2)^2]]^{1/2}$.

References:

1. S. J. Lippard and J. M. Berg, *Principles of Bioinorganic Chemistry*, University Science Books, Mill Valley, CA, 1st ed., 1994.
2. J. M. Berg and Z. Shi, *Science*, 1996, **271**, 1081-1085.
3. G. K. Andrews, *Biometals*, 2001, **14**, 223-237.
4. Z. H. Dai, X. D. Xu and J. W. Canary, *Chem. Commun.*, 2002, 1414-1415.
5. Z. K. Wu, Y. F. Zhang, J. S. Ma and G. Q. Yang, *Inorg. Chem.*, 2006, **45**, 3140-3142.
6. S. L. Sensi, L. M. Canzoniero, S. P. Yu, H. S. Ying, J. Y. Koh, G. A. Kershner and D. W. Choi, *J. Neurosci.*, 1997, **17**, 9554-9564.
7. J. E. Coleman, *Curr. Opin. Chem. Biol.*, 1998, **2**, 222-234.
8. B. L. Vallee and K. H. Falchuk, *Phys. Rev.*, 1993, **73**, 79-118.
9. K. H. Falchuk, *Mol. Cell. Biochem.*, 1998, **188**, 41-48.
10. A. C. Miu, O. Benga, P. A. Adlard and A. I. Bush, *J. Alzheimer's Dis.*, 2006, **10**, 145-163.
11. E. L. Que, D. Ws. Domaille and C. J. Chang, *Chem. Rev.*, 2008, **108**, 4328-4328.
12. M. P. Cuajungco and G. J. Lees, *Neurobiol. Dis*., 1997, **4**, 137-169.
13. A. I. Bush, W. H. Pettingell, G. Multhaup, M. D. Paradis, J. P. Vonsattel, J. F. Gusella, K. Beyreuther, C. L. Masters and R. E. Tanzi, *Science*, 1994, **265**, 1464-1467.
14. J.-Y. Koh, S. W. Suh, B. J. Gwag, Y. Y. He, C. Y. Hsu and D. W. Choi, *Science*, 1996, **272**, 1013-1016.
15. A. Q. Truong-Tran, J. Carter, R. E. Ruffin and P. D. Zalewski, *Biometals*, 2001, **14**, 315-330.
16. P. D. Zalewski, I. J. Forbes, R. F. Seamark, R. Borlinghaus, W. H. Betts, S. F. Lincoln and A. D. Ward, *Chem. Biol.*, 1994, **1**, 153-161.
17. E. Kimura, S. Aoki, E. Kikuta and T. Koike, *Proc. Natl. Acad. Sci. U.S.A.*, 2003, **100**, 3731-3736.
18. S. Sumiya, Y. Shiraishi and T. Hirai, *J. Phys. Chem. A*, 2013, **117**, 1474-1482.
19. J. An, M. Yan, Z. Yang, T. Li and Q. Zhou, *Dyes and Pigments*, 2013, **99**, 1-5.

20. K. B. Kim, H. Kim, E. J. Song, S. Kim, I. Noh and C. Kim, *Dalton Trans.*, 2013, **42**, 16569-16577.
21. T. Mistri, M. Dolai, D. Chakraborty, A. R. Khuda-Bukhsh, K. K. Das and M. Ali, *Org. Biomol. Chem.*, 2012, **10**, 2380-2384.
22. K. Komatsu, Y. Urano, H. Kojima and T. Nagano, *J. Am. Chem. Soc.*, 2007, **129**, 13447-13454.
23. J. Dessingou, R. Joseph and C. P. Rao, *Tetrahedron Lett.*, 2005, **46**, 7967-7971.
24. J. P. Cornard, L. Dangleterre and C. Lapouge, *Chem. Phys. Lett.*, 2006, **41**, 9304-9308.
25. S. Aoki, K. Sakurama, N. Matsuo, Y. Yamada, R. Takasawa, S. Tanuma, M. Shiro, K. Takeda and E. Kimura, *Chem. Eur. J.*, 2006, **12**, 9066-9080.
26. H. Wang, Q. Gan, X. Wang, L. Xue, S. Liu and H. Jiang, *Org. Lett.*, 2007, **9**, 4995-4998.
27. A. Hens, A. Maity and K. K. Rajak, *Inorg. Chim. Acta*, 2014, **423**, 408-420.
28. X. Tang, X. Peng, W. Dou, J. Mao, J. Zheng, W. Qin, W. Liu, J. Chang and X. Yao, *Org. Lett.*, 2008, **10**, 3653-3656.
29. E. M. Nolan, J. W. Ryu, J. Jaworski, R. P. Feazell, M. Sheng and S. J. Lippard, *J. Am. Chem. Soc.*, 2006, **128**, 15517-15528.
30. K. Komatsu, K. Kikuchi, H. Kojima, Y. Urano and T. Nagano, *J. Am. Chem. Soc.*, 2005, **27**, 10197-10204.
31. N. C. Lim, J. V. Schuster, M. C. Porto, M. A. Tanudra, L. Yao, H. C. Freake and C. Brückner, *Inorg. Chem.*, 2005, **44**, 2018-2030.
32. M. M. Henary, Y. G. Wu and C. J. Fahrni, *Chem. Eur. J.*, 2004, **10**, 3015-3025.
33. S. Y. Jiao, L. L. Peng, K. Li, Y. M. Xie, M. Z. Ao, X. Wang and X. Q. Yu, *Analyst*, 2013, **138**, 5762-5768.
34. G. Sivaraman, T. Anand and D. Chellappa, *Analyst*, 2012, **137**, 5881-5884.
35. P. G. Jiang and Z. Guo, *Coord. Chem. Rev.*, 2004, **248**, 205-229.
36. A. E. Majzoub, C. Cadiou, I. D. Olivier, B. Tinant and F. Chuburu, *Inorg. Chem.*, 2011, **50**, 4029-4038.
37. Z. Liu, C. Zhang, Y. Li, Z. Wu, F. Qian, X. Yang, W. He, X. Gao and Z. Guo, *Org. Lett.*, 2009, **11**, 795-798.

38. P. Molina, A. Tárraga and F. Otón, *Org. Biomol. Chem.*, 2012, **10**, 1711-1724.
39. P. Alreja and N. Kaur, *RSC Adv.*, 2016, **6**, 23169-23217.
40. C. Bhaumik, S. Das, D. Maity and S. Baitalik, *Dalton Trans.*, 2012, **41**, 2427-2438.
41. Z. Xu, J. Yoon and D. R. Spring, *Chem. Soc. Rev.*, 2010, **39**, 1996-2006.
42. P. Carol, S. Sreejith and A. Ajayaghosh, *Chem. Asian J.*, 2007, **2**, 338-348.
43. D. W. Domaille, E. L. Que and C. J. Chang, *Nat. Chem. Biol.*, 2008, **4**, 168-175.
44. Z. Dai and J. W. Canary, *New J. Chem.*, 2007, **31**, 1708-1718.
45. E. Tomat and S. J. Lippard, *Curr. Opin. Chem. Biol*., 2010, **14**, 225-230.
46. W. Linert, G. N. L. Jameson, R. F. Jameson, K. A. Jellinger, *Met. Ions Life Sci.*, 2006, **1**, 281-320.
47. E. Kimura and T. Koike, *Chem. Soc. Rev.*, 1998, **27**, 179-184.
48. H. A. Benesi and J. H. Hildebrand, *J. Am. Chem. Soc*., 1949, **71**, 2703-2707.
49. X. Y. Zhou, B. R. Yu, Y. L. Guo, X. L. Tang, H. H. Zhang and W. S. Liu, *Inorg. Chem*., 2010, **49**, 4002-4007.
50. Y. Mikata, M. Wakamatsu, A. Kawamura, N. Yamanaka, S. Yano, A. Odani, K. Morihiro and S. Tamotsu, *Inorg. Chem.*, 2006, **45**, 9262-9268.
51. E. M. Nolan, S. C. Burdette, J. H. Harvey, S. A. Hilderbrand and S. J. Lippard, *Inorg. Chem.*, 2004, **43**, 2624-2635.
52. S. C. Burdette, C. J. Frederickson, W. Bu and S. J. Lippard, *J. Am. Chem. Soc.*, 2003, **125**, 1778-1787.
53. S. Huang, R. J. Clark and L. Zhu, *Org. Lett.*, 2007, **9**, 4999-5002.
54. E. U. Akkaya, M. E. Huston and A. W. Czarnik, *J. Am. Chem. Soc.*, 1990, **112**, 3590-3593.
55. R. Krämer, *Angew. Chem. Int. Ed.*, 1998, **37**, 772-773.
56. Y. Tian, C. Y. Chen, C. C. Yang, A. C. Young, S. H. Jang, W. C. Chen and A. K. Y. Jen, *Chem. Mater.*, 2008, **20**, 1977-1987.
57. E. M. Nolan, J. Jaworski, M. E. Racine, M. Sheng and S. J. Lippard, *Inorg. Chem.*, 2006, **45**, 9748-9757.
58. T. D. Rae, P. J. Schmidt, R. A. Pufahl, V. C. Culotta and T. V. O'Halloran, *Science*, 1999, **284**, 805-808.

59. L. Xue, G. P. Li, D. J. Zhu, Q. Liu and H. Jiang, *Inorg. Chem.*, 2012, **51**, 10842-10849.
60. J. Luo, W. S. Li, P. Xu, L. Y. Zhang and Z. N. Chen, *Inorg. Chem.*, 2012, **51**, 9508-9516.
61. V. K. Fulwa, R. Sahu and H. S. Jena, V. Manivannan, *Tetrahedron Lett.*, 2009, **50**, 6264-6267.
62. M. J. Frisch, G. W. Trucks, H. B. Schlegel, G. E. Scuseria, M. A. Robb, J. R. Cheeseman, G. Scalmani, V. Barone, B. Mennucci, G. A. Petersson, H. Nakatsuji, M. Caricato, X. Li, H. P. Hratchian, A. F. Izmaylov, J. Bloino, G. Zheng, J. L. Sonnenberg, M. Hada, M. Ehara, K. Toyota, R. Fukuda, J. Hasegawa, M. Ishida, T. Nakajima, Y. Honda, O. Kitao, H. Nakai, T. Vreven, J. A. Montgomery, Jr., J. E. Peralta, F. Ogliaro, M. Bearpark, J. J. Heyd, E. Brothers, K. N. Kudin, V. N. Staroverov, R. Kobayashi, J. Normand, K. Raghavachari, A. Rendell, J. C. Burant, S. S. Iyengar, J. Tomasi, M. Cossi, N. Rega, J. M. Millam, M. Klene, J. E. Knox, J. B. Cross, V. Bakken, C. Adamo, J. Jaramillo, R. Gomperts, R. E. Stratmann, O. Yazyev, A. J. Austin, R. Cammi, C. Pomelli, J. W. Ochterski, R. L. Martin, K. Morokuma, V. G. Zakrzewski, G. A. Voth, P. Salvador, J. J. Dannenberg, S. Dapprich, A. D. Daniels, Ö. Farkas, J. B. Foresman, J. V. Ortiz, J. Cioslowski, and D. J. Fox, Gaussian 09, Revision D.01, Gaussian, Inc., Wallingford CT, 2009.
63. A. Baez-Castro, J. Baldenebro-Lopez, D. Glossman-Mitnik, H. Höpfl, A. Cruz-Enríquez , V. Miranda-Soto, M. Parra-Hake and J. J. Campos-Gaxiola, *J. Mol. Struct.*, 2015, **1099**, 126-134.

Appendix

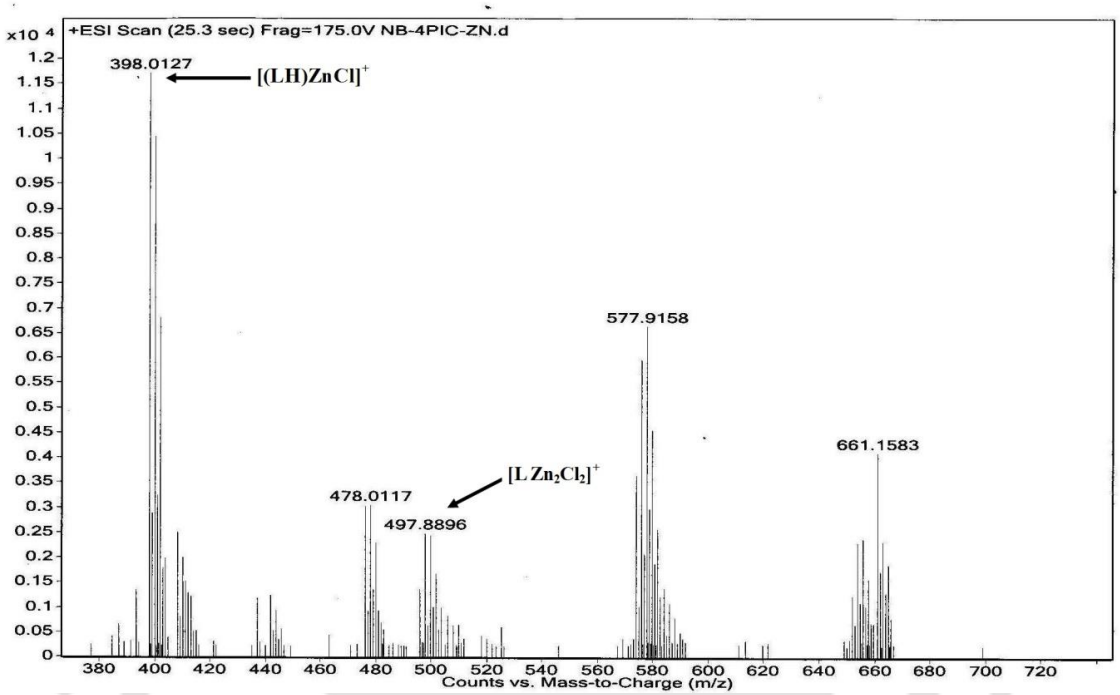

Figure A1. ESI-MS spectrum of complex **1**.

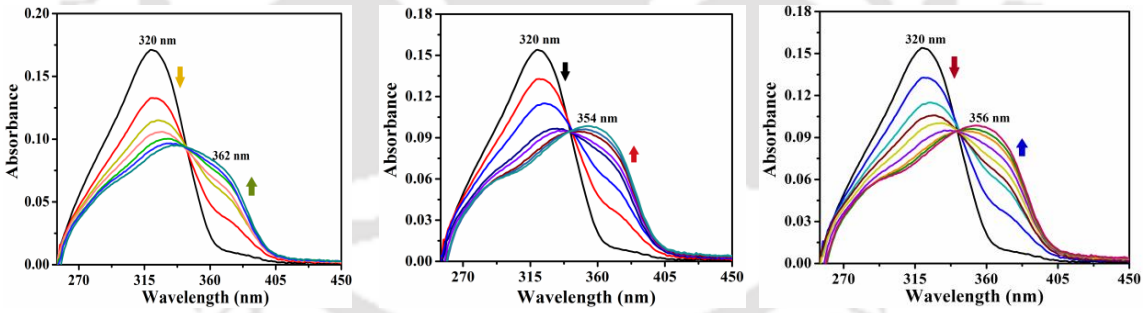

(**a**) (**b**) (**c**)

Figure A2. Changes in UV-Vis spectra of receptor **L1H** (10 µM) upon incremental addition of (a) $CuCl_2$ (b) $CoCl_2$ (c) $NiCl_2$ (0-3 equivalents) in HEPES buffered aqueous DMSO solution (5 mM, pH = 7.4, 2:8, *v*/*v*).

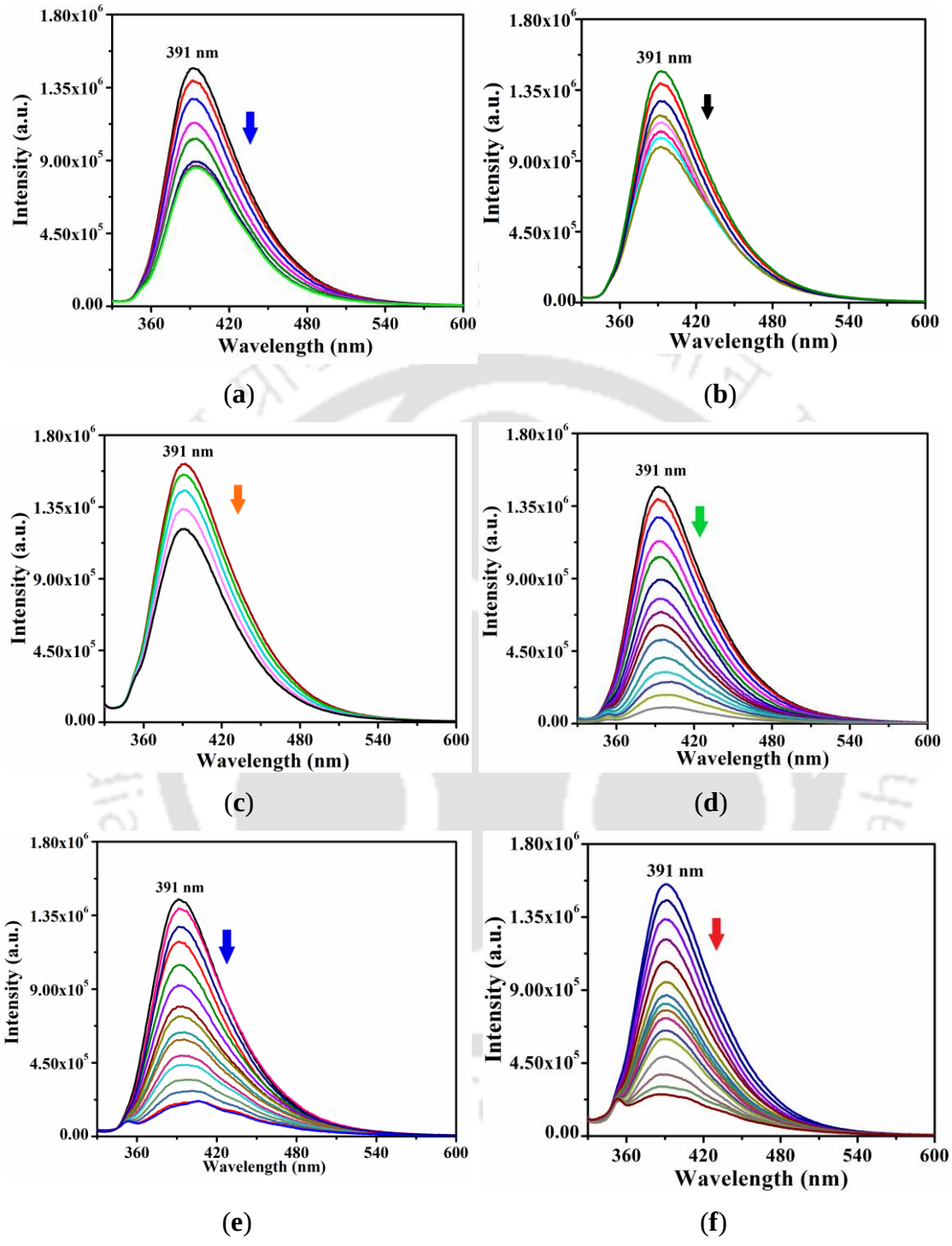

Figure A3. Fluorescence responses upon titration of **L1H** (10 μM) with (a) Mn^{2+} (b) Fe^{3+} (c) Cd^{2+} (d) Cu^{2+} (e) Co^{2+} (e) Ni^{2+} ions (0-3.5 equiv.) in DMSO.

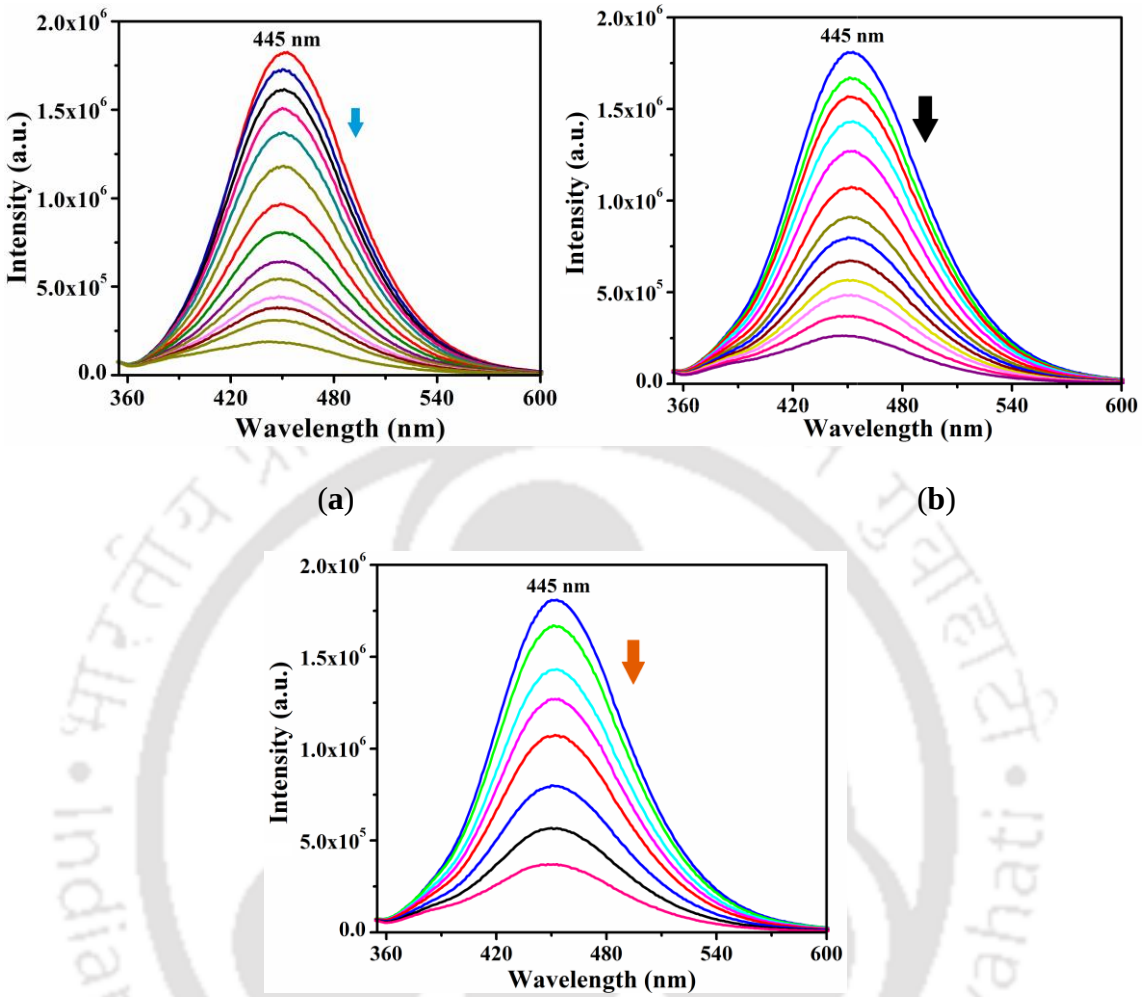

Figure A4. Fluorescence emission spectra of Zn^{2+}-**L1H** upon addition of noted metal ions in DMSO, λ_{ex} = 320 nm ([**L1H**] = 10 μM). (a) [Cu^{2+}] = 50 μM (b) [Co^{2+}] = 50 μM) (c) [Ni^{2+}] = 50 μM.

Chapter 4

Nanomolar Detection of Al(III) Ion by Hydrazones Carrying Benzothiazole and Substituted Phenol Groups

Abstract:

In this Chapter, two new hydrazones *viz.*, 2-(2-(2,3-dihydroxy)benzylidenehydrazinyl)benzothiazole (**L2H**) and 2-((2-(2-hydroxy)(4-*N*,*N*-diethylamino))benzylidenehydrazinyl)benzothiazole (**L3H**), were synthesized using 2-hydrazinylbenzothiazole and 2,3-dihydroxybenzaldehyde or 4-(diethylamino)-2-hydroxybenzaldehyde. The probe **L2H** showed an absorption peak at 340 nm while **L3H** at 375 nm, in MeOH/HEPES buffer (pH = 7.3, 8:2, *v*/*v*). Upon gradual addition of $AlCl_3$ to **L2H**, intensity of the peak at 340 nm decreased and a new band appeared with a peak at 400 nm. Similarly upon adding $AlCl_3$ to **L3H**, new peaks at 405 and 420 nm grew in intensity with concomitant decrease in absorbance peak at 375 nm, having quasi isosbestic point at 395 nm. Both these probes are weakly emissive in nature. Incremental addition of $AlCl_3$ to the MeOH/HEPES buffer solution of **L2H** gave "*turn-on*" response having emission maximum at 480 nm and **L3H** at 450 nm with a shoulder at 468 nm. *Turn-On* responses of **L2H** and **L3H** towards Al^{3+} ion were result of inhibition of PET process which in turn allowed chelation induced enhanced fluorescence (CHEF) effect becoming operational. Job's plot obtained from the titration experiments yielded 1:1 stoichiometry for Al^{3+} ion, hence the formulae [Al(**L2**)Cl_2(H_2O)] and [Al(**L3**)Cl_2(H_2O)] were assigned. Addition of Na_2EDTA to [Al(**L2**)Cl_2(H_2O)] and [Al(**L3**)Cl_2(H_2O)] reproduced UV-visible spectrum that is characteristic of free **L2H/L3H**.

* This work has been published in:

N. Behera and V. Manivannan, *ChemistrySelect*, 2017, **2**, 11048–11054.

4.1. Introduction:

Cations and anions have great impact in the field of biology and environment. They play crucial role in our daily life and in industrial processes as well as perform vital physiological functions. Though, the anionic and cationic species are essential for sustaining of life and growth, at the same time their excessive accumulation has adverse effects in human life and environment.[1,2] For sensing spectroscopically silent ions such as aluminium(III), fluorescence technique[3-11] has become more useful and sensitive method than other methods *viz*., atomic absorption spectroscopy, inductively coupled plasma-mass spectrometry and inductively coupled plasma-atomic emission spectrometry.[12,13] Therefore, search for new fluorescence probes for selective detection of aluminium is still in demand. Though aluminium is available in the earth's crust,[14] its intake by human is through the lifestyle.[15] Excessive accumulation of aluminium in human body is detrimental to the health[16-18] and can lead to diseases like Alzheimer's,[19] Parkinson's,[20] osteomalacia, osteoporosis,[21-22] kidney failure,[23] encephalopathy[24] *etc*. It is also deleterious to aquatic species and eco-systems.[25-27]

As aluminium lacks spectroscopic characteristics[28-30] and is a hard acid as per HSAB principle, fluorescence sensors containing harder O and N donor atoms along with suitable fluorophore as a part of the ligand framework, were effective.[31–34] Easy preparation, high yield and high selectivity properties of imine-based chemosensors, have made them most popular fluorescence probes in detection of metal ions.[35-40] In this article, we wish to report utilizations of two benzothiazohydrazones having substituted phenol groups (Scheme 1) as efficient chemosensors for Al^{3+} ion.

Apart from cation detection, simultaneous anion detection by the resultant ensemble is also in high demand in sensor field. Among all biologically relevant anions, fluoride ion has great impact in biology and environment. Fluoride ion has pre-eminent role in dental care and its overconsumption provoke gastric and kidney disorders, urolithiasis and skeletal fluorosis.[41-43] Furthermore, it is employed in hypnotic and psychiatric drugs, and also for refinement of uranium in nuclear technology.[44-46] On account of this, selective detection of biologically and chemically important fluoride ion is also achieved using these two aluminium complexes as probes.

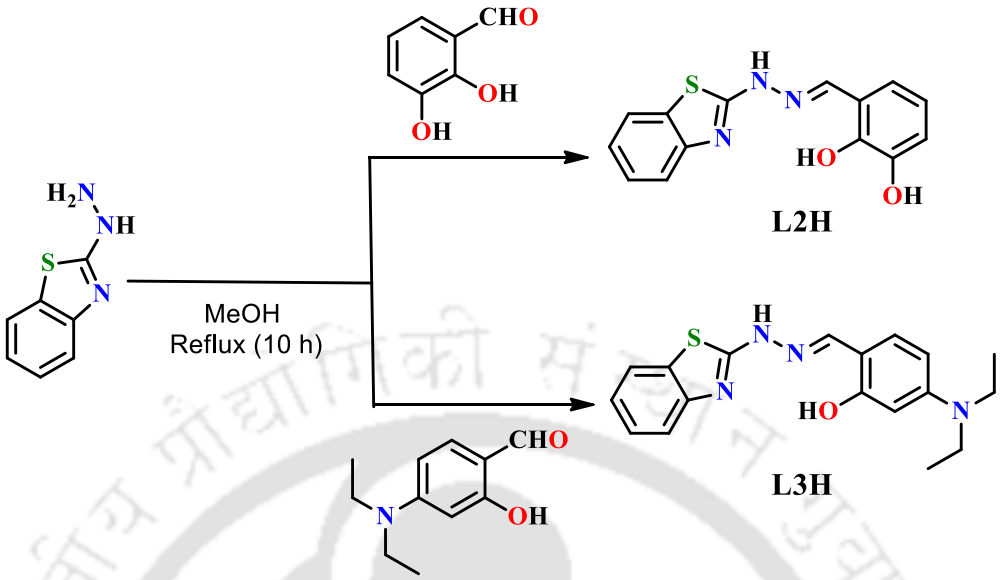

Scheme 1. Synthesis of **L2H** and **L3H**.

4.2. Experimental Section:

*4.2.1. Synthesis of **L2H** and **L3H**:*

A methanolic solution (50 mL) containing 2,3-dihydroxybenzaldehyde (0.5 g, 3.6 mmol) and 2-hydrazinylbenzothiazole (0.594 g, 3.6 mmol) was heated at reflux for 10 h and then the solution was allowed to cool to room temperature. The precipitate of **L2H** was collected through filtration and washed with ice-cold methanol. Yield 0.915 g (89 %). Anal. calcd. for $C_{14}H_{11}N_3O_2S$: C, 58.93; H, 3.89; N, 14.73. Found: C, 58.75; H, 3.80; N, 14.64. 600 MHz ^{1}H NMR (δ (*J*, Hz) DMSO-d_6): 12.15(1H, s), 10.07(1H, s), 9.45(1H, s), 8.43(1H, s), 7.71(1H, d, 7.7), 7.34(1H, d, 6.9), 7.28(1H, t, 7.6), 7.08(1H, t, 7.5), 7.04(1H, d, 7.7), 6.84(1H, d, 7.6), 6.73(1H, t, 7.8) (Figure A1). 150 MHz ^{13}C NMR (δ, DMSO-d_6): 166.54, 147.34, 145.71, 145.63, 127.21, 126.58, 122.11, 121.89, 120.03, 119.63, 118.94, 117.05, 115.88 (Figure A2). ESI-MS(+): *m/z* calcd. for $C_{14}H_{11}N_3O_2S$ 285.057 found (M^+ + H) 286.065. FTIR (KBr, cm^{-1}): 3251(w), 3159(w), 3101(w), 3050(w), 2922(w), 2856(w), 2791(w), 2658(w), 1616(s), 1583(m), 1559(m), 1540(m), 1474(s), 1400(m), 1365(w), 1288(w), 1265(w), 1248(s), 1160(w), 1127(w), 1089(w), 1074(w), 1055(w), 1015(w), 948(w), 932(w), 881(w), 848(w), 777(w), 751(m), 729(m), 690(m), 620(w), 534(w), 496(w).

The probe **L2H** was prepared by adopting the method described for **L3H**, by using 4-(diethylamino)-2-hydroxybenzaldehyde (0.7 g, 3.6 mmol) in place of 2,3-dihydroxybenzaldehyde. Yield 1.05 g (86 %). Anal. calcd. for $C_{18}H_{20}N_4OS$: C, 63.50; H, 5.92; N, 16.46. Found: C, 63.39; H, 5.84; N, 16.30. 600 MHz ^{1}H NMR (δ (*J*, Hz) DMSO-d_6): 11.79(1H, s), 10.67(1H, s), 8.26(1H, s), 7.64(1H, d, 7.8), 7.28–7.20(3H, m), 7.06–6.98(1H, m), 6.23(1H, dd, 8.8, 2.4), 6.11(1H, d, 2.3), 3.30(4H, q, 7.0), 1.06(6H, t, 7.0) (Figure A3). 150 MHz ^{13}C NMR (δ, DMSO-d_6): 164.77, 159.31, 150.18, 145.63, 131.13, 126.61, 126.30, 122.19, 121.51, 114.70, 107.27, 104.17, 97.58, 44.10, 12.74 (Figure A4). ESI-MS(+): *m/z* calcd. for $C_{18}H_{20}N_4OS$ 340.136 found (M^+ + H) 341.145. FTIR (KBr, cm^{-1}): 3418(b), 3075(w), 2965(m), 2927(w), 2865(w), 2816(w), 1634(w),1612(s), 1579(w), 1553(w), 1519(m), 1467(m), 1444(w), 1409(m), 1371(w), 1356(w), 1341(w), 1295(w), 1268(w), 1233(m), 1191(w), S1156(w), 1129(m), 1091(w), 1076(w), 1051(w), 1019(w), 956(w), 921(w), 897(w), 872(w), 826(m), 793(m), 742(m), 718(w), 707(w), 695(w), 684(w), 645(w), 609(m), 593(w), 567(w), 554(w), 494(w), 467(w), 459(w).

4.3. Results and Discussion:

4.3.1. UV-Vis spectroscopic studies of L2H and L3H in presence of metal ions:

The probe **L2H** showed the absorption peak at 340 nm in MeOH/HEPES buffer (pH = 7.3, 8:2, *v/v*). As inferred from the DFT/TDDFT calculations[47] absorption at 340 nm is of $n\rightarrow\pi^*$, in origin. Upon addition of $AlCl_3$ to **L2H**, intensity of the peak at 340 nm decreased and a new band appeared with a peak at 400 nm along with a shoulder at ~420 nm, accompanied by presence of a quasi isosbestic point at 375 nm (Figure 1). The probe **L3H** showed the absorption maximum at 375 nm having a shoulder at ~388 nm, in MeOH/HEPES buffer (pH = 7.3, 8:2, *v/v*). With incremental addition of aluminium chloride to the solution of **L3H**, decreasing of absorbance of 375 nm peak occurred which eventually disappeared. New peaks appeared at 405 and 420 nm with the quasi isosbestic point at 395 nm (Figure 2). Origin of these two new peaks are of $\pi\rightarrow\pi^*$ in nature and red shift is the result of decrease in the HOMO-LUMO energy gap (*vide infra*). Other metal ions are also expected to bind to these ligands but lacks shift in their

absorption spectra. This indicates that effect of binding of these metal ions on the energy gap between ground and excited states of intra-ligand transitions are minimal.

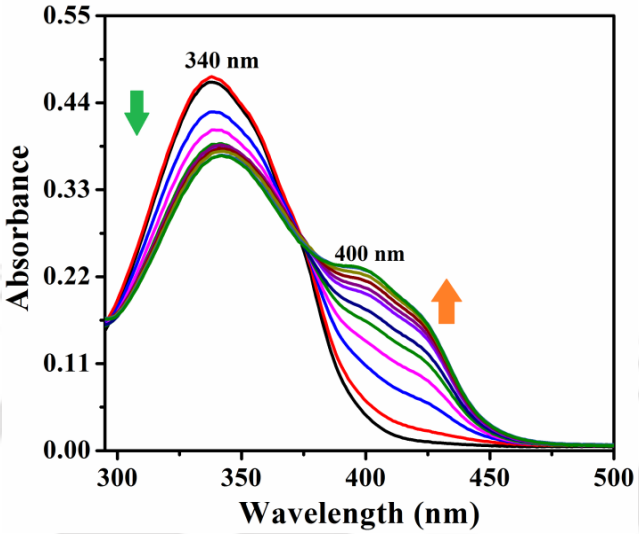

Figure 1. Changes in absorption spectra of **L2H** (10 μM) upon incremental addition of $AlCl_3$ (0-3 equivalents) in MeOH/HEPES buffer (pH = 7.3, 8:2, *v*/*v*).

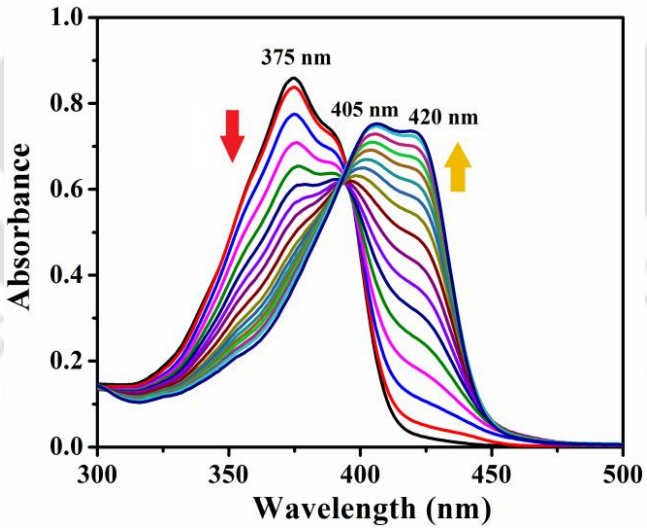

Figure 2. Changes in absorption spectra of **L3H** (10 μM) upon incremental addition of $AlCl_3$ (0-3 equivalents) in MeOH/HEPES buffer (pH = 7.3, 8:2, *v*/*v*).

In effect, bathochromic shifts of 63 and 45 nm were observed in the probes **L2H** and **L3H** respectively. These shifts indicate the formation of complex between Al^{3+} ion and the probes. The chloride salts of other metal ions *viz*., Li^{+}, Na^{+}, K^{+}, Ag^{+}, Ca^{2+}, Mg^{2+},

Cu^{2+}, Co^{2+}, Ni^{2+}, Mn^{2+}, Zn^{2+}, Cd^{2+}, Hg^{2+}, Cr^{3+}, Fe^{3+} and Pb^{2+} showed little or no change in spectral patterns of **L2H** and **L3H** (Figure 3).

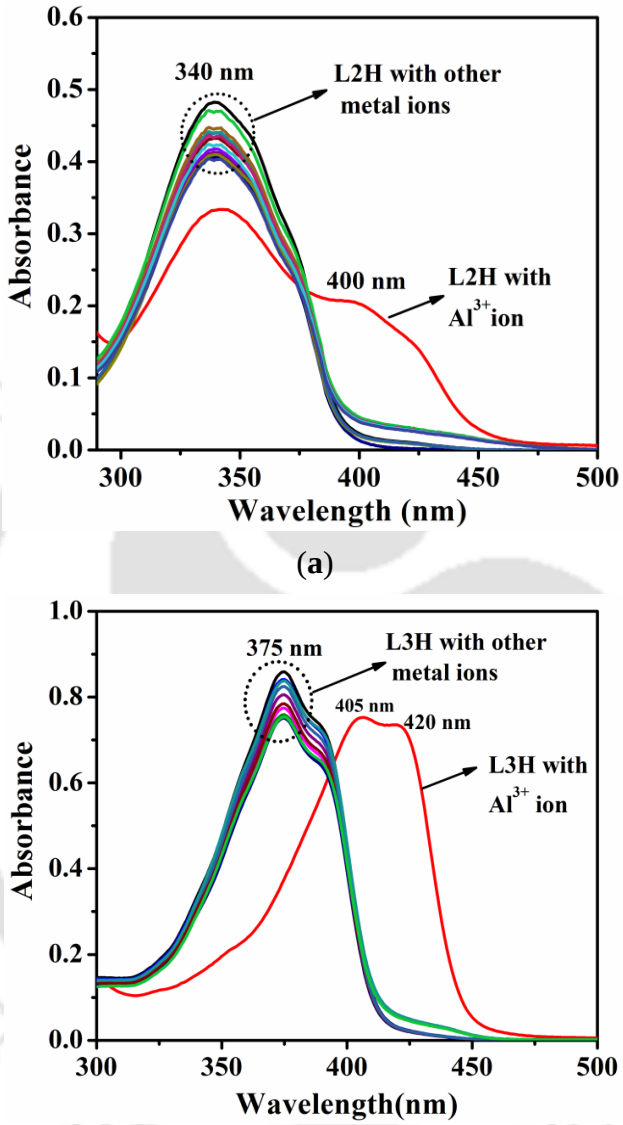

Figure 3. Changes in absorption spectra of (a) **L2H** (b) **L3H** (10 μM) upon incremental addition of chloride salts of other metal ions *viz.*, Li^{+}, Na^{+}, K^{+}, Ag^{+}, Ca^{2+}, Mg^{2+}, Cu^{2+}, Co^{2+}, Ni^{2+}, Mn^{2+}, Zn^{2+}, Cd^{2+}, Hg^{2+}, Al^{3+}, Cr^{3+}, Fe^{3+} and Pb^{2+} (0-3 equivalents) in MeOH/HEPES buffer (pH = 7.3, 8:2, *v*/*v*).

Addition of Na_2EDTA (metal ion sequestering agent) to the individual solutions obtained after titrating **L2H** and **L3H** with $AlCl_3$, yielded UV-visible spectrum that is

characteristics of free **L2H/L3H**. This indicates that the probes **L2H/L3H** bind to Al^{3+} ion without losing their identity (Figure 4).

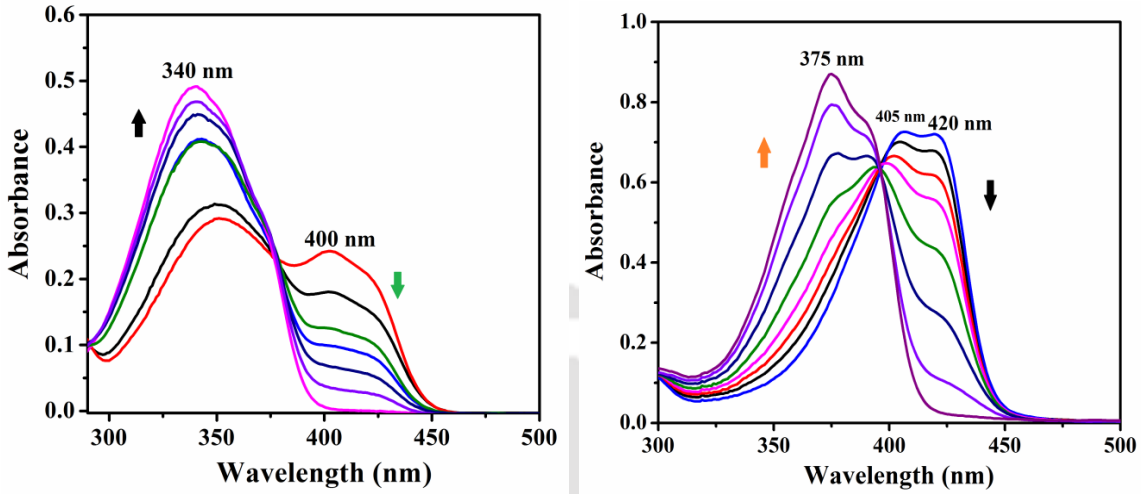

(**a**) (**b**)

Figure 4. Changes in absorption spectra of (a) **L2H** (b) **L3H** in the presence of $AlCl_3$ with Na_2EDTA in MeOH/HEPES buffer (pH = 7.3, 8:2, *v*/*v*).

4.3.2. Fluorescence spectroscopic studies of L2H and L3H in presence of metal ions:

Both the probes **L2H** and **L3H** were weakly/non emitting upon excitation at 375 and 395 nm respectively. The fluorescence response of **L2H** and **L3H** in presence of metal chlorides of Li^+, Na^+, K^+, Ag^+, Ca^{2+}, Mg^{2+}, Cu^{2+}, Co^{2+}, Ni^{2+}, Mn^{2+}, Zn^{2+}, Cd^{2+}, Hg^{2+}, Cr^{3+}, Fe^{3+}, Al^{3+} and Pb^{2+} were examined in MeOH/HEPES buffer (pH = 7.3, 8:2, *v*/*v*). The probe **L2H** upon excitation at 375 nm became emissive in presence of $AlCl_3$. Hence a titration experiment was carried out in which $AlCl_3$ solution was added in small quantities into **L2H**, during which the intensity of emissive peak at 480 nm gradually enhanced (Figure 5). Such enhancement in intensity has been observed only with Al^{3+} ion while other metal ions noted above didn't show any such increase in intensity of probe **L2H**. A similar behaviour was shown by **L3H** that weakly/non emissive probe upon gradual addition of $AlCl_3$, exhibited "*turn on*" fluorescence signal at 450 nm with a shoulder at 468 nm which grew in intensity with increasing amount of Al^{3+} ion (Figure 6). Overall, titrations of $AlCl_3$ with **L2H** and **L3H** respectively manifested ~150 and ~390 times increase in emission intensity. A small increase in the emission intensity (~30

times) upon addition of $CrCl_3$ has also been observed. The enhancement in emission intensity has not been exhibited by other metal ions examined in this study (Figure 7).

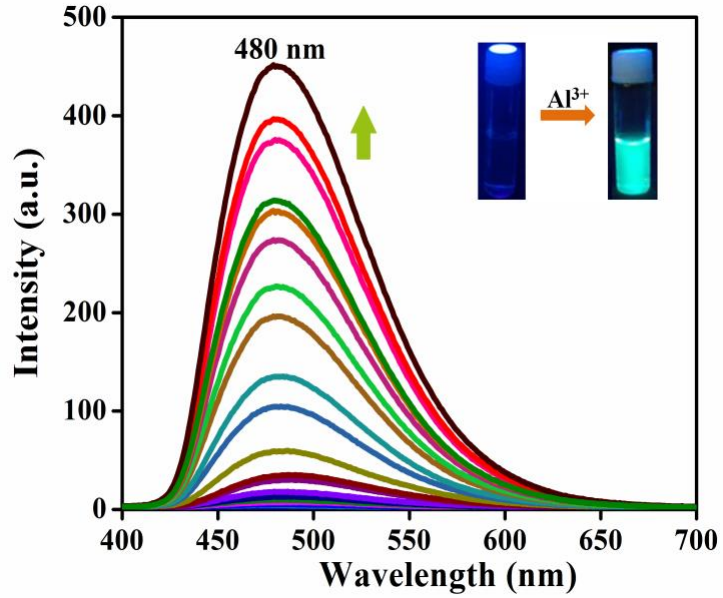

Figure 5. Fluorescence titration spectra of **L2H** (10 μM, λ_{ex} = 375 nm) upon incremental addition of $AlCl_3$ (0-3 equivalents) in MeOH/HEPES buffer (pH = 7.3, 8:2, *v*/*v*).

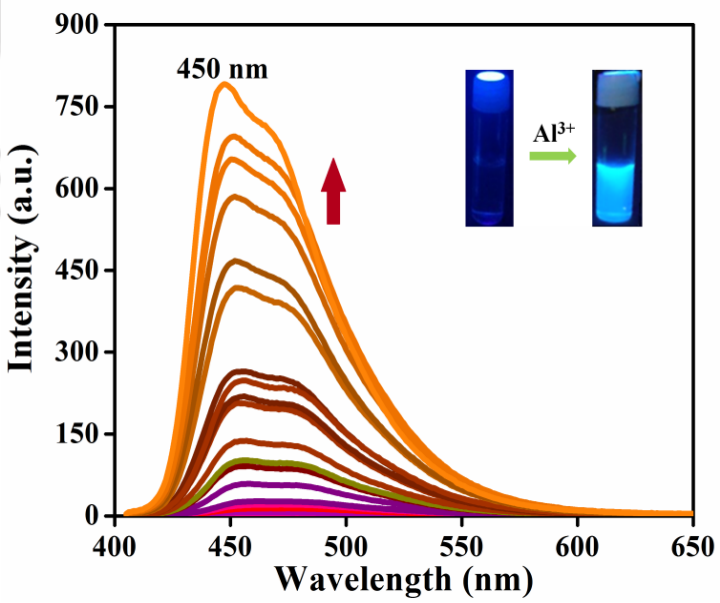

Figure 6. Fluorescence titration spectra of **L3H** (10 μM, λ_{ex} = 395 nm) upon incremental addition of $AlCl_3$ (0-3 equivalents) in MeOH/HEPES buffer (pH = 7.3, 8:2, *v*/*v*).

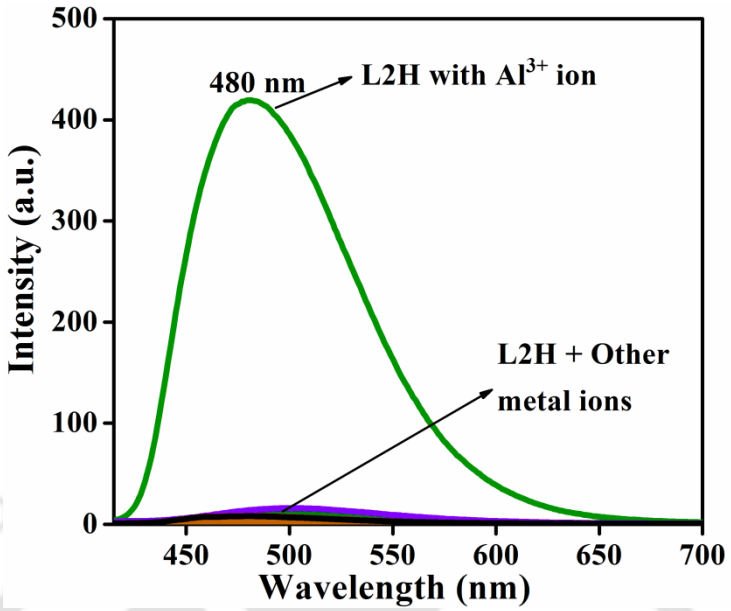

(a)

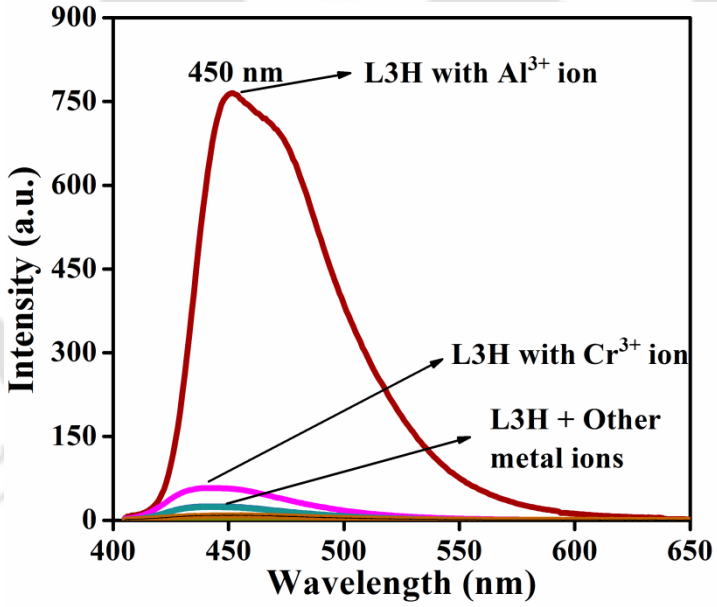

(b)

Figure 7. Changes in fluorescence emission of receptor (a) **L2H** (10 μM) and (b) **L3H** (10 μM) observed upon addition of chloride salts (50 μM) of Li^{+}, Na^{+}, K^{+}, Ag^{+}, Ca^{2+}, Mg^{2+}, Cu^{2+}, Co^{2+}, Ni^{2+}, Mn^{2+}, Zn^{2+}, Cd^{2+}, Hg^{2+}, Al^{3+}, Cr^{3+}, Fe^{3+} and Pb^{2+} (0-3 equivalents) in MeOH/HEPES buffer (pH = 7.3, 8:2, *v*/*v*).

This indicates that both **L2H** and **L3H** can be useful fluorescence probe selective for Al^{3+} ion. Both probes are expected to show *cis-trans* isomerisation along imine group

(–CH=N–) in the excited state[48,49] and photoinduced electron transfer (PET) involving lone-pair of electron on nitrogen atom of hydrazone group to large π-conjugated system of aromatic rings and these may be responsible for weak emission of both probes. Upon binding to metal ion, the lone-pair on nitrogen atom of imine is not free due to its involvement in coordination thereby imparting substantial increase in rigidity of the system. When **L2H** and **L3H** bind to metal Al^{3+} ion through imine nitrogen, phenolate oxygen and benzothiazole nitrogen atoms, result in inhibition of PET process that involves lone pair on imine N-atom (Scheme 2). As a result, chelation induced enhanced fluorescence (CHEF) effect becomes operational which induces a large enhancement in fluorescence intensity of **L2H** and **L3H**.

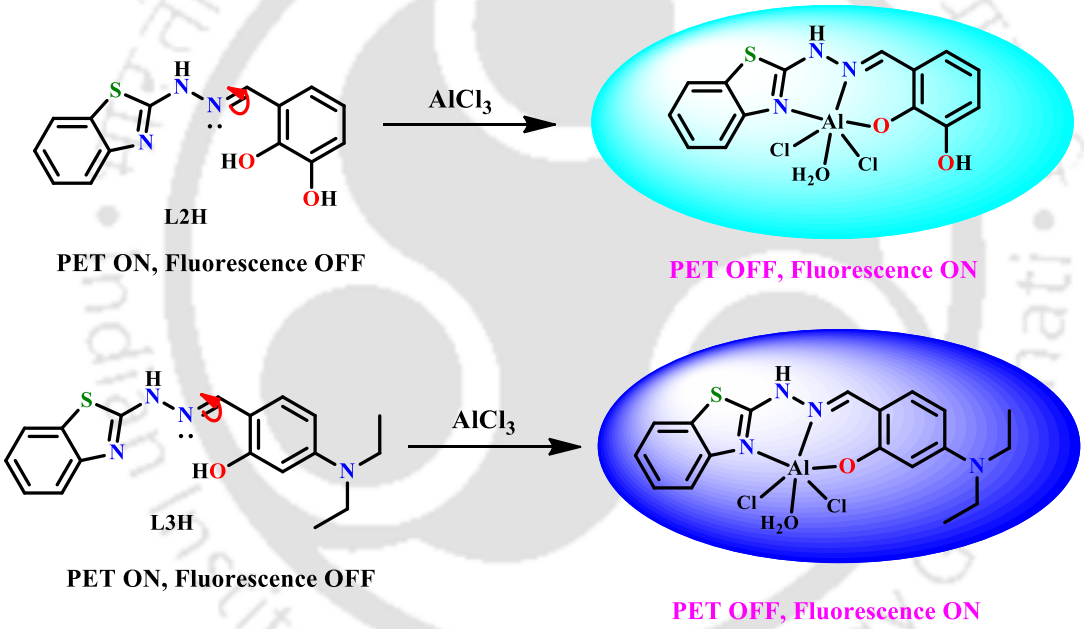

Scheme 2. Schematic diagram Al(III) complexes of **L2H** and **L3H**.

Job's plot obtained from the titration experiments yielded 1:1 stoichiometry for Al^{3+} ion with both **L2H** and **L3H** (Figure 8-9) and hence the formulations [Al(**L2**)$Cl_2(H_2O)$] and [Al(**L3**)$Cl_2(H_2O)$] were adopted throughout this study. In addition, the 1:1 stoichiometry of **L2H** and **L3H** towards Al^{3+} ion were further supported by the appearance of ESI-MS(+) *m/z* peak at 387.003 (calcd. for $AlClC_{16}H_{13}N_4O_2S^+$, 387.026) and 479.087 (calcd. for $AlClC_{20}H_{25}N_4O_2S_2^+$, 479.092) corresponding to $[Al(\mathbf{L2})(Cl)(CH_3CN)]^+$ and $[Al(\mathbf{L3})(Cl)(DMSO)]^+$ formulations (Figure A5-6). The

association constants of 4.0×10^6 M^{-1} and 2.5×10^6 M^{-1} for **L2H** and **L3H** respectively with respect to Al^{3+} ion, were derived using the Benesi–Hildebrand equation (Figure 10). This difference in association constants could be due to the electronic effects of 3-OH and 4-$N(Et)_2$ groups on the aromatic ring. The detection limits of **L2H** and **L3H** for Al^{3+} ion were calculated to be 3.6×10^{-9} M and 2.4×10^{-9} M respectively (Figure 11). The formulations $[Al(\mathbf{L2})Cl_2(H_2O)]$ and $[Al(\mathbf{L3})Cl_2(H_2O)]$ were adopted throughout this study based on the preferred coordination number of 6 in aqueous medium.[50]

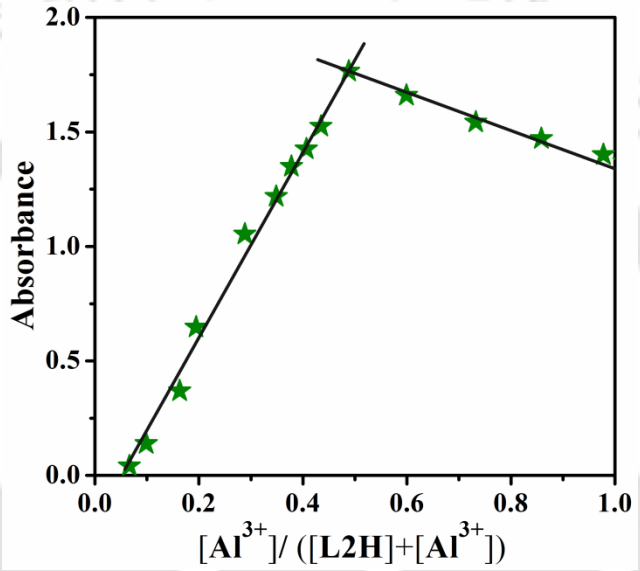

Figure 8. Job's Plot for **L2H** (10 μM) with Al^{3+} ion.

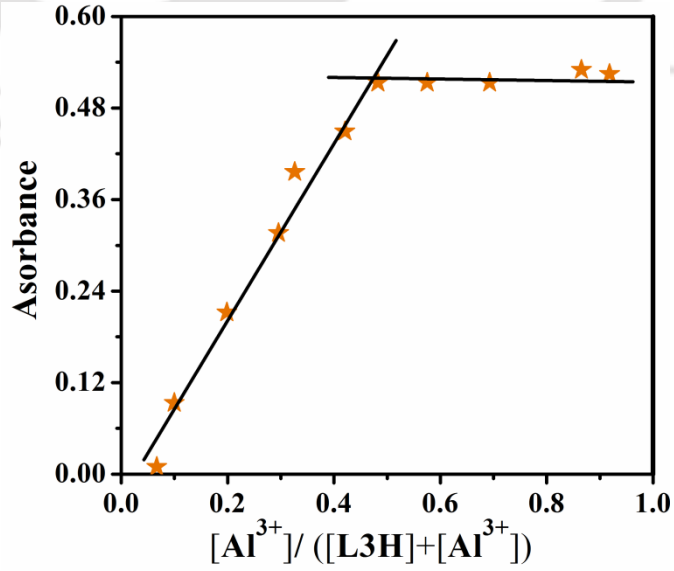

Figure 9. Job's Plot for **L3H** (10 μM) with Al^{3+} ion.

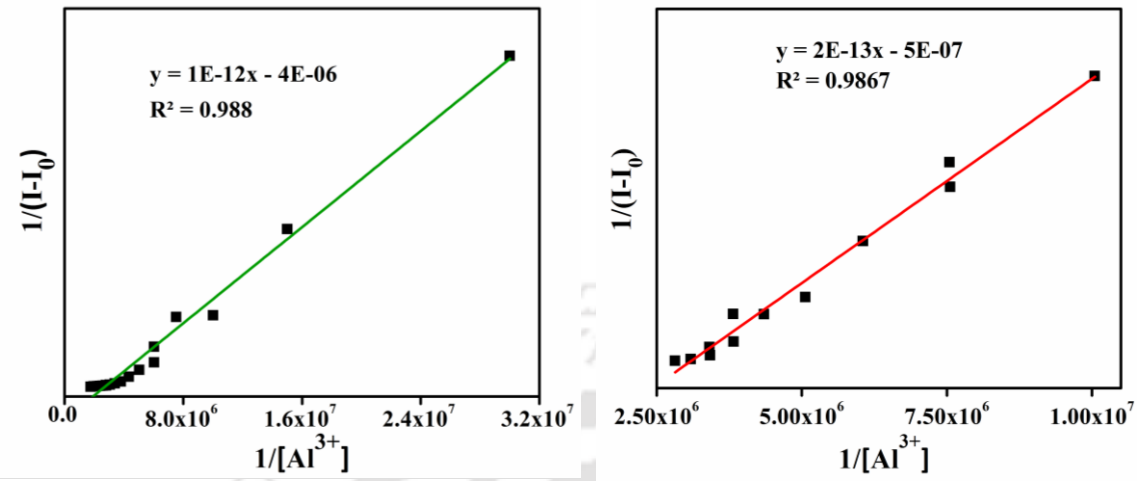

(**a**) (**b**)

Figure 10. Benesi-Hildebrand plot for determination of binding constant of (a) **L2H** (10 μM) and (b) **L3H** (10 μM) with Al^{3+} ion in MeOH/HEPES buffer (pH = 7.3, 8:2, *v/v*).

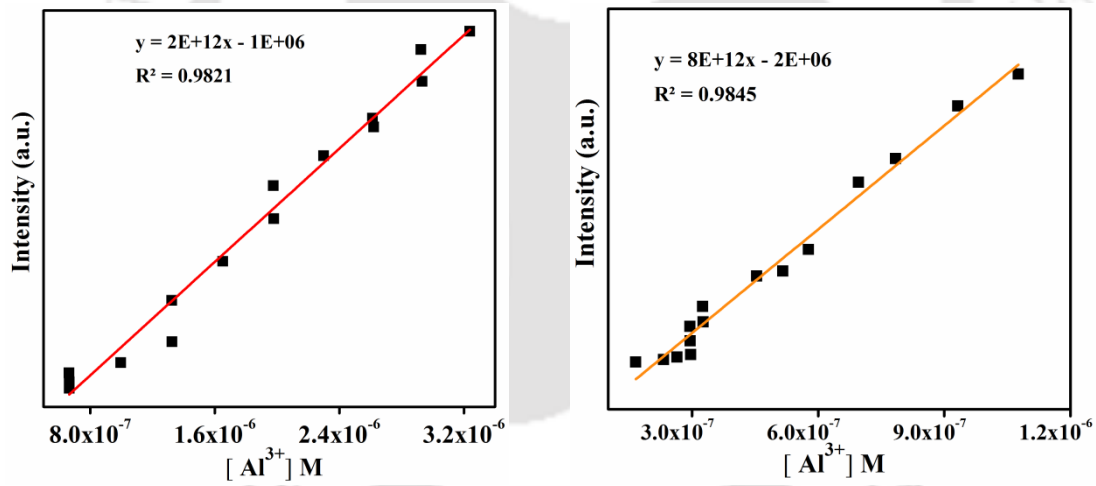

(**a**) (**b**)

Figure 11. Fluorescence intensity vs. concentration of Al^{3+} ion plot for determination of detection limit (a) [**L2H**] = 10 μM (b) **[L3H]** = 10 μM.

4.3.3. Metal ion competition studies:

For the practical applicability of **L2H** and **L3H** as Al^{3+} ion selective "*turn-on*" fluorescence receptors, competitive experiments were carried out in presence of other biologically and/or environmentally significant metal ions *viz*., Li^{+}, Na^{+}, K^{+}, Ag^{+}, Ca^{2+}, Mg^{2+}, Cu^{2+}, Co^{2+}, Ni^{2+}, Mn^{2+}, Zn^{2+}, Cd^{2+}, Hg^{2+}, Cr^{3+}, Fe^{3+} and Pb^{2+}. It was found that most of the metal ions did not interfere with the detection of Al^{3+} ion by **L2H** and **L3H**.

However, Cu^{2+} ion quenched about 10-15% of fluorescence intensity shown by [Al(**L2**)$Cl_2(H_2O)$] complex and Ni^{2+} ion quenched about 15-20% fluorescence intensity shown by [Al(**L3**)$Cl_2(H_2O)$] ensemble. Besides this, **L2H** and **L3H** still had sufficient "*turn-on*" ratios for detection of Al^{3+} ion in presence of other metal ions (Figure 12). These results indicate that **L2H** and **L3H** could be good sensor for Al^{3+} ion over competing metal ions.

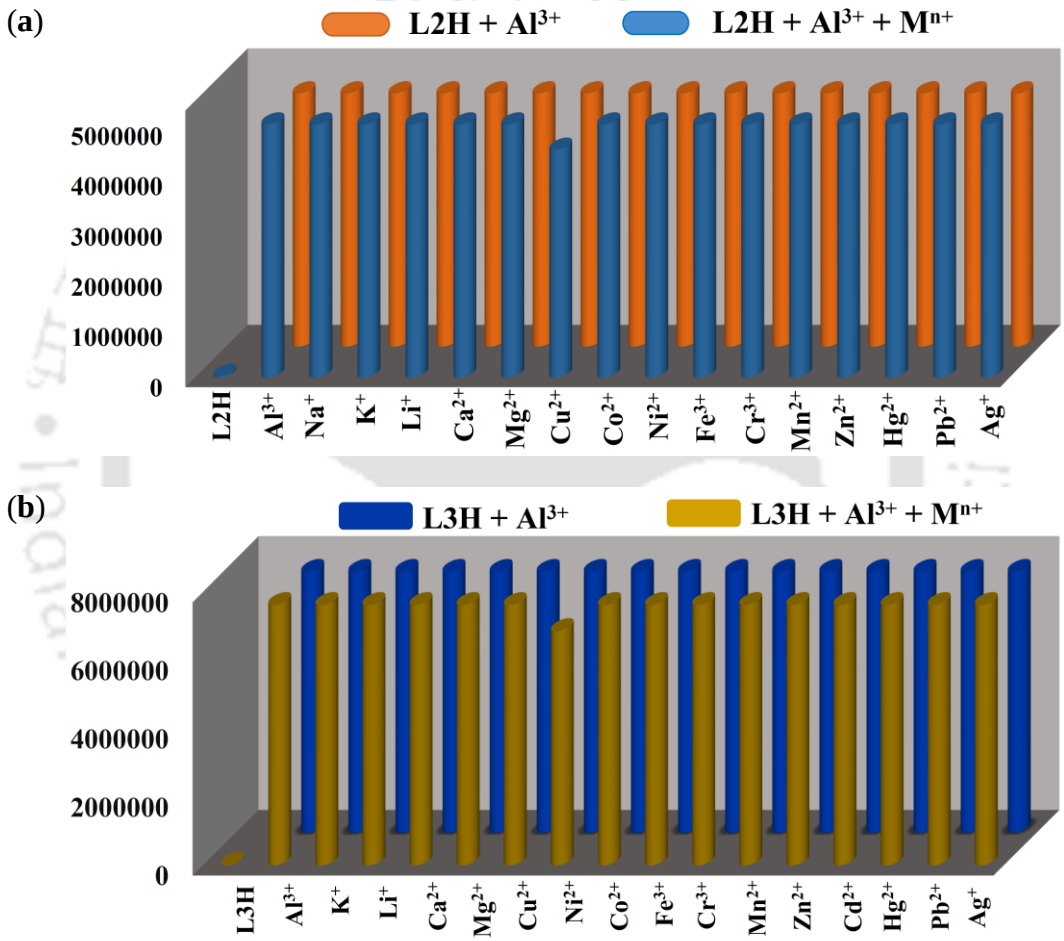

Figure 12. Fluorescence response of (a) **L2H** (b) **L3H** in presence of Al^{3+} ion (λ_{em} = 480 and 450 nm respectively) upon incremental addition of various metal ions (0-3 equivalents) in MeOH/HEPES buffer solution (5mM, pH = 7.3, 8:2, *v*/*v*).

4.3.4. pH effect:

To check the pH effect, the "*turn-on*" fluorescence ability of **L2H** and **L3H** were evaluated at different pH conditions in MeOH/HEPES buffer (8:2, *v*/*v*). Fluorescence behaviour of free probes **L2H** and **L3H** along with [Al(**L2**/**L3**)$Cl_2(H_2O)$] complexes,

were recorded in the pH range 2–12. The fluorescence intensity of both [Al(**L2**/**L3**)$Cl_2(H_2O)$] complexes remained nearly the same in pH 6–8 and this pH window is suitable for the use of these probes under physiological conditions (Figure 13).

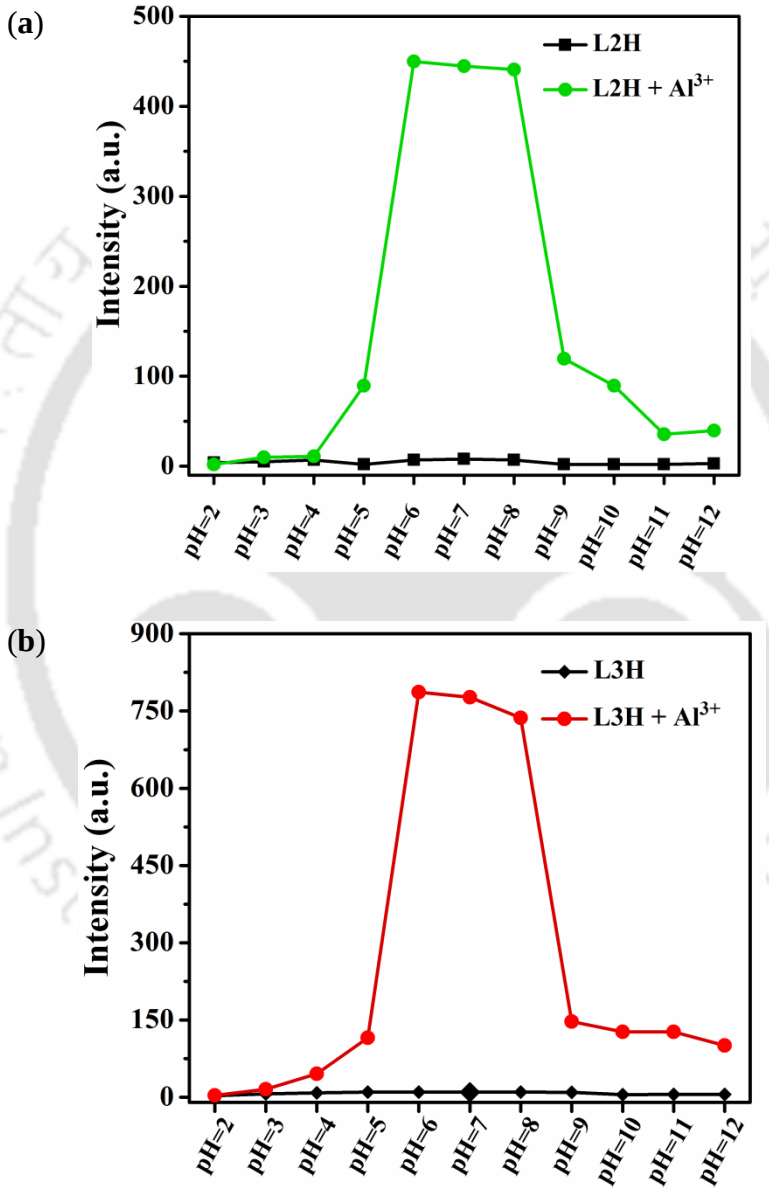

Figure 13. Fluorescence intensities of (a) **L2H** (10 μM, λ_{ex} = 375 nm) with [Al(**L2**)$Cl_2(H_2O)$] (λ_{em} = 480 nm) (b) **L3H** (10 μM, λ_{ex} = 395 nm) with [Al(**L3**)$Cl_2(H_2O)$] (λ_{em} = 450 nm) at various pH values in MeOH/HEPES buffer solution (5mM, 8:2, *v*/*v*).

4.3.5. TRPL Measurements:

The TRPL measurements were carried out to understand the mechanism of the "*turn-on*" sensor responses of **L2H** and **L3H** toward Al^{3+} ion and the decay profiles are shown in Figure 14-15. The fluorescence lifetimes (τ) of **L2H** and **L3H** in MeOH/HEPES buffer solution (5 mM, pH = 7.3, 8:2, *v*/*v*) are 0.62 and 0.02 ns respectively. On the other hand, average fluorescence lifetimes of Al(III) complexes of **L2H** and **L3H** are 3.56 and 1.87 ns respectively (Table 1). These lifetime values suggest that addition of $AlCl_3$ to **L2H** and **L3H**, allow CHEF to become operational as a result of complexation and thus fluorescence lifetimes of such emissive species become longer than the free probes. Both **L2H** and **L3H** were selective towards Al^{3+} ion by virtue of smaller charge-to-size ratio of Al^{3+} ion, thus stabilizing the excited state of the ligands and allowing them to decay through the emissive pathway. The excited state life time measurements were carried out on the diamagnetic metal ions like Zn^{2+} and Cd^{2+} show smaller changes with respect to the ligands (Figure A7) and this may not be sufficient to inhibit the non-radiative decay mechanism of the excited state.

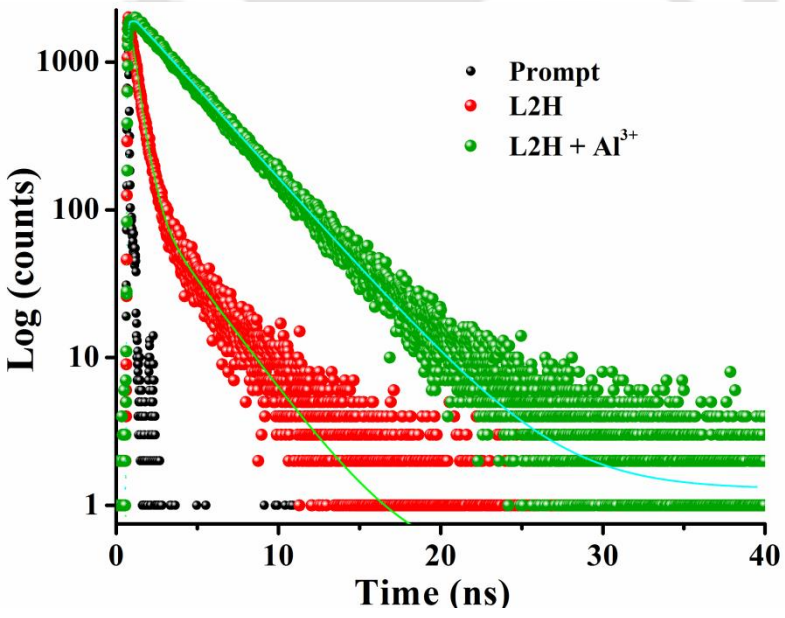

Figure 14. Time resolved decay profile of **L2H** upon addition of Al^{3+} ion.

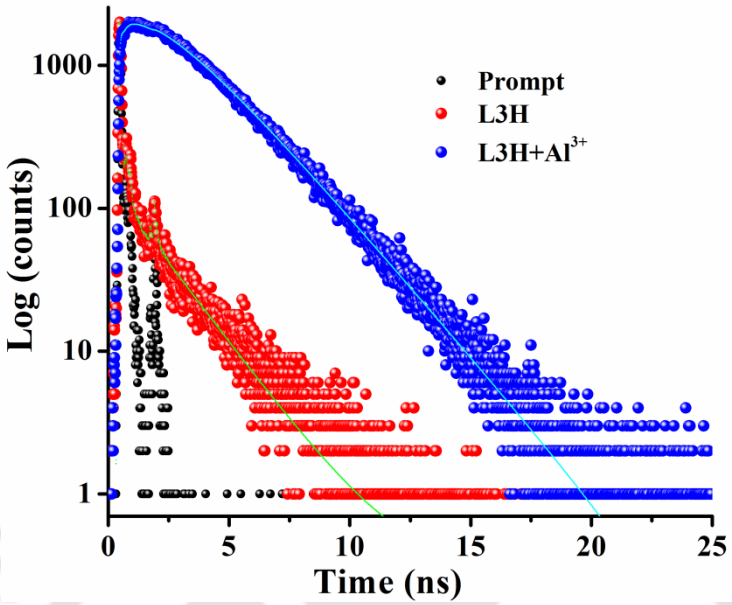

Figure 15. Time resolved decay profile of **L3H** upon addition of Al^{3+} ion.

Table 1: Fluorescence decay parameters of **L2H**, **L2H**+Al^{3+}, **L3H** and **L3H**+Al^{3+}

Sample	τ (ns)	χ^2
L2H	0.62	1.05
L2H+Al^{3+}	3.56	1.11
L2H+Zn^{2+}	0.13	1.01
L2H+Cd^{2+}	0.12	1.08
L3H	0.02	1.00
L3H+Al^{3+}	1.86	1.09
L3H+Zn^{2+}	0.09	1.00
L3H+Cd^{2+}	0.06	1.00

4.3.6. ^{1}H-NMR titration experiment of L2H and L3H with Al^{3+} ion:

The interactions between **L2H** and **L3H** with Al^{3+} ion were also followed by ^{1}H-NMR titration experiment. The ligand **L2H** has two phenolic OH groups out of which one that lie ortho to the imine function should involve in chelating to the metal ion. Hence upon **L2H** binding to Al^{3+} ion, OH peak at 12.15 ppm broadened initially and finally disappeared after addition of one equivalent of $AlCl_3$. Also all other peaks

broadened with the addition of $AlCl_3$, which indicated the complex formation of **L2H** and **L3H** with Al^{3+} ion. The above results strongly indicate that the phenolic –OH group and the Schiff base N-atoms bind with both the metal ions along with the deprotonation of the phenolic –OH group (Figure 16).

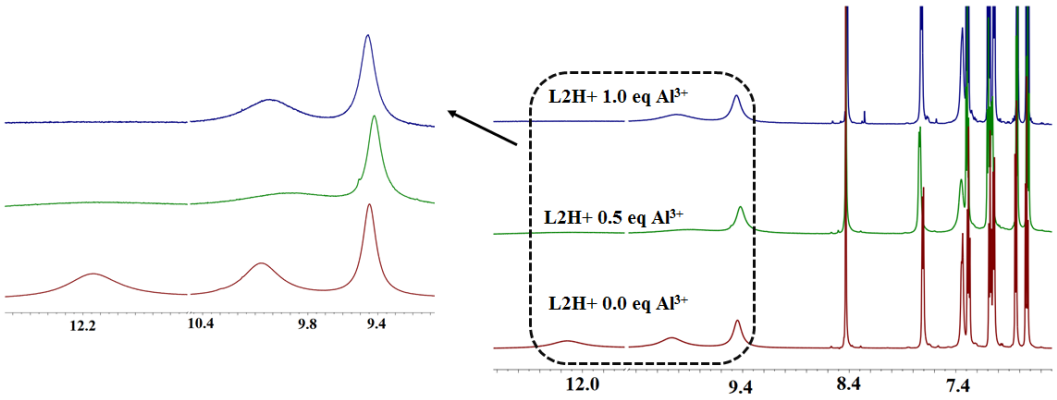

(**a**)

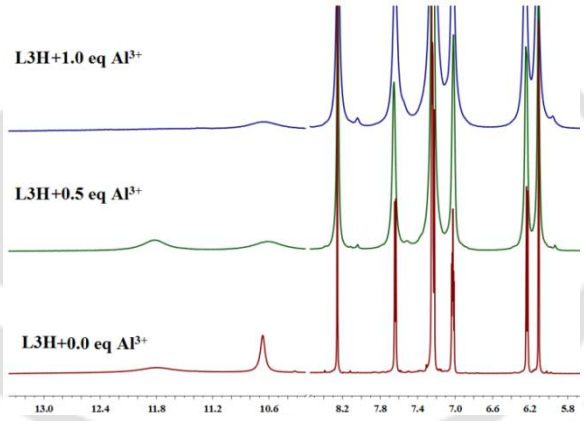

(**b**)

Figure 16. ^{1}H NMR titration study of (a) **L2H** and (b) **L3H** in DMSO-d_6/CD_3OD (9:1, *v*/*v*) at room temperature with $AlCl_3$.

4.3.7. Fluorescence studies of $[Al(L2)Cl_2(H_2O)]$ and $[Al(L3)Cl_2(H_2O)]$ species with various anions:

It is pronounced from the above results that **L2H** and **L3H** can selectively recognize Al^{3+} ion at different wavelengths in physiological condition even in presence of excess of other competitive metal ions. Emphasizing on the capability of metal complexes as a good binding ensemble for anions, we presume that resultant

mononuclear complexes can be used for anion recognition. So we investigated the impact of different anions on these complexes spectroscopically. The fluorescence response of complexes formed between **L2H**/**L3H** and Al^{3+} ion were examined in presence of various anions such as F^-, Cl^-, Br^-, I^-, SCN^-, PO_4^{3-}, $S_2O_3^{2-}$, $H_2PO_4^-$, HPO_4^{2-}, NO_3^-, SO_4^{2-}, $P_2O_7^{4-}$, S^{2-}, OH^-, HSO_4^-, CO_3^{2-}, HCO_3^-, AcO^-, ClO_4^- and $C_2O_4^{2-}$. Only F^- ion exhibited specific effect on fluorescence intensity of [Al(**L2**)$Cl_2(H_2O)$] and [Al(**L3**)$Cl_2(H_2O)$] complexes by completely quenching the emission intensity at 480 and 450 nm respectively and the resultant spectrum resembled to that of free ligand **L2H**/**L3H** (Figure 17).

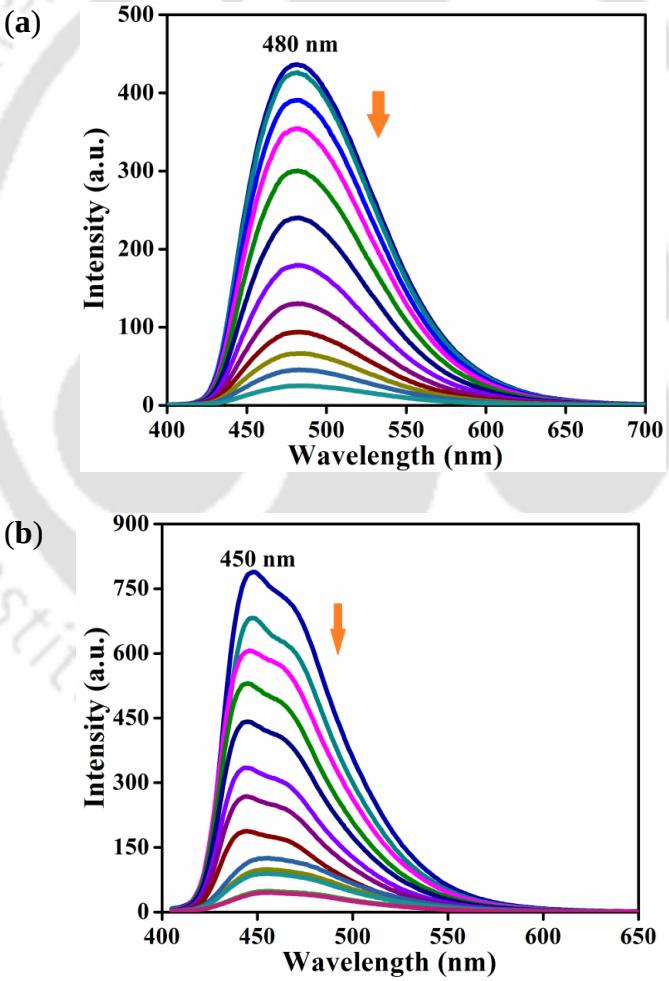

Figure 17. Changes in fluorescence spectra of (a) [Al(**L2**)$Cl_2(H_2O)$] (b) [Al(**L3**)$Cl_2(H_2O)$] ensemble upon incremental addition of F^- ion in MeOH/HEPES buffer (pH = 7.3, 8:2, *v/v*).

In contrast, all the other ions gave minimal or no significant change in intensity of [Al(**L2**)$Cl_2(H_2O)$]/[Al(**L3**)$Cl_2(H_2O)$] complexes (Figure 18). These results indicate that only F^- ion[51-56] form complex with Al^{3+} ion and release the free **L2H/L3H** into the solution. This selectivity is in accordance with the HSAB principle as both are hard ions in nature[57,58] and a similar result has been reported recently.[59]

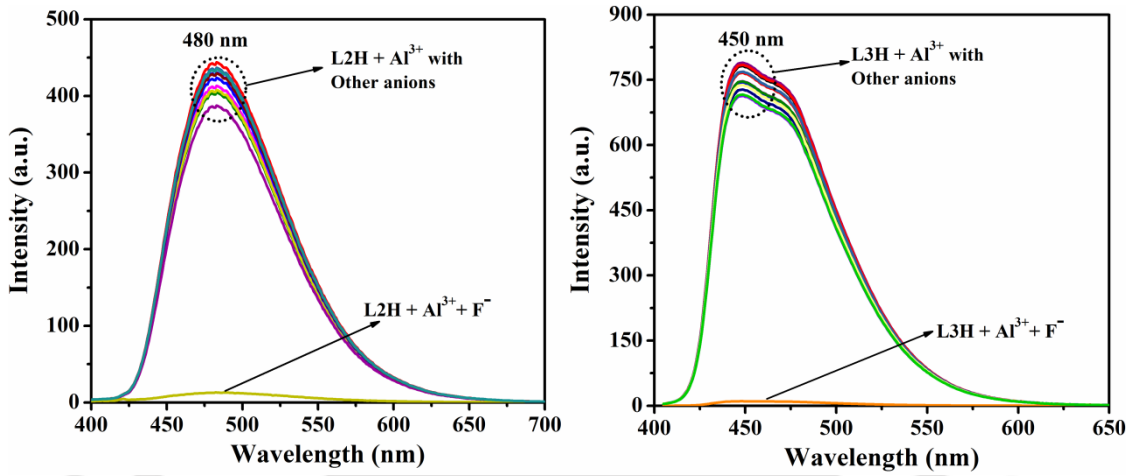

(**a**) (**b**)

Figure 18. Changes in fluorescence spectra of (a) [Al(**L2**)$Cl_2(H_2O)$] (b) [Al(**L3**)$Cl_2(H_2O)$] ensemble upon incremental addition of various anions such as F^-, Cl^-, Br^-, I^-, SCN^-, PO_4^{3-}, $S_2O_3^{2-}$, $H_2PO_4^-$, HPO_4^{2-}, NO_3^-, SO_4^{2-}, $P_2O_7^{4-}$, HSO_4^-, CO_3^{2-}, HCO_3^-, AcO^-, ClO_4^- and $C_2O_4^{2-}$ in MeOH/HEPES buffer (pH = 7.3, 8:2, *v/v*).

This indicates that extent of ionization of AlF_3 is not sufficient enough to leave fluoride-free (and solvated) Al^{3+} ion into the solution that will allow it to re-bind to the probes. As Al^{3+} and F^- ions are harder than the solvent system MeOH/H_2O (Sol) used in this study and ionization of AlF3 will be negligible. Any ionization of AlF_3 will lead to species like $[AlF_2(Sol)_4][AlF_4]$. Hence in presence of fluoride ions it is unlikely that fluoride free Al(III) ion will be present in solution. The binding constant of [Al(**L2**)$Cl_2(H_2O)$] and [Al(**L3**)$Cl_2(H_2O)$] with fluoride (Figure 19) ions are 5×10^5 M^{-1} and 3×10^5 M^{-1} respectively. The detection limit of [Al(**L2**)$Cl_2(H_2O)$] and [Al(**L3**)$Cl_2(H_2O)$] were evaluated to be 2.3×10^{-7} and 3.7×10^{-6} M respectively (Figure 20).

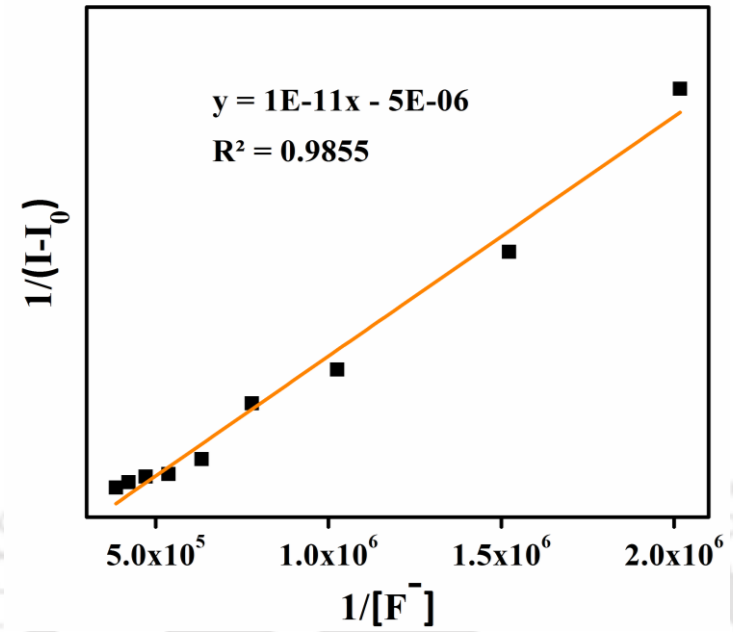

(**a**)

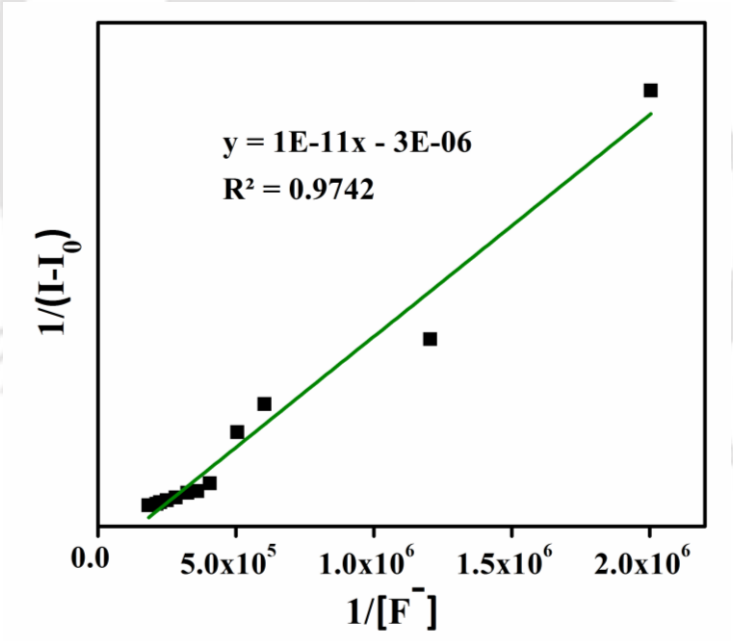

(**b**)

Figure 19. Benesi-Hildebrand plot for determination of binding constant of (a) [Al(**L2**)$Cl_2(H_2O)$] (b) [Al(**L3**)$Cl_2(H_2O)$] ensembles with F^- ion in MeOH/HEPES buffer (pH = 7.3, 8:2, *v*/*v*).

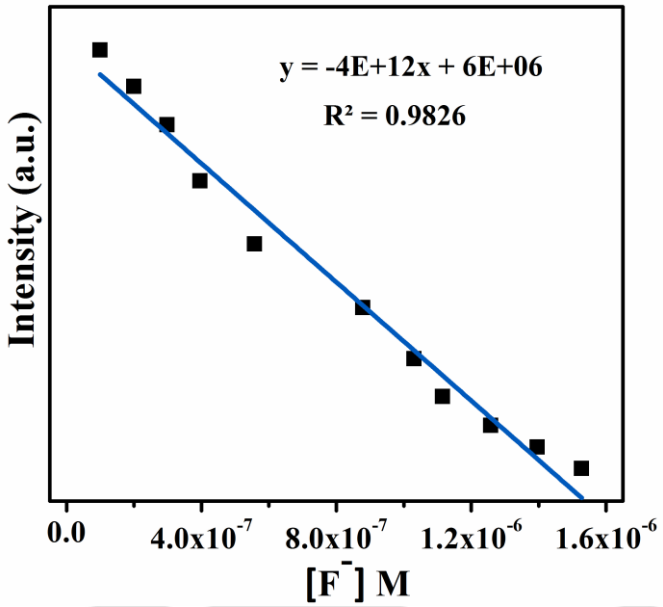

(a)

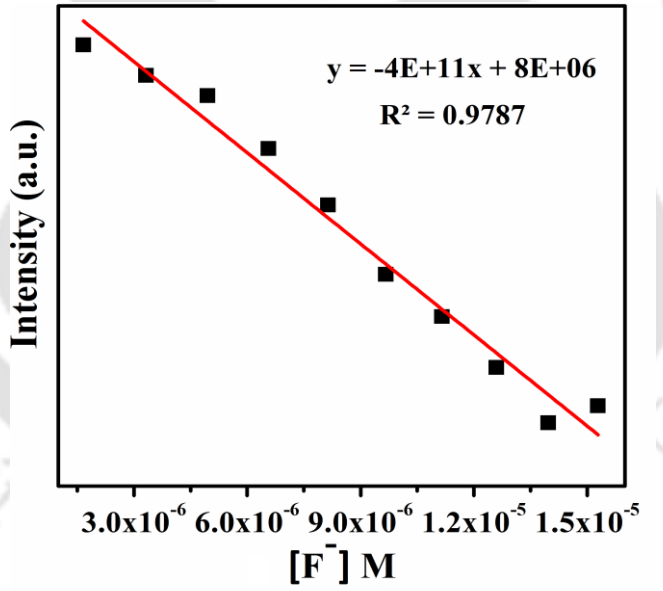

(b)

Figure 20. Fluorescence intensity vs. concentration of F^- ion plot for determination of detection limit (a) [**L2H**] = 10 μM (b) [**L3H**] = 10 μM.

4.3.8. Computational studies:

In order to have an insight into the structural changes that occur when **L2H** and **L3H** coordinate to Al^{3+} ion, extensive density functional theory (DFT/TDDFT)

calculations were performed on **L2H**, **L3H**, [Al(**L2**)$Cl_2(H_2O)$] and [Al(**L3**)$Cl_2(H_2O)$]. The formula for the complexes were chosen based on absorption and emission spectroscopic studies, which yielded the stoichiometries of complexes to be 1:1 with respect to the ligand. Both **L2H** and **L3H** are potential tridentate ligands and can coordinate through N_B, N_H and O_P {N_B = benzothiozole-N; N_H = hydrazone-N and O_P = phenolate-O} atoms. However both **L2H** and **L3H** can exist in two rotational isomeric forms with respect to the N–N bond leading to H_H and H_A {H_H = hydrazine-H and H_A = aldimine-H} orienting in *syn* and *anti* fashion (Figure 21-22) with respect to each other. The optimized structures of [Al(**L2**)$Cl_2(H_2O)$] and [Al(**L3**)$Cl_2(H_2O)$] are shown in Figure 23.

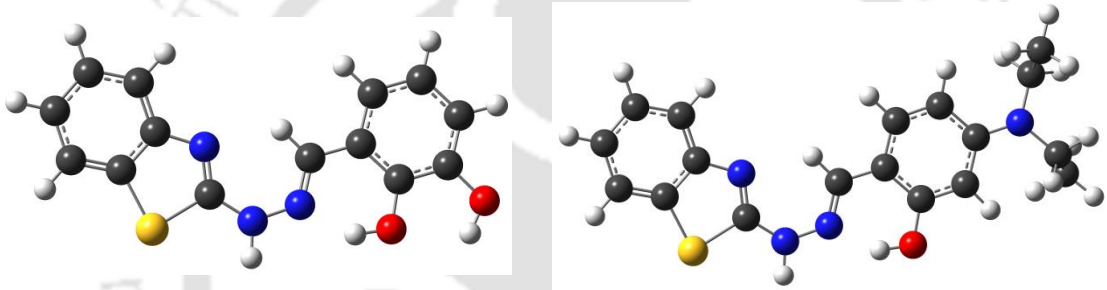

(**a**) (**b**)

Figure 21. Optimised structures *anti* form of (a) **L2H** and (b) **L3H**.

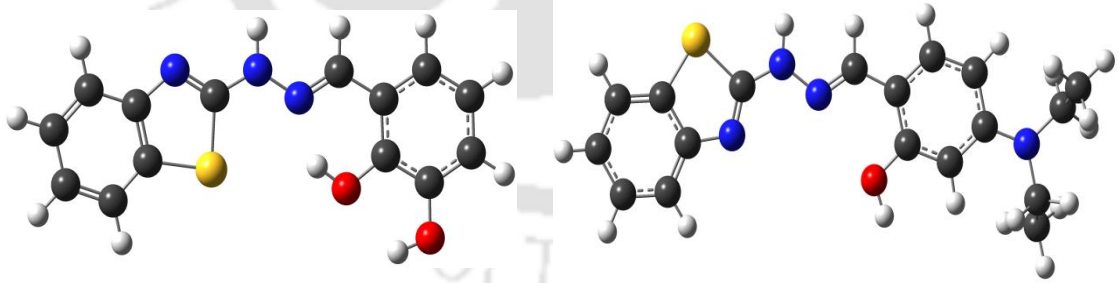

(**a**) (**b**)

Figure 22. Optimised structures *syn* form of (a) **L2H** and (b) **L3H**.

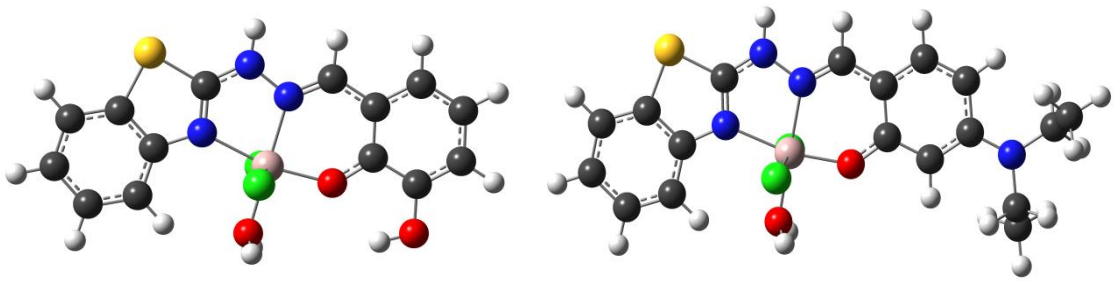

(**a**) (**b**)

Figure 23. Optimised structures of (a) [Al(**L2**)$Cl_2(H_2O)$] (b) [Al(**L3**)$Cl_2(H_2O)$].

Calculations on both forms of **L2H** and **L3H** suggest that *anti* form is more stable by 8.4 and 19.7 KJ/mol respectively. But in complexes, both ligands are required to exist in the *syn* form since all the three donor atoms should lie in same direction for effective chelation to metal center. Optimized structures of *syn* and *anti* forms of **L2H** and **L3H** are completely planar in nature. The relative energies and frontier molecular orbitals of **L2H** and [Al(**L2**)$Cl_2(H_2O)$] are depicted in (Figure 24). The HOMO/HOMO-1 of **L2H** are mainly localised on π-orbitals of benzothiazole ring, phenol ring and lone pair orbitals on oxygen and nitrogen atoms. The LUMO is corresponding antibonding orbital (Figure 24) of HOMO with energy gap between HOMO and LUMO being 3.934 eV. Both HOMO and LUMO of [Al(**L2**)$Cl_2(H_2O)$] more or less resemble those of **L2H** except some deviations on benzo moiety of benzothiazole ring. Upon coordination to Al(III), the energy of HOMO is raised while that of LUMO being lowered thereby bringing down HOMO-LUMO energy gap to 3.201 eV. The HOMO of **L3H** has contributions from the π-orbitals of the whole molecule including nitrogen atom of *N*,*N*-diethylamine group as well as benzothiazole moiety and the LUMO is corresponding antibonding orbitals. The HOMO and LUMO of [Al(**L3**)$Cl_2(H_2O)$] also resemble those of **L3H** but Al(III) ion stabilize LUMO to a greater extent than HOMO and effectively lower the HOMO-LUMO energy gap to 3.442 eV from 3.606 eV (Figure 25). The decrease in energy gap upon coordination to Al^{3+} ion implies a red shift of absorption band to occur in complexes which has indeed been observed experimentally. Also as the lone-pair on hydrazone-N atom is coordinated to the metal ion, PET process has been unfavoured totally.

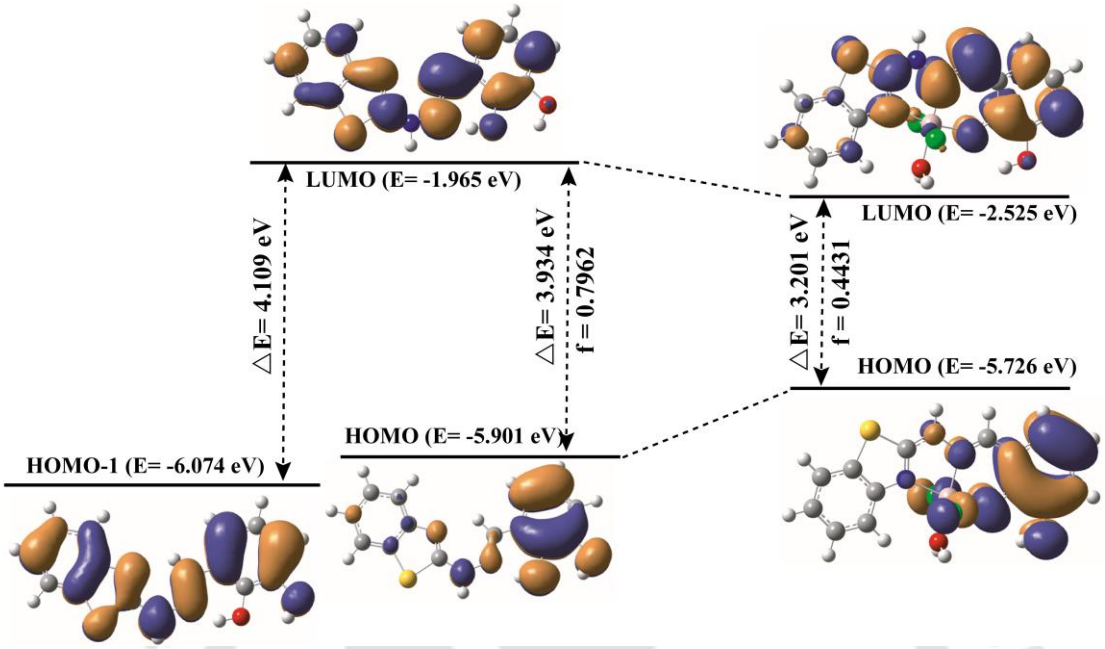

Figure 24. Energy level diagram depicting frontier orbitals of **L2H** and [Al(**L2**)$Cl_2(H_2O)$].

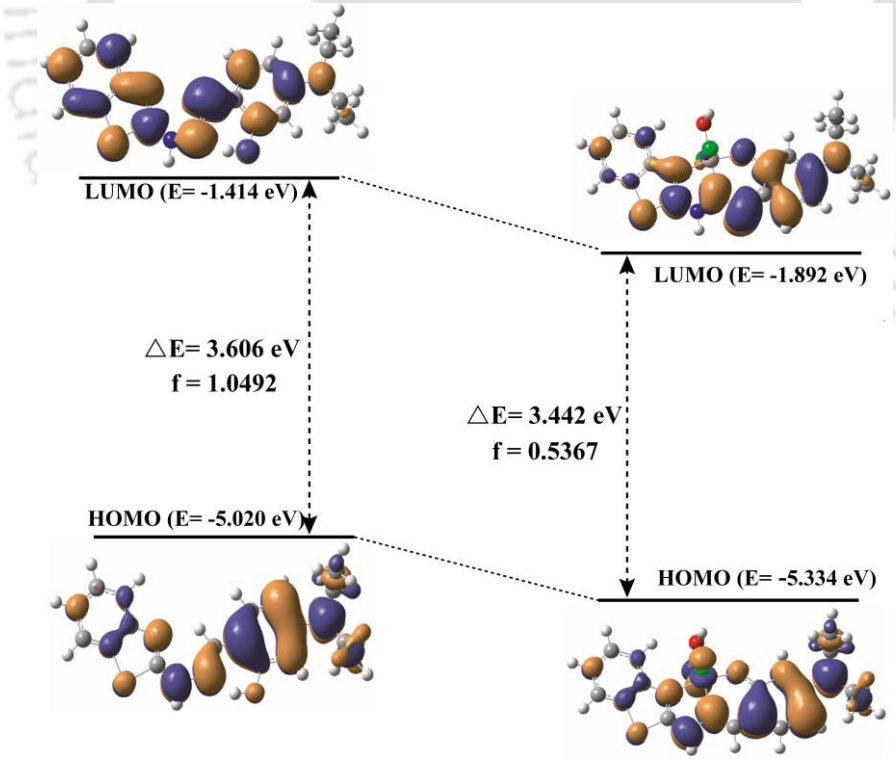

Figure 25. Energy level diagram depicting HOMO and LUMO of **L3H** and [Al(**L3**)$Cl_2(H_2O)$].

4.4. Conclusion:

In conclusion, condensation products of 2-hydrazinylbenzothiazole with 2,3-dihydroxybenzaldehyde (**L2H**) and 4-(diethylamino)-2-hydroxybenzaldehyde (**L3H**) were isolated as crystalline solid and characterized thoroughly using spectroscopic techniques. In MeOH/HEPES buffer, both **L2H** and **L3H** act as "OFF-ON" fluorescence sensors for Al^{3+} ion. Free probes show absorption band assignable to $n\rightarrow\pi^*$ transition, which undergo red-shift upon gradual addition of $AlCl_3$ along with a quasi isosbestic point in both cases. The probes are weakly emissive in nature due to photoinduced electron transfer process but upon irradiating with 375 and 395 nm light, **L2H** and **L3H** became strongly emissive only in presence of Al^{3+} ion having the maxima at 480 and 450 nm respectively. These results indicate that the PET process is quenched in presence of Al^{3+} ion. Both probes exhibit high sensitivity for Al^{3+} ion having detection limits in nanomolar levels. Fluoride ion exhibited specific "*Turn Off*" effect on fluorescence intensity by complete quenching of the respective emission intensity. The DFT/TDDFT calculations performed on **L2H**, **L3H**, [Al(**L2**)$Cl_2(H_2O)$] and [Al(**L3**)$Cl_2(H_2O)$] revealed that in [Al(**L2**)$Cl_2(H_2O)$] the energy of HOMO is raised while that of LUMO lowered and in [Al(**L3**)$Cl_2(H_2O)$] the energy of LUMO was lowered to a greater extent than the HOMO. Hence in both complexes, HOMO-LUMO energy gap has been reduced in comparison with free ligands.

References:

1. L. Lehninger, *Principles of Biochemistry*, CBS Publishers and Distributers, New Delhi, 1984.
2. J. J. Peirce, R. F. Weiner and P. A. Vesilind, *Environmental Pollution and Control.*, Butterworth-Heinemann, 225 Wildwood Avenue, Wuburn, USA, 1998.
3. H. N. Kim, W. X. Ren, J. S. Kim and J. Yoon, *Chem. Soc. Rev.*, 2012, **41**, 3210-3244.
4. H. N. Kim, Z. Guo, W. Zhu, J. Yoon and H. Tian, *Chem. Soc. Rev.*, 2011, **40**, 79-93.
5. D. T. Quang and J. S. Kim, *Chem. Rev.*, 2010, **110**, 6280-6301.
6. E. M. Nolan and S. J. Lippard, *Chem. Rev.*, 2008, **108**, 3443-3480.
7. J. S. Kim and D. T. Quang, *Chem. Rev.*, 2007, **107**, 3780-3799.
8. P. Das, A. Ghosh, H. Bhatt and A. Das, *RSC Adv.*, 2012, **2**, 3714-3721.
9. V. Luxami and S. Kumar, *RSC Adv.*, 2012, **2**, 8734-8740.
10. C. Kar, M. D. Adhikari, A. Ramesh and G. Das, *RSC Adv.*, 2012, **2**, 9201-9206.
11. Y. Wang, Y. Huang, B. Li, L. Zhang, H. Song, H. Jiang and J. Gao, *RSC Adv.*, 2011, **1**, 1294-1300.
12. W. J. McShane, R. S. Pappas, V. Wilson-McElprang and D. Paschal, *Spectrochim. Acta, Part B*, 2008, **63**, 638-644.
13. M. de la Guardia, A. R. Mauri and C. J. Mongay, *J. Anal. At. Spectrom.*, 1988, **3**, 1035-1038.
14. The special issue on Aluminium: Lithosphere to Biosphere (and Back): *J. Inorg. Biochem.*, 2005, **99**, 1747-1928.
15. W. S. Miller, L. Zhuang, J. Bottema, A. J. Wittebrood, P. De Smet, A. Haszler and A. Vierege, *Mater. Sci. Eng., A*, 2000, **280**, 37-49.
16. M. L. Mora, M. A. Alfara, S. C. Jarvis, R. Demanet and P. Cartes, *Soil Use Manage*, 2006, **22**, 95-101.
17. E. Alvarez, M. L. Fernandez, C. Monterroso and S. M. Fernandez, *Forest Ecol. Manage*, 2005, **211**, 227-239.
18. J. Barcello and C. Poschenrieder, *Environ. Exp. Bot.*, 2002, **48**, 75-92.
19. J. R. Walton, *NeuroToxicology*, 2006, **27**, 385-394.
20. S. Polizzi, *NeuroToxicology*, 2002, **23**, 761-774.

21. M. Baral, S. K. Sahoo and B. K. Kanungo, *J. Inorg. Biochem.*, 2008, **102**, 1581-1588.
22. V. K. Gupta, A. K. Jain and G. Maheshwari, *Talanta*, 2007, **72**, 1469-1473.
23. J. R. J. Sorenson, I. R. Campbell, L. B. Tepper and R. D. Lingg, *Environ. Health Perspect.*, 1974, **8**, 3-95.
24. S. H. Kim, H. S. Cho, J. Kim, S. J. Lee, D. T. Quang and J. S. Kim, *Org. Lett.*, 2010, **12**, 560-563.
25. E. Delhaize and P. R. Ryan, *Plant Physiol.*, **1995**, *107*, 315-321.
26. D. L. Godbold, E. Fritz and A. Huttermann, *Proc. Natl. Acad. Sci. U. S. A.*, 1988, **85**, 3888–3892.
27. J. Ren and H. Tian, *Sensors*, 2007, **7**, 3166-3178.
28. K. Soroka, R. Vithanage, D. A. Philips, B. Walker and P. K. Dasgupta, *Anal. Chem.*, 1987, **59**, 629-636.
29. K. K. Upadhyay and A. Kumar, *Org. Biomol.Chem.*, 2010, **8**, 4892-4897.
30. X. Sun, Y. W. Wang and Y. Peng, *Org. Lett.*, 2012, **14**, 3420-3423.
31. D. Maity and T. Govindaraju, *Inorg. Chem.*, 2010, **49**, 7229-7231.
32. D. Maity and T. Govindaraju, *Chem. Commun.*, 2010, **46**, 4499-4501.
33. D. Maity and T. Govindaraju, *Chem. Commun.*, 2012, **48**, 1039-1041.
34. D. Maity and T. Govindaraju, *Eur. J. Inorg. Chem.*, 2011, 5479-5485.
35. L. Wang, W. Qin, X. Tang, W. Dou and W. Liu, *J. Phys. Chem. A*, 2011, **115**, 1609-1616.
36. M. Suresh, A. K. Mandal, S. Saha, E. Suresh, A. Mandoli, R. D. Liddo, P. P. Parnigotto and A. Das, *Org. Lett.*, 2010, **12**, 5406-5409.
37. F. Zapata, A. Caballero, A. Espinosa, A. Tarraga and P. Molina, *Org. Lett.*, 2007, **9**, 2385-2388.
38. J. Wu, W. Liu, J. Ge, H. Zhang and P. Wang, *Chem. Soc. Rev.*, 2011, **40**, 3483-3495.
39. P. Ghosh and P. Banerjee, *Phys. Chem. Chem. Phys.*, 2016, **18**, 22805-22815.
40. P. Ghosh, P. Roy, A. Ghosh, S. Jana, N. C. Murmu, S. K. Mukhopadhyay and P. Banerjee, *J. Lumin.*, 2017, **185**, 272-278.
41. P. Ghosh, B. G. Roy, S. K. Mukhopadhyay and P. Banerjee, *RSC Adv.*, 2015, **5**, 27387-27392.

42. K. Youngmin and F. P. Gabbaï, *J. Am. Chem. Soc.*, 2009, **131**, 3363-3369.
43. S. Jagtap, M. K. Yenkie, N. Labhsetwar and S. Rayalu, *Chem. Rev.*, 2012, **112**, 2454-2466.
44. A. Roychowdhury, P. Ghosh, S. K. Saha, P. Mitra and P. Banerjee, *Spectrochim. Acta, Part A*, 2014, **124**, 492-499.
45. I.-S. Ke, M. Myahkostupov, F. N. Castellano and F. P. Gabbaï, *J. Am. Chem. Soc.*, 2012, **134**, 15309-15311.
46. H. Miyaji, W. Sato and J. L. Sessler, *Angew. Chem., Int. Ed.*, 2000, **39**, 1777-1780.
47. M. J. Frisch, G. W. Trucks, H. B. Schlegel, G. E. Scuseria, M. A. Robb, J. R. Cheeseman, G. Scalmani, V. Barone, B. Mennucci, G. A. Petersson, H. Nakatsuji, M. Caricato, X. Li, H. P. Hratchian, A. F. Izmaylov, J. Bloino, G. Zheng, J. L. Sonnenberg, M. Hada, M. Ehara, K. Toyota, R. Fukuda, J. Hasegawa, M. Ishida, T. Nakajima, Y. Honda, O. Kitao, H. Nakai, T. Vreven, J. A. Montgomery, Jr., J. E. Peralta, F. Ogliaro, M. Bearpark, J. J. Heyd, E. Brothers, K. N. Kudin, V. N. Staroverov, R. Kobayashi, J. Normand, K. Raghavachari, A. Rendell, J. C. Burant, S. S. Iyengar, J. Tomasi, M. Cossi, N. Rega, J. M. Millam, M. Klene, J. E. Knox, J. B. Cross, V. Bakken, C. Adamo, J. Jaramillo, R. Gomperts, R. E. Stratmann, O. Yazyev, A. J. Austin, R. Cammi, C. Pomelli, J. W. Ochterski, R. L. Martin, K. Morokuma, V. G. Zakrzewski, G. A. Voth, P. Salvador, J. J. Dannenberg, S. Dapprich, A. D. Daniels, Ö. Farkas, J. B. Foresman, J. V. Ortiz, J. Cioslowski, D. J. Fox, Gaussian 09, Revision D.01, Gaussian, Inc., Wallingford CT, 2009.
48. M. Shyamal, P. Mazumdar, S. Maity, S. Samanta, G. P. Sahoo and A. Misra, *ACS Sens.*, 2016, **1**, 739-747.
49. S. Goswami, A. Manna, S. Paul, K. Aich, A. K. Das and S. Chakraborty, *Dalton Trans.*, 2013, **42**, 8078-8085.
50. F. A. Cotton, G. Wilkinson, C. A. Murillo and M. Bochmann, *Advanced Inorganic Chemistry*, John Wiley and sons, inc. 6th edition, page 177.
51. P. Ghosh, B. G. Roy, S. Jana, S. K. Mukhopadhyay and P. Banerjee, *Phys. Chem. Chem. Phys.*, 2015, **17**, 20288-20295.
52. P. Ghosh, N. Kumar, S. K. Mukhopadhyay and P. Banerjee, *Sens. Actuators, B*, 2016, **224**, 899-906.

53. P. Ghosh and P. Banerjee, *Chem. Phys.*, 2016, **478**, 103-109.
54. P. Ghosh and P. Banerjee, *Anal. Chim. Acta*, 2017, **965**, 111-122.
55. A. R. Chowdhury, P. Ghosh, B. G. Roy, S. K. Mukhopadhyay, N. C. Murmu and P. Banerjee, *Sens. Actuators, B*, 2015, **220**, 347-355.
56. A. R. Chowdhury, P. Ghosh, B. G. Roy, S. K. Mukhopadhyay, P. Mitra and P. Banerjee, *RSC Adv.*, 2015, **5**, 62017-62023.
57. D. F. Shriver and P. W. Atkins, *Inorganic Chemistry*, Oxford University Press, 3rd edition, 1999, 169.
58. R. G. Pearson, *J. Chem. Edu.*, 1968, **45**, 581-587.
59. D. Sarkar, P. Ghosh, S. Gharami, T. K. Mondal and N. Murmu., *Sens. Actuators, B*, 2017, **242**, 338–346.

Appendix:

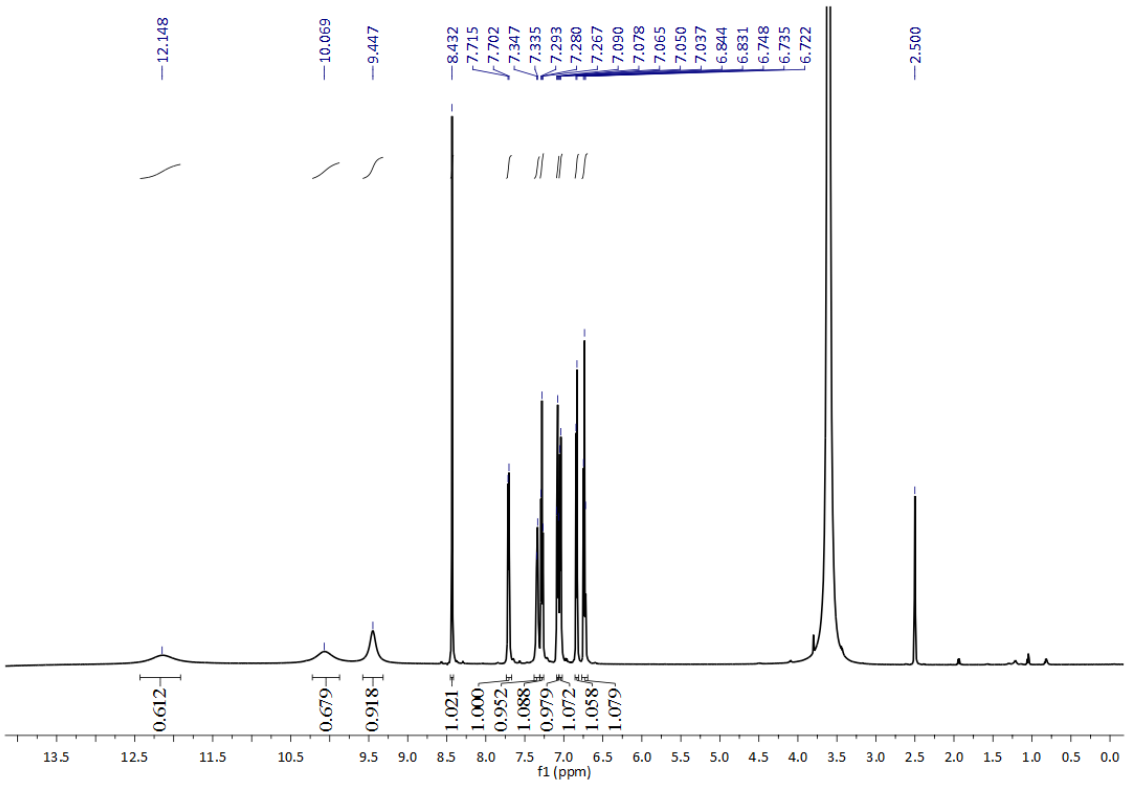

Figure A1. ^{1}H NMR of **L2H**.

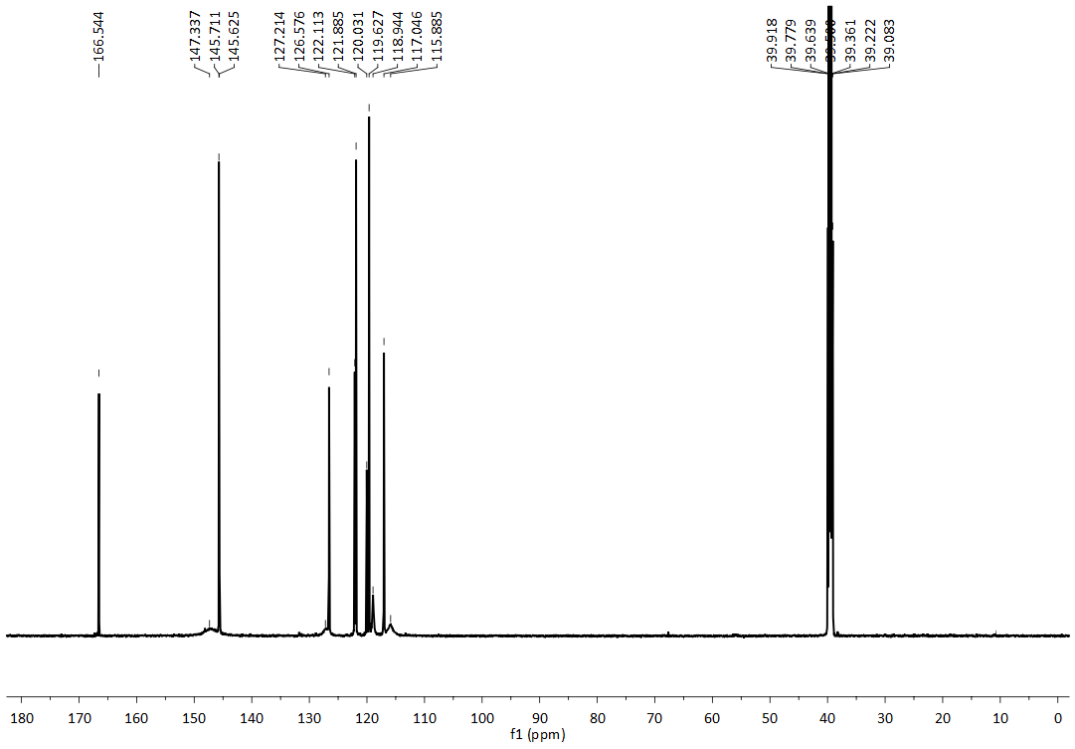

Figure A2. ^{13}C NMR of **L2H**.

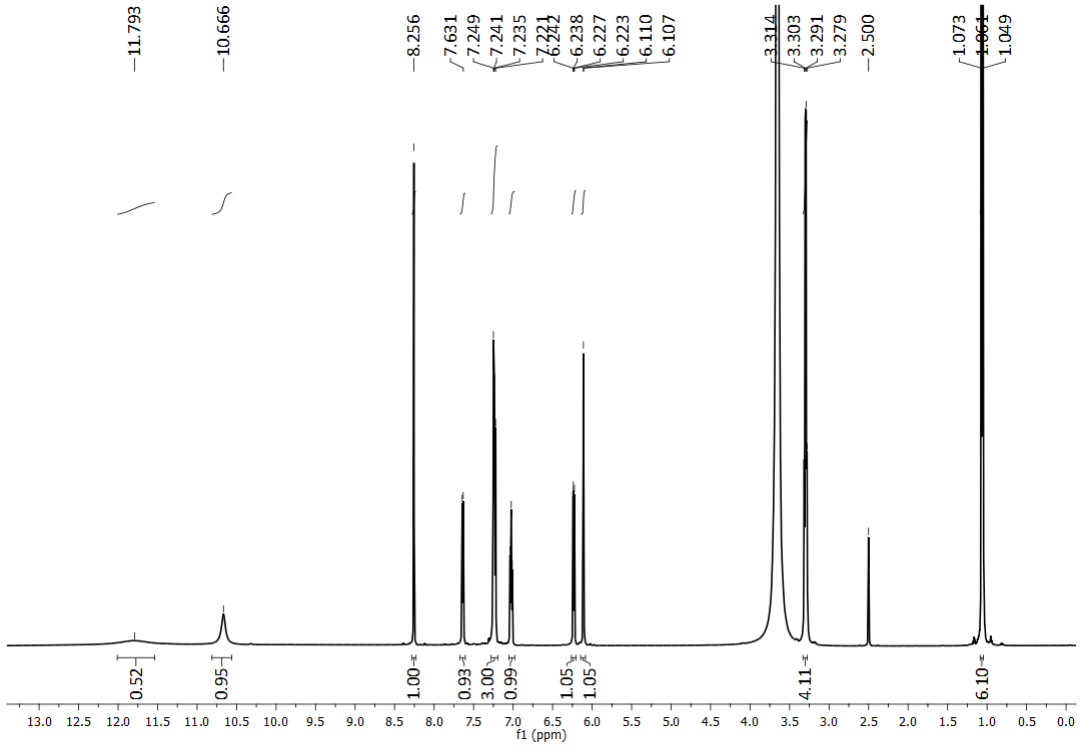

Figure A3. ^{1}H NMR of **L3H.**

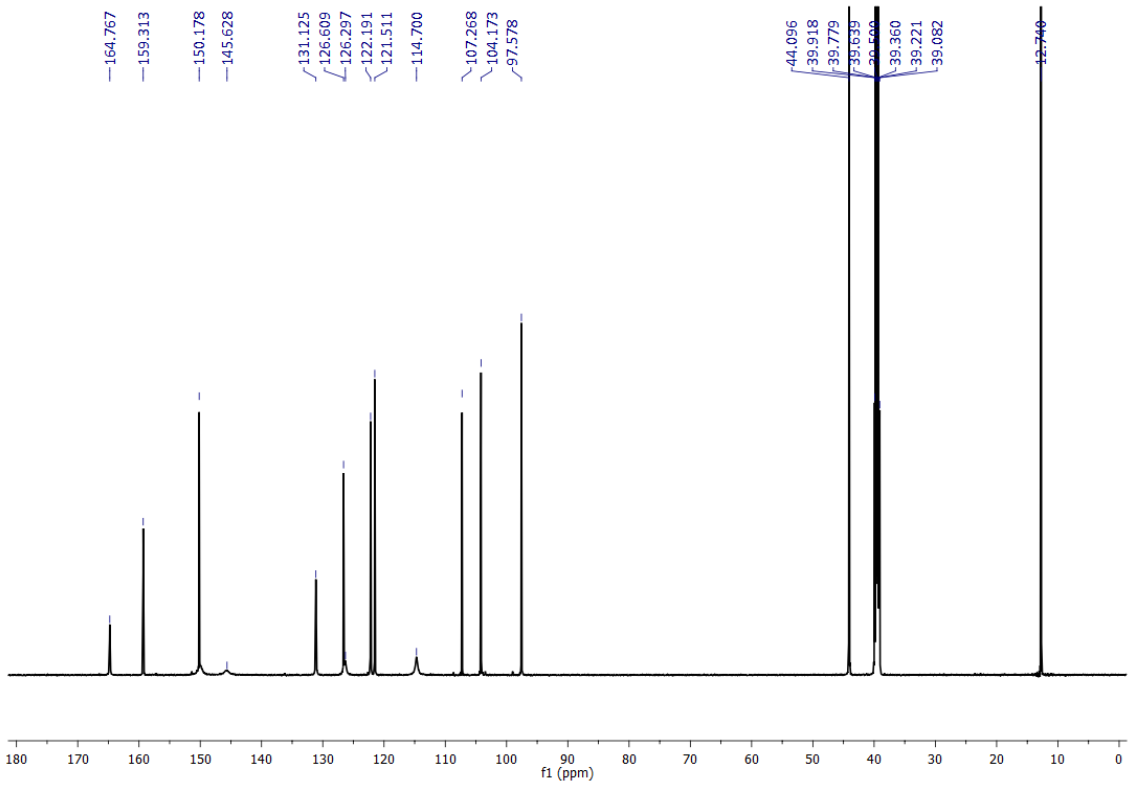

Figure A4. ^{13}C NMR of **L3H**.

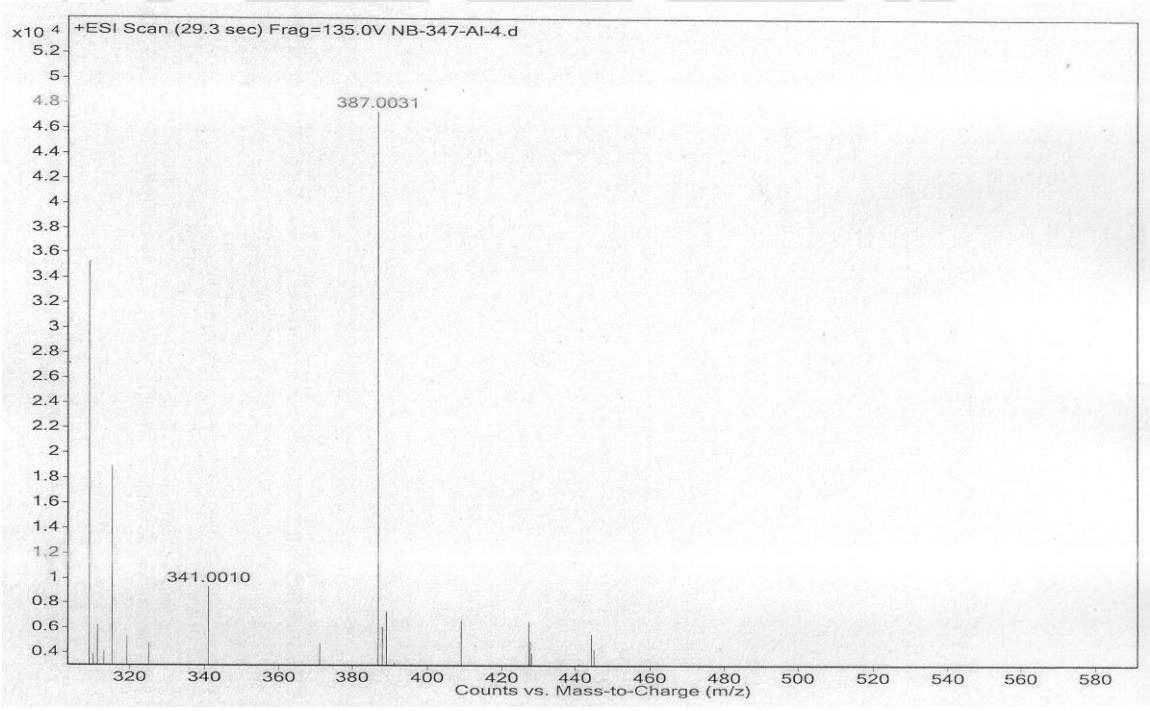

Figure A5. Mass spectrum of **L2H** complex of Al^{3+} ion.

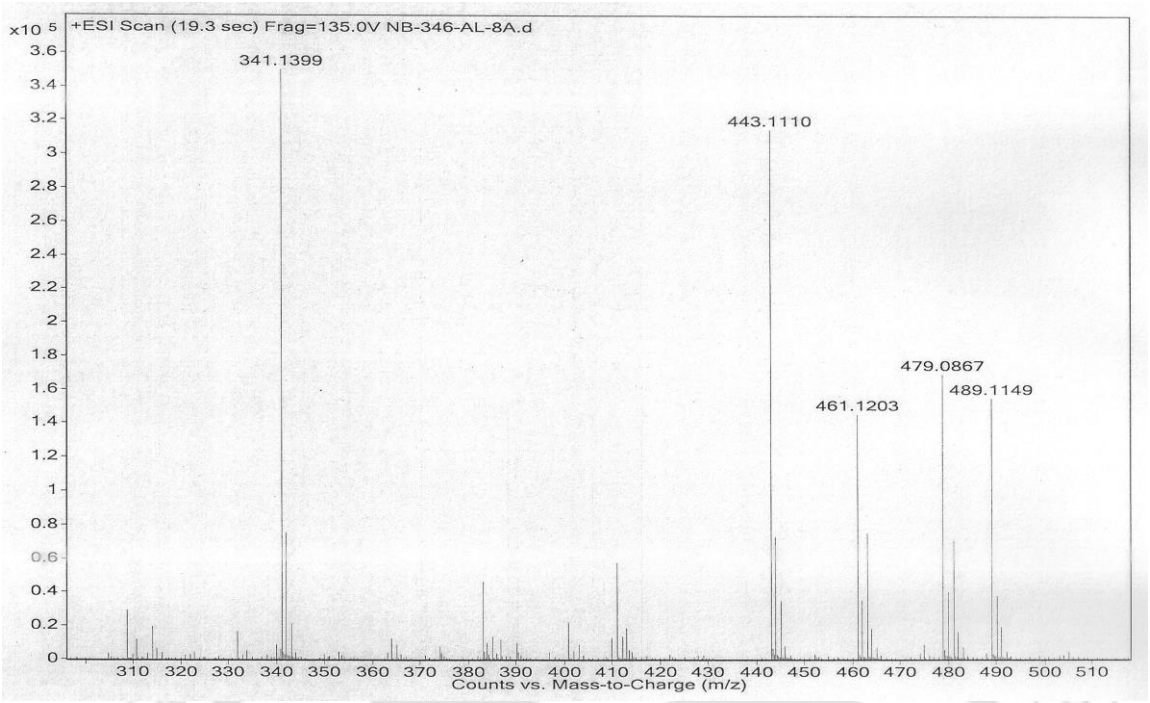

Figure A6. Mass spectrum of **L3H** complex of Al^{3+} ion.

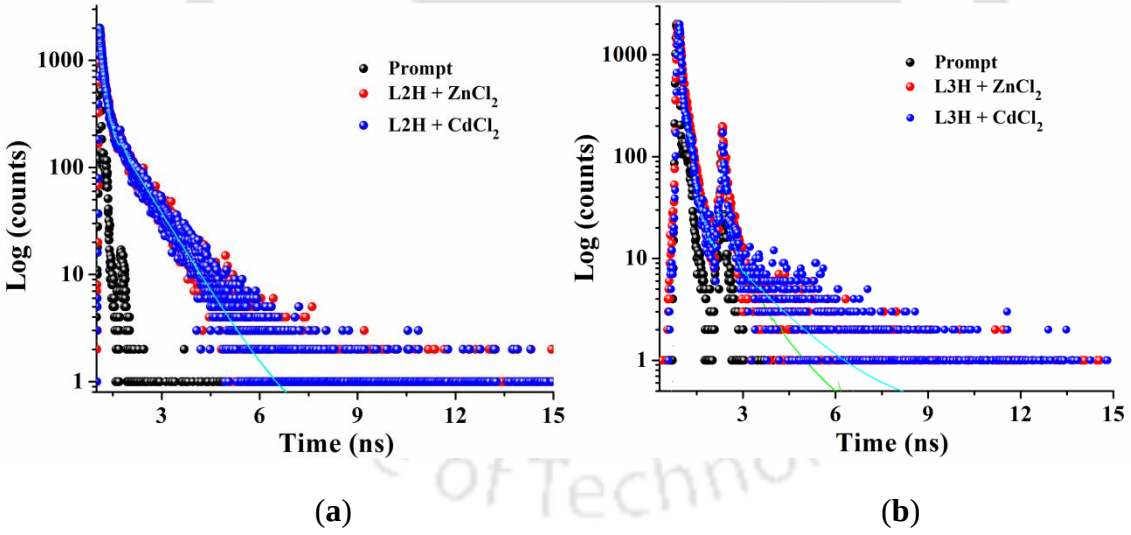

(**a**) (**b**)

Figure A7. Time resolved decay profile of (a) **L2H** (b) **L3H** upon addition of Zn^{2+} and Cd^{2+} ions.

Chapter 5

A Probe for Multi Detection of Al^{3+}, Zn^{2+} and Cd^{2+} Ions *via* *Turn-On* Fluorescence Responses*

Abstract:

In this Chapter, hydrazide (**L4H**) using 6-(hydroxymethyl)picolinohydrazide and 2-hydroxynapthaldehyde was synthesized and characterized. This acts as a "*TURN-ON"* fluorescence sensor for Al^{3+}, Zn^{2+} and Cd^{2+} ions by giving different emission maxima. The **L4H** itself is weakly emissive having the maximum at 495 nm. Gradual addition of chloride salts of Al^{3+}, Zn^{2+} and Cd^{2+} ions to **L4H**, gave rise to emission peaks at 485, 570 and 540 nm, in MeOH-HEPES buffer solution (5 mM, pH = 7.3, 7:3 *v*/*v*). Addition of Al^{3+}, Zn^{2+} and Cd^{2+} ions to a solution of **L4H** generates new absorbance and fluorescence peaks due to binding of $\mathbf{L4}^-$ with Al^{3+} ion in 2:1 ratio; Zn^{2+} and Cd^{2+} ions in 1:1 ratios. Reversibility of complexes of **L4H** with Al^{3+}, Zn^{2+} and Cd^{2+} ions was also studied by titrating with Na_2EDTA using UV-Vis spectroscopy. Calculated detection limits of **L4H** towards Al^{3+}, Zn^{2+} and Cd^{2+} ions are 5.7×10^{-9}, 1.09×10^{-6} and 1.64×10^{-6} M respectively. Based on experimental and theoretical results the formulae $[Al(\mathbf{L4})_2]^+$, $[Zn(\mathbf{L4})Cl(H_2O)_2]$ and $[Cd(\mathbf{L4})Cl(H_2O)_2]$ were assigned and these complexes generated *in situ* are useful fluorophore to detect fluoride and dihydrogen phosphate ions, which act by quenching the fluorescence responses. The results of DFT/TDDFT calculations on **L4H**, $[Al(\mathbf{L4})_2]^+$, $[Zn(\mathbf{L4})Cl(H_2O)_2]$ and $[Cd(\mathbf{L4})Cl(H_2O)_2]$ were consistent with the experimental results.

* This work has been published in:

N. Behera and V. Manivannan, *J. Photochem. Photobiol. A*, 2018, **353**, 77-85.

5.1. Introduction:

Metal ions play essential role in the fields of life sciences, medicine, chemistry and biotechnology.[1-3] Aluminium compounds are adequately used in many industries and pharmaceuticals.[4,5] Excess of Al^{3+} ion is toxic to fish, algae as well as to other aquatic species. In humans, excessive accumulation causes several diseases such as Parkinson's disease, Alzheimer's disease, osteomalacia, and rickets.[6,7] Potential impact on human health and environment of Al^{3+} ion having weak coordination and strong properties has created importance for estimation of this ion. On the other hand, zinc is the second most abundant transition metal ion, present in various classes of enzyme and plays a rudimentary role in metabolism of RNA and DNA, signal transduction, regulating apoptosis and gene expression.[12-16] Effects of zinc deficiency and overload on animals, plants and aquatic lives have been documented.[17-20] Heavy metal ion Cd^{2+} is toxic and carcinogenic in nature.[21,22] Use of Cd^{2+} ion in making battery, metal alloys, paint pigments, ceramic enamels and natural factors consequently lead to water and soil contamination.[23-25] As both Zn^{2+} and Cd^{2+} belong to same group, most of these Zn^{2+} and Cd^{2+} ion sensors have given very similar physicochemical properties. Thus, distinguishing Zn^{2+} and Cd^{2+} ions from one another at different wavelength is of critical importance.[26,27]

Fluoride[28-30] and $H_2PO_4^-$ ions[31-33] play an imperative role in various fields such as biological, medical and chemical processes. Fluoride has important role to prevent osteoporosis and also in dental care.[34] Excess intake of fluoride ion cause dental and skeletal fluorosis, urolithiasis.[35-38] Furthermore, dihydrogen phosphate ($H_2PO_4^-$) plays a pivotal role in signal transduction, energy storage and construction of the backbone of DNA and RNA.[39,40] Moreover, phosphates as pollutants can cause the eutrophication of water.[41] Therefore, detection of F^- and $H_2PO_4^-$ ions has received increasing attention.[42,43]

Ability of high sensitivity, fast response time and technical simplicity of probes along with detection of cations by producing distinct fluorescence signals has been created great impact recently.[44-50] Many probes having naphthyl, boron dipyrromethenedifluoride, coumarin, rhodamine and salicylyl moieties were reported to be useful fluorophores for the detection of single metal ion.[51-58] Fluorescent sensors

derived using 2-hydroxy-1-naphthaldehyde and suitable amine often provided an excellent functionalised fluorescent backbone.[59,60] The modularity, straightforward synthesis, and stability towards hydrolysis (cf. imines) make hydrazide backbone containing 2-hydroxy-1-naphthyl group, a useful probe for cation detection. There are very less number of reports for achieving multiple metal ion detection at distinct signals.[61-68] Search for new fluorescence probes for detection of different biologically and environmentally important metal ions at distinct emission wavelength is still continuing. We report here a new probe **L4H** (6-(hydroxymethyl)-*N'*-((2-hydroxy-1-naphthyl)methylene)picolinohydrazide) that can detect Al^{3+}, Zn^{2+} and Cd^{2+} ions by giving sharp "*TURN-ON*" fluorescence responses at different wavelengths at physiological conditions. In addition, thus obtained solutions containing these complex species are also useful for secondary detection of fluoride and $H_2PO_4^-$ ions.

5.2. Experimental section:

5.2.1. *Synthesis of 1–3*:

Compound **1**–**3** were prepared by adopting the procedures reported in the literature.[69,70] Typically **1** was prepared by refluxing 2,6-pyridinedicarboxylic acid in ethanol in presence of catalytic amount of aqueous H_2SO_4. Then **2** was obtained by reducing **1** with sodium borohydride in dry methanol. White precipitate of **3** was obtained by refluxing compound **2** with 1.5 equivalents of $NH_2NH_2{\cdot}H_2O$ in methanol as noted in Scheme 1.

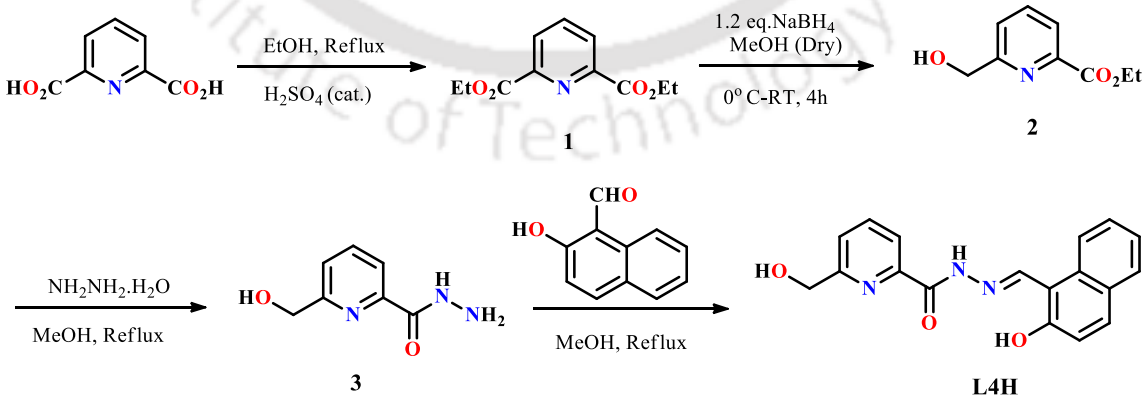

Scheme 1. Synthesis of **L4H**.

5.2.2. *Synthesis of the probe L4H [6-(hydroxymethyl)-N'-((2-hydroxy-1-naphthyl)methylene)picolinohydrazide]:*

To a hot methanol (50 mL) solution of 2-hydroxy-1-napthaldehyde (0.50 g, 3.0 mmol), 6-(hydroxymethyl)picolinohydrazide (0.52 g, 3.0 mmol) solid was added in small portions over a period of time and then heated under reflux for 6 h. The resulting reaction mixture was allowed to cool slowly to room temperature. The yellow coloured precipitate of **L4H** was separated by filtration and washed with ice-cold methanol. Yield 0.9 g (93.3%). Anal. Calcd. for $C_{18}H_{15}N_3O_3$: C, 67.28; H, 4.71; N, 13.08. Found: C, 67.05; H, 4.67; N, 12.99. 400 MHz ^{1}H NMR (δ (*J*, Hz), DMSO-d_6): 12.87(OH, s), 12.35(OH, s), 9.78(NH, s), 8.28(1H, d, 8.5), 8.10–8.02(2H, m), 7.95(1H, d, 9.0), 7.91(1H, d, 8.0), 7.75(1H, d, 7.2), 7.62(1H, t, 8.3), 7.42(1H, t, 7.4), 7.25(1H, d, 8.9), 5.63(1H, t, 5.8), 4.76(2H, d, 5.6). (Figure A1). 100 MHz ^{13}C NMR (δ, DMSO-d_6): 161.29, 160.05, 158.20, 148.49, 147.88, 138.51, 132.91, 131.89, 129.00, 127.86, 127.74, 123.78, 123.62, 120.98, 120.83, 118.98, 108.67, 63.98 (Figure A2). ESI-MS(+): *m/z* calcd. for $C_{18}H_{15}N_3O_3$ 321.111 found (M^+ + H) 322.119 (Figure A3). FTIR (KBr, cm^{-1}): 3389(m), 3259(m), 3080(w), 3029(w), 2912(w), 1692(s), 1620(m), 1594(m), 1572(w), 1532(s), 1467(m), 1454(m), 1410(m), 1386(m), 1358(w), 1324(m), 1281(m), 1240(m), 1226(m), 1190(m), 1164(m), 1048(s), 997(w), 966(m), 938(w), 863(w), 823(m), 789(m), 753(m), 719(w), 675(m), 645(w), 548(w), 488(w), 468(w), 425(w).

5.3. Results and discussion:

5.3.1. UV-Vis spectroscopic studies of L4H in presence of metal ions:

The binding affinities of **L4H** with various metal chlorides (Li^+, Na^+, K^+, Mg^{2+}, Ca^{2+}, Co^{2+}, Ni^{2+}, Cu^{2+}, Cd^{2+}, Ag^+, Pb^{2+}, Hg^{2+}, Mn^{2+}, Al^{3+}, Cr^{3+}, Fe^{3+} and Zn^{2+}) were performed in a MeOH-HEPES buffer solution (5 mM, pH = 7.3, 7:3, *v*/*v*) at room temperature. The probe **L4H** displayed well-defined four absorption bands with peak values at 316, 326, 365 and 378 nm (Figure 1). These bands are probably of $n\rightarrow\pi^*$ and $\pi\rightarrow\pi^*$ transitions, in origin. A titration experiment between $AlCl_3$ and **L4H** was performed in order to get a quantitative idea about the ability of **L4H** to interact with Al^{3+} ion. The gradual addition of $AlCl_3$ up to ½ equivalent to solution of **L4H** rendered systematic growth of the new absorbance bands at 432, 412 and 340 nm with a simultaneous decrease in intensity of

peaks at 316, 326, 364 and 378 nm (Figure 1). Distinct isosbestic points were also observed at 345 and 385 nm and beyond ½ equivalent of $AlCl_3$ no change in the spectra was observed. Similar titration experiments of **L4H** with Zn^{2+} and Cd^{2+} ions also show similar spectral changes *viz*., new peak appearing at 432 and 429 nm along with an isosbestic point at 394 and 392 nm, respectively (Figure 2-3). Whereas, other metal ions listed above, did not alter the absorption profile of free probe **L4H** (Figure 4).

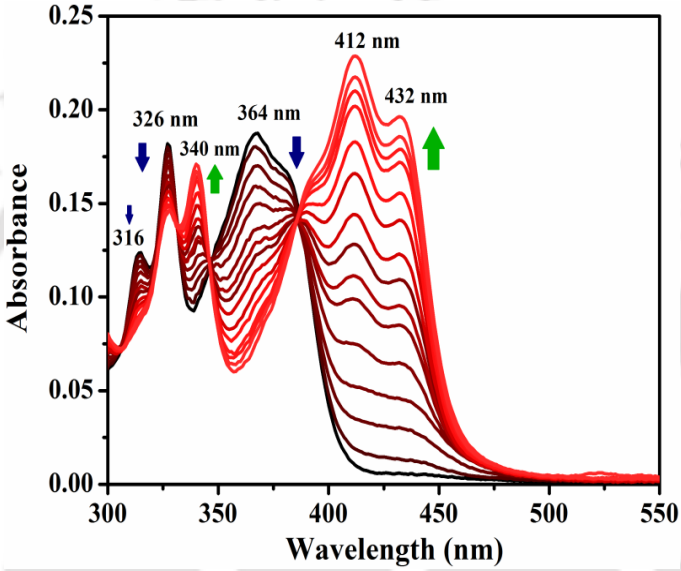

Figure 1. Changes in absorption spectra of **L4H** (10 μM) upon incremental addition of $AlCl_3$.

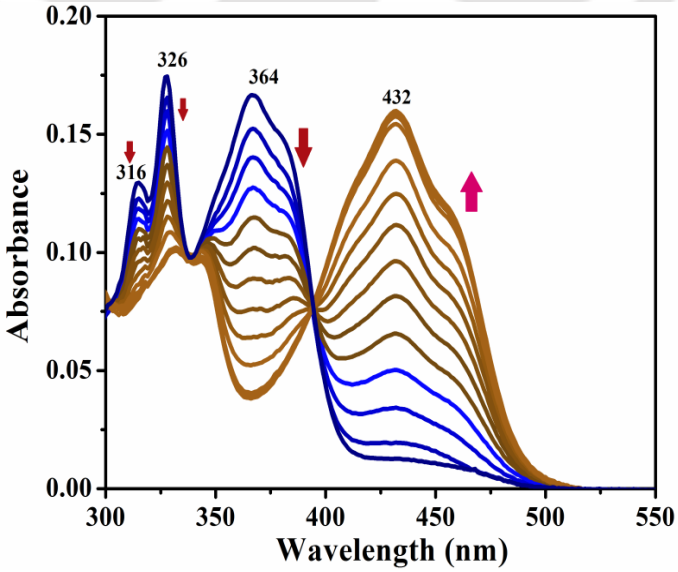

Figure 2. Changes in absorption spectra of **L4H** (10 μM) upon incremental addition of $ZnCl_2$.

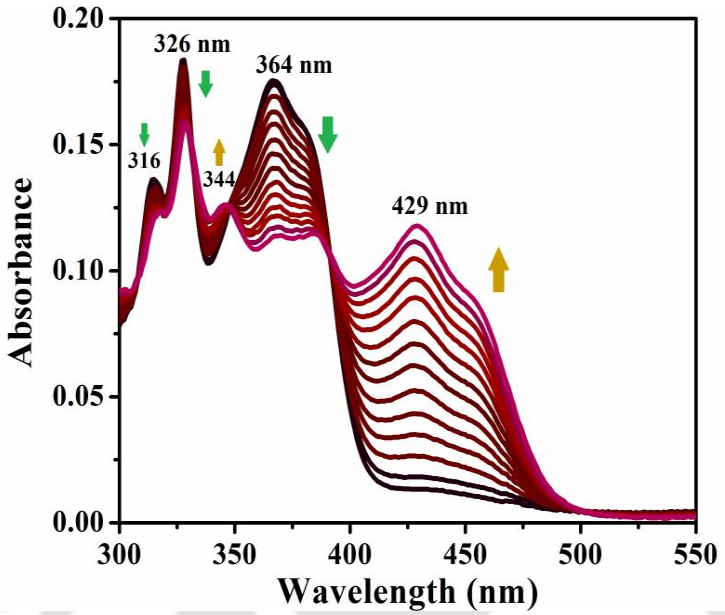

Figure 3. Changes in absorption spectra of **L4H** (10 μM) upon incremental addition of $CdCl_2$.

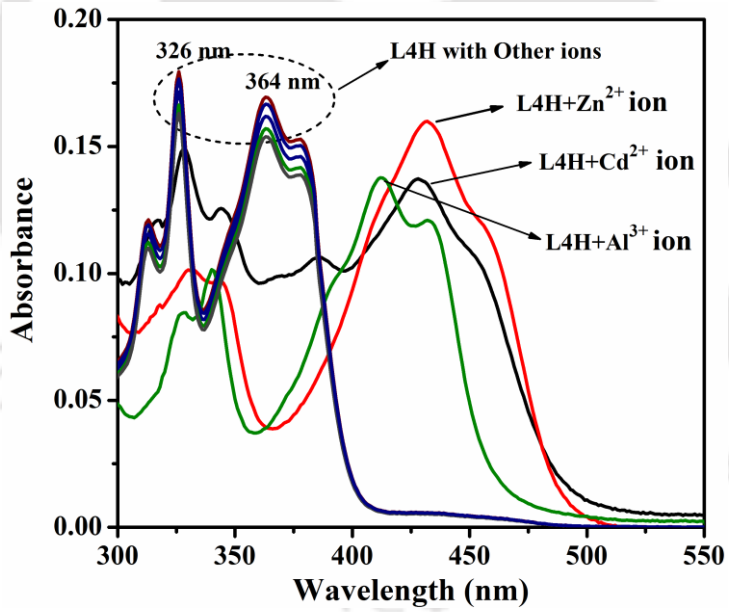

Figure 4. Changes in absorption spectra of **L4H** (10 μM) upon incremental addition of chlorides of Li^+, Na^+, K^+, Mg^{2+}, Ca^{2+}, Co^{2+}, Ni^{2+}, Cu^{2+}, Cd^{2+}, Ag^+, Pb^{2+}, Hg^{2+}, Mn^{2+}, Al^{3+}, Cr^{3+}, Fe^{3+} and Zn^{2+} (0-3 equivalents) in MeOH-HEPES buffer solution (5 mM, pH = 7.3, 7:3, *v*/*v*).

Such shift in absorption band of **L4H** may be ascribed to decrease in HOMO to LUMO energy gap of **L4H** upon coordination to the metal ion. Upon adding the metal ion sequestering agent Na_2EDTA to the individual solutions obtained after titrating **L4H**

with $AlCl_3$, $ZnCl_2$ and $CdCl_2$, reproduced UV-Visible spectrum of free **L4H**. This indicates that the probe **L4H** binds to these three metal ions without losing its identity (Figure 5).

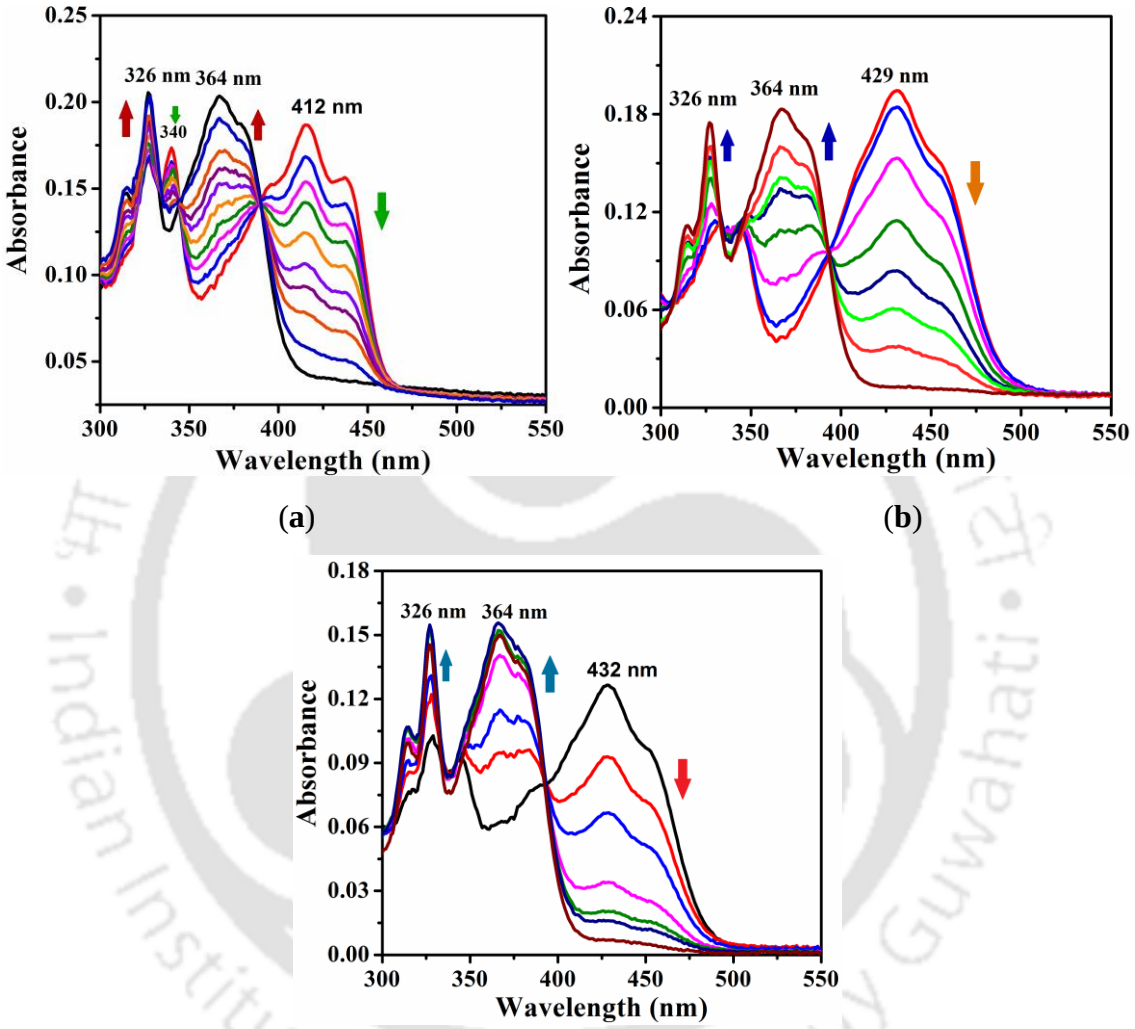

Figure 5. Changes in absorption spectra of **L4H** in the presence of (a) $AlCl_3$ (b) $ZnCl_2$ (c) $CdCl_2$ ion with EDTA disodium in MeOH-HEPES buffer solution (5mM, pH = 7.4, 7:3, *v/v*).

5.3.2. Fluorescence spectroscopic studies of L4H in the presence of metal ions:

The probe **L4H** displays a weak emission at 495 nm in MeOH-HEPES buffer solution (5 mM, pH = 7.3, 7:3, *v/v*) upon excitation at 435 nm. The weak fluorescence of **L4H** can be due to photo-induced electron transfer (PET) caused by electron transfer

from nitrogen atom of imino (–CH=N–) group to conjugated π system of naphthalene fluorophore. The emission spectra of **L4H** has been recorded as a function of $AlCl_3$ concentration in MeOH-HEPES buffer solution (5 mM, pH = 7.3, 7:3, *v*/*v*) at room temperature. It is significant to note that amongst the tested metal ions, Al^{3+} ion rendered significant TURN-ON fluorescence response.

Titration of $AlCl_3$ with **L4H** manifested ~95 times increase in emission intensity along with a 10 nm blue shift in wavelength as well as a new peak appearing at 485 nm (Figure 6). In cases of titration with $ZnCl_2$ ~43 times and $CdCl_2$ ~49 times, increase in

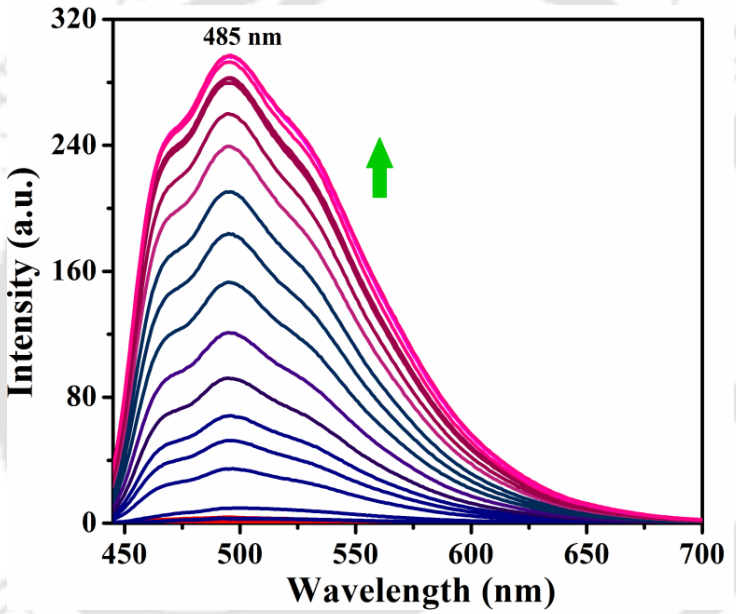

Figure 6. Fluorescence titration spectra of **L4H** (10 μM, λ_{ex} = 435 nm) upon incremental addition of $AlCl_3$ in MeOH-HEPES buffer solution (5 mM, pH = 7.3, 7:3, *v*/*v*).

emission intensity was observed but led to a large red shift in wavelength at 570 and 540 nm respectively. The extent of the red shift is 65 nm and 45 nm respectively in $ZnCl_2$ and $CdCl_2$ (Figure 7-8). A small increase in the emission intensity ~8 times upon addition of $CrCl_3$ has also been observed. The detection ability of **L4H** with chlorides of Li^+, Na^+, K^+, Mg^{2+}, Ca^{2+}, Co^{2+}, Ni^{2+}, Cu^{2+}, Ag^+, Pb^{2+}, Hg^{2+}, Mn^{2+}, Fe^{3+} were also been examined. In all these cases, negligible amount of increase in the emission intensity were observed (Figure 9).

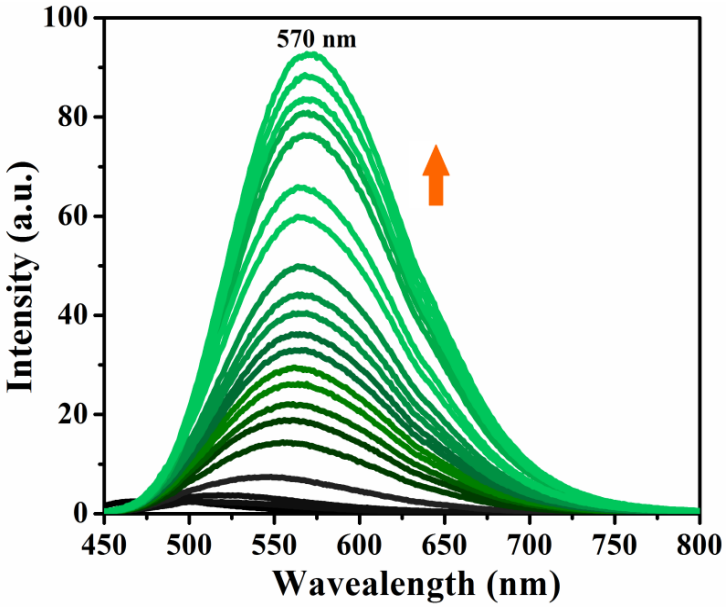

Figure 7. Fluorescence titration spectra of **L4H** (10 μM, λ_{ex} = 435 nm) upon incremental addition of $ZnCl_2$ in MeOH-HEPES buffer solution (5 mM, pH = 7.3, 7:3, *v*/*v*).

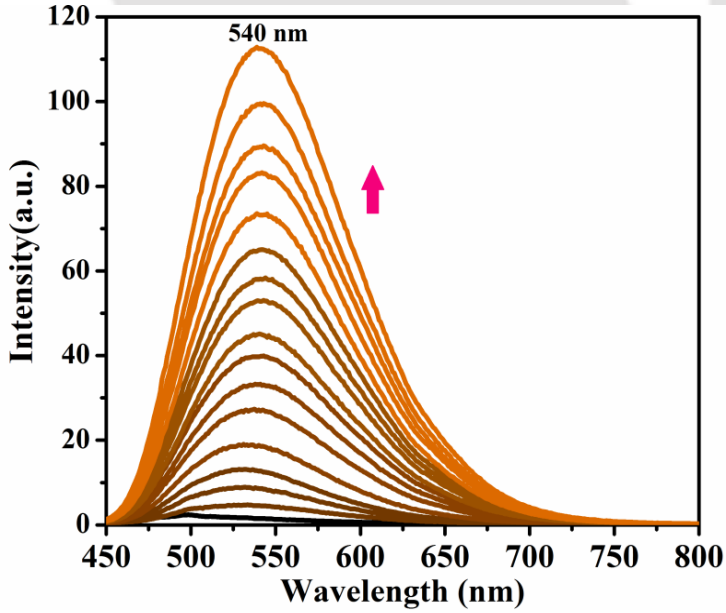

Figure 8. Fluorescence titration spectra of **L4H** (10 μM, λ_{ex} = 435 nm) upon incremental addition of $CdCl_2$ (0-3 equivalents) in MeOH-HEPES buffer solution (5 mM, pH = 7.3, 7:3, *v*/*v*).

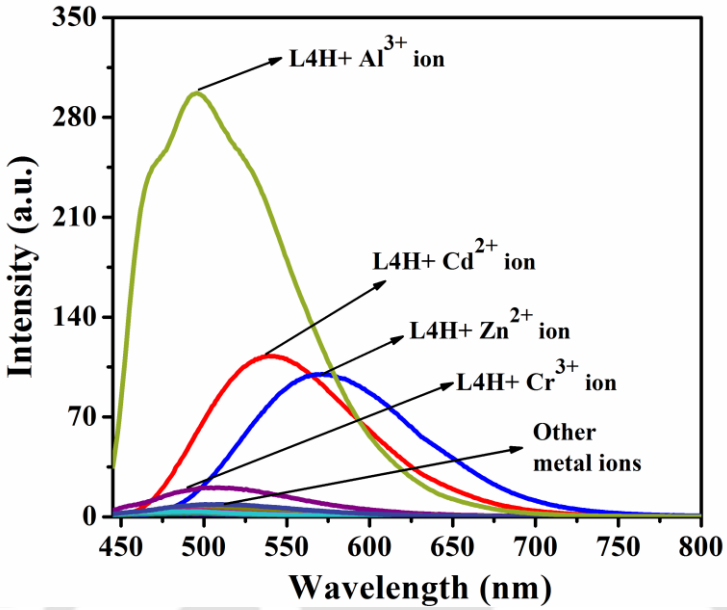

Figure 9. Changes in fluorescence emission of receptor **L4H** (10 μM) observed upon addition of chloride salts (50 μM) of Li^{+}, Na^{+}, K^{+}, Mg^{2+}, Ca^{2+}, Co^{2+}, Ni^{2+}, Cu^{2+}, Cd^{2+}, Ag^{+}, Pb^{2+}, Hg^{2+}, Mn^{2+}, Al^{3+}, Cr^{3+}, Fe^{3+} and Zn^{2+} (0-3 equivalents) in MeOH-HEPES buffer solution (5 mM, pH = 7.3, 7:3, *v*/*v*).

Job's plot obtained from titration experiments yielded a 2:1 stoichiometry for Al^{3+} ion but 1:1 stoichiometry for Zn^{2+} and Cd^{2+} ions (Figure 10). In addition, the binding stoichiometry of **L4H** towards Al^{3+}, Zn^{2+} and Cd^{2+} ions was further supported by the appearance of ESI-MS(+) *m*/*z* peak at 667.19 (calcd. for $AlC_{36}H_{28}N_6O_6^{+}$, 667.19), 462.05 (calcd. for $ZnC_{20}H_{20}N_3O_4S^{+}$, 462.05) and 512.02 (calcd. for $CdC_{20}H_{20}N_3O_4S^{+}$, 512.02) corresponding to $[Al(\mathbf{L4})_2]^{+}$, $[Zn(\mathbf{L4})(DMSO)]^{+}$ and $[Cd(\mathbf{L4})(DMSO)]^{+}$ respectively (Figure A4-A6). Hence the formulations $[Al(\mathbf{L4})_2]^{+}$, $[Zn(\mathbf{L4})Cl(H_2O)_2]$ and $[Cd(3\mathbf{L4})Cl(H_2O)_2]$ were adopted throughout this study based on the preferred coordination number of 6 in aqueous medium.[71] The association constants of **L4H** for Al^{3+}, Zn^{2+} and Cd^{2+} derived from the Benesi–Hildebrand equation were $1.5 \times 10^3\ M^{-½}$, $5 \times 10^5\ M^{-1}$ and $3.5 \times 10^5\ M^{-1}$ respectively (Figure 11-12). The detection limits of **L4H** for Al^{3+}, Zn^{2+} and Cd^{2+} were calculated to be 5.7×10^{-9}, 1.09×10^{-6} and 1.64×10^{-6} M respectively (Figure 13). The quantum yield of free **L4H** was 0.07 where as quantum yields for $\mathbf{L4}^{-}$ complexes of Al^{3+}, Zn^{2+} and Cd^{2+} ions were found to be 0.63, 0.21 and 0.20 respectively.

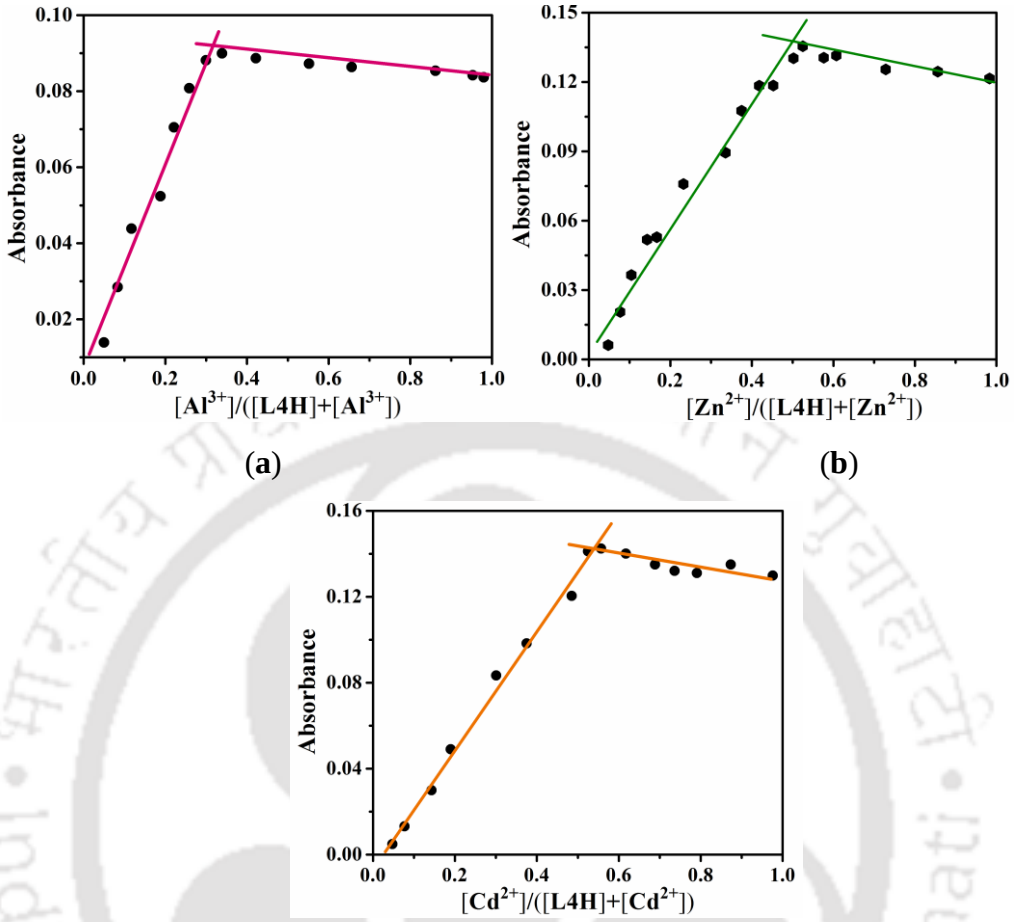

Figure 10. Job's Plot for **L4H** (10 µM) with (a) Al^{3+} (b) Zn^{2+} (c) Cd^{2+} ions.

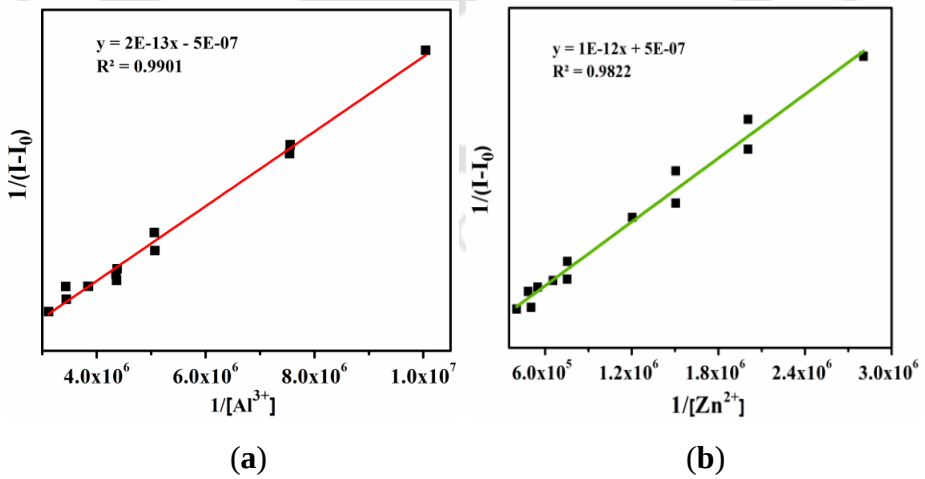

Figure 11. Benesi-Hildebrand plot for determination of binding constant of **L4H** (10 µM) with (a) Al^{3+} (b) Zn^{2+} ions in MeOH-HEPES buffer solution (5 mM, pH = 7.3, 7:3, *v/v*).

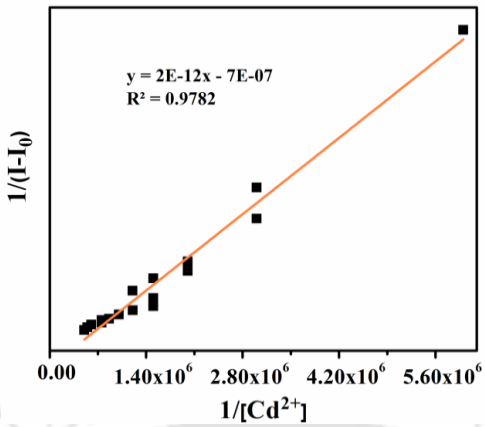

Figure 12. Benesi-Hildebrand plot for determination of binding constant of **L4H** (10 μM) with Cd^{2+} ion in MeOH-HEPES buffer solution (5 mM, pH = 7.3, 7:3, *v/v*).

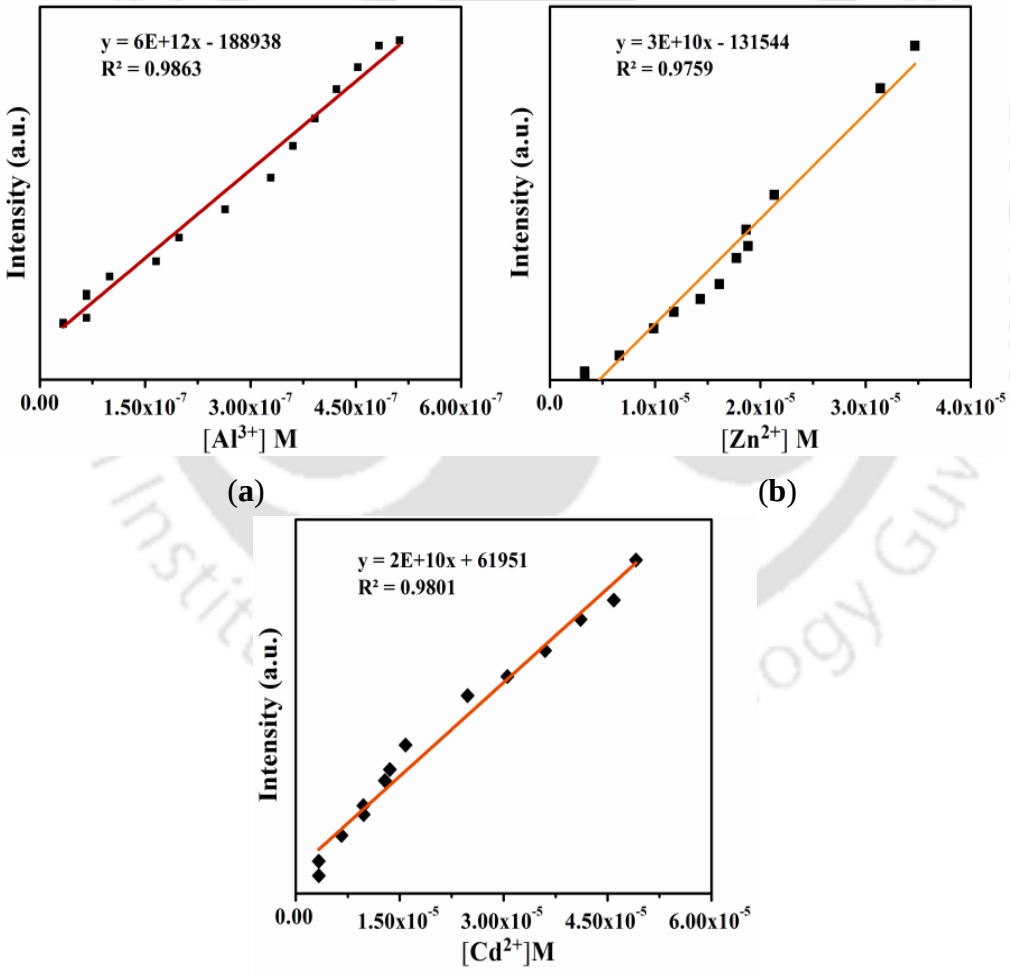

Figure 13. Fluorescence intensity *vs.* concentration of (a) Al^{3+} (b) Zn^{2+} (c) Cd^{2+} ions plot for determination of detection limit ([**L4H**] = 10 μM).

The fluorescence responses of **L4H** in presence of these three metal ions might primarily be attributed to chelation of metal ions by **L4H** in its conjugate base form $\mathbf{L4}^{-}$. In other words, the selective "*TURN-ON*" emission signals of **L4H** in presence of Al^{3+}, Zn^{2+} and Cd^{2+} ions were through chelation-enhanced fluorescence (CHEF) mechanism. The probe **L4H** is not a planar system due to rotation about the N–N bond in the ground state, *cis-trans* isomerisation along imine group (–CH=N–) in the excited state[72-74] and photoinduced electron transfer (PET) caused by electron transmission from nitrogen atom of imine to large π-conjugation system of naphthalene fluorophore. These are some predominant factors responsible for weak emission of **L4H**. Upon binding to metal ion, the lone-pair on nitrogen atom of imine is not free due to its involvement in coordination and the ligand framework attains a near planar geometry, thus imparting substantial increase in rigidity of the system. The probe **L4H** binds to metal ion through imine nitrogen, phenolate and amide oxygen atoms and results in inhibition of PET process that involves lone pair on imine N-atom. As a result, chelation induced enhanced fluorescence (CHEF) effect[75-79] becomes operational which induces a large enhancement in fluorescence intensity of **L4H**. Therefore, due to distinct electronic behaviour, size effect and charge density, the "*TURN-ON*" emission signals were observed for Al^{3+}, Zn^{2+} and Cd^{2+} ions with distinct emission maxima.

5.3.3. TRPL Measurements:

The TRPL measurements were carried out to understand the mechanism of the turn-on fluorescence responses of **L4H** toward Al^{3+}, Zn^{2+} and Cd^{2+} ions and the decay profiles are shown in Figure 14. Free **L4H** has a lifetime (τ) of 0.30 ns in MeOH-HEPES buffer solution (5 mM, pH = 7.3, 7:3, *v*/*v*). On the other hand, Al^{3+}, Zn^{2+} and Cd^{2+} complexes of **L4H** were having greater lifetimes as evident from average fluorescence lifetimes (Table 1) of 3.28, 1.26 and 3.44 ns respectively. This suggests that addition of these metal ions to **L4H** allow CHEF to become operational as a result of complexation and thus fluorescence lifetimes of such emissive species become longer than free probe **L4H**. In the free ligand, PET process and free rotation are responsible for the lack of fluorescence. These processes have been locked in the presence of metal ions due to complex formation and hence fluorescence has been observed. Hence, complexation

stops non-radiative decay process and changes in life time in presence of metal ions have been observed.

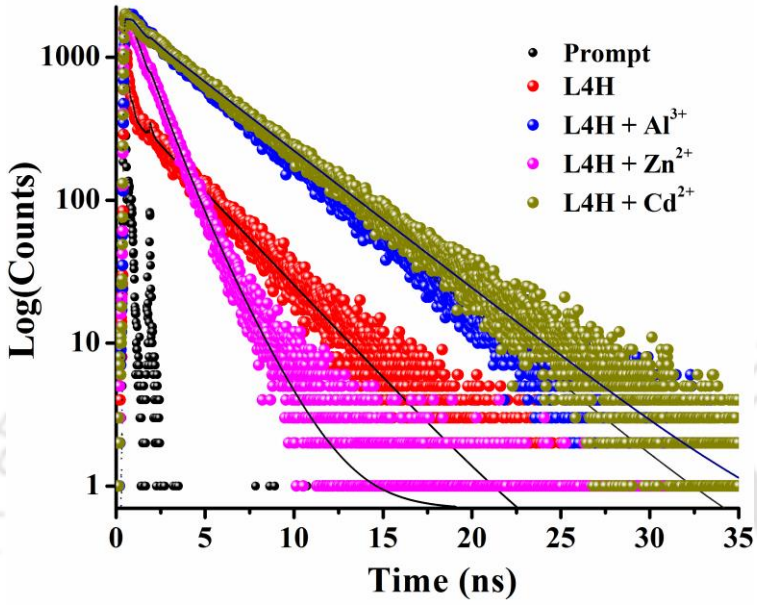

Figure 14. Time resolved decay profile of **L4H** upon addition of Al^{3+}, Zn^{2+} and Cd^{2+} ions.

Table 1: Fluorescence decay parameters of **L4H**, **L4H** with Al^{3+}, Zn^{2+} and Cd^{2+} ions.

Sample	τ (ns)	χ^2
L4H	0.30	1.03
L4H + $AlCl_3$	3.28	1.08
L4H + $ZnCl_2$	1.26	1.03
L4H + $CdCl_2$	3.44	1.09

5.3.4. ^{1}H-NMR titration experiment of L4H in the presence of Al^{3+}, Zn^{2+} and Cd^{2+} ions:

The interactions between **L4H** with Al^{3+}, Zn^{2+} and Cd^{2+} ions were also followed by ^{1}H-NMR titration experiments. With gradual addition of chloride salt of above noted metal ions, reduction in intensity along with an up field shift of phenolic–OH peak was observed in initial stages which finally disappeared (Figure 15), indicating deprotonation of **L4H** and binding as $\mathbf{L4}^-$ ion.

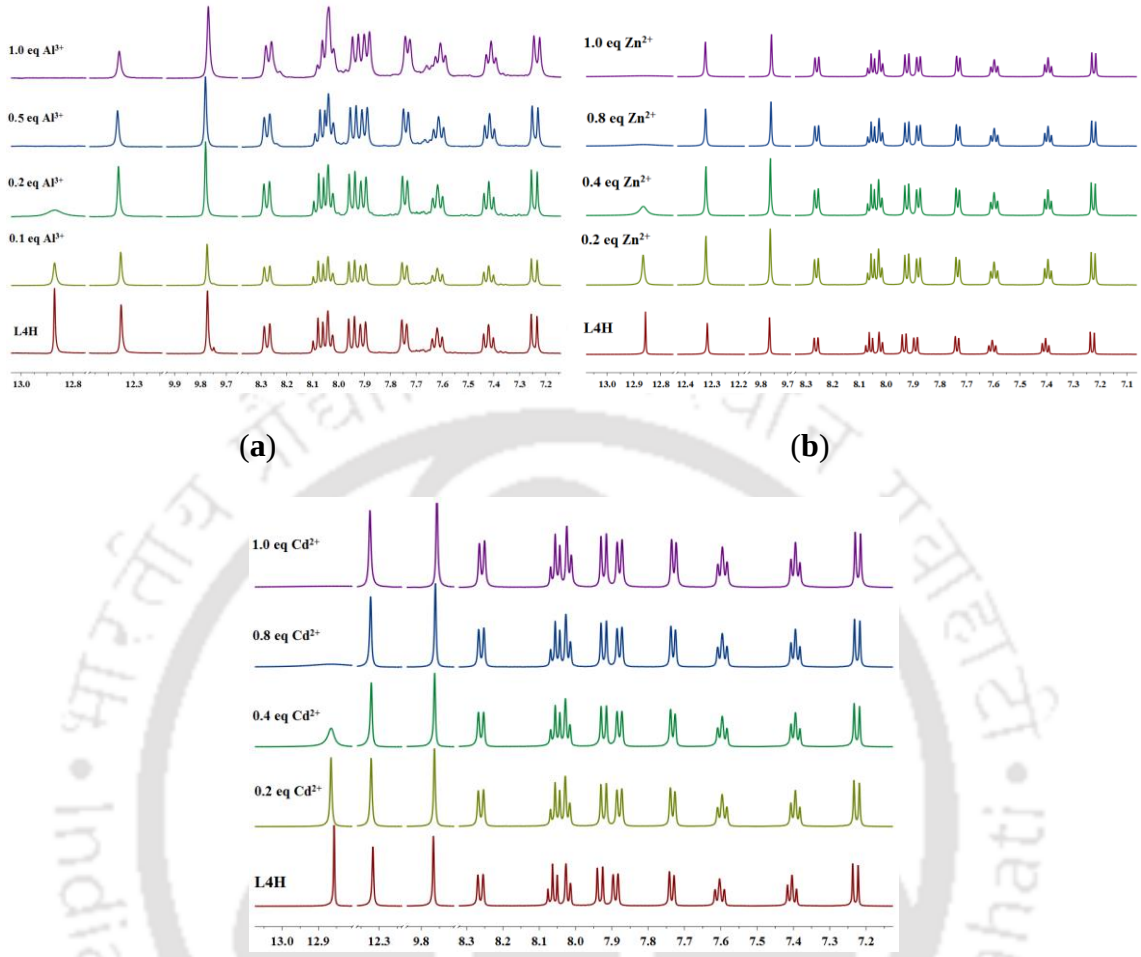

(**a**) (**b**)

(**c**)

Figure 15. ^{1}H NMR titration study of **L4H** in DMSO-d_6/CD_3OD (9:1, *v/v*) at room temperature with (a) $AlCl_3$ (b) $ZnCl_2$ (c) $CdCl_2$.

5.3.5. Fluorescence studies of $[Al(L4)_2]^+$, $[Zn(L4)Cl(H_2O)_2]$ and $[Cd(L4)Cl(H_2O)_2]$ species with various anions:

The inferences made from the above results indicate that **L4H** can recognize Al^{3+}, Zn^{2+} and Cd^{2+} ions at different wavelengths in physiological condition even in presence of excess of other competitive metal ions. These metal complexes can also be a good binding ensemble for anions through electrostatic and hydrogen bonding interactions. Hence attempts were made to use these complexes in solution for anion recognition and investigated the impact of different anions on these complexes spectroscopically. The fluorescence responses of solutions obtained after titrating **L4H** with Al^{3+}, Zn^{2+} and Cd^{2+}

chlorides, were examined by titrating again with the solutions of anions such as F^-, Cl^-, Br^-, I^-, CN^-, SCN^-, PO_4^{3-}, S^{2-}, OH^-, $S_2O_3^{2-}$, $H_2PO_4^-$, HPO_4^{2-}, NO_3^-, SO_4^{2-}, $P_2O_7^{4-}$, HSO_4^-, CO_3^{2-}, HCO_3^-, AcO^-, ClO_4^- and $C_2O_4^{2-}$. All these ions gave minimal or no significant change in emission intensity of $[Al(\mathbf{L4})_2]^+$, $[Zn(\mathbf{L4})Cl(H_2O)_2]$ and $[Cd(\mathbf{L4})Cl(H_2O)_2]$ complexes. In contrast, only F^- ion exhibited specific quenching of fluorescence intensity of $[Al(\mathbf{L4})_2]^+$ complex by complete quenching of emission at 485 nm and the resultant spectrum resembles that of free **L4H** (Figure 16). Whereas, $H_2PO_4^-$ ion gave substantial fluorescence change in $[Zn(\mathbf{L4})Cl(H_2O)_2]$ and $[Cd(\mathbf{L4})Cl(H_2O)_2]$ complexes by complete quenching of emission at 570 and 540 nm, the resultant spectrum resembles that of free **L4H** (Figure 17).

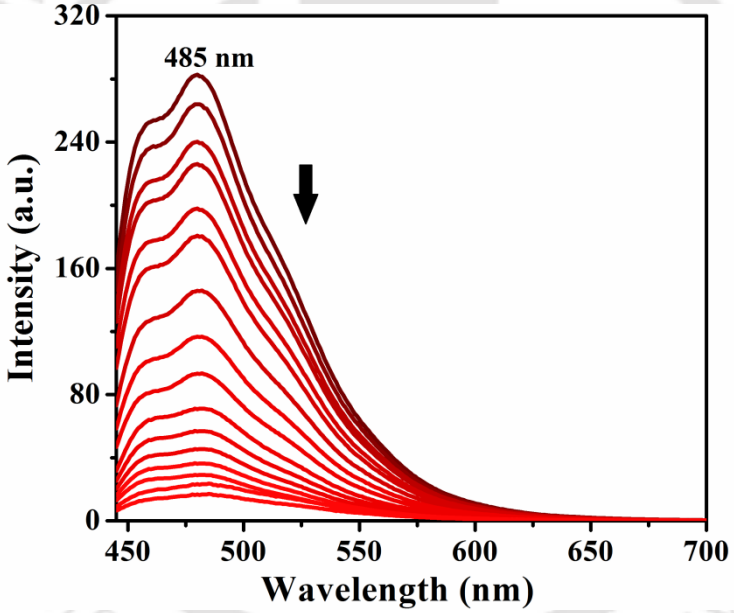

Figure 16. Changes in fluorescence spectra of $[Al(\mathbf{L4})_2]^+$ ensemble upon incremental addition of F^- ion in MeOH-HEPES buffer solution (5mM, pH = 7.3, 7:3, *v/v*).

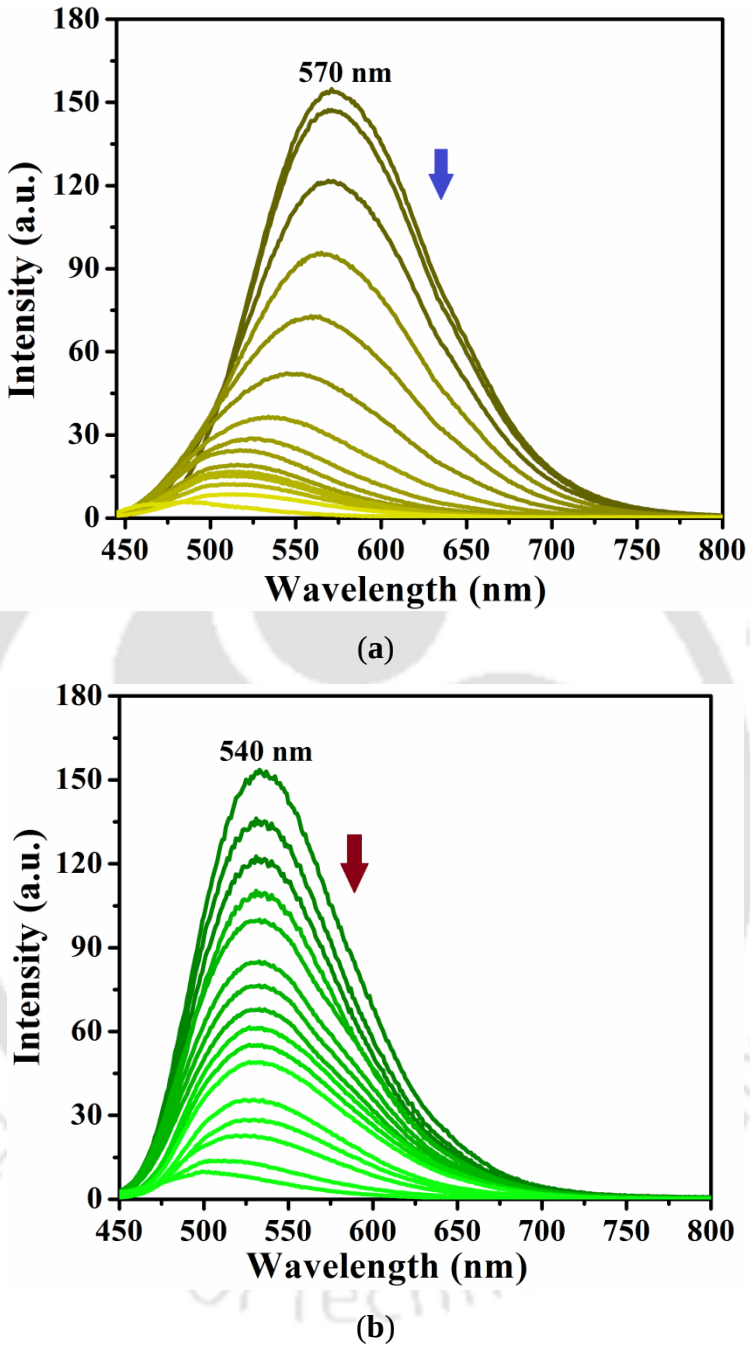

Figure 17. Changes in fluorescence spectra of (a) [Zn(**L4**)Cl(H_2O)$_2$] (b) [Cd(**L4**)Cl(H_2O)$_2$] ensemble upon incremental addition of $H_2PO_4^-$ ion in MeOH-HEPES buffer solution (5mM, pH = 7.3, 7:3, *v/v*).

These results indicate that these anions form complex with respective metal ions and release the free **L4H** into the solution and this selectivity is in accordance with the HSAB principle.[73] The detection limit of [Al(**L4**)$_2$]$^+$ (for F^-), [Zn(**L4**)Cl(H_2O)$_2$] and

[Cd(**L4**)Cl(H_2O)$_2$] (for $H_2PO_4^-$), were evaluated to be 2.5 × 10^{-6}, 1.43 × 10^{-5} and 2.11 × 10^{-5} M respectively (Figure 18-19).

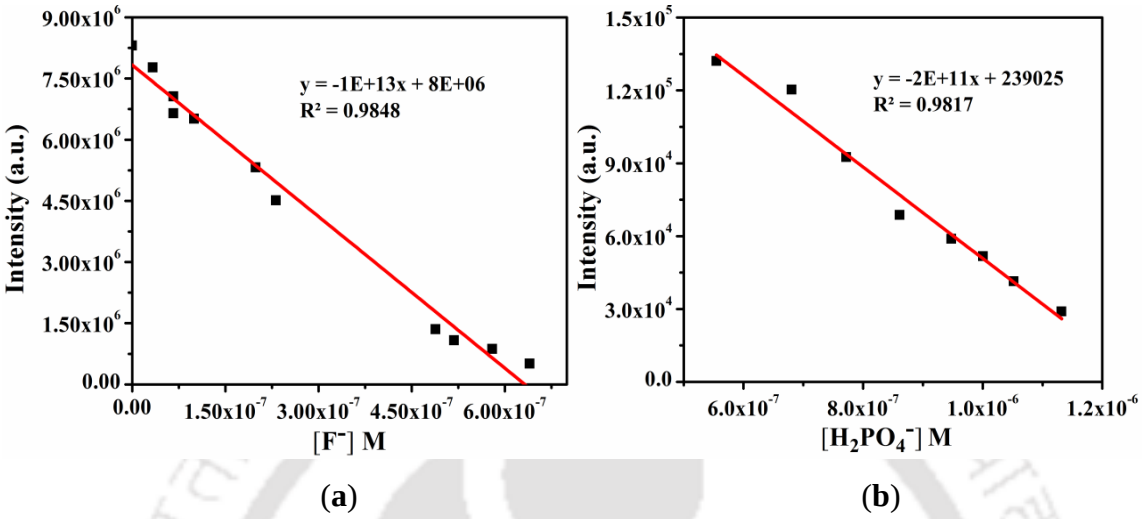

(**a**) (**b**)

Figure 18. Fluorescence intensity *vs.* concentration of (a) F^- (b) $H_2PO_4^-$ ions plot for determination of detection limit ([**L4H**] = 10 μM).

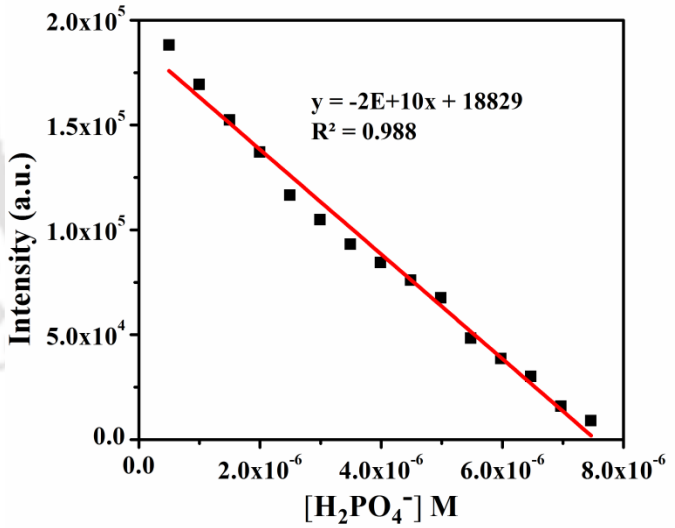

Figure 19. Fluorescence intensity *vs.* concentration of $H_2PO_4^-$ ion plot for determination of detection limit ([**L4H**] = 10 μM).

5.3.6. Metal ion competition studies:

In order to assess the ability of **L4H** as selective multi fluorescence receptor for Al^{3+}, Zn^{2+} and Cd^{2+} ions, competitive experiments were carried out. In these experiments, to each of the solutions obtained after titration of **L4H** with Al^{3+}, Zn^{2+} and Cd^{2+} ions, aqueous solutions of other metal ions listed earlier were added and then

fluorescence spectra of these solutions were recorded. All the metal ions did not show any perceptible effect on the ability of **L4H** with the detection of Al^{3+} Zn^{2+} and Cd^{2+} ions, but upon addition of up to four equivalents of Cu^{2+} ion quenched fluorescence intensity by about 20-30%. Despite this, **L4H** still has sufficient "turn-on" ratios for the detection of Al^{3+}, Zn^{2+} and Cd^{2+} ions in presence of other metal ions at different wavelengths (Figure 20-21).

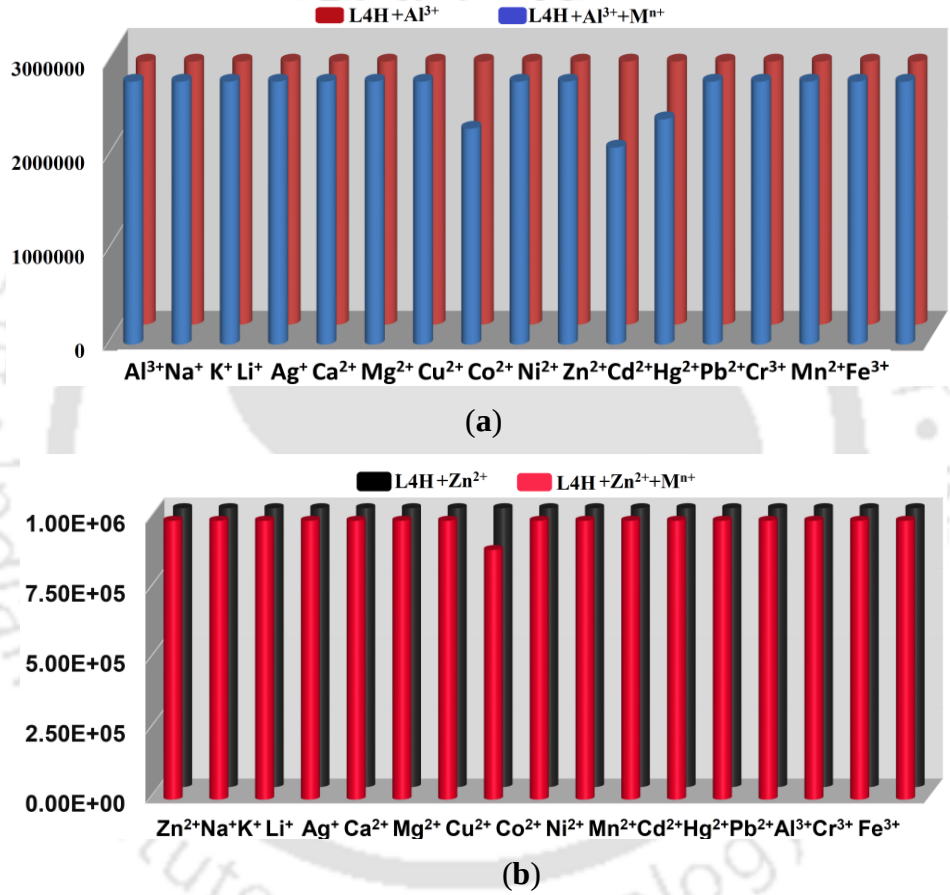

Figure 20. Fluorescence response of **L4H** in presence of (a) Al^{3+} (λ_{em} = 485 nm) (b) Zn^{2+} (λ_{em} = 570 nm) ions upon incremental addition of various metal ions (0-3 equivalents) in MeOH-HEPES buffer solution (5mM, pH = 7.3, 7:3, *v/v*).

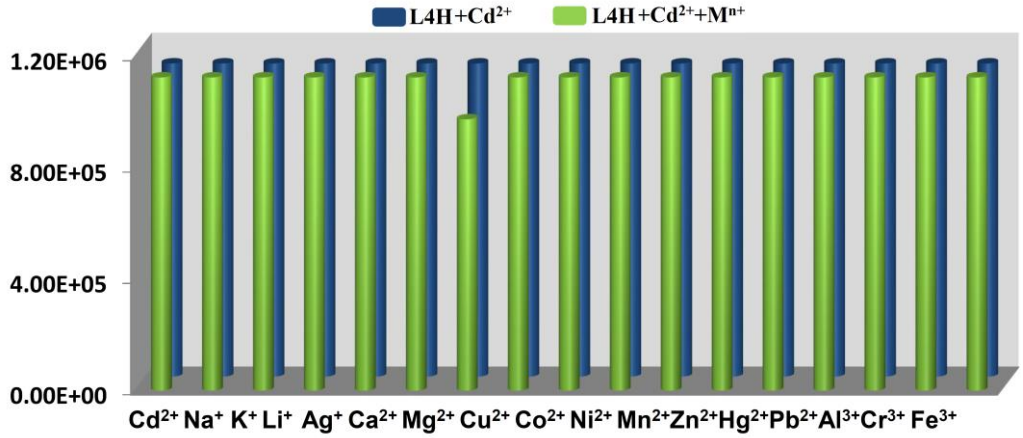

Figure 21. Fluorescence response of **L4H** in presence of Cd^{2+} (λ_{em} = 540 nm) ion upon incremental addition of various metal ions (0-3 equivalents) in MeOH-HEPES buffer solution (5mM, pH = 7 .3, 7:3, *v/v*).

While gradual addition of solutions of $ZnCl_2$ and $CdCl_2$ separately to the solution obtained after titrating **L4H** with Al^{3+} ion, red shifted peaks at 513 and 505 nm were observed (Figure 22). Titration experiments of **L4H** with a mixture of two or all three metal ions Al^{3+}, Zn^{2+} and Cd^{2+} were also been carried out. Titrations of **L4H** with solutions having equal quantities of (a) $AlCl_3$ and $ZnCl_2$ exhibited a new turn-on peak at 515 nm. (b) $AlCl_3$ and $CdCl_2$ exhibited a new turn-on peak at 505 nm (c) $ZnCl_2$ and $CdCl_2$ exhibited a new turn-on peak at 560 nm (Figure 23a-c). Similar titrations of **L4H** with a solution having equal quantities of $AlCl_3$, $ZnCl_2$ and $CdCl_2$ exhibited a new turn-on peak at 513 nm (Figure 23d). These results are consistent with the emission peaks observed in the individual titrations: that (a) in presence of $AlCl_3$ emission at 485 nm is red shifted by 30 nm (by $ZnCl_2$) and by 20 nm (by $CdCl_2$) (b) a mixture of $ZnCl_2$ and $CdCl_2$ show emission peak which is in between their respective individual emission peak of 570 and 540 nm. Thus metal ion competition studies indicate that **L4H** can detect Al^{3+}, Zn^{2+} and Cd^{2+} ions individually or a mixture of any two or all three together, with distinct signals.

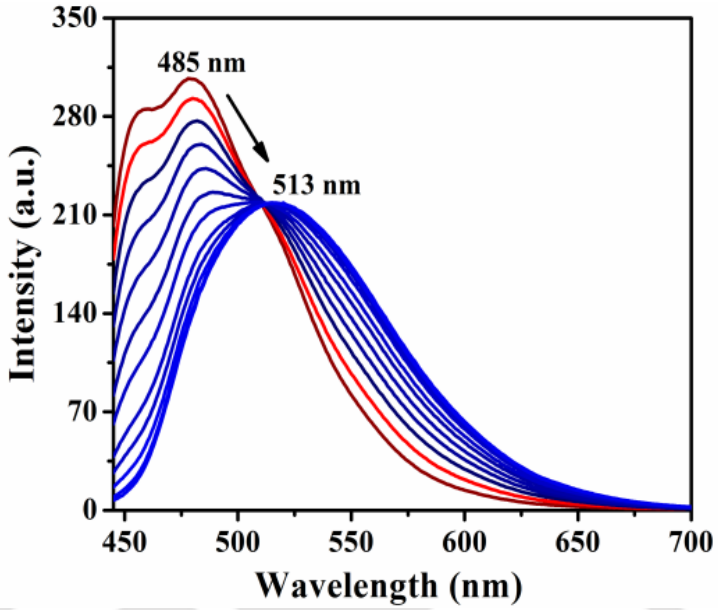

(**a**)

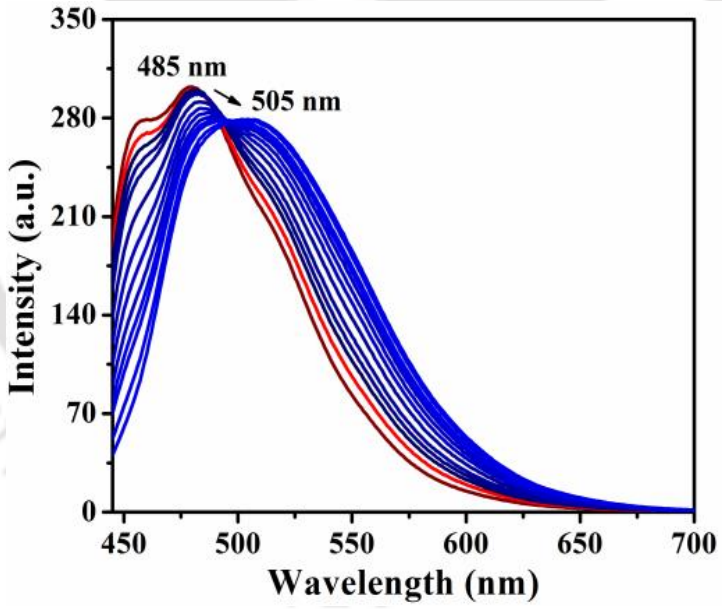

(**b**)

Figure 22. Changes in fluorescence spectra of $[Al(\mathbf{L4})_2]^+$ ensemble upon incremental addition of (a) Zn^{2+} (c) Cd^{2+} ions (0-3 equivalents) in MeOH-HEPES buffer solution (5mM, pH = 7.3, 7:3, *v*/*v*).

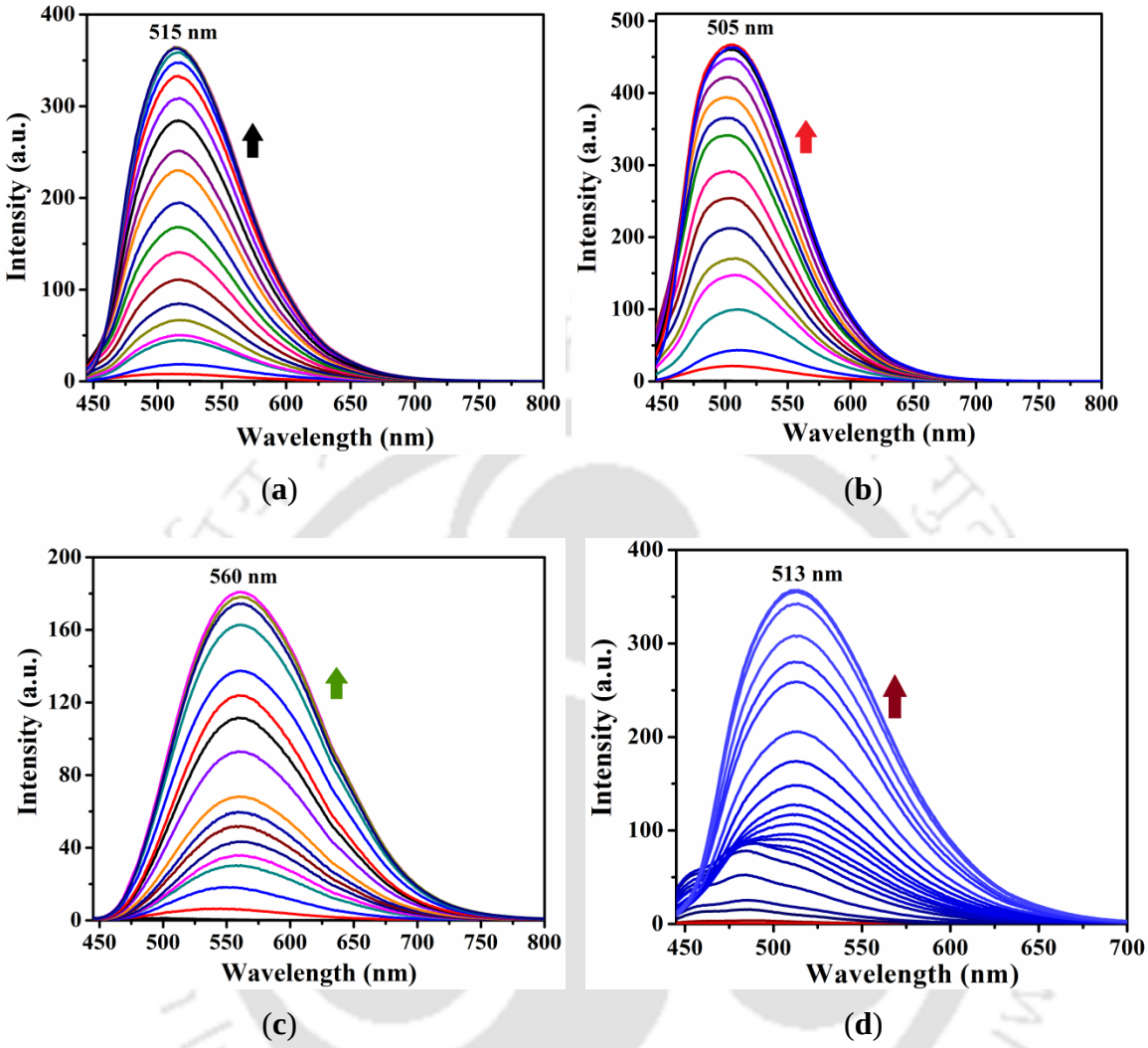

Figure 23. Changes in fluorescence spectra of **L4H** (10 μM) with upon incremental addition of mixture of chloride salt of (a) Al^{3+}/Zn^{2+} (b) Al^{3+}/Cd^{2+} (c) Zn^{2+}/Cd^{2+} (d) $Al^{3+}/Zn^{2+}/Cd^{2+}$ ions (0-3 equivalents) in MeOH-HEPES buffer solution (5mM, pH = 7.4, 7:3, *v/v*).

5.3.7. pH effect:

Effect of pH on these individual titrations was also examined using 5 mM HEPES buffer. Free ligand remained fluorescence inactive between pH ranges 2-12. The $[Al(\mathbf{L4})_2]^+$ complex ion exhibited a maximum intensity in the range 6-8, with a slight to moderate quenching up to pH 9 and no emission beyond these ranges. The same pH window was also observed in cases of $ZnCl_2$ and $CdCl_2$. This fluorescence behaviour of

L4H with Al^{3+}, Zn^{2+} and Cd^{2+} ions makes it a suitable sensor to the demands of physiological pH conditions (Figure 24).

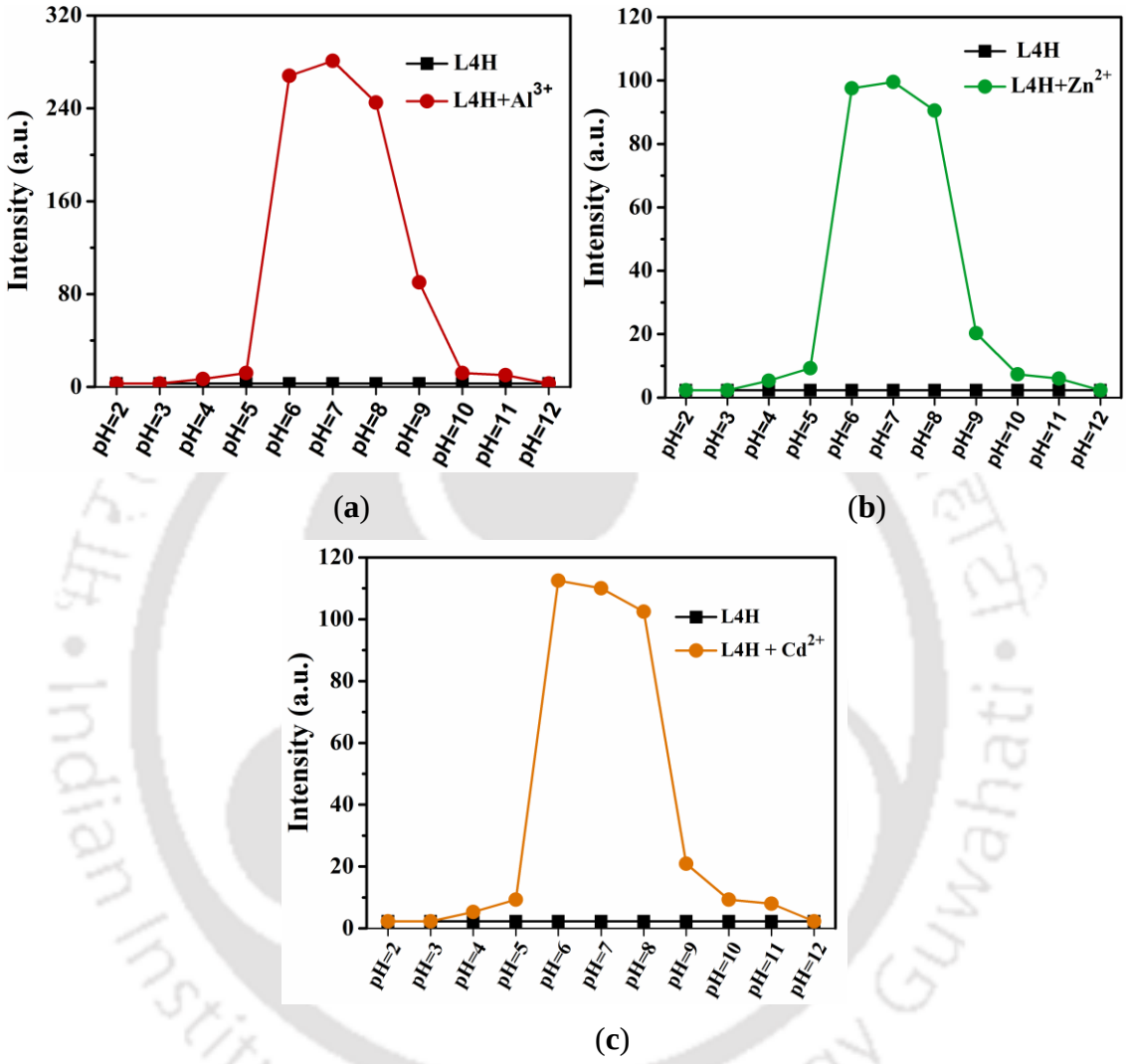

Figure 24. Fluorescence intensities of **L4H** (10 μM, λ_{em} = 495) with (a) $[Al(\mathbf{L4})_2]^+$ (λ_{em} = 485) (b) $[Zn(\mathbf{L4})Cl(H_2O)_2]$ (λ_{em} = 570 nm) and (c) $[Cd(\mathbf{L4})Cl(H_2O)_2]$ (λ_{em} = 540 nm) at various pH values (λ_{ex} = 435 nm) in MeOH-HEPES buffer solution (5mM, pH = 7.4, 7:3, *v*/*v*).

5.3.8. Detection of Al^{3+}, Zn^{2+} and Cd^{2+} ions in real samples:

To check the applicability of **L4H** towards sensing of Al^{3+}, Zn^{2+} and Cd^{2+} ions, fluorescence spectra of water samples containing these ions were also examined by using available real water samples collected from laboratory tap and Brahmaputra river (near I.I.T. Guwahati campus, Assam, India). A blank experiment was performed to check the

presence of these three metal ions in these samples and their presence is negligible as inferred from the no change in the fluorescence response. A stock solution of Al^{3+}, Zn^{2+} and Cd^{2+} ions were diluted with these two water samples. The fluorescence spectra of **L4H** (1×10^{-5} $molL^{-1}$)were recorded at 485, 570 and 540 nm for Al^{3+}, Zn^{2+} and Cd^{2+} ions respectively and the profiles are shown in Figure 25. These results indicate that **L4H** can be a suitable probe for the detection of Al^{3+}, Zn^{2+} and Cd^{2+} ions in the tap and river water samples.

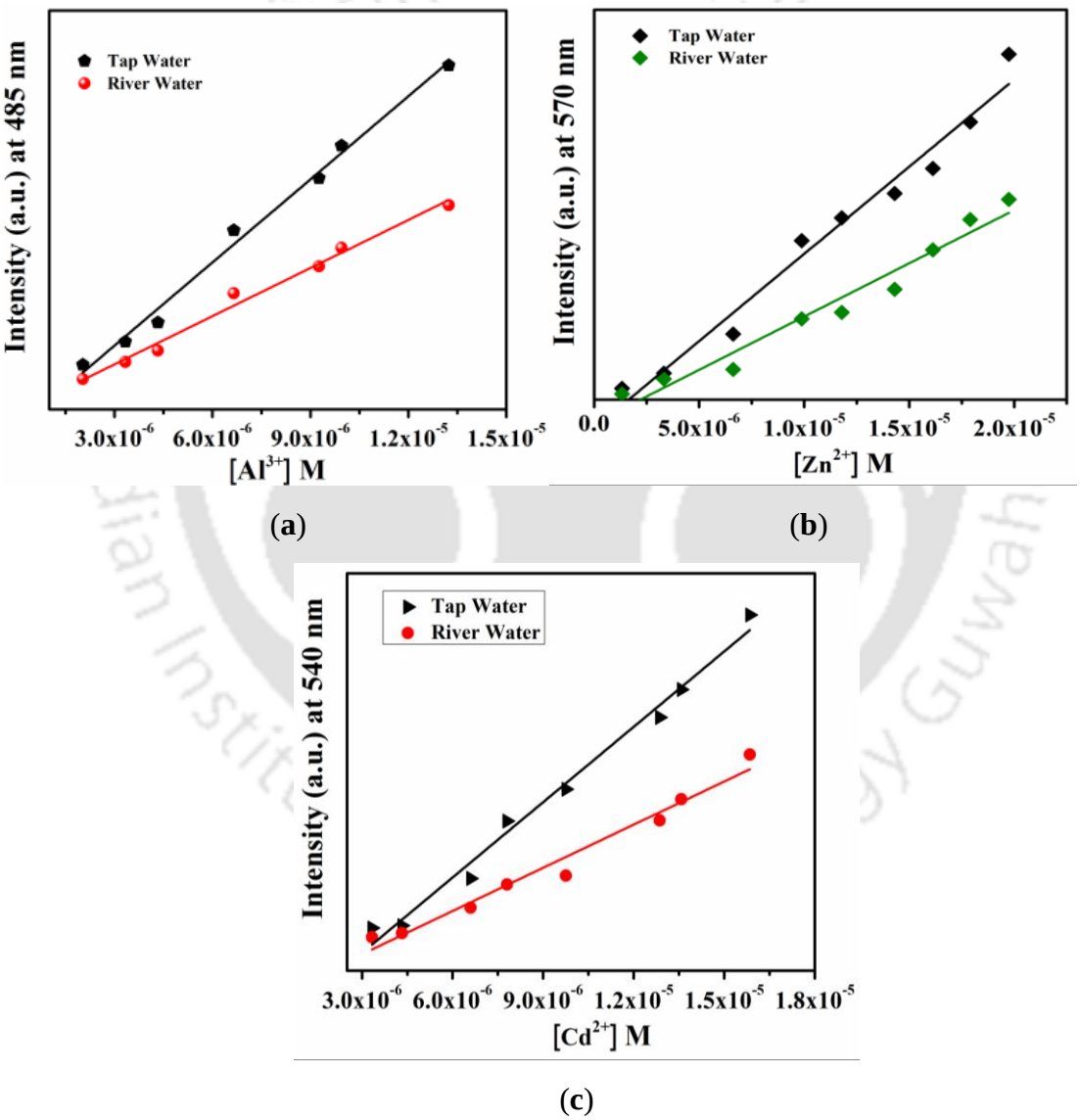

Figure 25. Plots of fluorescence intensity of **L4H** (1×10^{-5} $molL^{-1}$) noted in vertical axis as a function of (a) Al^{3+} (0-13.0 μmol/L), (b) Zn^{2+} (0-18.0 μmol/L) (c) Cd^{2+} (0-20.0 μmol/L) ion concentration.

5.3.9. Computational studies:

To obtain a theoretical aspect of the structural changes of **L4H** upon coordination with Al^{3+}, Zn^{2+} and Cd^{2+} ions, extensive density functional theory (DFT/TDDFT) calculations were performed. Based on the absorption and emission spectroscopic studies, the stoichiometry of the complexes were found to be 2:1 for Al^{3+} ion but 1:1 for Zn^{2+} and Cd^{2+} ions. Hence, complexes of composition $[Al(\mathbf{L4})_2]^+$, $[Zn(\mathbf{L4})Cl(H_2O)_2]$ and $[Cd(\mathbf{L4})Cl(H_2O)_2]$ {**L4** = conjugate base of **L4H** and as phenolate ion} as well as free **L4H** were optimized by DFT calculations. The optimized structure of **L4H** and its frontier molecular orbitals are depicted in Figure 26-27. The HOMO of **L4H** is mainly formed by π-orbitals of napthyl ring, lone pair orbitals on oxygen and nitrogen atoms and the LUMO is the corresponding antibonding orbitals. The calculated HOMO–LUMO energy gap in **L4H** is 4.01 eV which corresponds to 364 nm (Figure 27). The probe **L4H** comprises of large flexible backbone made up of N–N and C–N single bonds, that gives rise to non-planar structure due to possible rotations about these bonds.

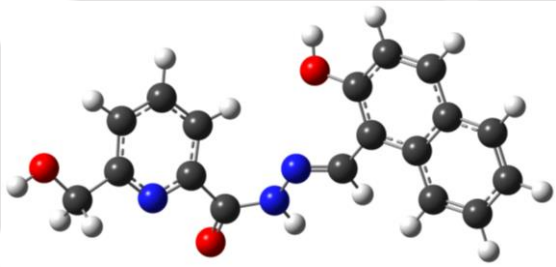

Figure 26. Optimized structure of **L4H**.

However, upon coordination to a metal center the ligand is expected to attain a rigid planar structure. In order to ascertain this, structure optimisations were also performed on complexes of **L4H** with three metal ions which had exhibited distinct fluorescence emission maxima *viz*., Al^{3+}, Zn^{2+} and Cd^{2+} ions. Since the ligand can coordinate in two coordination modes: (a) through NOO donor atoms with one five- and one six-membered chelate rings and (b) through NNO donor atoms with two six-membered chelate rings. The NOO coordination mode is composed of two O-atoms from phenolate and carbonyl group as well as N-atom from imine group where as NNO is composed of one O-atom from phenolate and two N-atoms from pyridine and amide nitrogen (Table 2). The structure optimisation was performed for these two different

coordination modes of **L4**$^{-}$. The results indicated that among the two coordination modes, complexes formed with NOO coordination modes are more stable than that with NNO mode. Hence NOO coordination mode has been considered for further discussions.

Table 2: Optimized structures of **L4H** complexes with Al^{3+}, $Zn^{2+}$and Cd^{2+} ions for both 'NOO' and 'NNO' coordination.

Complex	NOO-coordination mode	NNO-coordination mode	Total Energy (Hatree)
$[Al(\mathbf{L4})_2]^+$	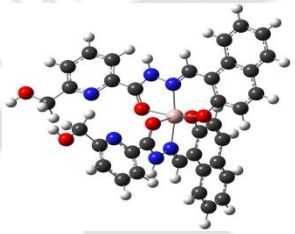	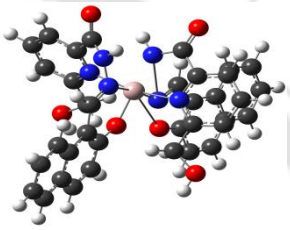	E_{NOO} = -2170.185 E_{NNO} = -2170.135
$[Zn(\mathbf{L4})Cl(H_2O)_2]$	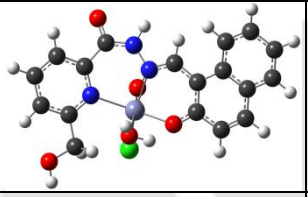	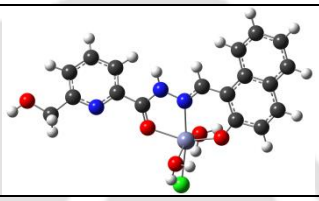	E_{NOO} = -1317.534 E_{NNO} = -1317.536
$[Cd(\mathbf{L4})Cl(H_2O)_2]$	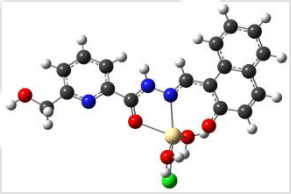	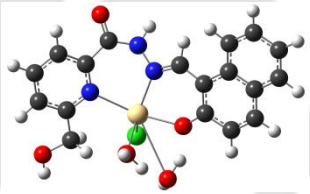	E_{NOO} = -1300.000 E_{NNO} = -1299.987

In $[Al(\mathbf{L4})_2]^+$, both HOMO and LUMO have similar characteristics as that in free **L4H** (except that pyridine ring system is also contributing to the LUMO) but the energies of both HOMO and LUMO has been lowered (Figure 27). Since the energy of LUMO is lowered to a greater extent than that of HOMO, energy gap between them is essentially lowered upon coordination to the Al(III) metal ion. However in $[Zn(\mathbf{L4})Cl(H_2O)_2]$ and $[Cd(\mathbf{L4})Cl(H_2O)_2]$ formulations, both HOMO and LUMO also have similar characteristics (with pyridine ring system is also contributing the LUMO) as that in free **L4H** but the energy of HOMO has been raised while that of LUMO has been lowered. This also resulted in lowering of HOMO-LUMO energy gap (Figure 28-29). The red shifts in absorption bands as observed in UV-Vis titration experiments are consistent with results of theoretical calculations (Figure A7). Also it is observed that

planarity of **L4**$^{-}$ has been enhanced in the complexes and become rigid as the lone-pair on imine-N is coordinated to the metal ion, PET process has been unfavoured totally.

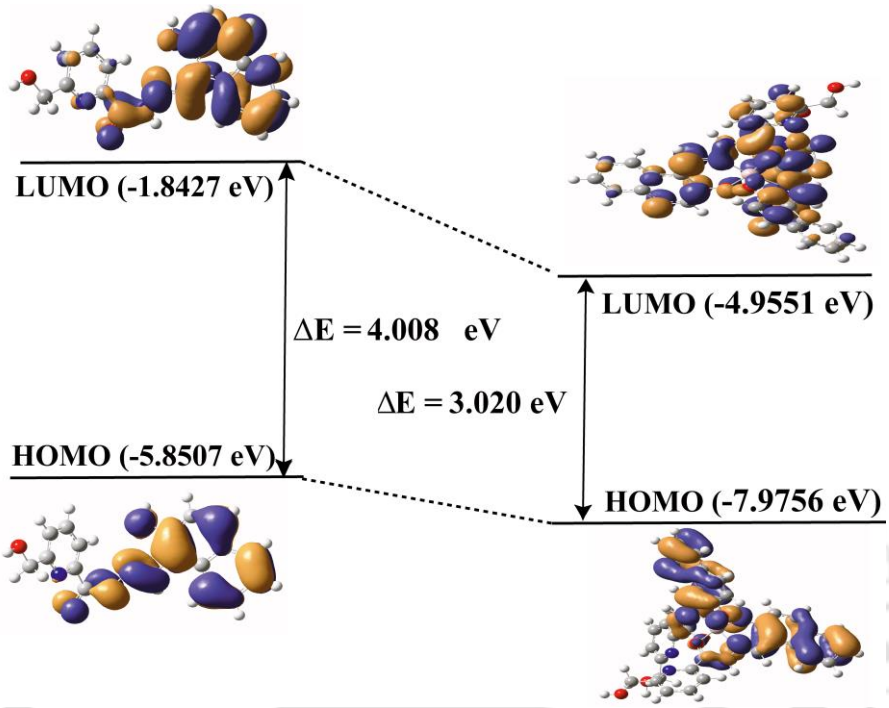

Figure 27. Energy level diagram depicting HOMO and LUMO of **L4H** and $[Al(\mathbf{L4})_2]^+$.

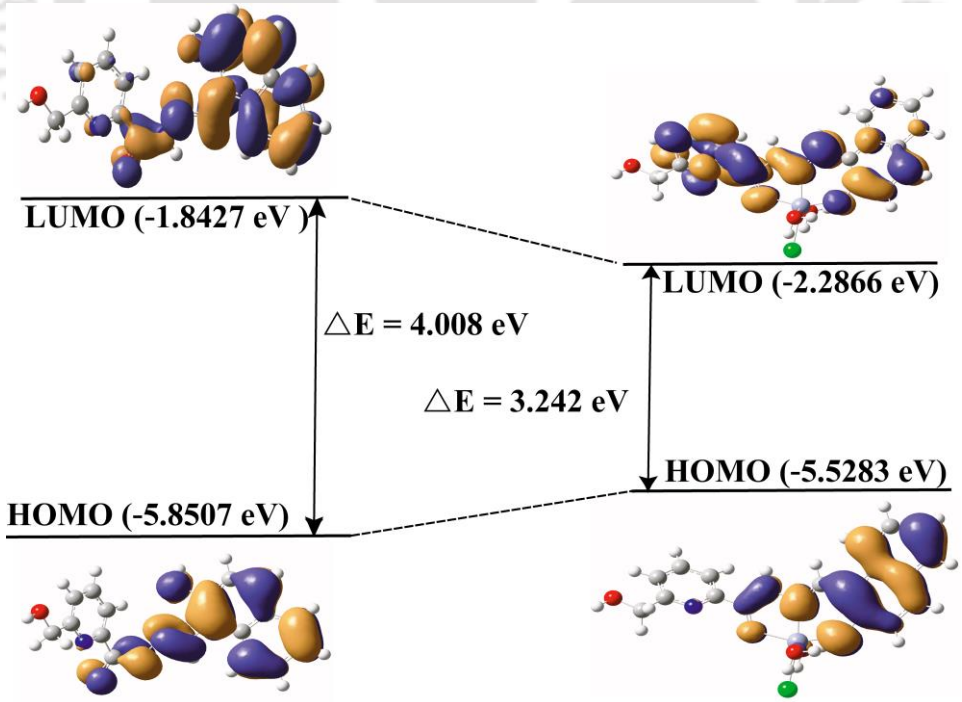

Figure 28. Energy level diagram depicting HOMO and LUMO of $[Zn(\mathbf{L4})Cl(H_2O)_2]$ complex.

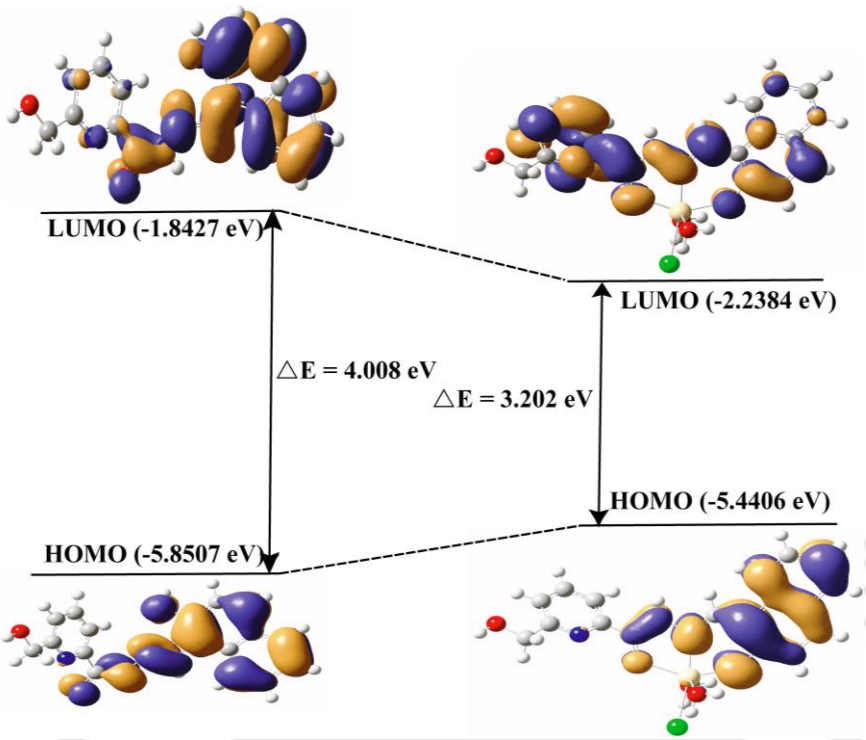

Figure 29. Energy level diagram depicting HOMO and LUMO of [Cd(**L4**)Cl(H_2O)$_2$] complex.

5.4. Conclusion:

In summary, a new probe (**L4H**) having a hydroxynapthyl group has been synthesized which acts as an *off–on* fluorescent sensor for single or multi detection of Al^{3+}, Zn^{2+} and Cd^{2+} ions in MeOH-HEPES buffer solution (5 mM, pH = 7.3, 7:3, *v*/*v*). The probe is weakly emissive in nature due to photoinduced electron transfer process involving the lone pair of electron on nitrogen atom of imine group. But upon irradiating with 435 nm light, **L4H** became strongly emissive only in presence of Al^{3+}, Zn^{2+} and Cd^{2+} ions having the maxima at 485, 570 and 540 nm, respectively. These results indicate that the PET process is quenched in presence of these three metal ions. These resultant solutions of metal-ligand species can detect anions by quenching the emission as a consequence of releasing the free **L4H** into the solution. Thus fluoride ion exhibited specific quenching of fluorescence intensity of aluminium complex but $H_2PO_4^-$ ion quenched those of zinc and cadmium complexes. Metal ion competition studies indicated that **L4H** can detect Al^{3+}, Zn^{2+} and Cd^{2+} ions individually or a mixture of any two or all three together, with distinct signals. Job's plot and mass spectra indicated that **L4H** binds

to Al^{3+} ion in 2:1 ratio and to Zn^{2+} and Cd^{2+} ions in 1:1 ratios. The results of DFT/TDDFT calculations on **L4H**, $[Al(\mathbf{L4})_2]^+$, $[Zn(\mathbf{L4})Cl(H_2O)_2]$ and $[Cd(\mathbf{L4})Cl(H_2O)_2]$ are in agreement with the experimentally observed results. In all cases, the HOMO is composed of π-orbitals of napthyl ring, lone pair orbitals on oxygen atom with some contribution from the pyridyl ring (in complexes) and nitrogen atom (in **L4H**). When compared to **L4H**, energies of both HOMO and LUMO have been lowered in $[Al(\mathbf{L4})_2]^+$ but in $[Zn(\mathbf{L4})Cl(H_2O)_2]$ and $[Cd(\mathbf{L4})Cl(H_2O)_2]$ energies of HOMO have been raised while that of LUMO has been lowered. There is a net lowering of HOMO-LUMO energy gap and also involvement of napthyl ring in the emissive process.

Reference:

1. R. P. Haugland, *The Molecular Probes Handbook: A Guide to Fluorescent Probes and Labeling Technologies*, Invitrogen, Carlsbad, CA, 10th edn, 2005.
2. A. P. de Silva, H. Q. N. Gunaratne, T. Gunnlaugsson, A. J. M. Huxley, C. P. McCoy, J. T. Rademacher and T. E. Rice, *Chem. Rev.*, 1997, **97**, 1515-1566.
3. S. C. Burdette and S. J. Lippard, *Coord. Chem. Rev.*, 2001, **216**, 333-361.
4. M. Mukherjee, S. Pal, S. Lohar, B. Sen, S. Sen, S. Banerjee, S. Banerjee and P. Chattopadhyay, *Analyst*, 2014, **139**, 4828-4835.
5. S. V. Verstraeten, L. Aimo and P. I. Oteiza, *Arch. Toxicol.*, 2008, **82**, 789−802.
6. J. Barcelo and C. Poschenrieder, *Environ. Exp. Bot.*, 2002, **48**, 75-92.
7. T. P. Flaten and M. Odegard, *Food Chem. Toxic.*, 1988, **26**, 959-960.
8. S. H. Kim, H. S. Choi, J. Kim, S. J. Lee, D. T. Quang and J. S. Kim, *Org. Lett.*, 2010, **12**, 560-563.
9. D. Maity and T. Govindaraju, *Chem. Commun.*, 2010, **46**, 4499-4501.
10. K. K. Upadhyay and A. Kumar, *Org. Biomol. Chem.*, 2010, **8**, 4892-4897.
11. Y. Zhao, Z. Lin, H. Liao, C. Duan and Q. Meng, *Inorg. Chem. Commun.*, 2006, **9**, 966-968.
12. E. L. Que, D. W. Domaille and C. J. Chang, *Chem. Rev.*, 2008, **108**, 1517-1519.
13. C. J. Frederickson, J. Y. Koh and A. I. Bush, *Nat. Rev. Neurosci.*, 2005, **6**, 449-462.
14. J. M. Berg and Y. Shi, *Science*, 1996, **271**, 1081-1085.
15. P. Jiang and Z. Guo, *Coord. Chem. Rev.*, 2004, **248**, 205-229.
16. E. J. Song, H. Kim, I. H. Hwang, K. B. Kim, A. R. Kim, I. Noh and C. Kim, *Sens. Actuators B*, 2014, **195**, 36-43.
17. A. I. Anzellotti and N. P. Farrell, *Chem. Soc. Rev.*, 2008, **37**, 1629-1651.
18. M. P. Cuajungco and G. J. Lees, *Neurobiol. Dis.*, 1997, **4**, 137-169.
19. A. I. Bush, W. H. Pettingell, G. Multhaup, M. D. Paradis, J. P. Vonsattel, J. F. Gusella, K. Beyreuther, C. L. Masters and R. E. Tanzi, *Science*, 1994, **265**, 1464-1467.
20. J. E. Kwon, S. Lee, Y. You, K.-H. Baek, K. Ohkubo, J. Cho, S. Fukuzumi, I. Shin, S. Y. Park and W. Nam, *Inorg. Chem.*, 2012, **51**, 8760-8774.
21. M. P. Waalkes, *J. Inorg. Biochem.*, 2000, **79**, 241-244.

22. M. P. Waalkes, T. P. Coogan and R. A. Barter, *Crit. Rev. Toxicol.*, 1992, **22**, 175-201.
23. R. E. Clement, P. W. Yang and C. Koester, *Anal. Chem.*, 1999, **71**, 257R-292R.
24. L. H. Thaller and A. H. Zimmerman, *J. Power Sources*, 1996, **63**, 53-61.
25. S. E. Bailey, T. J. Olin, R.M. Bricka and D. D. Adrian, *Water Res.*, 1999, **33**, 2469-2479.
26. E. M. Nolan, J. W. Ryu, J. Jaworski, R. P. Feazell, M. Sheng and S. J. Lippard, *J. Am. Chem. Soc.*, 2006, **128**, 15517-15528.
27. K. Komatsu, K. Kikuchi, H. Kojima, Y. Urano and T. Nagano, *J. Am. Chem. Soc.*, 2005, **27**, 10197-10204.
28. S. K. Kim and J. L. Sessler, *Chem. Soc. Rev.*, 2010, **39**, 3784-3809.
29. J. Aaseth, M. Shimshi, J. L. Gabrilove and G. S. Birketvedt, *J. Trace Elem. Exp. Med.*, 2004, **17**, 83-92.
30. J. Chen, P. Zhou, L. Zhao and T. Chu, *RSC Adv.*, 2014, **4**, 254-259.
31. S. W. Thomas III, G. D. Joly and T. M. Swager, *Chem. Rev.*, 2007, **107**, 1339-1386.
32. J. Yoon, S. K. Kim, N. J. Singh and K. S. Kim, *Chem. Soc. Rev.*, 2006, **35**, 355-360.
33. J. L. Sessler and J. M. Davis, *Acc. Chem. Res.*, 2001, **34**, 989-997.
34. J. Chen, P. Zhou, G. Li, T. Chu and G. He, *J. Phys. Chem. B*, 2013, **117**, 5212-5221.
35. Y. Kim and F. P. Gabbaï, *J. Am. Chem. Soc.*, 2009, **131**, 3363-3369.
36. A. E. J. Broomsgrove, D. A. Addy, A. D. Paolo, I. R. Morgan, C. Bresner, V. Chislett, I. A. Fallis, A. L. Thompson, D. Vidovic and S. Aldridge, *Inorg. Chem.*, 2010, **49**, 157-173.
37. K. Tayade, S. K. Sahoo, A. Singh, N. Singh, P. Mahulikar, S. Attarde and A. Kuwar, *Sens. Actuators, B*, 2014, **202**, 1333-1337.
38. A. Bamesberger, C. Schwartz, Q. Song, W. Han, Z. Wang and H. Cao, *New J. Chem.*, 2014, **38**, 884–888.
39. W. Scenger, *Principles of Nucleic Acid Structure*, Springer, New York, 1998.
40. D. H. Lee, S. Y. Kim and J. Hong, *Angew. Chem., Int. Ed.*, 2004, **43**, 4777-4780.
41. S. E. Manhan, *Fundamentals of Environmental Chemistry*, CRC Press, Taylor & Francis Group, LLC, 3rd edn, 2008.
42. C. Bazzicalupi, A. Bencini and V. Lippolis, *Chem. Soc. Rev.*, 2010, **39**, 3709-3728.

43. C. Spangler, M. Schaeferling and O. S. Wolfbeis, *Microchim. Acta*, 2008, **161**, 1-39.
44. H. Y. Li, R. A. Lalancette and F. Jäkle, *Chem. Commun.*, 2011, **47**, 9378-9380.
45. E. Tomat and S. J. Lippard, *Inorg. Chem.*, 2010, **49**, 9113-9115.
46. G. V. Zyryanov, M. A. Palacios and P. Anzenbacher Jr., *Angew. Chem., Int. Ed.*, 2007, **46**, 7849-7852.
47. S. O. Kang, J. M. Llinares, V. W. Day and K. Bowman-James, *Chem. Soc. Rev.*, 2010, **39**, 3980-4003.
48. Z. C. Xu, K. H. Baek, H. N. Kim, J. N. Cui, X. H. Qian, D. R. Spring, I. Shin and J. Y. Yoon, *J. Am. Chem. Soc.*, 2010, **132**, 601-610;
49. P. Jiang and Z. J. Guo, *Coord. Chem. Rev.*, 2004, **248**, 205-229.
50. N. Behera and V. Manivannan, *ChemistrySelect*, 2016, **1**, 4016-4023.
51. D. Maity and T. Govindaraju, *Chem. Commun.*, 2012, **48**, 1039–1041.
52. Y. Liu, C. Chen and A. Wu, *Analyst*, 2012, **137**, 5201–5203.
53. X. Xie and Y. Qin, *Sens. Actuator, B*, 2011, **156**, 213–217.
54. C. R. Lohani, J. Kim, S. Chung, J. Yoon and K. Lee, *Analyst*, 2010, **135**, 2079–2084.
55. S. Kim, J. Y. Noh, K. Y. Kim, J. H. Kim, H. K. Kang, S. W. Nam, S. H. Kim, S. Park, C. Kim and J. Kim, *Inorg. Chem.*, 2012, **51**, 3597–3602.
56. G. Albendín, M. P. Mánuel-Vez, C. Moreno and M. García-Vargas, *Talanta*, 2003, **60**, 425-431.
57. A. Garau, M. Oliver, M. Rosende, M. P. Mánuel-Vez and M. Miró, *Talanta*, 2015, **133**, 120–126.
58. J. Qin, Z. Yang and P. Yang, *Inorg. Chim. Acta*, 2015, **432**, 136-141.
59. A. K. Das and S. Goswami, *Sens. Actuators, B*, 2017, **245**, 1062-1125.
60. X. Su and I. Aprahamian, *Chem. Soc. Rev.*, 2014, **43**, 1963-1981.
61. J. L. Ren, J. Zhang, J. Q. Luo, X. K. Pei and Z. Xi Jiang, *Analyst*, 2001, **126**, 698-702.
62. S. M. Ng and R. Narayanaswamy, *Anal. Bioanal. Chem.*, 2006, **386**, 1235-1244.
63. J. Sun, B. Ye, G. Xia and H. Wang, *Sens. Actuators, B*, 2017, **249**, 386–394.
64. S. Nandi and D. Das, *ACS Sens.*, 2016, **1**, 81–87.
65. M. Shyamal, P. Mazumdar, S. Maity, S. Samanta, G. P. Sahoo and A. Misra, *ACS Sens.*, 2016, **1**, 144−150.

66. E. J. Song, J. Kang, G. R. You, G. J. Park, Y. Kim, S.-J. Kim, C. Kim and R. G. Harrison, *Dalton Trans.*, 2013, **42**, 15514-15520.
67. D. Maity and T. Govindaraju, *Chem. Commun.*, 2012, **48**, 1039–1041.
68. S. B. Roy, J. Mondal, A. R. K. Bukhsh and K. K. Rajak, *New J. Chem.*, 2016, **40**, 9593–9608.
69. S. Goswami, D. Sen and N. K. Das, *Tetrahedron Lett.*, 2010, **51**, 6707-6710.
70. S. Goswami, S. Das, K. Aich, D. Sarkar, T. K. Mondal, C. K. Quah, H.-K. Fun, *Dalton Trans.*, 2013, **42**, 15113-15119.
71. F. A. Cotton, G. Wilkinson, C. A. Murillo and M. Bochmann, *Advanced Inorganic Chemistry*, John Wiley and sons, inc. 6th edition, pp 600.
72. M. Shyamal, P. Mazumdar, S. Maity, S. Samanta, G. P. Sahoo and A. Misra, *ACS Sens.*, 2016, **1**, 739-747.
73. S. Goswami, A. Manna, S. Paul, K. Aich, A. K. Das and S. Chakraborty, *Dalton Trans.*, 2013, **42**, 8078-8085.
74. S. Goswami, K. Aich, S. Das, A. K. Das, D. Sarkar, S. Panja, T. K. Mondal and S. Mukhopadhyay, *Chem. Commun.*, 2013, **49**, 10739-10741.
75. S. Das, S. Goswami, K. Aich, K. Ghoshal, C. K. Quah, M. Bhattacharyya and H.-K. Fun, *New J. Chem.*, 2015, **39**, 8582-8587.
76. A. Gupta and N. Kumar, *RSC Adv.*, 2016, **6**, 106413-106434.
77. G. H. Aryal, C. H. Battle, T. A. Grusenmeyer, M. Zhu and J. Jayawickramarajah, *Chem. Commun.*, 2016, **52**, 2307-2310.
78. G. H. Aryal, L. Huang and K. W. Hunter, *RSC Adv.* 2013, **6**, 82566-82570.
79. D. F. Shriver and P. W. Atkins, *Inorganic Chemistry, Oxford University Press*, 3rd edition, 1999, 169.

Appendix:

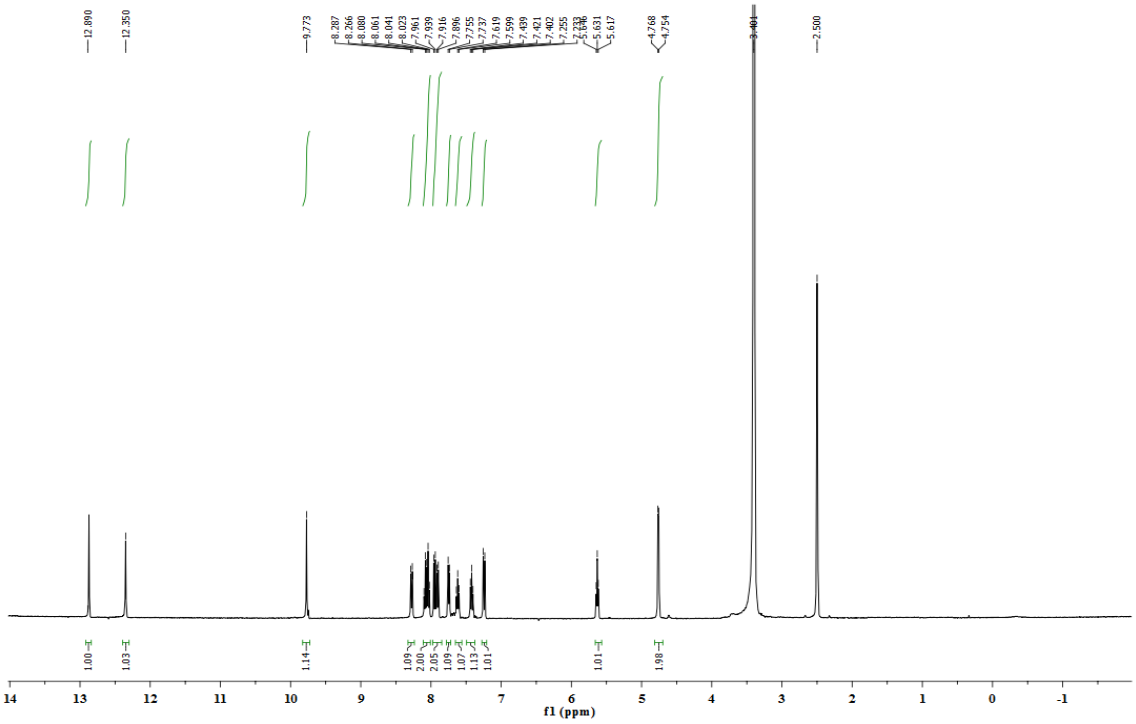

Figure A1. ^{1}H NMR of **L4H**.

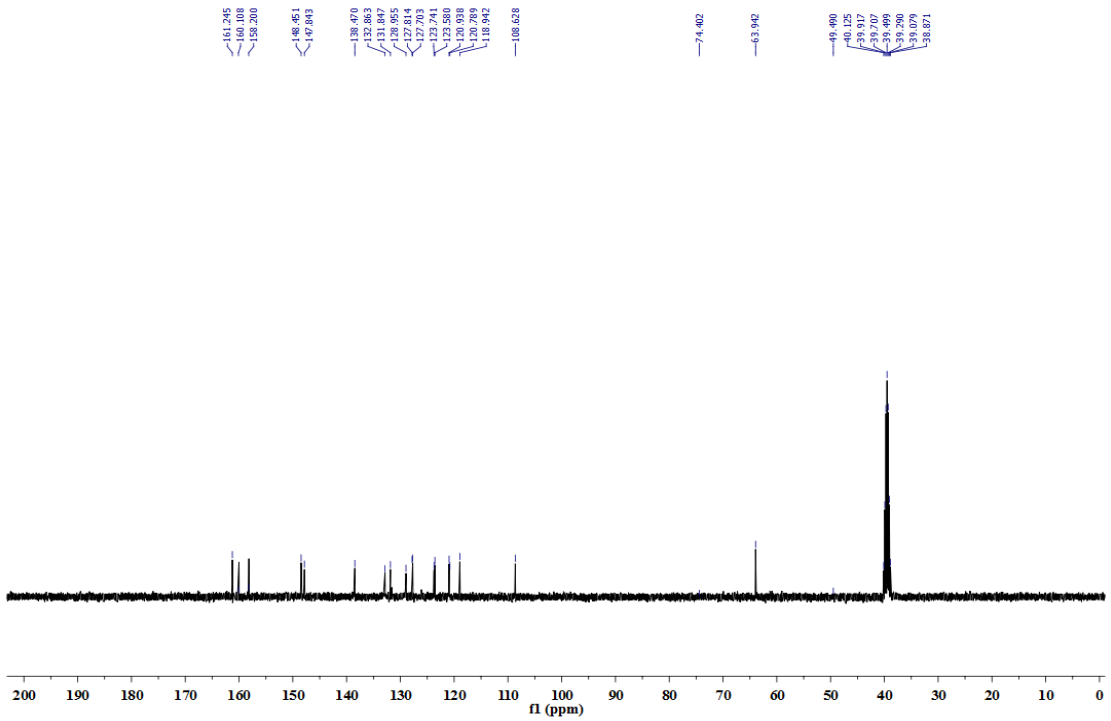

Figure A2. ^{13}C NMR of **L4H**.

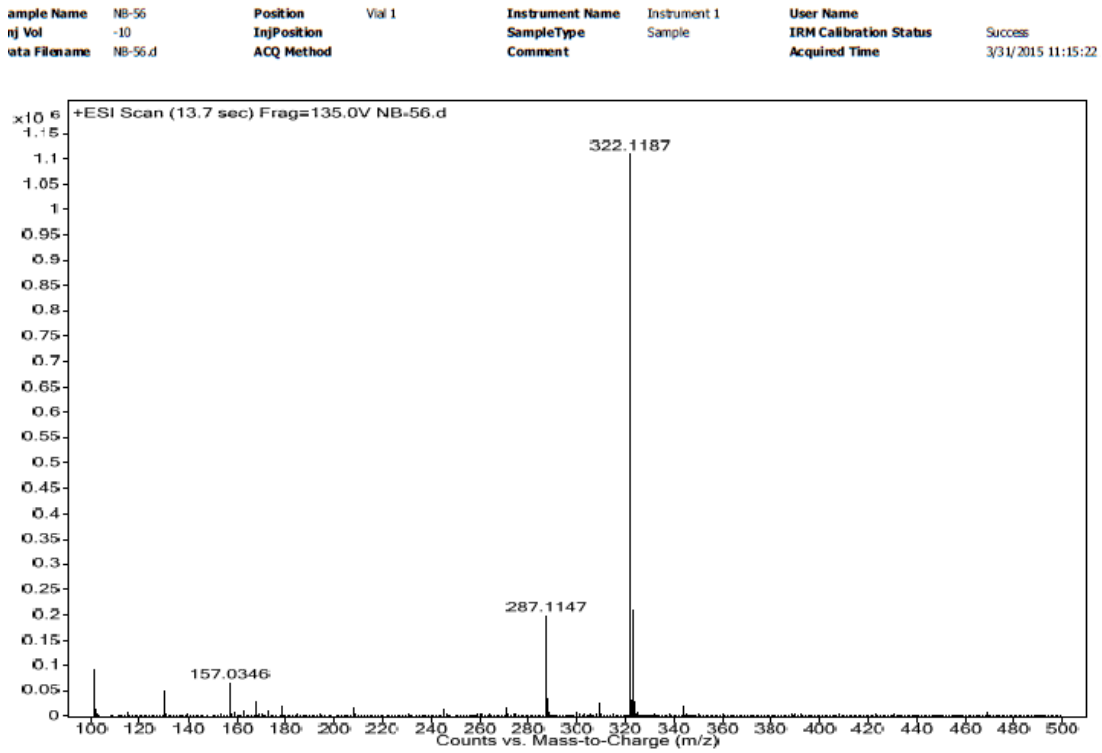

Figure A3. Mass spectrum of **L4H**.

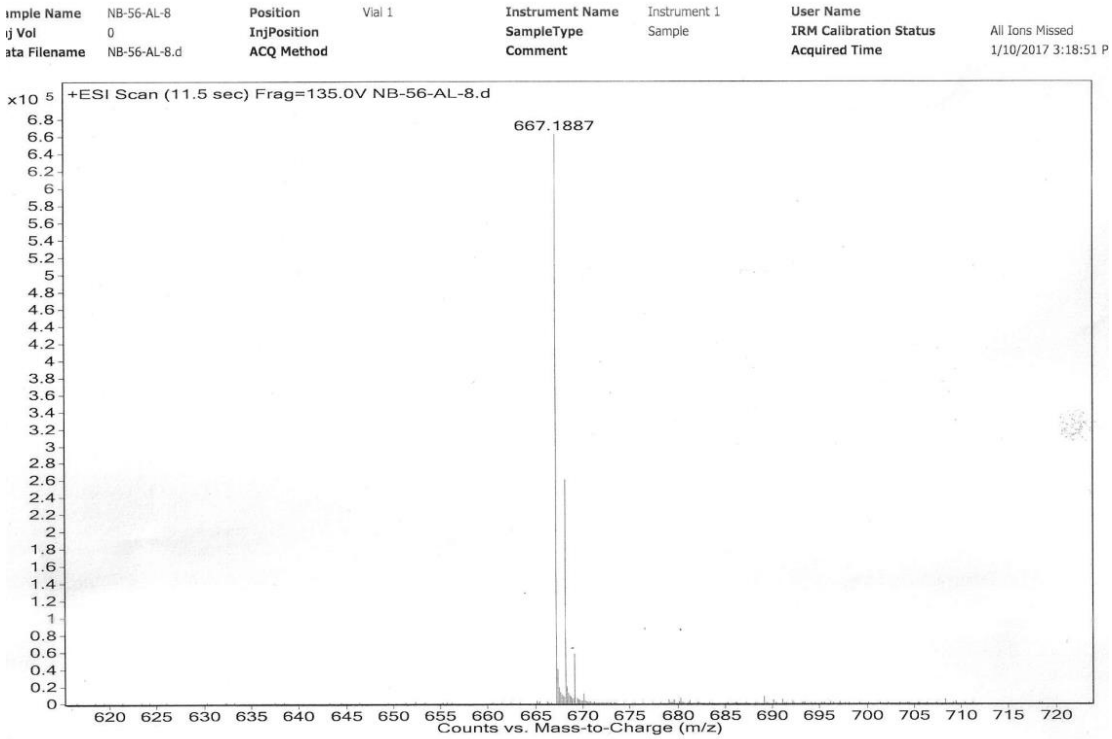

Figure A4. Mass spectrum of **L4H** complex of Al^{3+} ion.

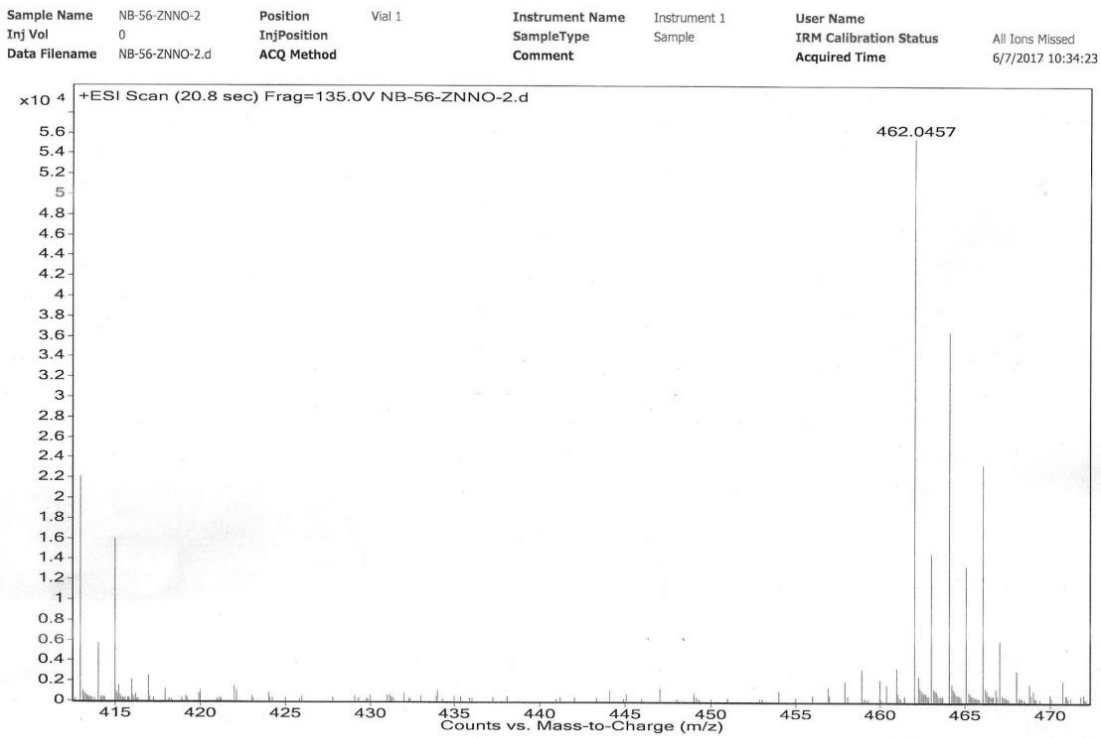

Figure A5. Mass spectrum of **L4H** complex of Zn^{2+} ion.

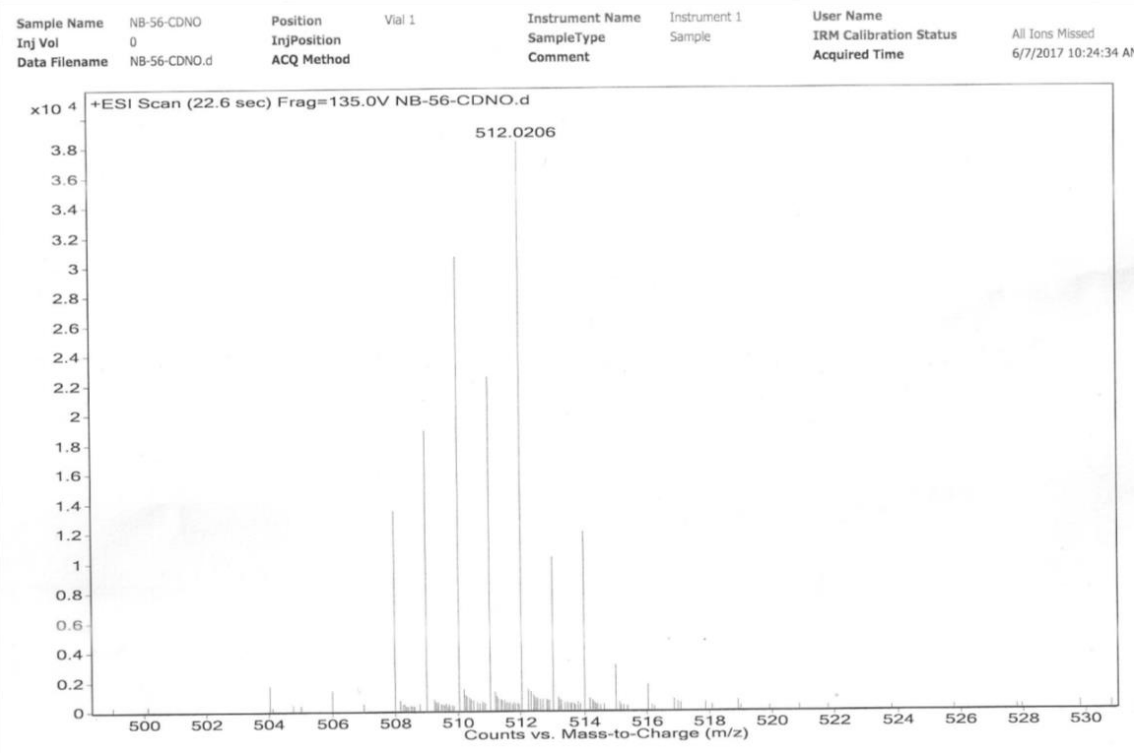

Figure A6. Mass spectrum of **L4H** complex of Cd^{2+} ion.

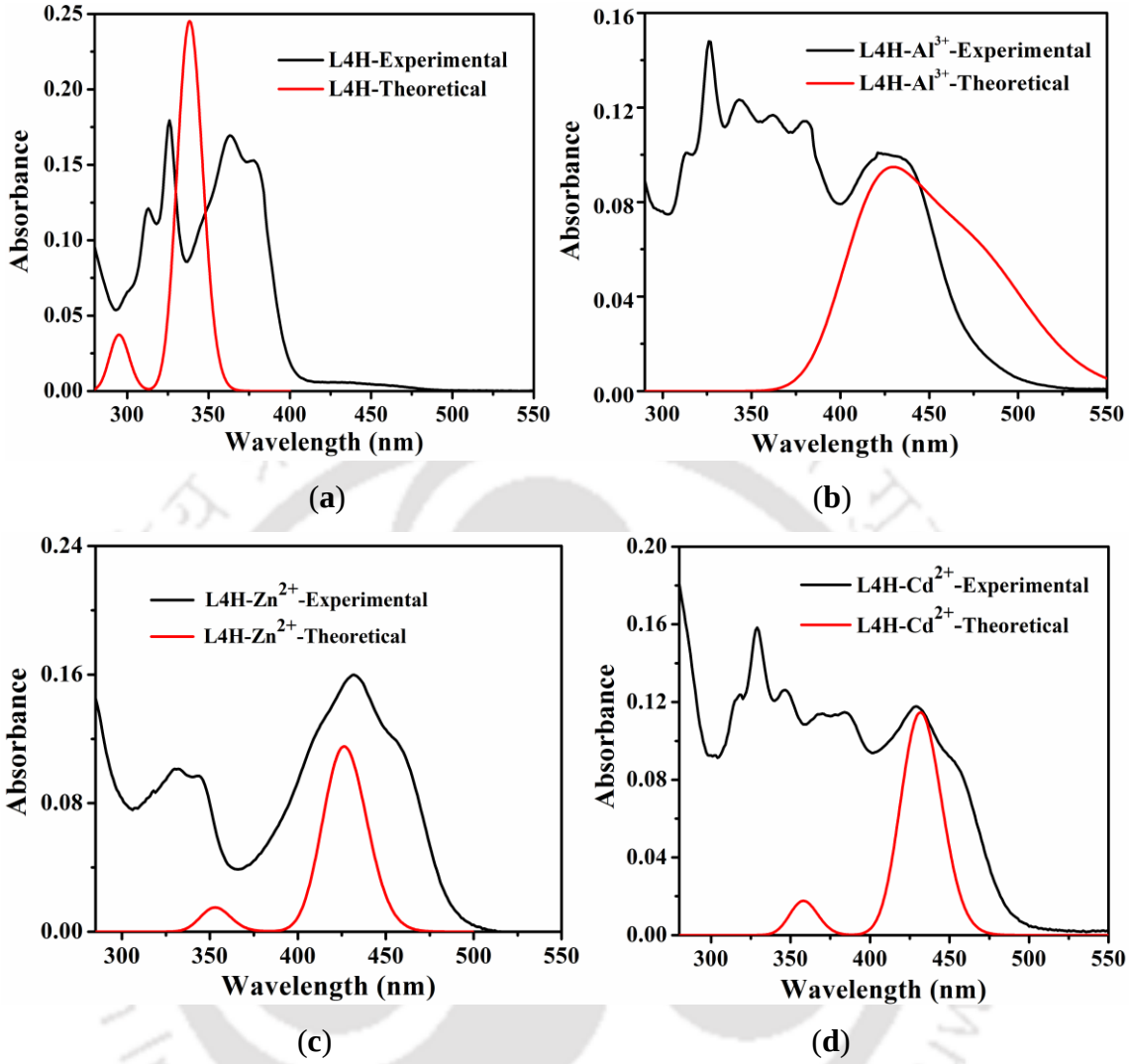

Figure A7. Experimental and simulated UV-Vis absorption spectra of **L4H** and its complex with Al^{3+}, Zn^{2+} and Cd^{2+} ions.

Overview

In Chapter 2, a mono-substituted imidazole ligand, 1-(4-acetylphenyl)imidazole (**L**) has been used to synthesize nine complexes which exhibit different supramolecular architectures with the help of weak interactions. This encouraged to try with a tri-substituted imidazole, which might show similar kind of supramolecular networks, hence, the 2,4-bis(2-pyridyl)-5-(4-pyridyl)imidazole (**L1H**) was used. A crystalline 1D coordination polymer of composition $[Zn_2(\mathbf{L1})Cl_3(H_2O)]$ was isolated and structurally characterized. In addition, **L1H** was found to act as a selective fluorescence sensor form Zn^{2+} ion. This prompted to design some new probes containing benzothiazole moiety and 2-(2-(2,3-dihydroxy)benzylidenehydrazinyl)benzothiazole (**L2H**) and 2-((2-(2-hydroxy)(4-*N*,*N*-diethylamino))benzylidenehydrazinyl)benzothiazole (**L3H**) were synthesized and both are found to be useful probes for the detection of aluminium(III) ion. As a continuation, a hydrazide having a fluorophoric hydroxynapthyl group, 6-(hydroxymethyl)-*N*'-((2-hydroxy-1-naphthyl)methylene)picolinohydrazide (**L4H**) was designed and synthesized. This hydrazide was found to be useful for the detection of Al^{3+}, Zn^{2+} and Cd^{2+} ions.

Conclusions

Nine bivalent metal complexes of monodentate ligand 1-(4-acetylphenyl)imidazole (**L**) and co-ligands, were synthesized and weak interactions such as; O–H···O, C–H···π, C–H···S, C–H···Cl, C–H···O and π···π stacking interactions were observed to be present in their molecular structures determined by single-crystal X-ray diffraction studies, which lead to different supramolecular architectures. In addition, coligand **Fum** coordinates to metal center in different binding fashions resulting in formation of 1D and 2D coordination polymers. The trisubstituted imidazole probe, 2,4,-bis(2-pyridyl)-5-(4-pyridyl)imidazole (**L1H**) can selectively recognize Zn^{2+} ion by giving red shifted peak in fluorescence and the complex $[Zn_2(\mathbf{L1})Cl_3(H_2O)]$ was isolated as crystalline solid, is a 1D coordination polymer. Two new benzothiazole probes 2-(2-(2,3-dihydroxy)benzylidenehydrazinyl)benzothiazole (**L2H**) and 2-((2-(2-hydroxy)(4-*N*,*N*-diethylamino))benzylidenehy-drazinyl)benzothiazole (**L3H**) can selectively

recognize Al^{3+} ion exhibiting "*Turn On*" responses at physiological pH. The results of DFT/TDDFT calculations on ligands and their Al^{3+} complexes support the changes in UV-Vis spectra upon complex formation. A hydrazide (**L4H**) containing 2-hydroxynaphthal moiety has been found to act as a "*TURN-ON"* fluorescence sensor for Al^{3+}, Zn^{2+} and Cd^{2+} ions by giving different emission maxima at physiological pH range. The results of DFT/TDDFT calculations on **L4H**, $[Al(\mathbf{L4})_2]^+$, $[Zn(\mathbf{L4})Cl(H_2O)_2]$ and $[Cd(\mathbf{L4})Cl(H_2O)_2]$ support the experimental UV-Vis results.

Future Perspective

In future, supramolecular interactions in complexes can further be studied by tuning the ligand by having different substituent on the imidazole ring and changing the reaction condition as well as utilizing different coligands. In metal ion recognition studies, the ability to detect metal ions in aqueous solution and at visible and NIR regions is still a challenging task. Modification in ligand motifs by incorporating suitable fluorophore groups can be undertaken in order for them to be employed as chromophore/fluorophore for the recognition of cation and anions.

List of Publications

From Thesis:

1. N. Behera and V. Manivannan, *ChemistrySelect*, 2016, **1**, 4016–4023
2. N. Behera and V. Manivannan, *ChemistrySelect*, 2017, **2**, 11048–11054.
3. N. Behera and V. Manivannan, *J. Photochem. Photobiol. A*, 2018, **353**, 77-85.

Others:

1. J. Bori, N. Behera, S. Mahata and V. Manivannan, *ChemistrySelect*, 2017, **2**, 11727–11731.